

REPORT DOCUMENTATION PAGE				Form Approved OMB No. 0704-0188	
Public reporting burden for this collection of information is estimated to average 1 hour per response, including the time for reviewing instructions, searching existing data sources, gathering and maintaining the data needed, and completing and reviewing the collection of information. Send comments regarding this burden estimate or any other aspect of this collection of information, including suggestions for reducing the burden, to Department of Defense, Washington Headquarters Services, Directorate for Information Operations and Reports (0704-0188), 1215 Jefferson Davis Highway, Suite 1204, Arlington, VA 22202-4302. Respondents should be aware that notwithstanding any other provision of law, no person shall be subject to any penalty for failing to comply with a collection of information if it does not display a currently valid OMB control number. PLEASE DO NOT RETURN YOUR FORM TO THE ABOVE ADDRESS.					
1. REPORT DATE (DD-MM-YYYY) 05-01-2005		2. REPORT TYPE Final Report		3. DATES COVERED (From – To) 20-Nov-01 - 11-Jan-05	
4. TITLE AND SUBTITLE Study of a Structural Plasma Influence on Characteristics of Viscous Friction and Separated Near-Surface Zone Position Under High-Speed Airflow			5a. CONTRACT NUMBER ISTC Registration No: 2084		
			5b. GRANT NUMBER		
			5c. PROGRAM ELEMENT NUMBER		
6. AUTHOR(S) Dr. Serguei Leonov			5d. PROJECT NUMBER		
			5d. TASK NUMBER		
			5e. WORK UNIT NUMBER		
7. PERFORMING ORGANIZATION NAME(S) AND ADDRESS(ES) Institute of High Temperatures RAS IVTAN, Izhorskaya str., 13/19 Moscow 125412 Russia				8. PERFORMING ORGANIZATION REPORT NUMBER N/A	
9. SPONSORING/MONITORING AGENCY NAME(S) AND ADDRESS(ES) EOARD PSC 802 BOX 14 FPO 09499-0014				10. SPONSOR/MONITOR'S ACRONYM(S)	
				11. SPONSOR/MONITOR'S REPORT NUMBER(S) ISTC 01-7001	
12. DISTRIBUTION/AVAILABILITY STATEMENT Approved for public release; distribution is unlimited.					
13. SUPPLEMENTARY NOTES					
14. ABSTRACT This report results from a contract tasking Institute of High Temperatures RAS as follows: The contractor will study the application of plasma technology for drag reduction and flow control. In particular, he will investigate the change in aerodynamic friction and the flow separation point using a modulated High Frequency (HF) multi-streamer electric discharge near a model's surface. In order to measure plasma effects on the viscous friction, the experiments will be made in a wind tunnel at transonic and subsonic speeds. The short duration wind tunnel, currently available at IVTAN will be used. The Mach numbers at which experiments will be made are $0.1 < M < 0.95$ and $M = 1.7$. Diagnostic investigations such as: Schlieren (for flow visualization); spectral system (for emission measurements); pressure sensors; tenso-balances; fast photo camera; thermocouples and others will allow to investigate in detail the process of interaction of surface plasma with aerodynamic bodies in high-speed flow.					
15. SUBJECT TERMS EOARD, Aviation Technology, Aerodynamics					
16. SECURITY CLASSIFICATION OF:			17. LIMITATION OF ABSTRACT UL	18. NUMBER OF PAGES 276	19a. NAME OF RESPONSIBLE PERSON William B. McClure, Col USAF
a. REPORT UNCLAS	b. ABSTRACT UNCLAS	c. THIS PAGE UNCLAS			19b. TELEPHONE NUMBER (Include area code) +44 (0)20 7514 4376



EOARD-IVTAN-ISTC Project# 2084p

Operative Commencement Date:

November 01, 2001

Institute of High Temperature
Russian Academy of Science (IVTAN)
Izhorskaya street, 13/19, of. 231
Moscow, 125412, Russia

Final Report

Study of Structural Plasma Influence on the Characteristics of Viscous Friction and Separated Near-Surface Zone Position under High-Speed Airflow.

(1 November 2002 – 31 October 2004)

Director of IHT RAS:

Corresponding Member of the RAS

Vyacheslav M. Batenin

Project Manager:

Dr. Sergey B. Leonov

Institute of High Temperature RAS, Moscow

November 2004

**This project is funded by EOARD and performed under the contract to the
International Science and Technology Center (ISTC), Moscow.**

ISTC Project #2084p

Title:

Study of Structural Plasma Influence on the Characteristics of Viscous Friction and Separated Near-Surface Zone Position under High-Speed Airflow

Institute: Institute of High Temperature Russian Academy of Science

Project Manager: Sergey Borisovich Leonov,
Izhorskaya str., 13/19, Moscow, 125412, Russia
Phone +7-(095) 484-1811, Fax +7-(095) 483-2285
E-mail: sleo@oivtran.iitp.ru

Partner: European Office of Aerospace Research and Development (EOARD)
223-231 Old Marylebone Road, London, UK
Phone: +44-171-514-4299; Fax: +44-171-514-4960
E-mail: Wayne.Donaldson@london.af.mil

Project Duration: From November 1, 2001 to October 31, 2004 for 36 months

Objectives:

The objective of the project is an experimental study a surface plasma influence on viscous friction and position of separation areas on simple models in transonic (supersonic) and subsonic airflow.

The general purpose of the activity is to continue a study of the fundamental plasma technology in a plasma -airflow interaction area, in particular, research of methods of control of structural (filamentary) plasma objects and application of such plasma for the control of airflow parameters near a streamlined surfaces (viscous friction and separation zones location). The work performed under this intention will also result in to obtain new data about interaction in an airflow-plasma system.

Keywords : Electrical Discharge, Plasma Aerodynamics, Plasma Non-uniformity, Boundary Layer, Separation Zone, Viscous Friction, Spectroscopy, Schlieren Measurement.

Contents.

- i. List of key personnel.
- ii. List of acronyms and definitions.

1. Introduction

1.1. Objectives and Motivation.

1.2. Tasks Description.

1.3. Background.

1.3.1. Aerodynamic Sequences of Near-Surface Plasma Generation.

1.3.2. Methods of the Discharge Control.

1.3.3. Weakly-Ionized Plasma Experiments on Flow Control.

1.4. Short Review of Results Year by Year.

2. Results.

2.1. Experimental Facility Description.

2.1.1. Gasdynamic Facilities PWT-10 and PWT-50.

2.1.2. Schemes of Electric Discharges Tested.

2.1.3. Schlieren Shadow System.

2.1.4. Spectroscopic Measurements. Method of the Spectrum Fitting.

2.1.5. Gasdynamic and Electrical Measurements.

2.2. Experimental Results on Quasi-DC Surface Plasma Effect.

2.2.1. Design of Quasi-DC Surface Plasma Generator.

2.2.2. Measurements of Filamentary Plasma Parameters.

2.2.3. Dynamics of Filamentary Plasma Inflow.

2.2.4. Simplified Physical Model of Interaction.

2.2.5. The Effect of Plasma-Induced Separation.

2.2.6. Duct-Driven Flow Control.

2.2.7. Separation Control by Filamentary Plasma.

2.2.8. Transonic Flow Control.

2.3. Experimental Results on DBD Plasma Effect.

2.3.1. Dielectric-Barrier Discharge Operation and Appearance.

2.3.2. Scheme Simulation.

2.3.3. Measurements of Electric Parameters.

2.3.4. Measurements of Barrier Discharge Plasma Parameters.

2.3.5. Experimental Arrangement and the Test Parameters.

2.3.6. Plasma-Induced Flow.

2.3.7. Subsonic Effects.

2.3.8. Transonic Effect.

2.3.9. Supersonic Effect.

2.4. Numerical Simulation of Near-Surface Plasma Effect.

2.4.1. Near-Surface Thermal Power Deposition (Euler Approach).

2.4.2. Near-Surface Energy Deposition (Navier-Stokes Approach).

2.4.3. Electrodynamic Effects in Boundary Layer.

3. Conclusion.

3.1. Conclusion.

3.2. Applications.

Attachment 1.

Summary of publications.

i. List of Key Personnel.

Dr. Felix A. Akopov	Senior Researcher,
Dr. Yury I. Isaenkov	Senior Researcher,
Dr. Valery G. Gromov	Senior Scientist,
Dr. Alexander P. Kuryachiy	Senior Researcher,
Dr. Sergey B. Leonov	Head of Laboratory, Project Manager,
Mr. Paul G. Makeev	Senior Engineer,
Mr. Konstantin V. Savelkin	Senior Engineer,
Dr. Victor R. Soloviev	Senior Researcher,
Mr. Vladimir A. Storozhenko	Mechanical Engineer,
Dr. Valery N. Suchov	Leading Engineer,
Mr. Dmitry A. Yarantsev	Engineer-Physicist,
Prof. Anatoly S. Yuriev	Senior Scientist.

Acknowledgements.

Dr. Valentin A Bityurin,
Mr. Wayne Donaldson,
Dr. Victor V. Kirichenko,
Dr. Anatoly I. Klimov,
Dr. Yury F. Kolesnichenko,
Prof. Artur V. Krasilnikov,
Prof. J. Reece Roth,
Dr. Valery N. Sermanov,
Dr. Vladimir V. Skvortsov.

ii. List of Definitions and Acronyms.

M -	Mach Number of the flow.
Kn-	Knudsen Number.
Re -	Reynolds Number.
Sc -	Struhal Number.
C -	capacitance.
E-	electric field strength.
E/N-	reduced electric field strength.
I -	electric current.
k -	Boltzman's constant.
L-	inductivity.
N _e -	concentration of electrons.
N -	concentration of neutral gas particles.
N _n -	concentration of the different chemical species.
P _{st} -	static pressure in airflow.
P _o -	stagnation pressure in airflow.
R	resistivity.
R _L = ω L	inductive resistivity.
S -	area of midsection.
T _g -	gas temperature.
T _v -	vibrational temperature of molecular gas.
T _e -	temperature of electrons in plasma.
V -	velocity of flow.
W -	power or power density.
ρ_0 -	gas density in flow.
ϵ_0 -	electrostatic constant.
δ -	boundary layer thickness.
λ -	wavelength.
τ -	relaxation time.
ω -	circular frequency of EM wave.
BL -	boundary layer.
AC -	alternative current.
DBD -	dielectric barrier discharge.
DC -	direct current.
EMF -	electromagnetic field.
EHD (EGD) -	electrohydrodynamics.
HF -	high frequency.
HV -	high voltage.
IR -	infra-red radiation.
MPA -	magneto plasma aerodynamics.
MW -	micro waves.
MF -	magnetic field.
MFD -	middle frequency discharge.
PD -	pulse discharge.
PG -	plasma generator.
PWT -	pulse wind tunnel.
SW -	shock wave.
SD -	surface discharge.
TS -	test section.
UV -	ultra-violet radiation.
WT -	wind tunnel.

1. Introduction

1.1. Objectives and Motivation.

The objective of the project as a whole is an experimental study of a surface plasma influence on viscous friction and position of separation areas on simple models in supersonic and subsonic airflow. Several ideas stimulate efforts in this field. Main ones from those are the following:

- ◇ Active control of the supersonic inlet/diffuser performance;
- ◇ Control of the flow structure near the foils;
- ◇ Stabilization of unsteady flow areas;
- ◇ Fixing of interference effects;
- ◇ Improvement of the supersonic combustion efficiency.

Conventional methods to advance aerodynamic characteristics of flight vehicles and its parts or to adjust the trajectory are based on application of mechanical elements, which use energy of oncoming airflow for re-distribution of pressure on surfaces, and application of jets' power in local areas near the surfaces. The method of chemical energy deposition is utilized for propulsion. The abilities of these methods of flow control are close to natural limitations due to a strict localization and slow response. A fast flow control can be realized through an electromagnetic mechanism of bulk force generation. Three main domains in this field are known, namely: heat energy release by plasma of electric discharge; magneto-hydrodynamic (MHD) interaction; and electrostatic (EHD) force generation. It is definite that heat release changes the flowfield. But in the case of non-uniform plasma the distribution of parameters depends on structure of flowfield itself. Here some important details of such an interaction are made clearer. General understanding now is that EHD forces are quite small and can be observed under low-speed flow. Here a weak EHD effect is demonstrated at high-speed conditions. The MHD body forces generation can be realized effectively under high bulk conductivity of the gas. This work describes the effects for near-surface plasma generation without external magnetic field.

Today a huge experience is gathered in a field of Plasma Aerodynamics, especially in model experiments and CFD [1-4]. As a result of the latest efforts there are no doubts that the

plasma method can be applied for flow/flight control. The problem is the effectiveness of method and realization of controllable/accurate energy release to airflow. An idea of the flow modification by plasma of electrical discharge can be formulated on the most simple manner as following: modification of flow-field structure and, consequently, changing a pressure and tangential tension near surfaces by means of an energy release into predefined space area with predefined parameters' distribution and at predefined tempering. The diagram below in Fig.1.1 shows a simple classification of types of the energetic effect on flow-body system. The blue-colored fields are related to plasma-based technique. An extended understanding of the MPA method for FFC includes not only gas heating but also MHD and electrostatic methods of ponderomotive forces production. Several main mechanisms of the electric discharges influence on moving gas can be described: (1) change of thermodynamic and chemical properties of medium, (2) modification of flow-field structure, (3) local artificial separation and (4) boundary layer modification. Technically the effects have become apparent in bow shock transformation, wave drag reduction (thermodynamic and form-factor shares), base drag reduction, skin friction change, thermal flux redistribution, adjustment of flow-field structure in inlets/diffusers, etc. Such possibilities can be realized by means of plasma generation in DC-AC electrical discharge; free-localized plasma generation in electromagnetic wave beams; blowing out of high enthalpy plasma jets; and by the other similar phenomena [5-24].

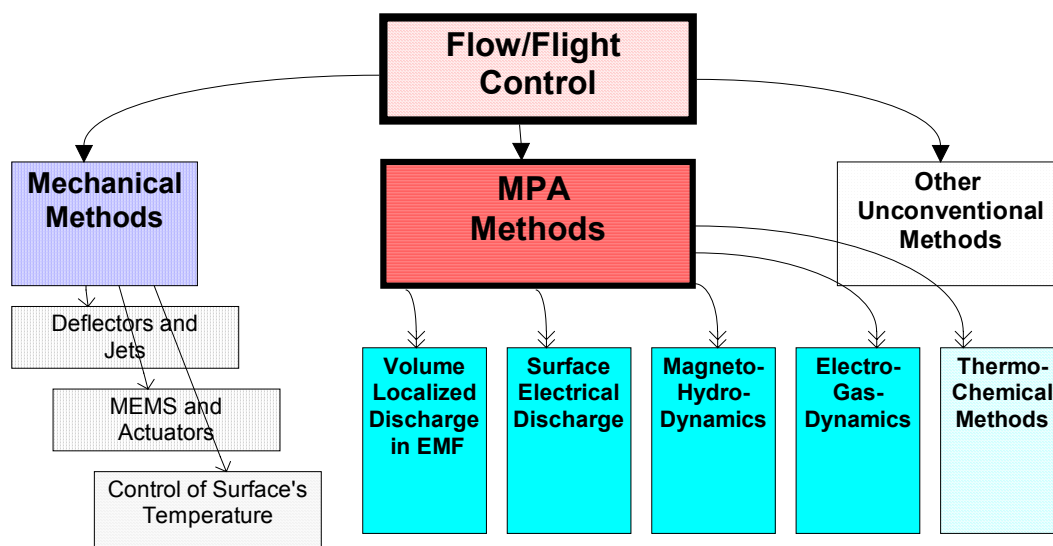


Fig.1.1. Simplified classification of plasma methods of FFC.

Typically, in-flow generated plasma appears as nonequilibrium, non-uniform and unsteady formation. The experiments related to the filamentary discharge influence on the

drag of a supersonic streamlined body were reported in paper [18]. At 1998 two types of single-electrode HF discharges and its combination were observed: quasi-homogeneous mode and filamentary one. The first mode occurred at 100Torr and lower of static pressure when the discharge appeared as a diffuse glow around the needle protruding from the nose tip. At higher pressures, plasma filaments (streamers) from the nose-tip are observed by shadow photo as well as from self-emission. A visible influence of such HF filaments on SW appearance (structure) and parameters of airflow were considered. The experiments devoted to a surface plasma effect on boundary layer parameters have been conducted at the three last years [14-18, 20-27]. They have shown that the plasma influences on processes of airflow-surface interaction are significant. A main problem within this field is to ensure enough frequent occupation of the interaction volume by the plasma formations. It can be reduced to the problem of multi-filamentary mode of the discharge generation. Well known that in the most cases the specific plasma instability takes place: a presence of one plasma object prevents the next one by means of mechanism of electrical field redistribution. At high frequency or short-pulses types of plasma excitation the multi-streamer mode can be realized under the conditions of high-speed flow. At the same time we still have no an evidence of multi-filamentary discharge generation between electrodes pair.

Speaking about duct-driven flow modification a special interest in surface plasma generation is arisen due to its possibility to provide the energy deposition and gas property modifications at a pre-defined zone of the flow-field, prospectively, under the effective electronic control of plasma location. Typically, in-flow generated plasma appears as a non-uniform and unsteady formation. At some important cases unsteady plasma manipulation can give a large benefit in power consumption. The idea of plasma strong non-uniformity in space structure, non-equilibrium composition and unsteady temporal behavior gives chance to decrease needed energy deposition down to reasonable level at quite sufficient effect.

Close problems are typical at attempts of plasma applications in a field of internal flows and combustion. The technique of the surface located discharges in high-speed flow renders the flow structure modification possible. The ability of the plasma layer to decrease losses by friction and damping of spatial and temporal instabilities in flow is prospective as an element of ducts design. The experimental evidences on shocks generation, instabilities dumping and artificial separation are published in [14-18]. Important practical consequences of the effect of plasma-induced artificial unsteady separation are discussed in this report (see section 2.2).

Last several years the interest grows in boundary layer modification by means of plasma actuators application [8-12, 22-24]. In those publications the plasma affects on flow-field through directed electrostatic forces. It was shown many times that the electrostatic bulk forces may be effective at low velocity or low density of the gas (see section 1.2). This work demonstrates a valuable electrostatic effect in transonic mode for specific gasdynamic conditions. It occurs due to a weak DBD influence amplified by periodic (quasi-resonant) forcing (see section 2.3). At the same time a main conclusion is done that the EHD interaction is too delicate for the conditions of high-speed gasdynamic.

CFD efforts were fulfilled to explain some features of the interaction in plasma-flow system (see section 2.4). The surface discharge effect on supersonic airflow was simulated on the base of Euler and Navier-Stocks equations. It is noted that simplified models did not give satisfactory agreement with experimental data. The periodic DBD discharge influence on BL properties was simulated on the base of EHD approach. Important predictions were done on the magnitude of BL modification.

In accordance with the ideas above the project, as a whole, was focused on two problems: generation of the near-surface controllable discharge in a proper operation mode and study of such a discharge influence on parameters of viscous friction between the solid surface and airflow [25-27]. The work performed under this intention will result in to obtain new data about interaction in an airflow-plasma system. This "Report" describes the experimental results in plasma generation and study of plasma effect on near-surface gasdynamic processes. This Report is comprehensive in frames of the three-years period of the Project #2084p activity.

References to Section 1.1.

1. G. G. Chernyi, The impact of electromagnetic energy addition to air near the flying body on its aerodynamic characteristics. 2-nd WIG Workshop, proceeding, Norfolk, VA, April 24-25, 1998. // G. Chernyi "Energy release effect in areas of electric discharge near bodies in airflow." Eight All-Russian Congress on Theoretical and Applied Mechanics, August 23-29, 2001 / Perm, Russia, p.594.
2. V.Bityurin, A.Klimov, S.Leonov "Assessment of a Concept of Advanced Flow/Flight Control for Hypersonic Flights in Atmosphere." 3rd Workshop on WIG. November 1-5, 1999 / Norfolk, Virginia, AIAA 99-4820.

3. T. Cain, D. Boyd "Electrodynamics and the effect of an electric discharge on cone/cylinder drag at Mach 5", 37th AIAA Aerospace Sciences Meeting and Exhibit, January 11-14, 1999/Reno, NV, AIAA 99-0602.
4. Poggie, J. and Gaitonde, D., "Simulation of Magnetogasdynamic Flow Control Techniques", AIAA Paper 2000-2326, 2000.
5. Kazakov A., Kogan M., Kuriachi A., Influence on the friction of local heat addition to the turbulent boundary layer. Mech. Of Fluids and Gases, N1, 1997.
6. Kurjachi A. P., Boundary layer transition by means of electrodynamics method. Prikl. Math. I Mech., vol.49, issue 1,1985.
7. A.V. Kazakov, A.P. Kuryachii, Electrogasdynamic influence on the development of the small disturbances in a boundary layer in the thin profile Izv. AN USSR, Mekhanika zhidkosti i gaza, 1, 1986.
8. J. R. Roth, H. Sin, R. Chandra, M. Madhan, S. P. Wilkinson "Flow re-attachmenr and acceleration by paraelectric and peristaltic EHD effects", 41th AIAA Aerospace Meeting and Exhibit, 6-10 January, Reno, NV, 2003.
9. Roth J. R., Sherman D. M. and Wilkinson S. P. "Electrohydrodynamic Flow Control with a Glow Discharge Surface Plasma" *AIAA Journal*, Vol. 38, No. 7, July 2000, pp 1166-1172.
10. S. Khabiry, G. Colver, "Drag reduction by DC corona discharge along an electrically conductive flat plate for small Reynolds number flow", Phys. Fluids, 9 (3), March 1997, p. 587-599.
11. Yu.V. Shcherbakov, N.S. Ivanov, and others, Drag Reduction by AC Streamer Corona Discharges along a Wing-like profile Plate. AIAA Paper 2000-2670.
12. M. Post, T. Corke "Separation control on high angle of attack airfoil using plasma actuators", AIAA Paper 2003-1024, 41th AIAA Aerospace Meeting and Exhibit, 6-10 January, Reno, NV, 2003.
13. Bityurin V.A., Gubertov A.M., Ivanov V.A., Kuranov M.L., Okunev V.I. MHD Control Estimation of Supersonic Boundary Layer. // Twelfth International Conference on Magnetohydrodynamic Electrical Power Generation, Yokohama, Japan, October 15-18, 1996, vol.12 p.618.
14. S. Leonov, V. Bityurin, K. Savelkin, D. Yarantsev "The Features of Electro-Discharge Plasma Control of High-Speed Gas Flows." AIAA-2002-2180, 33-th Plasmadynamic and Laser Conference, 20-24 May, 2002, Maui, HI.

15. S. Leonov, V. Bityurin, A. Klimov "Effectiveness of Plasma Method of Flow/Flight Control." Proceedings of the Symposium on Thermal-Chemical Processes, St-Petersburg, "Leninets", July, 2002.
16. S. Leonov, V. Bityurin, K. Savelkin, D. Yarantsev "Effect of Electrical Discharge on Separation Processes and Shocks Position in Supersonic Airflow." 40th AIAA Aerospace Sciences Meeting & Exhibit, 13-17 January 2002 / Reno, NV, AIAA 2002-0355.
17. S. Leonov, V. Bityurin, N. Savischenko, A. Yuriev, "Study of Surface Electrical Discharge Influence on Friction of Plate in Transonic Airflow". AIAA-2001-0640, 39th AIAA Aerospace Meeting and Exhibit, 8-11 January, Reno, NV, 2001.
18. S. Leonov, V. Bityurin, A. Klimov, Yu. Kolesnichenko, A. Yuriev "Influence of Structural Electric Discharges on Parameters of Streamlined Bodies in Airflow." 32th AIAA Plasmadynamics and Lasers Conference and 4th Weakly Ionized Gases Workshop 11-14 June 2001 / Anaheim, CA, AIAA-2001-3057.
19. S. Macheret, M. Schneider, R. Miles "Nonequilibrium Magnetohydrodynamic Control of Turbojet and Ram/Scramjet Inlets", AIAA-2002-2251, 33th Plasmadynamic and Laser Conference, 20-24 May, 2002, Maui, HI.
20. S. Leonov, V. Bityurin, A. Bocharov, E. Gubanov, Yu. Kolesnichenko, K. Savelkin, A. Yuriev, N. Savischenko "Discharge plasma influence on flow characteristics near wall step in a high-speed duct." The 3rd Workshop on Magneto-Plasma Aerodynamics in Aerospace Applications, Proceedings, Moscow, IVTAN, 24-26 April, 2001.
21. S. Leonov, V. Bityurin, K. Savelkin, D. Yarantsev D. VanWie "Hydrocarbon Fuel Ignition in Separation Zone of High Speed Duct by Discharge Plasma." The 4th Workshop on Magneto-Plasma Aerodynamics in Aerospace Applications, Proceedings, Moscow, IVTAN, April, 2002.
22. S. Leonov, V. Bityurin, D. Yarantsev "The Effect of Plasma-Induced Separation", AIAA-2003-3853, 34th Plasmadynamic and Laser Conference, 23-26 June 2003 / Orlando, FL.
23. S. Leonov, V. Bityurin, K. Savelkin, D. Yarantsev "Progress in Investigation for Plasma Control of Duct-Driven Flows." AIAA-2003-0699 41th AIAA Aerospace Meeting and Exhibit, 6-10 January, Reno, NV, 2003.
24. S. Leonov, K. Savelkin, D. Yarantsev, A. Yuriev "Supersonic Gas Flow Control by Electrical Discharges" International Scientific Conference "High-Speed Flow: Fundamental Problems", Zhukovsky, 21-24 September 2004.

25. S. Leonov “Study of Structural Plasma Influence on the Characteristics of Viscous Friction and Separated Near-Surface Zone Position under High-Speed Airflow.” The first year Report, Delivery 4, IVTAN-EOARD-ISTC Project 2084P, October 2002.
26. S. Leonov “Study of Structural Plasma Influence on the Characteristics of Viscous Friction and Separated Near-Surface Zone Position under High-Speed Airflow.” The second year Report, Delivery 8, IVTAN-EOARD-ISTC Project 2084P, October 2003.
27. S. Leonov “Influence of Surface Plasma on Characteristics of Viscous Friction and Separation Zones Location.” Final report, Delivery 4, IVTAN-EOARD-ISTC Project 1780P, April 2001.

1.2. Tasks Description.

The work under this project is aimed at study of the plasma properties in high-speed flow and plasma effect on near-surface layers. The efforts were being kept on three-year period of time. It contained two separate tasks, which are related to a one distinct idea. The tasks are listed below.

Task 1. **Investigations of multi-filament plasma generation process.**

- 1.1. Design of experimental setup and electrode configuration.
- 1.2. Design of resonant distributive electrode configuration.
- 1.3. Experiments with multi-streamer HF plasma generator.
- 1.4. Measurements/estimations of plasma parameters.
- 1.5. Design of combined HF-HV plasma generator.
- 1.6. Design of plasma filament generator with laser or UV pre-ionization.
- 1.7. Experiments on control of plasma filament propagation. Structural evolution of plasma filaments at interaction with airflow.
- 1.8. Measurements of DBD plasma parameters.
- 1.9. Design of DBD generator electrode configuration and power supply.
- 1.10. Test of surface plasma generation in high-speed flow.
- 1.11. Adjustment of plasma characteristics for high-speed test.
- 1.12. Analysis of available data. Final Report issuing.

Task 2. **Application of a multi-streamer mode of the plasma generator for a viscous friction reduction.**

- 2.1. Design and preparation of multi-streamer HF generator for experiment on plasma control of the viscous friction.
- 2.2. Short time wind tunnel's runs. Measurements of plasma effect on the viscous friction at transonic airflow.
- 2.3. Analyses of data. Preparation of the First-Year Report.
- 2.4. Design and preparation of controlled plasma filamentary HF generator for experiment on plasma control of the viscous friction and separation zones location.
- 2.5. Short time wind tunnel's runs. Measurements of plasma effect on the viscous friction at transonic and subsonic airflow.
- 2.6. Analyses of data. Preparation of the Second-Year Report.

- 2.7. Preparation of Wind Tunnel experiment on separation zone control. Modification of profiled AD model and other parts.
- 2.8. Wind tunnel's runs. Measurements of plasma effect on separation zone location.
- 2.9. Analysis of experimental data. Preparation of the Final Report.

As it can be considered under the tasks observation, the first year efforts were directed on the experimental apparatus development as well as study of the filamentary plasma interaction with high-speed airflow.

In the second year the work were devoted to multi-filamentary plasma generation and study of such a discharge effects in near-surface layers under high-speed subsonic, supersonic and transonic flow.

The third year work was fulfilled for the DBD plasma panel technique development and the experimental study of surface plasma effect on stabilization of separation line and control of the position of the separation line under high-speed flow.

Short description of the main results on each year of the Project is given in the Section 1.4.

1.3. Background.

1.3.1. Aerodynamic Sequences at Near-Surface Plasma Generation.

In a general case a drag force of the flying vehicle is represented as a sum of two components: pressure drag and friction drag. The first one contains a forebody drag (wave, mainly, at $M > 1$), and base drag. The contributions of each of the components to the total drag on subsonic, transonic and supersonic flight modes are different. On supersonic and hypersonic modes the wave drag is 60 % and more of the total value. For modern long-distance airplanes at Mach numbers $M = 0.7 - 0.9$ the friction drag value is approximately 60% of the total drag value (and fuselage is 30%, and wing friction drag is 20-25%). Well-known statement is that energy release to airflow near/fore streamlined bodies can reduce a total drag of these bodies. Sometimes it occurs at high level of energetic efficiency [1-7]. At most cases the attention is directed to pressure and/or wave shares of total drag. Several important works were devoted to air friction reduction by mechanical and electrical methods [8-16]. Last time the interest to a near-surface layers control increases significantly [17, 18].

Now we will try to analysis of the possible plasma effect in three separate domains:

- Near-surface heat release;
- Electric dipole bulk forces excitation (electro-hydrodynamic);
- Volume forces on electric current in magnetic field (MHD control of BL).

Traditional methods of viscous friction reduction are based on a directed mechanical influence on airflow near-body surface, actually, it is a control of laminar and turbulent boundary layer. Such control can occur by means of two ways: change of velocity vector of an external airflow or/and properties and temperature of the surface. An energetic method of boundary layer control (volume energy release to gas near surface by means of electrical discharge, for instance) leads to non-trivial response. Papers of different authors show that a lot of different factors defines a behavior and conditions of a boundary layer. Namely, these are three main groups:

- parameters and conditions of outer non-viscous flow;
- parameters of a gas and flow inside boundary layer;
- parameters and conditions of wall itself.

Well known that the position of laminar-turbulent transition of the boundary layer can be changed by means of cooling or heating of the surface or heat deposition directly to gas inside of boundary layer [19-21]. The viscous friction in laminar BL is much less than in turbulent one. The problem is that the BL is laminar on a small part of the surface at the practical implementation. Thus the more important thing is to reduce turbulent friction or “re-laminarize” the BL.

At volume type of energy deposition in boundary layer the gas is “hot” not only near a point of heating but in region below due to airflow (independently on velocity of outer flow). Below the point (line) of energy input there is a heated boundary layer and relatively “cold” wall. In this case a BL is stabilized due to more full profile of it. A gas temperature in BL is changed slower along streamlines due to recombination processes. Thus a local Reynolds number changes slower also.

The best place for a plasma formation (heat release) is area with maximal mechanical energy losses, namely: area of critical point and line of reconnection after flow separation, fore part of plates and profiles and areas of shock waves interaction with BL. A laminar-turbulent transition removes below. In case of flow separation due to interaction of BL with SW on a profile, plasma formation prevented a separation process. Generally, volume type of energy input into the BL effects on external non-viscous flow.

At high level of input energy and thin BL (high power density) a gas density in BL could occur so low, that mode of flow passes continuous to transitional or free-molecular one. Knudsen number in this case can be less than 1. For example, at altitude 20-30km and gas temperature 3000-10000K Knudsen number will be in range $Kn=0.02-0.1$. Plasma influence in such places is just unpredictable.

A character of plasma thermal effect depends on specific model of interaction between discharge and gas flow. Two different modes: “streamlining” and “flowing through” can be released [22]. Really both mechanisms take place in a different proportion. In the first case an influence on external flow is more than in second one. Speed of flow is important at description of specific mechanism of interaction. At location of such discharge in a special geometrical configuration there is possible to provide a frictionless flow around a body. In second case an energy release or plasma formation influences more on a boundary layer itself, in particular, leads to increase of a kinetic energy of gas.

There is a strong correlation between the factors, influencing the aerodynamic drag components [23-28]. Therefore an attempt of changing of one component results in changing

of others and this change can have both identical and opposite signs. For example, friction coefficient reduction in front of the base shear results in base rarefaction increase and, as a consequence, in base drag increase.

The existing ways of friction drag reduction are based on a directed influence upon airflow near the surface and in fact are the ways of control laminar and turbulent boundary layers. Under the flow laminar mode the friction drag is ten times less than the one under the turbulent mode. Therefore preservation of a gas flow laminar mode in a boundary layer permitting in separate cases make the drag friction 90% less underlies a way called "laminarization of a boundary layer". As is well known, the laminarization can be reached by means of a surface shape selection, by the suction of small gas portions through the permeable skin, by utilization of elastic-damping coverings and influence of MHD effect on transition from a laminar flow mode to a turbulent one.

Considering this or another way of friction drag reduction it should be kept in mind that a laminar boundary layer is more predisposed to a separation than a turbulent one. Therefore an influence on a boundary layer in order to reduce friction drag raises the possibility of its separation that can result in the appearance of non-computational (calculated) modes. If these modes result in more negative consequences than the friction increase it is necessary to take measures for separation preventing. Such measures can be body surface shape change or boundary layer turbulization by application of mechanical vortex generators with a various design and surface arrangement. The opposite case is possible as well - for example, boundary layer turbulization in order to separation shift at "thick" low-streamlined bodies (an orb) and at "thin" bodies (wing profiles). In the first case, providing base drag reduction with friction drag increase due to turbulization we obtain reduction of total drag. In the second - the friction drag increase value exceeds the base component reduction value what results in the total drag growth.

It should be noted that methods of friction drag reduction considered are based on either removal of high-entropy gas layers at the wall (suction), or additional mechanical energy transfer to these layers (mobile walls, tangential ejection, mixing intensification with upper layers of a boundary layer etc.).

Other well-known ways of friction drag reduction use wall heating or wall cooling, as the wall temperature change influences a lot both the drag value itself under this or that flow mode and laminar-turbulent transition, i.e. the critical Reynolds number value. It is known that heat supply from a wall to a boundary layer decreases velocity gradient increasing the

layer thickness that results in reduction of friction stress. The physical explanation is that the relative wall temperature increases with Mach number at the thermal insulating surface grows. As a result the boundary layer thickness increases, the velocity profiles completeness decreases, and the laminar boundary layer becomes less steady. As it could be seen well-known methods are based for the particular body on the influence on a boundary layer using as a rule the wall condition change.

Recently in search of new economic and simply realized methods of boundary layer control the possibility of control by means of gas property and gas state changes in a boundary layer itself and in an external non-viscous flow is considered. This direction is connected to the development of power methods of streamlining control based on energy supply to a flow streamlined body. Though the theoretical and experimental researches carried out within the framework of this direction are mainly devoted to the wave drag reduction, the results of some of them demonstrate the possibility of influence on a boundary layer as well.

A value of friction tension depends on Mach number of non-viscous flow and longitudinal gradient of velocity strongly. From the other side a degree of initial turbulence essential influences on a boundary layer instability development. It effects on laminar-turbulent transition point, i.e. on a critical value of Reynolds number.

Roughness of a streamlined body wall exerts a similar influence as a degree of initial turbulence. At turbulent mode the roughness of a wall defines a friction tension. Besides, a curvature of the wall (influence of centrifugal forces), permeability of surface (blowing out, sucking of a gas through the wall, erosion of wall substance...), flexibility, relative temperature of the wall, catalytic ability of a wall surface influence on a friction drag and a separation point. Two last factors are rather important for a high temperature, chemical active layers. Recombination will do on a different way in dependence on relation between a wall temperature and stagnation temperature of flow. It directly influences on a value of thermal load on a wall and on viscous tension. The plasma deposition to boundary layer can lead to significant decrease of the turbulence magnitude due to the mechanism of effective ballooning of the boundary layer (surface roughness occurs relatively less). A catalytic ability of the surface also effects on processes inside of boundary layer.

Besides of factors in outer airflow and conditions on a wall, role of gas properties inside of boundary layer is important as well as thermal and chemical processes [29]. They are viscosity, heat transfer, diffusion, character and intensity of direct and inverse chemical reactions, rate of them and relative rates of relaxation processes.

At mathematical simulation of boundary layer problem on continuation there was defined that initial data on left edge effect on BL development below in flow. At the same time they (initial condition) depend on formation processes of BL. An essential difference exists in initial state of turbulent BL in case of development at reconnection after laminar separation or in case of laminar-turbulent transition. The similar difference might be at formation of BL in critical point of blunted bodies in supersonic airflow in dependence on condition in points of reconnection on bodies with nose needles. A further development of BL depends on type of transition or initial conditions. At any cases (on profiled bodies and plane plate) viscous tension has a maximal value in places of BL occurring. It shows that namely in such places losses of mechanical energy are maximal. So a parameter, which presents ratio a thickness of energy losses via thickness of impulse losses, has a significant importance. Seems that namely on this reason a gas blowing out near fore part is the most effective. Moreover, heating of simple plate near fore edge decreases a friction drag and leads to stabilization of laminar boundary layer (in contradiction with general conception).

As a sample of thermal approach the paper [30] can be pointed where the experimental work was accompanied with proper CFD simulations.

Thermal methods of boundary layer stability control.

In a Kogan's group works [9-10] the possibility of laminar boundary layer stabilization by means of plate heating at a leading edge was studied. It is shown that the heating increases stability of a laminar boundary layer. The result is interesting especially as usually such effect results in wall cooling because of known reasons. Electro-gasdynamics influence on the development of the small disturbances in a boundary layer at the plate and in the thin profile was considered. Here the unipolarly charged ionic jet spreads along a surface. The system of electrodes used for an ionic jet in glow discharge generation was simulated by two semi-infinite gauze electrodes (not causing a flow disturbances) installed in a profile perpendicular to a running flow and by one electrode inside a profile in its tip. It was shown that at the electro-gasdynamics streamlining Reynolds number of a boundary layer transition could increase up to 13% for a plane plate and up to 8-11% for a thin profile.

The influence of the heating or cooling surface on the laminar boundary layer stability characteristics was considered in theoretical and experimental works in which the stability self-similar boundary layers at constant surface temperature were studied [27, 33]. At subsonic speeds the surface cooling leads to improving of the boundary layer stability and

increasing the laminar part of the boundary layer. In one's turn, the surface heating leads to significant flow destabilization and more early transition to turbulent regime. However, if the streamlined surface is heated non-uniformly, one can obtain perfectly opposite results. In studies [34-35] on the base of numerical solution of linear stability problem it was first shown, that the local surface heating of the flat plate near its leading edge can lead to boundary layer stabilization and laminar region extension.

At the same time, the studies of the possibility of boundary layer flow control by the local surface heating at the some distance from the body leading edge have been carried out [36-38]. It has been shown that the periodic temperature variation of the small surface region can induce the disturbances like the Tollmien-Schlichting waves. Depending on the phase of the oscillations one can obtain the intensification or cancellation of the disturbances [39]. These studies are the expansion of the previous ideas and investigation carried out in [40], where the active control ideas have been considered for the first time. However, the possibility of the laminar-turbulent transition control was not considered in these works because the influence of the induced disturbances on the transition has not been shown.

It is known that unfavorable pressure gradient destabilizes the boundary layer and leads usually to the earlier laminar-turbulent transition. Nevertheless, it was shown that local surface heating near the thin airfoil leading edge can provide the significant laminar region extension including the region with adverse pressure gradient [41].

In [42-44] it was shown that not only the surface heating but also the volume energy supply can lead to the significant flow stabilization. One of the distinguishing feature of the laminarization on the nonisothermal surface is the essential boundary layer destabilization inside the surface heating region. This local destabilization can effect on the laminar-turbulent transition appearance in this region if the disturbance growth will be sufficiently large [45].

The investigation of the influence of the temperature gradient along the wall surface on the boundary layer stability has been carried out. The importance of the size of the surface heating region for an achievement a positive effect of transition delay has been shown [46]. At the same time the experimental studies have been carried out [47-49, 58] in which the propositions of the theoretical considerations have been confirmed. It should be noted the works concerning the search of the optimal methods of the surface heating when the surface behind the heating region is considered as heat-insulated one, because in usual situation the surface cooling is required for a maintenance of necessary temperature [50-52].

On the body streamlined with nonzero sweep angle the situation becomes more complicated because of an appearance of the cross flow and another type of the instability – cross-flow instability. On the swept wing namely the growth of these disturbances leads to laminar-turbulent transition. Another type of the instability peculiar to the boundary layer on the swept wing is the instability of the attachment line boundary layer. This instability can be the initial reason of the boundary layer turbulization from the leading edge of the wing. Therefore the investigation of the influence of local surface heating on the stability of the attachment line boundary layer is one of the important problem of the thermal methods usage. Earlier this problem was studied on the base of inviscid fluid model [53-54].

In [55] the influence of the compressibility and surface temperature on the attachment line boundary layer stability was considered on the base of linear stability calculations for viscous heat-conductive gas flow. It was shown that at subsonic speeds the Mach number and the surface temperature influence on the disturbance growth and critical Reynolds number of the attachment line boundary layer. It was shown also that the temperature increase leads to the decrease of the critical Reynolds number and the increase of the increment of disturbance growth.

At supersonic speeds for the swept wing with supersonic edges the surface temperature influence on the stability characteristics is more complicated because of different influence of the surface temperature on the various instability modes [56-57]. It was shown that the heating and the volume energy supply can increase the stability of the attachment line boundary layer in some temperature range [57].

Electrodynamic effects in BL.

The next domain of the plasma effect becomes apparent due to electrostatic (dipole) forces. Recently considerable attention has been given to the study of the possibility of controlling weakly ionized gas flows by means of the electrodynamic (EGD) interaction [59]. This method is based on the acceleration of the ions in an electric field and transfer of the momentum to neutral molecules during ion-molecule collisions. Appreciable electrostatic forces can arise in flows with unipolar space charge in the presence of a fairly strong applied electric field [60]. The corona discharge is one of the most convenient methods of producing such conditions for practical applications.

In the usual corona air discharge the space charge density is small (of the order of 10^{-4} C/m³) and the mean electric field strength in the discharge gap is not greater than breakdown

value (of the order $3 \cdot 10^6$ V/m for air). In case of homogeneous distribution of medium parameters we could compare the gas-kinetic power density of the gas $W_g = 1/2 \rho V^2$ with electrical power density $W_e = 1/2 \epsilon E^2$, where E is self-consistent electrical field. For the atmospheric conditions and close to breakdown field the resulted velocity is not more than $V=10$ m/s. Therefore, for typical flow velocities of the order of 100 m/s the electric terms in the momentum and energy equations (the volume Coulomb force and Joule dissipation respectively) are small as compared with convective terms. As they say in [59], "if there is to be a practical application, a mechanism is required to greatly amplify the small perturbations that are possible. The boundary layer is one region within a flowfield where small disturbances can lead to significant modification of aerodynamic forces either by moving the laminar/turbulent transition or by forcing/delaying boundary layer separation".

Under the conditions of boundary layer and strong non-homogeneity of the medium parameters the mechanisms of charge separation and thermal electromotive force generation should be taking into account. The first effect can be realized due to strong transversal gradient of gas velocity; the second occurs due to temperature gradients: $E_{tg} = \frac{1}{e} \times grad(kT_e)$.

The electrostatic forces are small compared to the total momentum in flow at high speed. An electrostatic effect could be realized under low-speed conditions or in distances compared with Debay radius:

$$R_D = \sqrt{kT_e / (4\pi e^2 n_e)} \approx 700 \sqrt{T_e (eV) / n_e (cm^{-3})} (cm), .$$

For typical conditions of one-atmospheric discharge, where $T_e \approx 1$ eV and $n_e > 10^{10} cm^{-3}$, the Debay radius is less than 0.1 mm. Actually, the Debay radius is a small parameter in the most practical aerodynamic applications. It means that the electrostatic forces can be realized only in BL conditions or under low pressure.

The idea of plasma strong non-uniformity in space structure, non-equilibrium composition and unsteady temporal behavior gives chance to get a quite sufficient effect in flow-field structure under high-speed flows. The characteristic parameters of impact in this case could be estimated roughly on the following manner. A thickness of boundary layer under the aerodynamic conditions is in a range $\delta \approx 1$ mm. To achieve large electrical field strength gradient the inter-electrodes gap has to be about $d \approx 1$ mm. Such a distance can be related to frequency of excited electrical power. If the characteristic flow velocity $V=100$ m/s the frequency of electrical field alteration has to be in range $f=100$ kHz. By the other words a big

velocity of flow required large frequency of electric field to expect a visible aerodynamic effect.

Boundary layer separation control and direct drag reduction methods.

The first experimental researches of boundary layer separation control by near surface corona discharge have been carried out in Kiev Institute of Civil Aviation Engineering [15, 61, 62]. The flow acceleration in an alternating-current (at a frequency up to 570 Hz) corona discharge directed along a flow made it possible to obtain a maximum induced velocity up to 5m/s in these experiments, and the separation on an airfoil with deflected flap has been removed at low free-stream velocity (of the order of 20m/s).

In recent years, a near surface HF capacity discharge technique has been applied for boundary layer separation control in University of Tennessee [13, 63] and in BAe [64]. These experiments showed, in particular, that the surface plasma produced by streamwise electrodes results in streamwise vortices generation and an increase the skin friction. On the other hand, an energizing the boundary layer due to streamwise vortices, similarly to direct its acceleration in the case of asymmetric staggered spanwise electrodes, can lead to separation delay.

A possibility of total drag reduction (a sum of skin friction and electrostatic reaction of streamlined surface) of the conductive flat plate on the basis of a creation of the “ion wind” thrust due to laminar boundary layer acceleration by the near surface DC corona discharge has been considered theoretically in [65]. But the effect of total drag reduction in this case is too small for practical application. Experimental research of DC corona discharge near a streamlined dielectric wall has been carried out in [66] where the “ion wind” velocity up to 7 m/s has been achieved at atmospheric condition.

The “ion wind” technique has been applied for direct skin friction reduction in situation when the electrostatic forces are mainly directed along the normal to the surface and force back the boundary layer flow in the neighborhood of the surface thereby providing a “blowing” effect (converting the tangential velocity into normal one) with no net mass transfer through the wall [67]. A remarkable drag reduction has been observed on a flat plate in turbulent boundary layer at free-stream velocities less than 10 m/s.

However, the reduction in friction obtained by initiating an “ion wind” along the normal to the surface is very inefficient with respect to the power expended. The ratio of the gain in mechanical power due to drag reduction to the electric power of the corona discharge is of the order of 0,01 [67]. This low energy efficiency is associated with the fact that the

discharge power is expended on producing additional normal momentum not only in the neighborhood of the surface but also in the outer inviscid region, where this action no longer has any effect in reduction the surface friction.

Laminar-turbulent transition control due to EGD interaction. The level of the corona induced velocity achieved, particularly, in [66] can be sufficient to change such sensitive characteristic of laminar boundary layer as its stability. Previous theoretical estimations [10, 68] have shown that EGD acceleration of laminar boundary layer leads to a deceleration of partial growth of the Tollmien-Schlichting type disturbances and, as a consequence, to a laminar-turbulent transition delay. A relative increase of laminar part of boundary layer has achieved 13% on a flat plate [10] and 8-11% on thin airfoils [68] in these estimations.

It has been shown theoretically in [69] that the remarkable total drag reduction can be obtained as a result of the laminar-turbulent transition delay due to boundary layer acceleration by the DC corona and that this method of drag reduction can be energy beneficial. The unipolar region of the DC corona discharge near a dielectric flat plate in air flow has been simulated in [69] by a linear ion source of intensity $I = 2 \cdot 10^{-5}$ A/m located on the plate surface at a distance l from the leading edge. There is a uniform electric field of strength $E_0 = 10^6$ V/m directed along the free-stream velocity. The Reynolds number corresponding to the ion source location has been defined as $Re = \rho_\infty u_\infty l / \mu_\infty = 10^6$ for the free-stream velocity $u_\infty = 30$ m/s. The numerical solution of the equation system of electrohydrodynamics has been obtained. Over the investigated range of variation of the local Reynolds number the maximum velocity induced behind the ion source u_{im} was not much more than 3% of free-stream velocity, i.e., $u_{im} \approx 1$ m/s for the above mentioned value of u_∞ . This appreciably lower than the value of u_{im} reached experimentally [66]. This indicates that the task parameters for which the calculations were carried out are not the maximum attainable ones when a corona discharge is used for acting on a boundary layer.

The linear stability problem has been solved numerically and laminar-turbulent transition location has been defined by the usage of the well known e^N -method. The transition Reynolds number $Re_{tr0} = 1.76 \cdot 10^6$ and $Re_{tr} = 2.56 \cdot 10^6$ without and with EHD interaction has been defined for $N=10$.

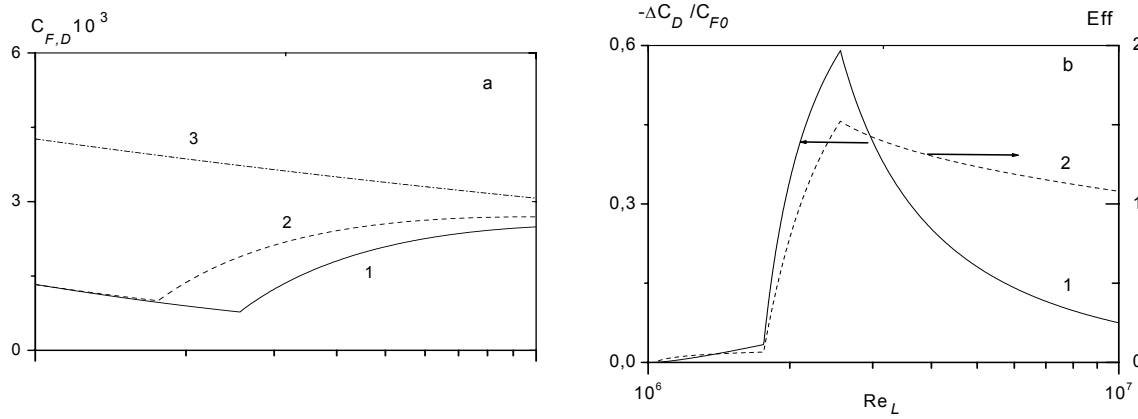


Fig.1.3.1.1. Integral friction and drag coefficients (a), relative reduction of total drag (b, curve 1), and efficiency criterion (b, curve 2) as functions of plate Reynolds number.

The integral drag coefficients C_D are plotted in Fig.1.3.1.1a as a function of the plate Reynolds number $Re_L = \rho_\infty u_\infty L / \mu_\infty$, where L is the plate length, with and without EHD interaction (curves 1 and 2, respectively). For comparison, the integral friction coefficient for completely turbulent boundary layer is plotted also in Fig.1.3.1.1a (curve 3). In Fig.1.3.1.1b the curves of the relative integral plate drag reduction (curve 1), and the efficiency criterion (curve 2) are reproduced. Here $\Delta C_D = C_D - C_{F0}$, C_D and C_{F0} are presented by curves 1 and 2 in Fig.1.3.1.1a, respectively.

The efficiency criterion is defined as follows: $Eff = \Delta D u_\infty / E_0 L_d I$, where ΔD is the total drag reduction, L_d is the distance from the ion source to the boundary layer cross-section considered or to the transition point if that cross-section is located downstream of this point. The space charge is assumed to relax on the plate trailing edge if the variable value of the Re_L number is lower than the transition Reynolds number. Otherwise, the charge relaxes in the cross-section corresponding to the laminar-turbulent transition point.

Clearly, for completely laminar flow on the plate the efficiency parameter Eff is significantly less than unity, i.e., the drag reduction due to “ion wind” thrust is energetically uneconomical only. At the same time, one can achieve $Eff > 1$ simultaneously with a very significant relative reduction in total drag if $Re_L > Re_{tr}$, i.e. at a presence of turbulent part of the boundary layer. Optimization of the method proposed should lead to a further increase in the efficiency.

An influence of the EGD interaction on linear stability of flows with curvilinear lines of flow has been studied in [70] for the case of flow between rotating cylinders. It has been shown that the critical Taylor number of instability rise and corresponding wave number of

vortical disturbances are highly sensitive to distributions of both radial electric field strength and volume charge density between the cylinders. One can assume that the influence of the EGD interaction on Taylor-vortices evolution can become apparent also in the case of Görtler-vortices which appear in boundary layer flow over a concave surface as a result of its instability. Another possible application of EGD action on concentrated vortex structures (the nature of this interaction is still not clear) can be associated with control of generation of so-called “streaks” in turbulent boundary layer. In this case a method of direct turbulent friction control can be developed.

The problem of MHD control of supersonic boundary layer is widely discussed in the domains of internal and external ballistics [16]. It is supposed to change pressure distribution and, consequently, balance of aerodynamics forces along surface flowing around with use of the decelerating or accelerating MHD force which able to cause a separation or reattachment of supersonic boundary layer [31]. The analysis of the turbulent boundary layer separation carried out in paper [31] has been based on the traditional approach widely used for example in paper [32] to treat separation phenomena in conventional gas dynamics. A positive pressure gradient in the flow leads to the flow deceleration in the inviscous core as well as in the boundary layer. Due to a difference between the core and boundary layer velocity (the boundary layer velocity is significantly lower) positive pressure gradient results in a much higher deceleration near the wall than in the flow core. Thus, the velocity profile becomes less filled and the friction tension $C_f = \frac{\tau_w}{\rho u_e^2}$ at the wall decreases. As we understand a main problem here is to make and to hold an enough level of gas electrical conductivity.

The last couple years the interest to the problem of electrical and electromagnetic actuators is increased significantly [71-78]. The comprehensive analysis of these efforts is still not fulfilled.

An observation of BL and recognition of the gas parameters inside of BL are difficult due to low thickness and small gradients of gas density. New informative methods are complex technically, as a rule [79, 80]. More conventional methods give limited information and have to be used together one with others [81].

References to Section 1.3.1.

1. Workshops on Weakly Ionized Gases. ##1-6, USA, 1997-2004.
2. International Workshops on Magneto-Plasma Aerodynamics in Aerospace Applications. ##1-5, IVTAN, Moscow, Russia, 1999-2004.
3. G. G. Chernyi, The impact of electromagnetic energy addition to air near the flying body on its aerodynamic characteristics. 2-nd WIG Workshop, proceeding, Norfolk, VA, April 24-25, 1998.
4. Levin V. A., Afonina N. E., Gromov V. G., Influence of Energy Input by Electric Discharge Supersonic flows around bodies. 2nd WIG Workshop, Proceedings, Norfolk, VA, April 24-25, 1998.
5. V.Bityurin, A.Klimov, S.Leonov "Assessment of a Concept of Advanced Flow/Flight Control for Hypersonic Flights in Atmosphere." 3rd Workshop on WIG. November 1-5, 1999 / Norfolk, Virginia, AIAA 99-4820.
6. T. Cain, D. Boyd "Electrodynamics and the effect of an electric discharge on cone/cylinder drag at Mach 5", 37th AIAA Aerospace Sciences Meeting and Exhibit, January 11-14, 1999/Reno, NV, AIAA 99-0602.
7. S. Leonov, V. Nebolsin, V. Shilov "Effectiveness of plasma jet Effect on Bodies in an Airflow", Proceedings of Workshop "Perspectives of MHD and Plasma Technologies in Aerospace Applications", Moscow, IVTAN, 1999, pp. 58-65.
8. D. Bushnell, C. McGinley Turbulence Control in Wall Flows, Ann. Rev. Fluid Mech., 21, 1-20, 1989.
9. Kazakov A., Kogan M., Kuriachi A., Influence on the friction of local heat addition to the turbulent boundary layer. Mech. Of Fluids and Gases, N1, 1997.
10. Kurjachi A. P., Boundary layer transition by means of electrodynamics method. Prikl. Math. I Mech.(rus), vol.49, issue 1,1985.
11. Yu.V. Shcherbakov, N.S. Ivanov, and others, Drag Reduction by AC Streamer Corona Discharges along a Wing-like profile Plate. AIAA 2000-2670.
12. A. Smith, Progress in Hypersonic Turbulent Boundary Layer Control, AIAA-2000-2322.
13. Roth J. R., Sherman D. M. and Wilkinson S. P. "Electrohydrodynamic Flow Control with a Glow Discharge Surface Plasma", AIAA Journal, Vol. 38, No. 7, July 2000, pp 1166-1172.
14. Soldati, A. and Banerjee, S. "Turbulence Modification by Large-Scale Organized Electrohydrodynamic Flows". Phys. Fluids, Vol. 10, No. 7 (1998) pp 1742-1756.

15. Mhitaryan A.M., Labinov C.D., Fridland V.Ya., "Electro-hydrodynamic method of boundary layer control", in paper collection "Some problems of aerodynamics and electro-hydrodynamics", vol.1, Kiev's Institute of Civil Aviation Engineers, Kiev, 1964.
16. Bityurin V.A., Gubertov A.M., Ivanov V.A., Kuranov M.L., Okunev V.I. MHD Control Estimation of Supersonic Boundary Layer. // Twelfth International Conference on Magnetohydrodynamic Electrical Power Generation, Yokohama, Japan, October 15-18, 1996, vol.12 p.618.
17. S. Leonov, V. Bityurin, D. Yarantsev "The Effect of Plasma-Induced Separation", AIAA-2003-3853, 34-th Plasmadynamic and Laser Conference, 23-26 June 2003 / Orlando, FL.
18. M. Post, T. Corke "Separation control on high angle of attack airfoil using plasma actuators", AIAA Paper 2003-1024, 41th AIAA Aerospace Meeting and Exhibit, 6-10 January, Reno, NV, 2003.
19. A. Kazakov, M. Kogan, V. Kuparev, "About stability of subsonic boundary layer under heating of the surface...", Izvestiay AN, Mechanics of Fluids and Gases, vol.3, 1985, p.68-75.
20. D. Bushell, "Turbulent drag reduction for external flows", AIAA paper No 227, 1983, 20pp.
21. Yu. Lapin, "Turbulent boundary layer in supersonic gas flows", Moscow: Science, 1982, 312pp.
22. Yu. Rayzer Physics of gas discharge. Moscow: Science. 1987. pp 479.
23. D. Kyukheman, Aerodynamic Planes Designing. M.: Mashinostroyeniye, 1983, p.555.
24. P. Chzhen, Separation flow. Moscow: Mir, 1973 v.3, p.14.
25. P. K. Chang., Control of Flow Separation. M.: MIR, 1979.
26. Goshek, High-speed Aerodynamics, S.: "Inostrannaya literatura", 1954
27. G. Schlichting, The theory of a boundary layer, M.: Nauka, 1974
28. A.P. Mel'nikov, I.A. Sychyov, N.F. Fillipov, Gashydrodynamics, L. p. 470, 1968
29. P. Baronets, A. Kolesnikov, S. Kubarev... Superequilibrium heating of surface in subsonic jet of dissociated air. Izvestiya RAS, MZhG (rus) 3, 1991, p.144-149.
30. S. Leonov, V. Bityurin N. Savischenko, A. Yuriev V. Gromov "Influence of Surface Electrical Discharge on Friction of Plate in Subsonic and Transonic Airflow." Paper AIAA-2001-0640.
31. Ivanov V.A. et.al "The Development of a Method of the MHD Separation Flow Calculation", Tech. Report, 95/7, IVTAN-ANRA, Moscow, 1995, 42p (in Russian).

32. Ivanov V.A., "The Method of the Flow and Head Transfer Calculation in a Nozzle under Off-Design Mode", Thesis, MPTI-NIITP, Moscow, 1985.
33. Gaponov S.A., Maslov A.A., "Development of Disturbances in Compressible Flows" (in Russian). Nauka, Novosibirsk, 1980, 144 p.
34. Kazakov A.V., Kogan M.N., Kuparev V.A., "On Subsonic Boundary Layer Stability at Surface Heating Near the Leading Edge of Flat Plate," *Fluid Dynamics*, 1985, No.3.
35. Kazakov A.V., Kogan M.N., Kuparev V.A., "On Increase of Subsonic Boundary Layer Stability Due to Surface Heating the Near Leading Edge of Streamlined Body," (in Russian) *Dokl. Akad. Nauk SSSR*, 1985, Vol. 283, No. 2.
36. Maestrello L. "Analysis of Active Control by Surface Heating," *AIAA-84-0173*, 1984, 8 p.
37. Bayliss A., Maestrello L., Prikh P., Turkel E., "Numerical Simulation of Boundary Layer Excitation by Surface Heating/Cooling," *AIAA-85-0565*, 1985, 8 p.
38. Metcalfe R.W., Rutland C., Duncan J.H., Riley J.J., "Numerical Simulations of Active Stabilization of Laminar Boundary Layers," *AIAA-85-0567*, 1985, 9 p.
39. Maestrello L., "Active Transition Fixing and Control of the Boundary Layer in Air," *AIAA Journal*, 1986, Vol. 24, No. 10, pp. 1577-1581.
40. Liepmann H.W., Nosenchuck D.M., "Active Control of Laminar-Turbulent Transition," *Journal of Fluid Mech.*, 1982, Vol. 118, pp.201-204.
41. Kazakov A.V., Kuryachii A.P., "Influence of Heating of the Thin Airfoil Surface on Laminar Boundary Layer Stability," *Fluid Dynamics*, 1986, Vol. 26, No. 5.
42. Kazakov A.V., Kogan M.N., "Stability of Subsonic Laminar Boundary Layer on a Flat Plate at Volume Energy Supply," *Fluid Dynamics*, 1988, Vol. 28, No. 2.
43. Kazakov A.V., Kogan M.N., Kuparev V.A., Kuryachii A.P., "About Off-Centre Methods of Stability Control Of Laminar Subsonic Boundary Layer" (in Russian), *Trudy TsAGI*, 1988, issue 2412.
44. Kazakov A.V., Kuparev V.A., "Boundary Layer Laminarization on a Thermally Insulated Surface with Energy Supply to the Flow," *Fluid Dynamics*, 1988, Vol. 23, No. 5.
45. Belov I.A., Litvinov V.M., Kazakov A.V., Kogan M.N., Kuparev V.A., "Laminar Boundary Layer Stability and Delayed Transition on a Nonisothermal Surface," *Fluid Dynamics*, 1989, Vol. 24, No. 2, pp.205-210.
46. Struminskii V.V., Lebedev Yu.B., Phomichev V.M., "Influence of Temperature Gradient Along a Surface on the Extension of Laminar Part of Gas Boundary Layer," (in Russian) *Dokl. Akad. Nauk SSSR*, 1986, Vol. 289, No. 4, pp. 813-816.

47. Belov I.A., Litvinov V.M., Kazakov A.V., Kuparev V.A., "Experimental Investigation of Influence of Surface Nonisothermality on Characteristics of Stability of the Flat Plate Laminar Boundary Layer," (in Russian) *Uchenii. Zapiski TsAGI*, 1989, Vol. 20, No. 3, pp. 106-110.
48. Struminskii V.V., Dovgal' A.V., Lebedev Yu.B., Levchenko V.Ya., Timofeev V.A., Phomichev V.M., "Theoretical and Experimental Research of Boundary Layer Stability at Nonuniform Surface Heating," (in Russian) *Preprint ITAM* # 3, 1987, 22 p.
49. Maestrello L., Nagabushana K.A., "Relaminarization of Turbulent Flow on a Flat Plate by Localized Surface Heating," *AIAA-89-0985*, 1989, 7 p.
50. Kazakov A.V., Kogan M.N., Kuparev V.A., "Optimization of Laminar-Turbulent Transition Delay by Means of Local Heating of the Surface," *Fluid Dynamics*, 1995, Vol. 30, No. 4, pp. 563-569.
51. Kazakov A.V., Kogan M.N., Kuparev V.A., "Delay of Laminar-Turbulent Transition by Means of Intensive Localized Heating of the Surface in the Vicinity of the Plate Leading Edge," *High Temperature*, 1996, Vol. 34, No. 1, pp. 46-51.
52. Kazakov A.V., Kogan M.N., Kuparev V.A., "Laminarization of Boundary Layer Under Condition of the Negative Pressure Gradient," *High Temperature*, 1996, Vol. 34, No. 2, pp. 244-249.
53. Poll D.I.A., "Transition in the Infinite Swept Attachment Line Boundary Layer," *Aeron. Quart.*, 1979, Vol. 30, No. 4, pp. 607-629.
54. Poll D.I.A., "Development of Intermittent Turbulence on a Swept Attachment Line Including the Effects of Compressibility," *Aeron. Quart.*, 1983, Vol. 34, No. 1, pp. 1-23.
55. Kazakov A.V., "Effect of Surface Temperature on the Stability of the Swept Attachment Line Boundary Layer," *Fluid Dynamics*, 1990, Vol. 25, No. 6, pp. 875-878.
56. Kazakov A.V., "Effect of the Surface Temperature on the Stability of the Supersonic Swept Attachment Line Boundary Layer," *Fluid Dynamics*, 1997, Vol. 32, No. 5, pp. 648-653.
57. Kazakov A.V., "Effect of Heat Supply on the Stability of the Supersonic Swept Attachment Line Boundary Layer," *Fluid Dynamics*, 1998, Vol. 33, No. 5, pp. 710-715.
58. Philippov V.M., "Influence of Heating of Plate Bow on Boundary Layer Evolution," *Fluid Dynamics*, 2002, Vol. 37, No. 1, pp. 32-42.
59. Cain T., "Progress in Plasma Aerodynamics," *DERA/WSS/WX9/CR980688/1.1*, 1998, 60p.

60. Vatazhin A.B., Grabovskii V.I., Likhter V.A., Shul'gin V.I., "Electrostatic Flows," (in Russian), Nauka, Moscow, 1983.
61. Mhitaryan A.M., Phridland V.Ya., Boyarskii G.N., Kas'yanov V.A., "Experimental Studies of an Influence of the Electrohydrodynamic Effect on Aerodynamic Characteristics of an Airfoil," in: *Some Problems of Aerodynamics and Electrohydrodynamics*, Vol.2 (in Russian), Kiev. Institute of Civil Aviation Engineering, Kiev, 1966.
62. Mhitaryan A.M., Boyarskii G.N., Kas'yanov V.A., Tishkov A.Ph., "Experimental Study of an Influence of Supply Voltage Frequency on an Effectiveness of EHD BLC," in: *Some Problems of Aerodynamics and Electrohydrodynamics*, Vol.3 (in Russian), Kiev. Institute of Civil Aviation Engineering, Kiev, 1968.
63. Roth J.R., Sherman D.M., Wilkinson S.P., "Boundary Layer Flow Control with a One Atmosphere Uniform Glow Discharge," *AIAA-98-0328*, Jan 1998.
64. Johnson G.A., Scott S.J., "Plasma-Aerodynamic Boundary Layer Interaction Studies," *AIAA-2001-3052*, 2001.
65. Khabiry S., Colver G., "Drag Reduction by DC Corona Discharge Along an Electrically Conductive Flat Plate for Small Reynolds Number Flow," *Physics of Fluids*, Vol. 9, No. 3, 1997, pp. 587-599.
66. Artana G., D'Adamo J., Leger L., Moreau E., Touchard G., "Flow Control with Electrohydrodynamic Actuators," *AIAA Journal*, Vol. 40, No.9, 2002, pp. 1773-1779.
67. Malik M.R., Weinstein L.M., Hussaini M.Y., "Ion Wind Drag Reduction," *AIAA-83-0231*, 1983, 10 p.
68. Kazakov A.V., Kuryachii A.P., "Influence of Electrostatic Impact on Evolution of Small Disturbances in the Boundary Layer on Thin Profile," *Fluid Dynamics*, Vol. 21, No.1, 1986, pp. 25-33.
69. Kazakov A.V., Kuryachii A.P., "Estimate of the Effectiveness of the Electrostatic Method for Reducing Aerodynamic Drag," *Fluid Dynamics*, Vol. 36, No. 2, 2001, pp. 236-243.
70. Kuryachii A.P., "The Stability of Couette-Taylor Electrohydrodynamic Flow," *J. Appl. Math. and Mech.*, 1989, Vol.53, part 3.
71. Kimmel R.L. "Aspects of Hypersonic Boundary-Layer Transition Control", *AIAA-2003-0772*.

72. Levin V.A., Larin O.B., “Skin-Friction Reduction by Energy Addition into a Turbulent Boundary Layer”, AIAA-2003-0036.
73. Roth J.R., Madhan R.C.,Yadav M., Rahel J., Wilkinson S.P., “Flow Field Measurements of Paraelectric, Peristaltic, and Combined Plasma Actuators Based on OAUGDP”, AIAA 2004-845.
74. Lacoste D., Pai D., Laux C., “Ion Wind Effect in a Positive DC Corona Discharge in Atmospheric Pressure Air”, AIAA 2004-0354.
75. Samimy M., Adamovich I., Webb B., Kastner J., Hileman J., Keshav S., Palm P., “Development and Application of Localized Arc Filament Plasma Actuators for Jet Flow and Noise Control”, AIAA 2004-0184.
76. Samimy M., Adamovich I., Kim J.-H.,Webb B., Keshav S., Utkin Y., “Active Control of High Speed Jets Using Localized Arc Filament Plasma Actuators”, AIAA 2004-2130.
77. Jukes T., Choi K.-S., Johnson G., Scott S., “Turbulent Boundary-Layer Control for Drag Reduction Using Surface Plasma”, AIAA 2004-2216.
78. Post M., Corke T., “Separation Control using Plasma Actuators – Dynamic Stall Control on an Oscillating Airfoil”, AIAA 2004-2517.
79. P. Wu, R. Miles, “MHz Rate Visualization of Separation Shock Wave Structure”, AIAA-2000-0647.
80. A. Yalin, W. Lempert and others, Planar imaging in a Mach 8 flow using sodium laser-induced fluorescence. AIAA-96-2270.
81. J. Naughton, M. Sheplak, Modern Skin Friction Measurement Techniques: Description, Use, and What to do With the Data. AIAA-2000-2521.

1.3.2. Methods of the Discharge Control.

One of main subjects of the investigations in frame of the task 1 is a high-frequency filamentary discharge. Similar phenomena were studied at ambient conditions (without airflow) from 50th [1-3]. The results of the latest investigations can be found in [4-7]. A special technique was used to produce directed filaments: mixture of HF and HV voltage (additional applying of high voltage to HF electrode). Investigators have named this phenomena as “HF flash”. Images of such discharges are presented in Fig.1.3.2.1a,b. We can see that they look like plasma filaments at pulse HV of HF type of excitation, including their shape and dimensions.

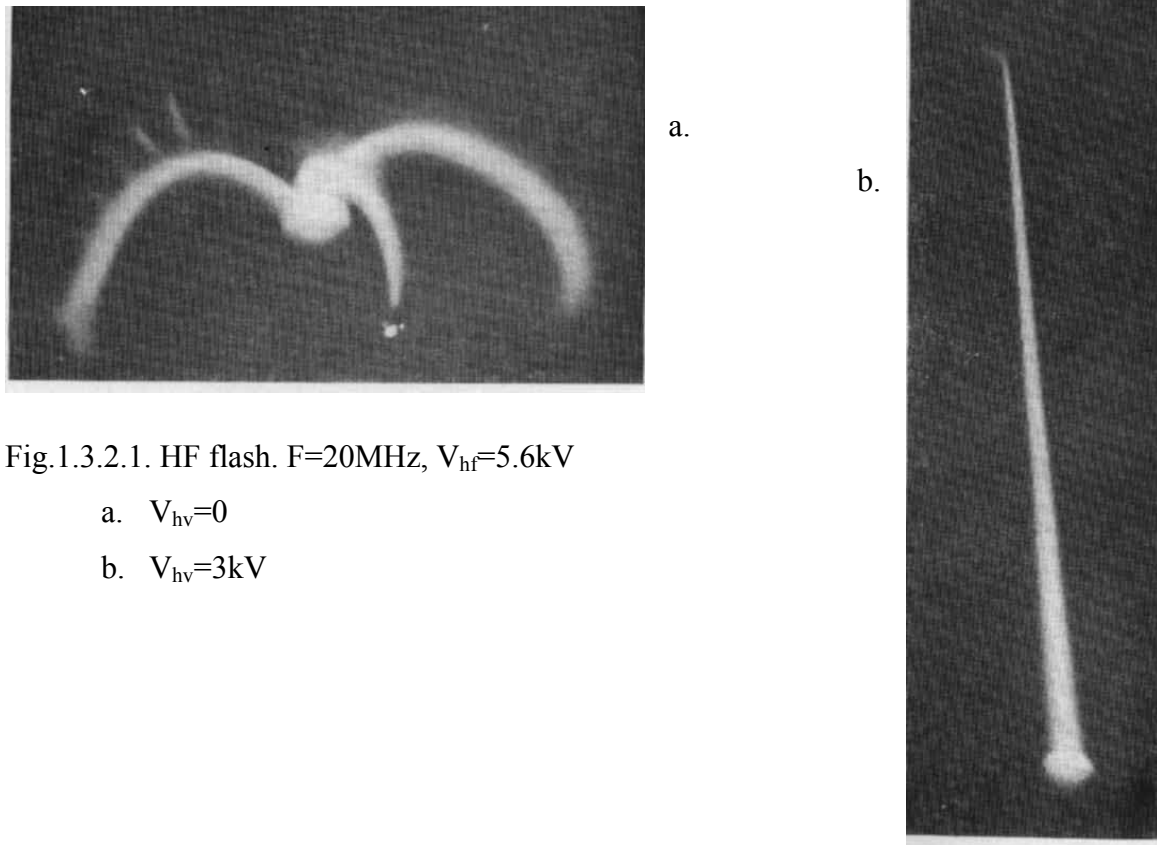


Fig.1.3.2.1. HF flash. $F=20\text{MHz}$, $V_{hf}=5.6\text{kV}$

- a. $V_{hv}=0$
- b. $V_{hv}=3\text{kV}$

In these works a systematical study of discharges appearance was done and several parameters of plasma filaments were measured. A sample of systematic diagram for a $F=10\text{MHz}$ frequency of exciting power is presented in Fig.1.3.2.2. It shows a visible shape of discharge and oscillograms of plasma luminosity in dependence on amplitudes of HF and HV voltage. The process of HF discharge channel appearance and propagation is as follows. At the positive half-period of the applied voltage a streamer is appeared at a point electrode. This streamer reserves a trace of excited and ionized gas after itself. Under the next positive half-

periods the waves of ionization and excitation are propagated along this trace. These waves can be treated as the secondary streamers. Their difference from the streamer in its classic foundation is that they propagate in previously disturbed, ionized media. The secondary streamers form a brighter main channel of the discharge, which develops with velocity sufficiently less than the first streamer. The process of HF discharge developing resembles the development of long spark. The role of leader is played by the main channel of HF discharge and the streamers in the vicinity of the main channel form the streamer zone, as in the case of long spark.

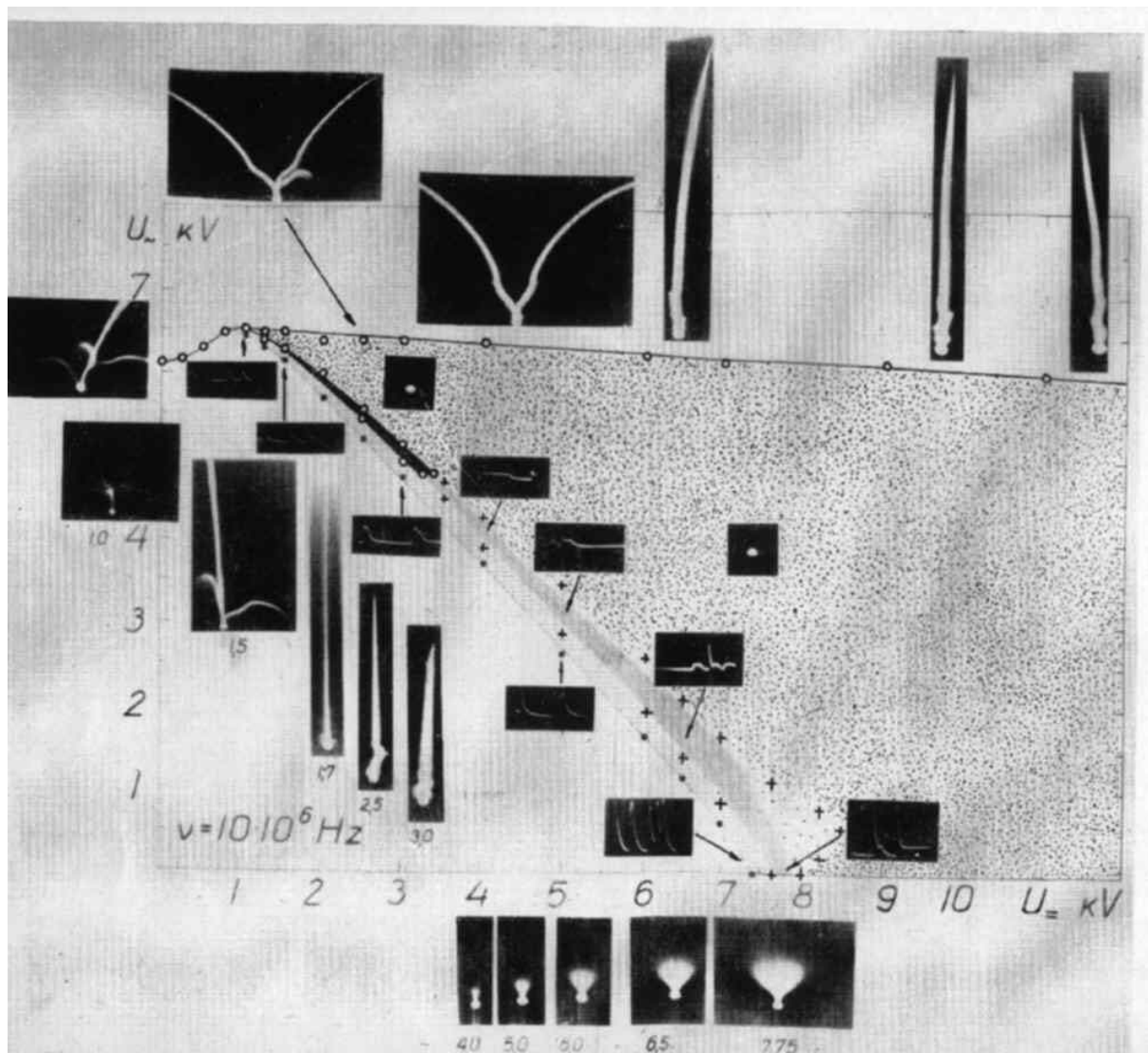


Fig.1.3.2.2. Systematic diagram of HF-HV discharge appearance.

On base of these data, it is possible to summarize main physical parameters of such type of HF discharge:

- Length of plasma filaments 1-10cm;
- Life-time 10-500 μ s;

- Frequency of appearance up to 30kHz (wide range);
- Velocity of propagation $3 \times 10^2 \div 10^7$ cm/sec;
- Temperature at low velocity mode 10^3 K at $50 \mu\text{s}$,
 3×10^3 at $200 \mu\text{s}$ of duration.

A plasma transition temperature was measured by spectroscopy (second positive system of nitrogen). Measurements were produced at normal atmospheric pressure. Under the certain conditions (HF-pulses of special form and an additional DC potential to the point electrode) the HF discharge channel propagates straight along the gap axis and the propagating velocity is nearly constant. Investigations were made for the two channel propagation velocities: 5×10^3 cm/s and 1.2×10^4 cm/s. Radiation of the discharge in this case consists of the second and first positive systems of nitrogen molecule and the first negative system of nitrogen molecule ion. For plasma diagnostics a small part of the discharge channel about 0.3mm on the point tip was taken under observation. For the determination of the neutral gas temperature the intensities of two second positive system bands – 0-0 and 0-2 were measured and compared each other (the neutral gas temperature was assumed to be equal to the rotational one, that is true for the atmospheric pressure discharges with high precision). In Fig.1.3.2.3 the time dependence of the gas temperature is presented for the two cited above values of channel propagation velocity.

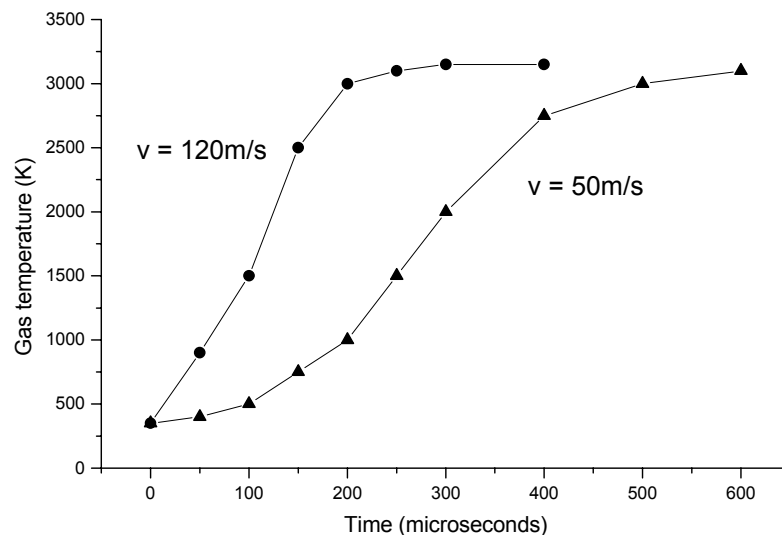


Fig.1.3.2.3. Gas temperature in the discharge channel for two propagating velocities

It can be seen that the greater is the propagation velocity, the faster is the temperature rise. This means that the plasma parameters versus the channel length do not depend much on the

propagating velocity. A similar conclusion was drawn in previous investigations for the electrical parameters of HF discharge in the ambient air.

Electrical Breakdown Control by Pre-Ionization. With relation to breakdown the pre-ionization technique allows to reduce a breakdown voltage and delay time needed for the start of initiated streamer (wave of ionization). Several different methods are used for creation of primary electrons. Among of them the most popular ones are following:

- Short-wavelength laser irradiation,
- Ultra-violet (UV) irradiation by quartz discharge lamp,
- HV pulse pre-discharge or corona discharge,
- Radioactive sources,
- X-rays pulse generators,
- Heating, etc.

The effect of decrease in breakdown voltage in plane-to-plane air gaps can be observed when increasing the frequency of the applied HF field over a certain value. This decrease takes place when the peak-to-peak amplitude of electron oscillation in the discharge gap becomes smaller than the distance d between electrodes. Material of the electrode surface influences on the breakdown essentially. Besides the influence on the onset potential there are some peculiarities in initiation of corona pulses by x-ray radiation for electrodes of different materials. A corona pulse can be created below the onset potential for Al electrode whereas it is impossible for Pt electrode, for instance.

Repetition rate of streamers is proportional to the frequency and amplitude of the AC voltage at conditions of mixed voltage $U_{\text{str}} - U_{\text{AC}} < U_{\text{DC}} < U_{\text{str}} + U_{\text{AC}}$, where U_{str} is the onset potential of streamers at the DC-case.

There have been demonstrated that branching behavior of the streamers in air depends on geometry of electrodes. About 10 times more branches had been observed in the point-wire configuration compared to the plane-plane one. The number of streamers depends also on the impedance of the pulsed power circuit: a resistive circuit gives a high number of thin streamers and an inductive circuit gives fewer streamers with a larger diameter. The current density in a single streamer differs an order of magnitude in these two cases.

An analysis has shown that the pre-ionization by corona discharge can be effective under the conditions of high-speed flow. Our suggestion is an exploiting the plasma panels on the base of barrier discharge with self-sustained pre-ionization by high-voltage pulse corona.

The most important characteristic of Barrier discharges is that non-equilibrium plasma conditions can be provided at elevated pressure, for example atmospheric pressure. In Barrier discharges this can be achieved in a much simpler way than with other alternative techniques like low pressure discharges, fast pulsed high pressure discharges or electron beam injection. The flexibility of barrier discharge configurations with respect to geometrical shape, operating medium and operating parameters is remarkable. In many cases discharge conditions optimized in small laboratory experiments can be scaled up to large industrial installations. Efficient low cost power supplies are available up to very high power levels.

Barrier discharges are characterized by the presence of one or more insulating layers in the current path between metal electrodes in addition to the discharge gap(s). A discharge having one or two dielectric boundaries has many similarities with discharges operated between metal electrodes. For the first ignition breakdown in a homogeneous electrical field is governed by the same Paschen's law that is known from breakdown between metal electrodes. One fundamental difference is, of course, that Barrier discharges cannot be operated with dc voltages because the capacitive coupling of the dielectric(s) necessitates an alternating electric field to drive a displacement current. Prudent utilization of the current limiting properties of the dielectric barriers is one of the major features in designing barrier discharge configurations and their matching to the power supplies. As soon as charges are deposited on the dielectric they have an influence on local fields. After the first ignition these memory charges soon dominate barrier discharge behavior. Barrier discharges can be operated with sinusoidal or square-wave currents between line frequency and microwave frequencies or with special pulsed wave forms. For large-scale industrial applications power supplies operating between 500 Hz and 500 kHz are preferred.

In atmospheric pressure gases breakdown in a plane parallel gap with insulated electrodes normally occurs in a large number of individual tiny breakdown channels, referred to as micro-discharges. When an over-voltage is applied to the discharge gap electron avalanches soon reach a critical stage where the local "edge-field" caused by space charge accumulation at the avalanche heads leads to a situation where extremely fast streamer propagation becomes possible. As a result thin conductive channels are formed. The properties of these micro-discharges have been investigated experimentally as well as theoretically [8-12]. Typical parameters for air filamentary discharges in a 1 mm gap are summarized below.

Duration: 10^{-9} - 10^{-8} s	Total Charge: $10^{-10} - 10^{-9}$ C
Filament Radius: about 10^{-4} m	Electron Density: $10^{14} - 10^{15}$ cm $^{-3}$
Peak Current 0.1 A	Mean Electron Energy: 1-10 eV
Current Density: 100 – 1000 A cm $^{-2}$	Filament Temperature: close to average gas temperature in the gap

The micro-discharge filaments can be characterized as weakly ionized plasmas with properties resembling those of transient high pressure glow discharges. They start when the breakdown field is reached locally and extinguish when the field is reduced to such an extent that electron attachment and recombination dominate over ionization. Due to charge build-up on the dielectric surfaces the field at the location of a micro-discharge collapses within a few ns after breakdown, thus terminating the current flow at this location. The short duration results in little transient gas heating of the current channel. Humidity tends to increase the strength of a micro-discharge while irradiating the cathode with UV photons tends to decrease it. The dielectric barrier limits the amount of charge and energy deposited in an individual micro-discharge and distributes the micro-discharges evenly over the entire electrode surface. As long as the external voltage is rising additional micro-discharges are initiated at new locations because the presence of residual charges on the dielectric has reduced the electric fields at positions where micro-discharges have already occurred. When the voltage is reversed, however, the next micro-discharges will form at old micro-discharge locations. Consequently, high voltage low frequency operation tends to spread the micro-discharges, while low voltage high frequency operation tends to reignite the old micro-discharge channels every half period. This memory effect due to charge accumulation on the dielectrics is a dominant feature in all barrier discharges.

At a dielectric surface the micro-discharge channels spread into surface discharges covering a much larger region than the original channel diameter. Under the low pressure the discharge occurs much more homogeneous. The electron density drops on several orders down to $10^9 - 10^{10}$ cm $^{-3}$.

With relation to breakdown preionisation allows to reduce a breakdown voltage and delay time needed for the start of initiated streamer. Different methods are used for creation of primary electrons. Laser radiation utilizing is published in [8-10]. In [9] electrons were released from the cathode by photo-effect: a divergent radiation of excimer laser (wavelength

$\lambda=308\text{nm}$) was directed to the electrode. Another method is to focus laser radiation on the gap axis between electrodes [9]. It is shown schematically in Fig.1.3.2.4. The α -active source was utilized by some researchers. It possesses to adjust a required level of preionisation by using orifice plates of different apertures in front of the α -source [11]. Among the other methods of preionisation the following could be named: using a β -active source [8]; corona ionizer [11]; x-ray pulse generator [10].

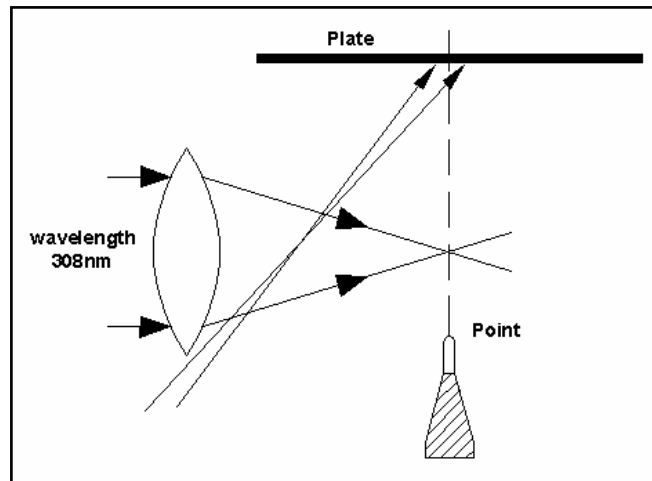


Fig.1.3.2.4. Scheme of laser initiation of the discharge.

Frequency of the applied HF field. The effect of decrease in breakdown voltage in plane-to-plane air gaps can be observed when increasing the frequency of the applied HF field over a certain value. This decrease takes place when the peak-to-peak amplitude of electron oscillation in the discharge gap becomes smaller than the distance d between electrodes. The frequency F at which this decrease begins is called the second critical frequency at given d . (At the first critical frequency the breakdown voltage drop is caused due to ion accumulation in the discharge gap, since the ion oscillation amplitude becomes smaller than the distance between electrodes.) On increasing the distance between electrodes at constant frequency the breakdown field drop can be observed as well. As an example following results have been obtained in [8]: for an ambient air and for discharge gap having been irradiated by a β -active source (ten pairs of ions per cm^3 per second) the first critical frequency was 3.333MHz ($d=1\text{--}8\text{mm}$), the second one 10MHz ($d_e=4.5\text{mm}$), 20MHz ($d_e=2.2\text{mm}$). Authors of [8] found out that a good agreement between theoretical and experimental data is achieved if taking into account electron detachment from negative ions. The sequence of attachment and detachment processes in the HF electric field yields a result equivalent to an extra diffusion of electrons

along the field. Analyzes of the breakdown criterion for two cases – with consideration of detachment and without one are the following:

The balance equations for average concentrations of electrons and negative ions in the first case:

$$\frac{\partial n_e}{\partial t} = n_e(v_i - v_a) + \nabla^2(D_{eHF}n_e) + v_d n_i; \dots \frac{\partial n_i}{\partial t} = n_e v_a - n_i v_d.$$

Assuming that $\partial n_e / \partial t = \partial n_i / \partial t = 0$ at the onset of breakdown, these equations give for the breakdown criterion:

$$v_i = \frac{\pi^2 D_{eHF}}{d^2}.$$

Here d is a discharge gap. The balance equations without consideration of electron detachment from negative ions are the following:

$$\frac{\partial n_e}{\partial t} = n_e(v_i - v_a) + \nabla^2(D_{eHF}n_e); \quad \frac{\partial n_i}{\partial t} = n_e v_a.$$

So breakdown criterion is:

$$v_i - v_a = \frac{\pi^2 D_{eHF}}{d^2}.$$

A qualitative difference between these two cases is that first criterion allows breakdown to take place at field strength $v_i < v_a$.

Influence of electrode surface conditions. Material of the electrode surface influences on the breakdown essentially. For instance, the DC-corona of negative polarity in a point-to-plane discharge gap was observed in the [10], and it was found out that an onset potential for platinum electrode is lower than for aluminum one. Besides the influence on the onset potential there are some peculiarities in initiation of corona pulses by x-ray radiation for electrodes of different materials. A corona pulse can be created below the onset potential for Al electrode whereas it is impossible for Pt electrode.

Discharge appearance.

Constant shift HV + HF. Repetition rate of streamers is proportional to the frequency and amplitude of the AC voltage at conditions of mixed voltage $U_{str} - U_{AC} < U_{DC} < U_{str} + U_{AC}$, where U_{str} is the onset potential of streamers at the DC-case [11].

Geometry of the electrodes and peculiarities of the power circuit. There have been demonstrated in [12] that branching behavior of the streamers in air depends on geometry of electrodes. About 10 times more branches had been observed in the point-wire configuration compared to the plane-plane one. The number of streamers depends also on the impedance of the pulsed power circuit: a resistive circuit gives a high number of thin streamers and an inductive circuit gives fewer streamers with a larger diameter. The current density in a single streamer differs an order of magnitude in these two cases.

Multi-streamer and multi-filamentary modes of the discharge. Pulse or high-frequency electrical discharge goes through a few phases in its development. The first stage is an ionization wave propagation – the streamer phase. The second stage is a leader stage, which can be characterized by the formation of the discharge channel. And the third stage is the spark phase, when the filamentary plasma channel is formed. The two first stages have to be considered as a low level input energy to an individual plasma object (typically less than 1mJ). During the spark phase the input energy is much more and can be defined by power and the pulse duration.

During the streamers' development there is a typical situation when a multi-streamer mode is realized under the enough high level of power of electrical supply system. For the illustration the photo of the streamer phase of the single-electrode pulse discharge is presented in Fig.1.3.2.5.

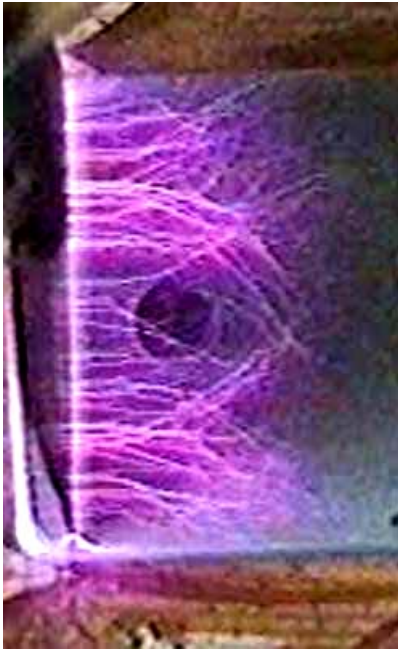


Fig.1.3.2.5. Streamer phase of the pulse discharge.

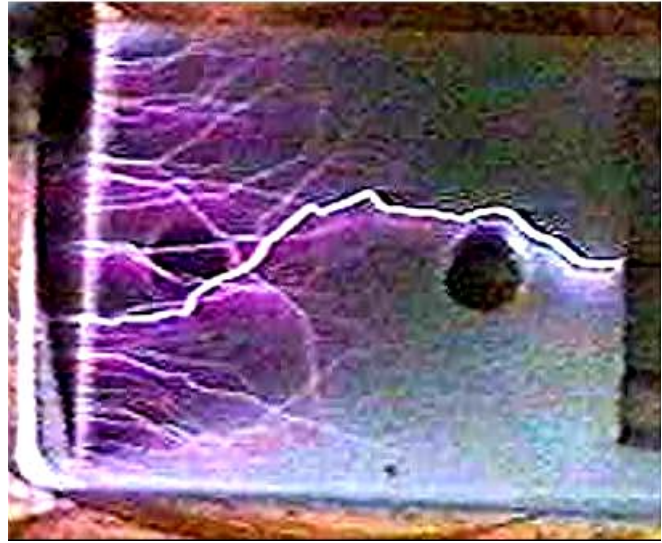


Fig.1.3.2.6. Spark phase of the pulse discharge.

When the discharge is transformed to filamentary-type of the plasma object, the specific plasma instability is developed on a very fast manner (typically, faster than 10^{-8} sec). As the result, only single plasma filament is evolved from the numbers of initial ionized channels. For the illustration the photo of such latest phase of the single-electrode pulse discharge is presented in Fig.1.3.2.6.

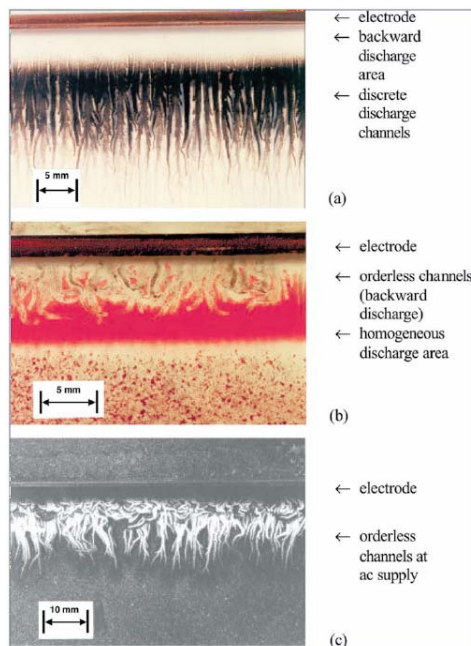
It should be considered, that up to now we have no reliable evidences of the multi-filamentary mode of electrical discharge. But it is clear that in case of separate power supply and separate electrode systems it can be demonstrated.

DBD Properties.

Experimental and theoretical study of barrier discharges has a long history in connection with their wide industrial application in ozone generation technologies. However, despite considerable progress in understanding the structure and properties of these discharges, which principally occurred during the last few decades, the knowledge of this subject nowadays appears to be insufficient to provide an adequate quantitative theoretical description for DBD behavior. This subsection is built on the base of available publications, mostly on [13], and reflects the data on surface barrier discharge specifically.

Dielectric barrier discharges (DBDs) occur in configurations, which are characterized by a dielectric layer between conducting electrodes. Two basic configurations can be distinguished: a volume discharge with a gas gap; and a surface discharge with surface electrode(s) on a dielectric layer and an extensive counter electrode on its reverse side. At atmospheric pressure the DBD consists of numerous microdischarges (multicoronas). Their number is proportional to the amplitude of the voltage. These events have a short duration in the range of some 10 ns transferring a certain amount of charge within the discharge region. The total transferred charge determines the current and hence the volt–ampere characteristic of each configuration. The discharge patterns on the dielectric surface depend on the polarity and amplitude of the applied voltage as well as on the specific capacity of the dielectric. The DBD is a highly transient, low-temperature non-equilibrium discharge formed from electrons of high mean energy which exists in a broad range of pressures.

While the DBD in volume configuration has been investigated intensively ([14–19] for instance), investigations of surface discharges are scarce [20–23]. Much knowledge on DBDs is accumulated in [24]; a more recent review of the state of the art of DBDs and their applications is given in [25].



Depending on the gas mixture, pressure, discharge cell geometry and other parameters, a wide range of discharge forms were observed [27]. There were diffuse and continuously burning discharges as well as self-pulsing microdischarges of short duration, which are randomly distributed in time and space over the surface of the electrodes.

Fig.1.3.2.7. [13]. Discharge patterns on the dielectric surface of an SD arrangement: (a) a positive voltage pulse of 20 kV at the surface electrode; (b) a negative voltage pulse of 20 kV; and (c) an ac voltage of 10 kV.

The bases of microchannels on the surface of the dielectric depend on the polarity of the applied voltage. In the surface discharge (SD) case with positive polarity (a positive voltage at the surface electrode) distinct channels appear on the dielectric with widths in the order of magnitude of 1 mm (Fig.1.3.2.7(a)). With the opposite polarity the discharge is

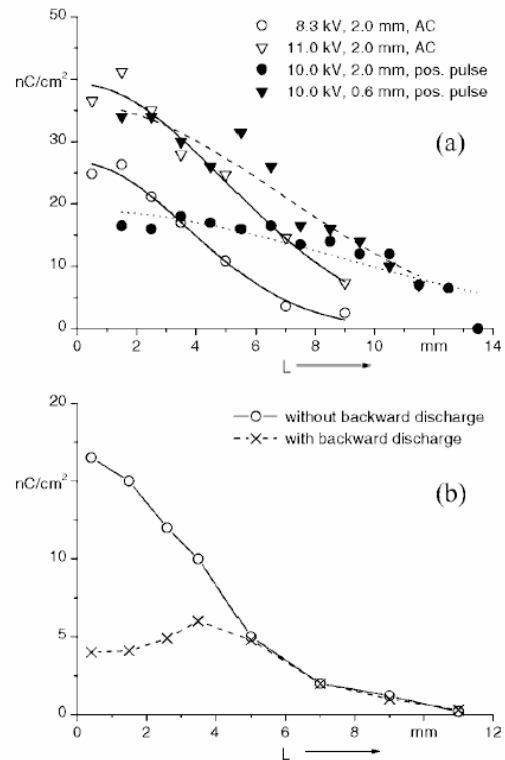
uniformly distributed in a certain area along the electrode (Fig.1.3.2.7(b)). As the voltage is decreased the potential difference between the surface charges and the electrode reaches breakdown field strength and 'backward' discharges with opposite polarity appear near the electrode. These back discharges have the patterns of the opposite polarity: at positive polarity they look uniform while at negative polarity they consist of orderless channels. With an AC voltage a mixture of both patterns can be observed. However, there is a distinct difference between the discharge mechanisms in the VD and SD arrangements. In VD arrangements microdischarge channels bridge the gas gap. The charge is transferred through these channels. With increasing voltage the number of microdischarges per period increases. In SD arrangements, however, there is no defined discharge gap. An increase in the voltage leads to an enlargement of the discharged area on the dielectric. In this case the charge transfer takes place in a thin layer on the dielectric surface.

Apart from the capacitance current, the current in DBDs consists of (numerous) short current pulses, which are a measure of the transferred charge. The time durations are about 10-100ns. The repetition frequency depends on the shape of the voltage pulse, the dimensions of the arrangement and the permittivity of the dielectric.

The actual quality of charge transferred through the discharge gap depends (apart from gas type and pressure) on the design parameters of the discharge arrangement, e.g. on the width of the discharge gap and the specific capacitance of the dielectric layer. The electrode material has been found to have no effect on this value. In SD arrangements the charges are distributed on the dielectric surface (Fig.1.3.2.8). The length of the charged area perpendicular to the electrode depends on the polarity and amplitude of the applied voltage. For a single voltage pulse after discharge ignition, the SD grows stepwise as the voltage rises to its maximum. During a voltage decrease, the potential difference between surface charges and the electrode causes backward discharges. Backward discharges reduce the charge density near the surface electrode; however, they do not influence on its value a long distance from the electrode (Fig.1.3.2.8(b)). In fact, the charge distribution on the dielectric surface is not homogeneous. From the measurements it follows that, with negative polarity, successive discharge steps enlarge the size of the uniformly discharged layer on the surface with an increasing voltage only. With positive polarity the discharge step consists of a set of channels (Fig.1.3.2.7). The positive polarity channels leave strips of charges on the dielectric surface. As voltage is increased, breakdown conditions are restored near the tips of the charge strips and the channels grow stepwise.

The stepwise growth of the channels is accompanied by short current impulses in the external circuit.

Fig.1.3.2.8. [13] Measured charge density distribution on the dielectric surface of an SD arrangement in air at atmospheric pressure: (a) at different ac voltage amplitudes and single positive voltage pulses, respectively, and with different thickness of the dielectric; and (b) charge density before and after the backward discharge took place, ac voltage.



The charged area on the dielectric surface is extended by approximately several millimeters with negative polarity. With positive polarity the channel extension is considerably larger. With an AC voltage the discharge extension is between that with positive and negative polarity. The outer boundary of the charged area is determined by the first positive half-cycle of the applied voltage. In the succeeding negative half-period the negative charged layer is extended by the outer positive charges on the surface, enhancing the field strength component parallel to the surface. It has been proved experimentally that with an AC voltage the outer region of the surface charge layer is charged positively [20].

With constant level of applied voltage the length of the discharge patterns depends on the relative permittivity value of the dielectric. The larger the permittivity is the shorter the discharge length becomes. As already mentioned, the size (or length) of the charged area in SD arrangements also depends on the amplitude of the voltage. From this, it follows that the dielectric area involved in the discharge process is not constant or, in other words, the capacitance of the discharged area depends on the voltage amplitude. This is quite different to VD arrangements and results in different current–voltage characteristics.

The DBD is one of the most effective non-thermal plasma sources [13]. It is characterized by an effective conversion of electric field energy to chemical or physical processes in gases or onto surfaces for many applications. On one hand, the efficiency is

determined by the total amount of energy released in the discharge in general. On the other, the efficiency depends on the value of the field strength, which has to be adapted to the process under consideration. From this it follows that the effectiveness of a special application of DBDs crucially depends on the dynamics of charge transfer within the discharge. The energy release is connected to a movement of charged particles, of electrons and ions. As the DBD is a nonequilibrium phenomenon, there is a significant gap between the mean energy of electrons and heavy particles. The mean electron energy in the discharge is about several eV, that of the heavy particles is around 0.03 eV (~ 300 K) at the conditions under consideration. While the energy of the electrons is utilized for chemical and physical purposes, the energy of the ions is, in general, useless. The energy consumption in DBDs is combined with the movement of charge carriers, i.e. current. The energy release starts simultaneously with the development of the initial avalanche; however, a remarkable value is not reached until the appearance of the streamer in VD arrangements. The energy density reaches its maximum value after cathode-layer formation and decreases again during charge accumulation on the dielectric. During cathode-layer formation, the current density reaches a level in the order of a hundred A/cm^2 . After cathode-layer formation and surface charge accumulation the main charge transfer and energy release are shifted to the peripheral region of the discharge channel at higher field strengths. The radial boundary of the surface charge determines the position of the radial current density maximum. The maximum moves with expansion of the surface charge.

In SDs with the boundary conditions under consideration, no cathode layer, in general, exists. This is an important difference between VDs and SDs. In the absence of an efficient source of secondary electrons, the current density is low, about $1 \text{ A}/\text{cm}^2$. In any case, a shielding effect caused by surface charges exists as well. In SDs, the drift distance of electrons on the dielectric becomes longer with time (at each successive discharge step). The charge transfer process is shifted to a region with lower field strength where the effective ionization coefficient is negative. In any case, in SDs the charge transfer as well as the energy release is less intensive.

A distinct cathode layer appears only if the discharge process is well developed. Depending on construction of the discharge arrangement and gas properties, the discharge process can be quenched early. In this case the field strength in front of the cathode may reach values in between the initial one and that of a well-developed cathode layer. This means in certain circumstances that the discharge may be quenched before cathode-layer formation.

The field strength distribution has a maximum in the cathode layer and an almost constant value in the conductive channel, which is nearly frozen after the appearance of the cathode layer. The constant value of the field strength in the conductive channel is determined by the equilibrium between electron generation and loss processes. In air and oxygen at atmospheric pressure it is about 100 Td.

In any configuration the DBD has a certain spatial structure; it consists of a series of microdischarges (VD) or discharge steps (SD). The interaction between surface charges and charge carrier flow in the gas region determines the density of the discharge patterns on the dielectric surface. The microdischarge energy density is comparatively low. The resulting temperature jump in the discharge region is estimated to be in the order of a few Kelvin after the termination of the microdischarge.

Experimental and theoretical study of barrier discharges has a long history [28] in connection with their wide industrial application in ozone generation technologies. However, despite of considerable progress in understanding the structure and properties of these discharges, which principally occurred during the last few decades, the knowledge of this subject nowadays appears to be insufficient to provide an adequate quantitative theoretical description for DBD behavior.

Reference to Section 1.3.2.

1. K. Kudu "About initial stages of discharge from tip in air." (in rus.) Tartu (Estonia): Tartu State University, 1960.
2. M. Laan, J. Suzi, "Optical Diagnostics of the propagating HF discharge in nitrogen", Proceedings of Tartu University, Tartu (Estonia), 1987, p.3-9.
3. Electrical insulation of HF installations of high voltage. Ed. M.A. Aronov, V.P. Larionov, (in rus.), Moscow: "Znak", 1994, 228pp.
4. E.M.Bazelyan, Yu.P.Raizer. Spark Discharge, CRC Press, Boca Raton, Florida, 1997.
5. Yu.P.Raizer. Laser Spark and Discharge Propagation, Moscow, Nauka, 1974 (in russian).
6. Raizer Yu. P. Gas discharge physics, Moscow, Nauka, 1987, p.591.
7. High-frequency Discharge in Wave Fields. Ed. by A.G.Litvak, IAP USSR Academy of Sciences, Gorky, 1988 (in Russian).
8. M.Aints, A.Haljaste, K.Kudu, V.Adamson, *The role of negative ions in high-frequency discharge*, J. Phys.D: Appl. Phys. 28 (1995) 81-89.

9. M. Laan, P. Paris, *The multi-avalanche nature of streamer formation in inhomogeneous fields*, J. Phys.D: Appl. Phys. 27 (1994) 970-978.
10. H. Korge, M. Laan, P. Paris, *On the formation of negative coronas*, J. Phys.D: Appl. Phys. 26 (1993) 231-236.
11. M. Aints, A. Haljaste, K. Kudu and T. Plank, *Repetition rate of streamers as a measure of content of electronegative additives in the air*, J. Phys.D: Appl. Phys. 30 (1997) 210-220.
12. E. M. van Veldhuizen and W. R. Rutgers, *Pulsed positive corona streamer propagation and branching*, J. Phys.D: Appl. Phys. 35 (2002) 2169-2179.
13. Valentin I Gibalov and Gerhard J Pietsch "The development of dielectric barrier discharges in gas gaps and on surfaces", J. Phys. D: Appl. Phys. **33** (2000) 2618–2636.
14. Eliasson B, Hirth M and Kogelschatz U 1987 Ozone synthesis from oxygen in dielectric barrier discharges *J. Phys. D: Appl. Phys.* **20** 1421–37
15. Eliasson B and Kogelschatz U 1991 Modelling and application of silent discharge plasmas *IEEE Trans. Plasma Sci.* **19** 309–22
16. Braun D, Kuchler U and Pietsch G J 1991 Microdischarges in air-fed ozonizers *J. Phys. D: Appl. Phys.* **24** 564–72
17. Braun D, Gibalov V I and Pietsch G J 1992 Two-dimensional modelling of the dielectric barrier discharge in air *Plasma Sources Sci. Technol.* **1** 166–74
18. Neiger M 1992 Dielectric barrier discharges: an unusual new light source *Proc. Science and Technology of Light Sources (LS6) (Budapest)* ed L Bartha and F J Kedves, pp 75–82
19. Steinle G, Neundorf D, Hiller W and Pietralla M 1999 Two-dimensional simulation of filaments in barrier discharges *J. Phys. D: Appl. Phys.* **32** 1350–6
20. Richter R and Pietsch G 1995 Discharge phenomena on a dielectric surface with extended electrodes *Proc. 11th Int. Conf. on Gas Discharges and Their Applications* vol 2, pp 280–3
21. Murata T, Okita Y and Terai K 1997 Distribution of surface discharge for ozone generation *Proc. XXIII Int. Conf. on Phenomena in Ionized Gases (Toulouse)* vol III, pp 82–3
22. Boeuf J-P, Punset C, Hirech A and Doyeux H 1997 Physics and modeling of plasma display panels *J. Physique* **IV** C4 p3–14

23. Pietsch G J and Gibalov V I 1997 Discharge phenomena on a dielectric surface with extended electrodes *Proc. 12th Int. Conf. on Gas Discharges and Their Applications* vol 2, pp 750–7
24. Samoilovich V, Gibalov V and Kozlov K 1997 *Physical Chemistry of the Barrier Discharge* 2nd edn (Dusseldorf: DVS)
25. Kogelschatz U, Eliasson B and Egli W 1997 Dielectric barrier discharges—principle and applications *J. Physique* **IV** C4 47–66
26. Pietsch G J, Braun D and Gibalov V I 1993 Modeling of dielectric barrier discharges *Non-Thermal Plasma Techniques for Pollution Control (NATO ASI Series Part A)* vol 34, ed B M Penetrante and S E Schultheis, pp 273–86
27. Muller S and Zahn R-J 1996 On various kinds of dielectric barrier discharges *Contrib. Plasma Phys.* **36** 697–709
28. K V Kozlov, H-E Wagner, R Brandenburg and P Michel. Spatio-temporally resolved spectroscopic diagnostics of the barrier discharge in air at atmospheric pressure. *J. Phys. D: Appl. Phys.* **34** (2001) 3164–3176

1.3.3. Weakly-Ionized Plasma Experiments on Flow Control.

The problem of flight control by energy and mass deposition was analyzed and discussed by several scientists and engineers (Oswatitch, Billig and others) in the last century. Starting from 1970th a serious interest to the problem of plasma generation inflow and the interaction of plasma with flow and flying bodies was appeared. At 1980th the specialized ballistic experiments have been done. Some results have been published later [1]. There was shown that plasma of electrical discharge effects on parameters (stand off) of bow shock and drag of flying bodies. But the regular investigations in wind tunnels have started at 1988.

Practically, simultaneously the experimental works began in TsAGI, MRTI, NIIRP, GosNIIAS, ITAM, MESU and TsNIIMash. The experiments have been simulated and supported by the theoretical investigations in Institute of Mechanics MSU and Keldysh IAM. Probably, the first publications were the [2-9]. Starting from 1995 these works have been supported by BAe/DERA, Rockwell/Boeing Co., APL/JHU and EOARD/AFOSR. At that time the most part of experimental works have been condensed by the Moscow Technical Company (MTC), which has been incorporated to IVTAN in 1998.

Conditionally all efforts can be separated to three cans: background (before 1997), main experiments on drag reduction in 1996-99 and the last years' works in frames of Advance Flow/Flight Concept (AFFC).

The most results from the first group are presented in the proceedings of WIG workshops [10] and Russian publications. That time very popular notion was the "plasma magic" approach. Different plasma generators were used by authors to explore the plasma effect on drag and lift [11] of bodies, namely: plasma jets, laser sparks, longitudinal AC/DC electric discharge, HF corona, discharge on body's surface. There were found the following results:

- Plasma of electrical discharges and laser beam decreases the drag of axe-symmetrical bodies in supersonic and subsonic flow in value up to 50% of initial level.
- The effectiveness of plasma influence can be more than 1 for blunt model.
- Stand off of the BSW is increased and stagnation pressure in top point is decreased due to plasma generation.
- Lift/drag ratio of a simple airfoil can be enhanced.

As a sample of early work the results of counterblow plasma jet effect can be described [7,11]. Some results of this work have been repeated and improved later [12-14].

A high enthalpy erosive plasma jet has features, which are important for application it as a factor of drag reduction: large specific length of initial laminar part of jet and high level of specific pressure counteraction. Using a hydro-carbon working medium gives possibility to obtain less value of mass density in comparison with air at same temperature (due to large share of H₂ in a thermo-destructive mixture). Besides of this, hydro-carbonic plasma has got high level of chemical activity: there is a lot of energy release at mixing with air. Aerodynamic models were a combination of cylinder (40, 60 and 70mm of diameter) and the cone with 30° of half angle or hemisphere. Base area was plain. Preliminary runs had shown that drag factor of such models was about 0.8-1.0 at Mach number 1.7-2.0. Sample of Schlieren photo of the plasma jet blowing out is shown in Fig.1.3.3.1. In the Schlieren photos a change of stand off of BSW is seen as well as generation of weak turbulent heat layer around the model. Weak parasitic shocks in a field of observation were due to mechanical junctures on a wall of WT.

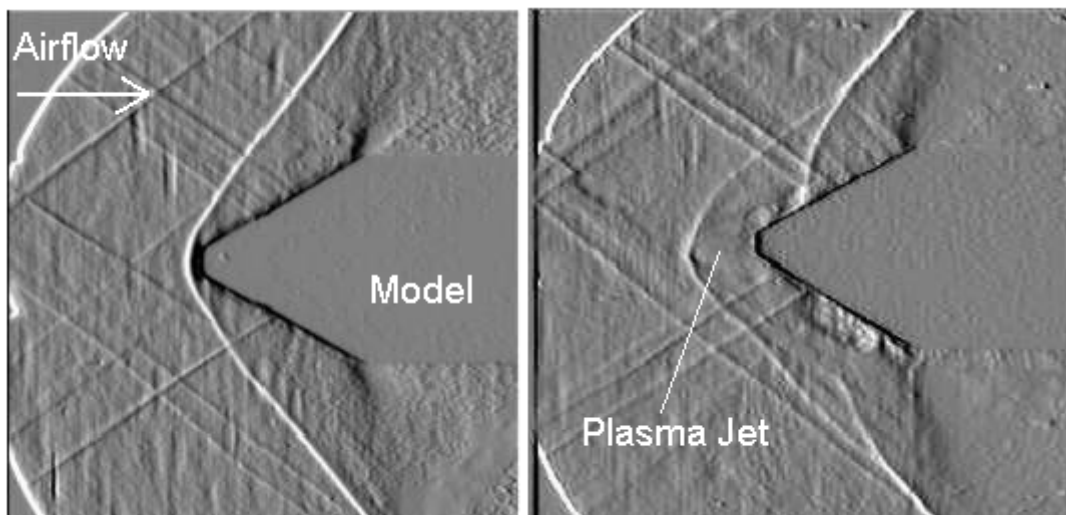


Fig.1.3.3.1. Schlieren photo of plasma jet interaction with supersonic airflow.

A sample of balance measured parameters and primary calculations for one of runs at $M=1.6$ is presented in Fig.1.3.3.2. It is seen, that pressure in airflow is changed during a time of experiment. It happens due to blow in WT pumped contour and some increase of temperature of air during the run. Resulting values of C_d are well compensated by taking into account all data at procedure.

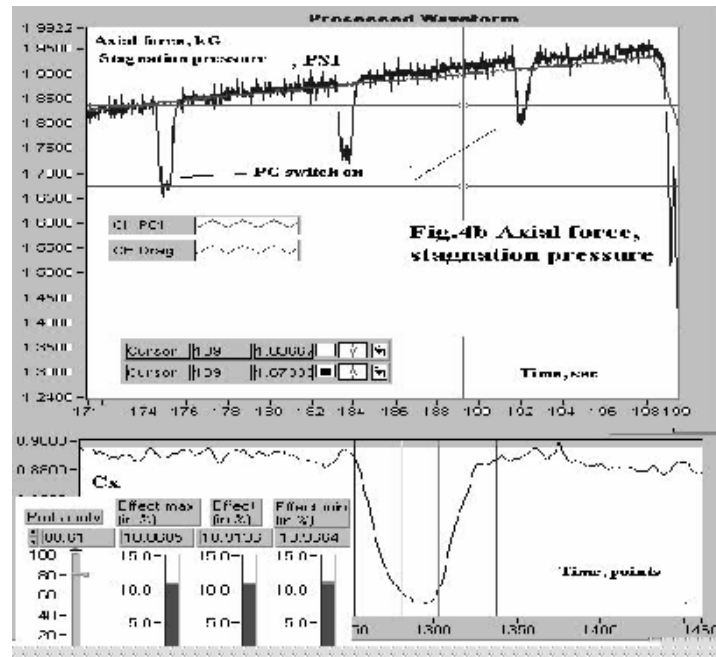


Fig.1.3.3.2. Sample of the drag measurements at plasma jet generation.

In Fig.1.3.3.3 the data on physical efficiency η_1 of Plasma Jet influence on drag of model are presented in dependence on Mach number. Well seen that the efficiency of interaction is maximal at transonic mode. In this case the stand-off of BSW was maximal too. The value of efficiency in this work is large and, important, more than 1.

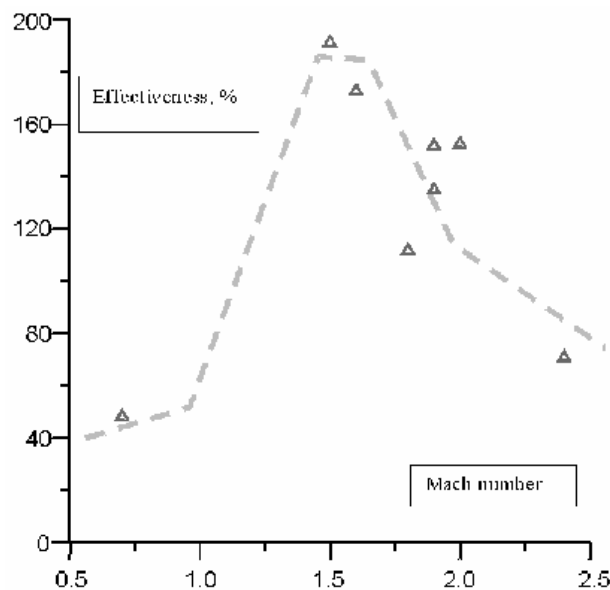


Fig.1.3.3.3. Effectiveness of plasma jet influence vs Mach number.

The increase of efficiency of plasma influence more than 1 is the key moment of this work. Well known that calculations show such exceeding in many times [15]. But at experimental

conditions and for “non-blunted” bodies it is not so simple problem. In that work statistically reliable results on drag reduction in dependence on input power, Mach number and model parameters were obtained as well as the first summarizing of experimental results on plasma jets influence on airflow-body system was made.

Several important experimental works are related to the second group. The first of those was the work, which has been supported by BAe and DERA in 1996-97 [16]. The combination of plasma jet generator with the surface discharge was utilized. The feature of the experiment was the low initial drag factor of the model $C_d=0.09-0.14$. The main result was that at low drag the plasma effect is small and non-effective. Later, the analysis of the data shows that a skin friction reduction can explain such an effect.

In 1997-98 the experiment on AC/DC plasma influence on drag of the axial-symmetric model was made at EOARD/AFOSR support [17]. The wind tunnel of TsAGI is used. The measurements of plasma parameters were done by MSU team. Different modes of the discharge were described (see Fig.1.3.3.4). The resulting drag reduction was $\Delta C_d/C_d=10-15\%$ at physical efficiency 30-100%.

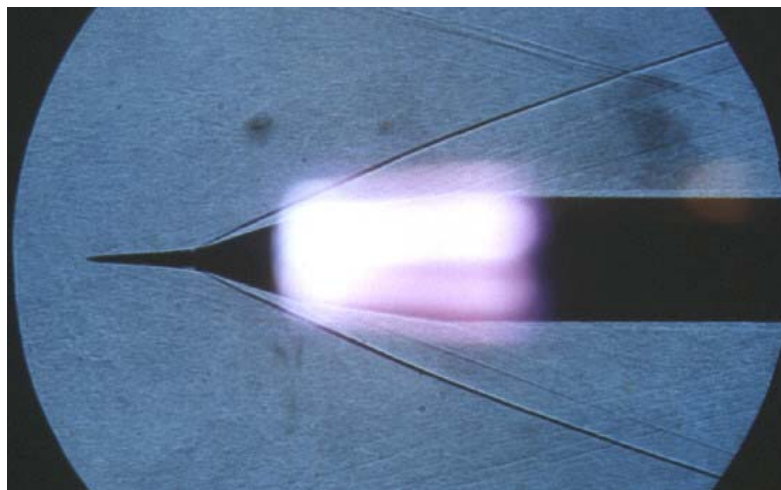


Fig.1.3.3.4. Longitudinal surface discharge at supersonic airflow.

A sufficiently different type of the interaction has been observed at short pulse plasma excitation with a sequential influence of heated (“processed”) area of flow-field on the shock structure and the body. In such a case the essentially unsteady and non-linear processes play the role. The work on short-pulse MW free-localized discharge effect on flow and drag was performed in 1997-98 at Boeing Co. support [18-19]. The gasdynamic installation of IMM St-Petersburg University and MW installation of RDI of Radioapparature were utilized.

A sample of Schlieren photo of shock wave structure is presented in Fig.1.3.3.5. The photo has been obtained under the following conditions: microwave pulse duration 1.5 μ s, pulse period 1.1ms, MW pulse power about 200kW, localization 5cm and 3cm upstream the model, exposure 1 μ s, time delay between MW pulse and photo 30 μ s, Mach number of airflow $M=1.5$.

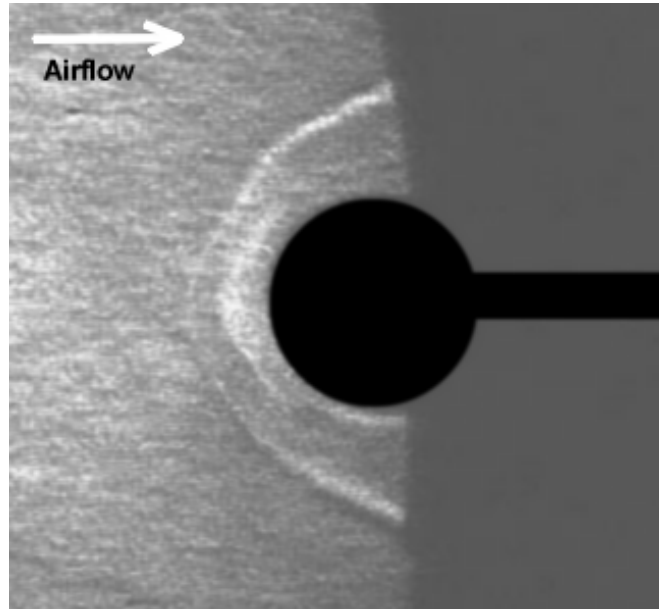


Fig.1.3.3.5. Unsteady shock wave structure at free-localized MW discharge excitation in upstream airflow.

It is clear that such a SW structure like a “splitting” can be observed only at unsteady conditions. The mechanism of interaction includes three main stages: momentary (during the MW pulse) plasma generation (1) in volume about 20cm³, streamlining of the model by relaxing plasma (2) at unsteady SW structure realization and reconstruction of the initial SW structure (3). Whole process spends up to 120÷160 μ s and it is repeated again in about 1ms. The measured mean drag reduction has been in a range 5÷9% on a spherical model. The sample of the balance’s record is shown in Fig.1.3.3.6. At the same time the measurements of the stagnation pressure on the top of the model show a large level of fluctuations. A formal recalculation of instant effect gives 30÷40% of drag reduction at efficiency $\eta_1=50\div100\%$.

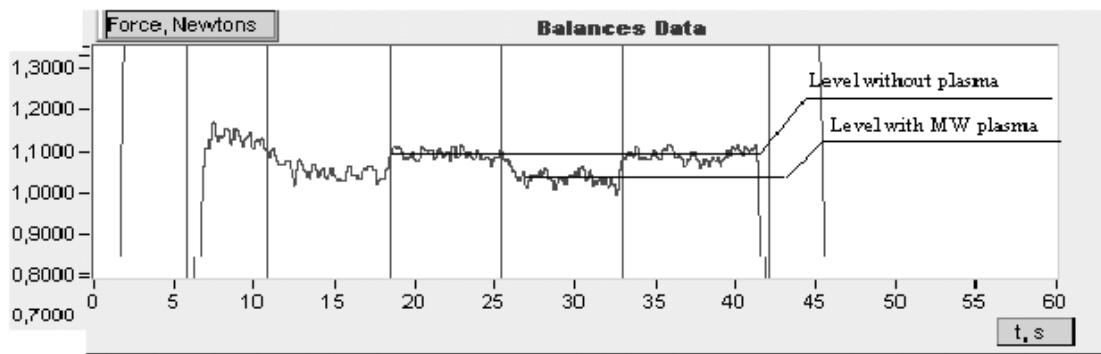


Fig.1.3.3.6. Sample of balance's record at MW plasma effect. $M=1.5$.

Analyzing this specific situation the conclusion might be considered that the unsteady type of interaction at the volume type of the energy release can provide a sufficient positive effect in drag reduction of bodies in supersonic airflow.

An effort of drag reduction with single-electrode high frequency (HF) filamentary discharge has been done in 1998-99 at BAe support [20,21] in experimental facilities of GosNIIAS, TsAGI and IVTAN. In frames of this work at the first time there was demonstrated specific behavior of plasma filaments in high-speed flow and effect of plasma filament penetration through the BSW with sequential modification of BSW (see Schlieren photo in Fig.1.3.3.7). Several different mechanisms of interaction were found. Among of them the mechanism of drag reduction of well-shaped bodies with drag factor $C_d \approx 0.1$ gave the effect $\Delta C_d / C_d = 5 \div 6\%$ at physical efficiency 30-180%.

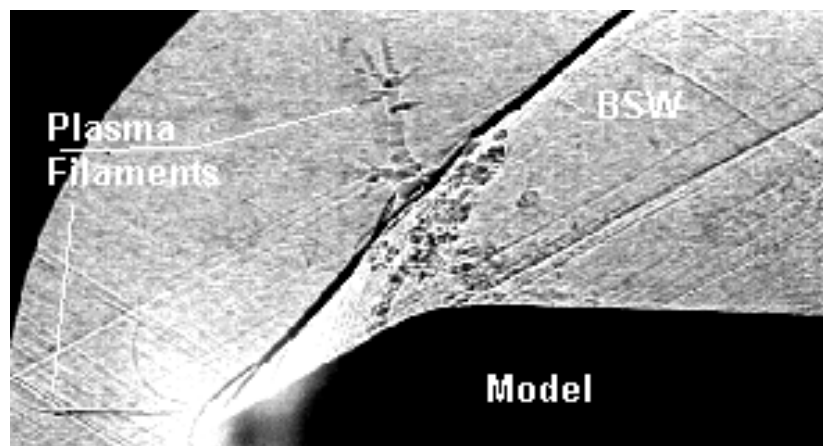


Fig.1.3.3.7. Single-electrode plasma filament interaction with BSW at $M=2$.

A comparison of data on HF discharge with another results allows suggesting, that a main mechanism of drag reduction at HF discharge could differ specifically from plasma jets and AC/DC discharges as well as at MW free localized discharge.

In 1997-99 the WT experiments with large models were fulfilled at Boeing Co. support on test facilities of TsNIIMash and, later, TsAGI. The first model was 1/3 scale nose part of F-15 vehicle (320mm of diameter), the diameter of the second model was two times less. Unfortunately, the work with large model has not been completed due to technical faults. A preliminary result was $\Delta C_d/C_d = 4 \pm 3\%$ at physical efficiency $20 \div 100\%$. The 1/6 scale model test was conducted with specific plasma generators arrangement. Formally, the highest efficiency has been demonstrated in case of AC discharge on forehead spike, namely $\Delta C_d/C_d = 6\%$ at up to 360% of physical efficiency [18,22,23].

These efforts show that plasma method of flow/flight control makes a sense. The problem is in understanding of specific mechanisms of the plasma effects in details and sequential optimization. In general case the drag force of a vehicle at atmospheric flight and/or in inlets and ducts is represented as the sum of the friction drag and the pressure drag. At the same time the pressure drag includes the wave drag, the base/obstacle drag, the interference drag etc. The contribution of each component to the total impulse losses at subsonic, transonic and supersonic flight modes are different. Usually the main attention was paid to pressure/wave shares of the total drag. Analysis of aerodynamic situation shows that the friction and interference effects can play an important role as well.

The third group of works in the field of AFFC is devoted to the problems of boundary layer and separation control. These efforts have own extensive background, for example [24]. Our experimental works have started in 1999 at support by EOARD/AFOSR. In [25-29] the preliminary results of these researches were considered.

At the same time the anticipated positive effect in FFC (drag reduction) due to inflow energy release are associated with some penalties to be paid for. This statement can be illustrated by several examples. Reducing the wave drag of the vehicle forehead leads to pressure redistribution in the base area. Simple analysis shows that such a pressure change can has the same sign, i.e. the resulting net effect for whole body is much less, than for individually considered forepart. If the air-breathing engine is utilized in the vehicle a drag reduction can lead to decrease of air mass flow-rate through the inlet. Thus, any specific AD situation requires the analysis of all aspects and possible negative sequences.

Some additional information on the problem of plasma method of flow/flight control can be found in [33].

References to Section 1.3.3.

1. G. Mishin, Yu. Serov, I. Yavor "Streamlining of the sphere in plasma of gas discharge at supersonic speed", J. of Technical Physics, Letters (Rus), 1991, v.17, No.11, p.65.
2. P. Georgievsky, V. Levin "Supersonic flow over space-distributed energy sources", Mechanics, modern problems. Moscow, MSU Pub. 1987, pp. 93-99.
3. A. Yuriev, V. Borzov, N. Savischenko et all. "Method of Flight Control", Patent RU-2173657, May 1990.
4. V. Vstovsky, L. Grachev, Yu. Kuznetsov et all. "Study of unsteady supersonic flow over the body in longitudinal electrical discharge", TVT (rus.), 1990, v.28, No 6, p.1156.
5. V. Borzov, I. Rybka, A. Yuriev "The influence of local energy supply at hypersonic flow on wave drag of bodies of different blunting", IFJ (rus), 1994, v. 67, No 5-6, pp.355-361.
6. V. Alatortsev, Yu. Kuznetsov, V. Skvortsov, L. Grachev, K. Khodataev et all. "Experimental study of drag force control on the model at the flow excitation by the longitudinal electrical discharge", TsAGI Proceedings, No 2552, 1994.
7. Leonov S.B., Pankova M.B., Shipilin A.V. "Modeling of ball lightning interaction with bodies in atmosphere" "Ball Lightning in Laboratory." ed. Avramenko R.F., Klimov A.I. and oth. Moscow: Chemistry, 1994.
8. A. Gridin, A. Zabrodin, A. Klimov, Yu. Kuznetsov, A. Lutsky, V. Skvortsov, K. Hodataev et all "Numerical and experimental research of supersonic flow over bluntnose body in presence of electric discharge", KIAM RAS Preprint No 19, 1995, Moscow.
9. Burdakov V.P., Baranovsky S.I., Klimov A.I., Lebedev P.D., Leonov S.B., Pankova M.B., Puhov A.P. "Improvement of aerodynamic and thrust-energetic parameters of hypersonic aircrafts and engines using algorithmic discharges and plasmoid formations". Proceeding of the International Conference of Advance Technology, Moscow, MSU, 1995.
10. Workshop on Weakly Ionized Gases. Proceedings. USAF Academy, Colorado, 9-13 June 1997; Second Workshop on Weakly Ionized Gases. Proceedings. Norfolk, 24-25 April 1998.
11. Workshop on Weakly Ionized Gases, USAF Academy, Colorado, 9-12 June 1997. Proceedings , Vol.1, section J.; Leonov S.B. "Plasma Jet Generation for influence on drag of bodies in a supersonic airflow". \Contributed Papers of HAKONE VI, Cork, Ireland, 1998, p.318-323.
12. Gordeev V.P., Krasilnikov A.V., Lagutin V.I. "Experimental study of possibility of drag reduction by means of plasma", MLG (rus.), N2, p.177-182, 1996.

13. J. Chang, J. Hayes, J. Menart, "Hypersonic flow over a Blunt Body with Plasma Injection", AIAA 2001-0344.
14. Fomin V.P., Maslov A.A., Fomichev V.P. Review of IPTM works on plasma aerodynamics. Proceedings of Meeting "Perspectives of MPA Technology in Aerospace Applications", March, 24-25, IVTAN, Moscow, 1999.
15. Levin V.A., Afonina, N.E., Georgievsky P.Y., Gromov V.G., Larin O.B., Terenteva L.V. "Study of possibility of control of supersonic airflow...", Preprint IM MSU, N24-97, Moscow, 1997.
16. MCEwen R & Gilmor M. Plasma Aerodynamics Meeting Report SRC BAe, II Nov1996; R. MCEwen, Workshop on Weakly Ionized Gases, USAF Academy, Colorado, 9-12 June 1997. Proceedings, Vol.1.
17. Chuvashev S.N., Ershov A.P., Klimov A.I., Leonov S.B., Shibkov V.M., Timofeev I.B. "Flow around body and characteristics of AC/DC discharges in plasma aerodynamic experiment." In Proceedings of 2nd Weakly Ionized Gases Workshop, AIAA, Norfolk, VA, April 24-25, 1998. P.59-61.
18. W. Beaulieu, A. Klimov, S Leonov, Yu. Kolesnichenko, V. Brovkin, "Development of Cold Plasma Technology Joint BNA and Russian Program", Second Weakly Ionized Gases Workshop, Proceedings supplement, April 24-25, 1998, Norfolk, p.207.
19. V.G. Brovkin, Yu.F. Kolesnichenko, S.B. Leonov, A.I. Klimov, A.A. Krylov, V.A. Lashkov, I.C. Mashek, M.I. Ryvkin, "Study of Microwave Plasma-Body Interaction in Supersonic Airflow", AIAA 99-3740, 30th AIAA Plasmadynamics and Lasers Conference, June 28-July 1, 1999 / Norfolk, Virginia.
20. S. Leonov, T. Cain, A. Klimov, A. Pashina, V. Skvortsov, B. Timofeev "Influence of a HF Corona Plasma Structure on Drag of an Axial-Symmetric Body in a Supersonic Airflow." 3rd Workshop on WIG, November 1-5, 1999 / Norfolk, Virginia, AIAA 99-4856.
21. S. Leonov, V. Bityurin, Yu. Kolesnichenko "Dynamic of a Single-electrode HF Plasma Filament in Supersonic Airflow." 39th AIAA Aerospace Sciences Meeting & Exhibit, 8-11 January 2001 / Reno, NV AIAA-2001-0493.
22. Beaulieu W., Bityurin V., Klimov A., Leonov S. et al., Plasma Aerodynamic WT Tests with 1/6 Scale Model of Nose Part of F-15, AIAA 99-4825 Paper, 3rd WIG Workshop, Norfolk, 1999.

28. W. Beaulieu, V. Bityurin, A. Klimov, S. Leonov, A. Pashina, B. Timofeev, Study of characteristics of 1/6 scale model...- Proceedings of Meeting "Perspectives...", March, 24-25, IVTRAS, Moscow, 1999.
29. Kazakov A., Kogan M., Kuriachi A., Influence on the friction of local heat addition to the turbulent boundary layer. Mech. Of Fluids and Gases, N1, 1997. // Kurjachi A. P., Boundary layer transition by means of electrodynamics method. Prikl. Math. I Mech., vol.49, issue 1, 1985. // A.V. Kazakov, A.P. Kuryachii, Electrogasdynamic influence on the development of the small disturbances in a boundary layer in the thin profile Izv. AN USSR, Mekhanika zhidkosti i gaza, 1, 1986
30. S. Leonov, V. Bityurin, N. Savischenko, A. Yuriev, "Study of Surface Electrical Discharge Influence on Friction of Plate in Transonic Airflow". AIAA-2001-0640, 39th AIAA Aerospace Meeting and Exhibit, 8-11 January, Reno, NV, 2001.
31. S. Leonov, V. Bityurin, A. Bocharov, E. Gubanov, Yu. Kolesnichenko, K. Savelkin, A. Yuriev, N. Savischenko "Discharge plasma influence on flow characteristics near wall step in a high-speed duct." The 3-rd Workshop on Magneto-Plasma Aerodynamics in Aerospace Applications, Proceedings, Moscow, IVTAN, 24-26 April, 2001.
32. S. Leonov, V. Bityurin, A. Klimov, Yu. Kolesnichenko, A. Yuriev "Influence of Structural Electric Discharges on Parameters of Streamlined Bodies in Airflow", AIAA-2001-3057, AIAA 32nd Plasmadynamic and Laser Conference, June, 2001, Anaheim, CA.
33. S. Leonov, V. Bityurin, K. Savelkin, D. Yarantsev "Effect of Electrical Discharge on Separation Processes and Shocks Position at Supersonic Airflow" AIAA-2002-0355, 40th AIAA Aerospace Meeting and Exhibit, 14-17 January, 2002, Reno, NV.
34. S. Leonov, V. Bityurin, K. Savelkin, D. Yarantsev "The Features of Electro-Discharge Plasma Control of High-Speed Gas Flows." AIAA-2002-2180, 33-th Plasmadynamic and Laser Conference, 20-24 May, 2002, Maui, HI.
35. V. M. Fomin, P. K. Tretyakov, J.-P. Taran, "Flow control using various plasma and aerodynamic approaches", Aerospace Science and Technology, 8, 2004, pp.411-421.

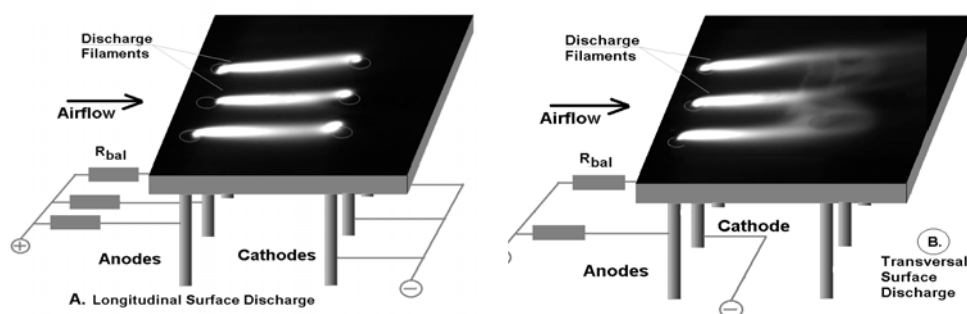
1.4. Short Review of Results Year by Year.

The first year of the Project.

The design of experimental setup and the electrode's configuration were fulfilled. The facility PWT-10 has been designed for short time runs. The special dielectric test section has a rectangular cross-section with dimensions 20*50mm. A subsonic and supersonic operation modes were realized and described in details. A base diagnostic system of the experimental installation was assembled. It includes the following parts:

- Schlieren-system, allowing to visualize the flow under investigation with separation of the needed phase of a process to the account of time gating;
- Spectral system, allowing to obtain emission spectrums of plasma;
- Pressure sensors, with the possibility to select a necessary phase of a process;
- Fast photo and video cameras;
- Electromagnetic sensors;
- Thermocouples and some original methodic.

Preliminary experiments on the filamentary plasma generation had been carried out that time. A self-vibration mode of the power feeding has been used. In this variant of the plasma generator the high voltage Tesla-type transformer with shock excitation was chosen as the power supply. The measurements were done for defining the input energy to the individual plasma filament. The preliminary experiments show that the filamentary plasma can be generated successfully by the shock excited HV transformer as well as by the high frequency generator.



1.4.1. Design of standard electrodes configuration.

The scheme of standard electrodes configuration is shown in Fig.1.4.1. It related to DC type of the discharge excitation. A new scheme of the surface discharge excitation was proposed on the base of resonant distributive electrode configuration. Such a type of

electrodes system was applied for excitation of distributive surface discharge in experiments on plasma influence on parameters of viscous friction and generation of artificial separation zones. The high frequency power generator was used as a primary source of the resonant contours supplying. That scheme was tested but it occurred unstable in operation and didn't utilize in further tests.

The experiments with multi-streamer HF plasma generator were carried out. The tests were conducted in the short time wind tunnel PWT-10 at static pressures from 100 to 300Torr and at Mach number 0.02, 0.8 and 1.7. The following conclusions were done on base of data mentioned above.

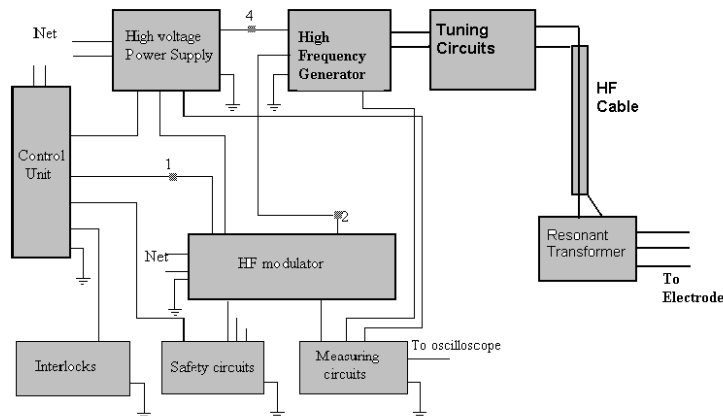
- Specific regime of plasma filamentary HF discharge generation in supersonic airflow has been found. The HF energy input to the individual filament can achieve the value 0.1J at the condition of the experiment.
- The frequency of filament generation can be up to 100kHz. The maximal frequency is realized at condition of supersonic airflow.
- The gas temperature in filamentary HF plasma occurs rather large: up to 4000K at 120Torr of a static pressure.
- Plasma filament diameter at the initial stage of breakdown is not larger than 0.3mm at length up to 30mm.

Plasma temperatures within the discharge were measured using optic spectroscopy, although it should be noted that the measurements of plasma parameters are difficult and present uncertainties due to the strong non-homogeneity of the discharge structure. A small addition of CO₂ was used for the CN generation. The method of processing is found on accurate fitting of experimental and calculated spectra at rotational and vibrational temperatures variation. Such a method has a relatively low accuracy, about $\pm 10\%$. The results are presented in table below for the case of longitudinal DC discharge.

Total Current /pressure	10Amperes	2Amperes
100Torr	5000 \pm 500K	3500 \pm 400K
200Torr	4500 \pm 500K	3000 \pm 400K

Spectrums of CN($B^2\Sigma^+ \rightarrow X^2\Sigma^+$), 2nd positive system of N₂($C^3\Pi_u \rightarrow B^3\Pi_g$) and the first negative system on nitrogen molecular ion N₂⁺ ($\lambda=3905\text{\AA}$) have been measured and analyzed for transversal mode of the surface discharge with different levels of the input power. During the first tests there was found out that the value of rotational temperature in this case much exceeds those for longitudinal discharge. At the same time the rotational

temperature measured by the spectroscopy of neutral molecular nitrogen occurs significantly less than by CN spectra at the same conditions. Under these conditions we have been forced to verify the discrepant data by means the analysis of spectrums of the molecular ions. It was recognized that the temperature of the medium is, at least, 7kK. The later tests verified this result.



The HF generator had been designed and tested. The general layout of the plasma generator's power supply is shown in Fig.1.4.2. The main parts are High Frequency Generator, Tuning Circuits with Transmitting Line and Resonant Transformer. A standard HF generator of 27.4MHz of

frequency and output power up to 4kW has been used for the HF discharge excitation.

The wind tunnel experiments have been conducted under the condition of supersonic airflow in short time blow-down wind tunnel. Several aspects of the problem of flow control by the surface plasma generation are considered. Namely, simplified physical model of the discharge interaction, duct-driven flow modification, shocks position control, shocks reflection control and transonic effects. In accordance with the experimental data and analysis of the situation the following conclusions were done.

- The structured plasma changes the flow parameters on a controllable manner. It occurs due to local heating, shocks generation and plasma induced separation.
- The transversal surface discharge is much more effective than longitudinal discharge in terms of energy input density and flow structure control.
- Global separation in duct-driven flow due to the surface plasma generation has been demonstrated experimentally.
- The energetic threshold for global boundary layer separation is defined in level about $5 \div 8 \text{ W/cm} \times \text{Torr}$ under the conditions of that test.
- The generation of plasma overlayer is the method to control the shocks position near the surface as well as the flow parameters in whole duct.

- Structural (non-homogeneous and unsteady controlled modes) plasma generation allows one to decrease required power for the realization of flow control effect.

The Second Year Efforts.

Two main aspects were aimed by this work and sequentially have been described in the Report on the second year activity: the features of the surface plasma generation in high-speed flow and such electrical discharges influence on the parameters of boundary layer including artificial separation.

The local heat release near the surface in high-speed flow leads to boundary layer separation if the level of power is high enough. Several types of discharges were tested for this mean. Important effect of unsteady flow separation by pulse filamentary transversal discharge was described. From the other side the effective viscous friction reduction at reasonable power deposition requires a consideration of non-thermal mechanisms. There was inferred that non-equilibrium surface plasma can be generated by multi-trace barrier discharge. Such a discharge may effect on the boundary layer parameters under relatively small power deposition. That time we didn't see any technical limitation in manufacturing large plasma panels on the base of multi-trace barrier MFD-HV discharge.

Several schemes of the dielectric barrier discharge generators have been tested for this objective. This plasma generator was designed and constructed for aerodynamic applications on the base of experimental results, obtained during the previous study of pulse periodic discharges, and plasma generator of continuous and modulated HF- discharges. The preliminary data on non-thermal non-equilibrium plasma behavior in high-speed flow was described.

Efforts have been undertaken to observe any electrostatic effect of nonequilibrium plasma on boundary layer integral parameters under high-speed dense flow. The quasi-continuous multi-trace surface barrier discharge was used for the plasma excitation. A specially designed power supply has been utilized. It can be characterized by high frequency of oscillations and triangle shape of initial pulses. In dependence on electrodes configuration and gas parameters the different plasma parameters could be obtained, as a rule, non-equilibrium. As a result, in combined discharge the additional mechanisms for effective control of plasma thermal and chemical processes (such as gas dissociation, secondary emission and gas heating inside the cathode layer) may be realized. Plasma effect on the airflow was observed when using discharge plate with cylindrical profile. Schlieren photos of such a mode are shown on the

Fig.1.4.3. It was well seen that transition zone between subsonic mode of the airflow and supersonic one is shifted down flow when the discharge is switched on (second photo). Nevertheless, such a behavior of the flow structure can be explained by the non-stability of the airflow mode.

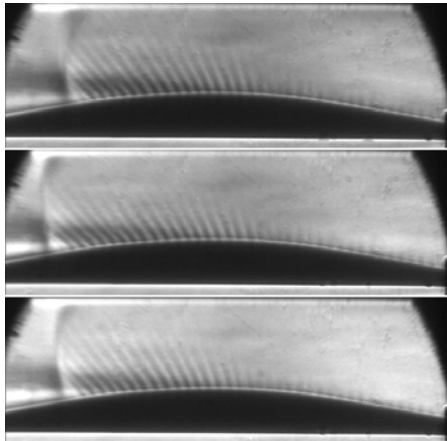


Fig.1.4.3. Schlieren photos of plasma flow interaction. Flow direction from right to left.

A simplified physical model of the interaction was proposed. The transversal surface discharge between flush-mounted electrodes generates relatively equilibrium non-uniform unsteady plasma with significant share of heat deposition. The transversal discharge is an unstable system of relaxation type with hot plasma filaments, which moves with the flow. Such a discharge influences on the flow structure sufficiently. The control of parameters of fixed separation zone behind wall backstep was demonstrated in two years. Two main regimes can be realized: expansion of circulation zone and transformation to separation-less mode. This year a new data on the plasma-flow interaction were obtained.

That time the pulse-repetitive modes of the filamentary spark discharge in airflow were obtained experimentally under the air speed 0 – 500m/s. Photo-ionization and photo-dissociation effects have been detected. Generation of the shock wave was obtained at such influence on the airflow. The test on pulse discharge influence on flow structure under supersonic conditions has been carried out in a renewed test section of PWT-10 facility. It is important that while the plasma channel is excited inflow it moves downstream with a main flow at the same velocity. The plasma influence occurs in a gas portion and the energy release doesn't lead to a dramatic change of the bulk parameters of the flow in duct and to thermal chocking.

Two different modes of the discharge operation have been found in case of separation zone. At the first mode the discharge is excited between electrodes. At the second mode the discharge current is being connected to the metallic wall in separation zone. The fast video shows that the length of plasma “cords” is much more in the case of the second discharge mode, which is reflected in the gap voltage increasing. The sample of photo of the discharge appearance in the separation zone at mode 2 is presented in Fig.1.4.4.

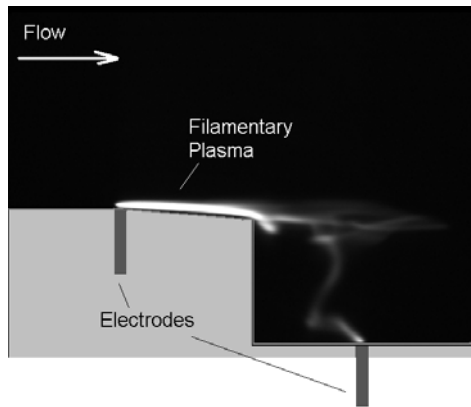


Fig.1.4.4. Surface discharge appearance in separation zone.

A large problem of plasma experiments generally and inflow specifically is the proper measurements of parameters at suitable time and spatial resolution. We paid a special attention to this. The detailed data on plasma parameters were shown in the Report on the second year activity. One of the important problems was in significant improving of measurement's techniques for plasma diagnostics as well as for boundary layer parameters estimation.

The method of spectrum fitting of N_2 Second positive band was applied for gas temperature measurements. Two plasma sources were examined, an arc discharge in the airflow and a dielectric barrier discharge. It was pointed out that filamentary discharge gas temperature depends on the static pressure in separated zone: a higher the pressure leads to raise the rotational temperature in plasma filament, see Table 1.4.2.

Table 1.4.2. Temperature in dependence on pressure.

Pressure in the separation zone.	Temperature of the gas.
100 Torr	$5 \pm 0,1$ kK
220 Torr	$5,5 \pm 0,1$ kK
500 Torr	$6 \pm 0,1$ kK

In the most condensed manner the second year's results can be formulated as following:

- Combined HF-HV plasma generator has been designed in different modifications and tested.
- The plasma generator of filamentary type with corona preionization was designed and tested.
- Structural evolution of plasma filaments at interaction with airflow was studied.
- Measuring system and application software were produced for spectroscopic diagnostic of electric discharges. Main parameters of plasma were measured.
- The experimental apparatus was modified for test on viscous friction and separation control by filamentary and barrier-discharge plasma.
- Short time wind tunnel's runs were fulfilled for study of plasma effect on boundary layer conditions.

- A preliminary analysis of experimental data was done.

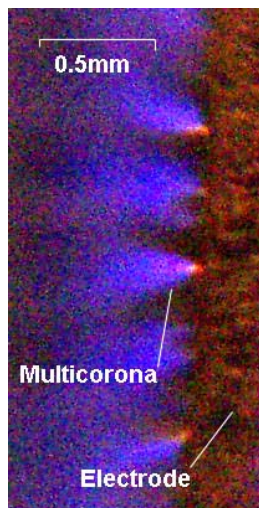
The Third Year Efforts.

After the two-years activity the work was extended with a general aim to study the nonequilibrium plasma effect on separation processes in high-speed flow.

An analysis of aerodynamic situation was executed on the base of available publications. It was shown that the heating and the volume energy supply can increase the stability of the attachment line boundary layer in some temperature range. The estimations demonstrated that the “ion wind” mechanism of drag reduction is ineffective itself. But in some specific cases the electro-hydrodynamic (EHD) effects could be important. One of possible fields is the EHD method application for laminar-turbulent transition control where it may be effective.

A modified experimental arrangement was designed for the further test on separation control at high-speed flow. The resonant type of power supply for DBD plasma panel was designed, simulated and tested preliminary.

The quasi-continuous multi-trace surface barrier discharge was used for the plasma excitation. Two modifications of the electrodes arrangement were tested: symmetric and non-symmetric. There was found out that the structure of such a discharge is non-uniform in micro-scale. Two important problems were studied in that period: fine structure of the multi-coronas discharge and spatial-temporal distribution of the discharge.



The efforts to recognize a fine structure of DBD were done on the base of micro-photographs observations. The Fig.1.4.5 shows a sample of such a photo, which was done by means of extra lens application. As the result the enhanced spatial resolution was obtained, not worse than $\delta=0.2\text{mm}$. In this case the exposure was 1/30sec. The density of plasma spots was measured in dependence on test parameters.

The velocity of the plasma-induced flow was measured by means of analysis of Schlieren images and Schlieren streak video scanning. The registered values of induced speed occurs in a range 1-3m/sec under the experimental conditions. This measurements also show that the velocity is increased when pressure is reduced.

Two types of experiments were being prepared. In the first case the sequences of the friction modification are going to be explored. In the second case an effect of separation control was studied. During the first test a tiny effect of DBD plane plate interaction with

supersonic turbulent boundary layer was observed. To avoid an undesirable shocks reflection and the duct choking this configuration includes the backwise wallstep. As a result the DBD plate locates in area of homogeneous supersonic flow.

The second experiment was conducted in a deeply modified short-duration blowdown wind tunnel PWT-50 of IVTAN with a closed-type of the test section. The tests were done at the following conditions:

- Mach number of undisturbed flow $M=0.1-0.95$;
- static pressure $P_{st} \approx 600-750 \text{ Torr}$,
- Reynolds number about $Re=10^6$ (on the model length),
- Initial boundary layer thickness at on-wall model's location $\delta=0.5-0.7 \text{ mm}$,
- duration of steady-stage operation $0.2-0.5 \text{ sec}$,
- typical air mass flow-rate through the duct about $G \approx 0.5 \text{ kg/sec}$.

Two different power supplies are used for DBD discharge excitation. The first one generates triangle bipolar pulses with frequency $f=100-200 \text{ kHz}$ and power density up to $W=20 \text{ W/cm}^2$. The second one is built on the resonant scheme and differs from the previous one by more effective adjustment with the plasma panel in particular test. The experimental testing of the schemes was done with the DBD load. The first device allows obtaining a large peak power. The second power supply demonstrates a good adjustment with DBD panel and relatively low level of EM noise.

Two methods are mainly exploited for the registration of the flow structure, namely, the Schlieren shadow method and measuring of the pressure distribution. Several methods give the additional information: Preston tube data downstream plasma area, pressure distribution measurements in test section, monitoring of transonic shocks position (under transonic mode), monitoring of separation line. A few original methods were designed specifically for these experiments. The method of Schlieren streak scanning gave the value of flow velocity on the base of analysis of disturbances moving. A fine structure of flow at weak shock reflection from the wall depends on boundary layer conditions. The level of flow disturbances in boundary layer was recorded by means of diode-laser based Schlieren technique.

The experiments on separation control were done at zero angle of attack $\alpha=0^\circ$ and significant inclination $\alpha=12^\circ$. Tests were performed under different velocity of the flow in a range $10-40 \text{ m/s}$. Sequence of separation zone visualization photos is shown in Fig.1.4.6.

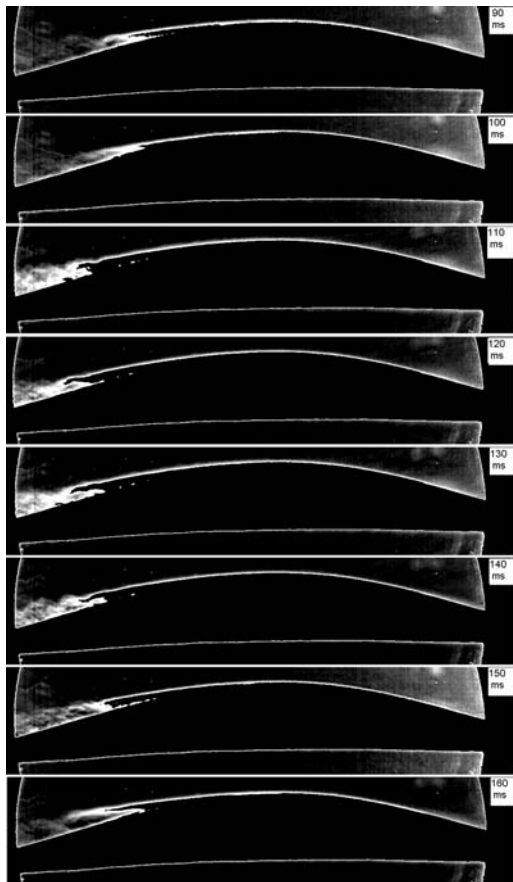


Fig.1.4.6. Schlieren photos under the DBD operation. Flow from right to left.

Discharge was turning on at 100ms from the start of the flow and it is turning off at 150ms. So, the first frame with the DBD is related to 110ms point. It is well seen that separation line changes its position after the discharge turning on. In the case of attack angle $\alpha=0^\circ$ there was an obvious the effect dependence on flow velocity (the pressure in vacuum tank), namely, the lower the pressure the wider the separation zone. The measurements of DBD effect on pressure in separation zone were also done at different conditions. The EM noise was rejected by

formalized procedure. It was easy to recognize that the DBD effect is not valuable but noticeable. It was appeared in some increase of the pressure in separation zone under the DBD operation. The procedure of data averaging was applied for estimation of the value of pressure increase ΔP . It was found out that ΔP is almost independent on the initial flow velocity and the model orientation and it was from $\Delta P=+0.12\pm0.8\text{Torr}$ up to $\Delta P=+0.6\pm0.5\text{Torr}$ for different realizations (runs). The accuracy of those measurements was limited by gasdynamic and electromagnetic noise.

Computational analysis was fulfilled to explain some features of the interaction in plasma-flow system. The surface discharge effect on supersonic airflow was simulated on the base of Euler and Navier-Stocks equations. It was noted that simplified models did not give satisfactory agreement with experimental data. The periodic DBD discharge influence on BL properties was simulated on the base of EHD approach. Important predictions were done on the magnitude of BL modification.

The analytical and experimental efforts in frame of the third year activity yield the following results:

- Analysis of aerodynamic consequences and DBD (surface type) properties was done on the base of available publications.
- The statement of the problem for the electric discharge effect numerical simulation was executed. Numerical simulations of surface discharge and periodic DBD effect on the conditions in BL were made. They gave non-trivial results in flow velocity profile near the surface.
- The “ion wind” mechanism of drag reduction is ineffective itself. But in some specific cases the EHD effect could be important.
- A new experimental data on the DBD properties in ambient air and airflow were obtained and described. The velocity of plasma-induced flow was measured in dependence on pressure by newly developed technique (Schlieren streak scanning).
- Deeply modified experimental arrangement was prepared for the supersonic test on BL modification and transonic test on separation control at high-speed flow. Experimental technique was enhanced.
- Measurements of rotational and vibrational temperature of DBD plasma were fulfilled. As it was expected the vibrational temperature occurs much larger then rotational one: $T_v \approx 2200K \gg T_{tr} \approx 350K$. On the base of general information the parameters of DBD plasma were estimated.
- Method of the separation zone visualization on the base of Schlieren device with sequential images' processing was tuned and tested.
- The DBD effect on the shape and position of separation zone were studied in dependence on test conditions. The separation line shifts the position downstream in about 10% of the model length.
- A small effect of the DBD on pressure in separation area was found out: level of the pressure increases in about 0.5Torr at one-atmospheric conditions.
- DBD influence on flow disturbances in separation zone was studied. The frequency of disturbances $f=1-5kHz$ depends on the flow velocity closely to the linear law.
- The data analysis was performed for three-year activity. The present Report was prepared and issued.

2. Results.

2.1. Experimental Facility Description.

The experimental facility contains following main parts:

- Gasdynamic facility PWT-10/PWT-50;
- Plasma Generators of different types;
- Measuring and control systems.

2.1.1. Gasdynamic Facilities PWT-10 and PWT-50.

Installation PWT-10 of IVTAN has been designed for short time runs under the conditions of supersonic and transonic airflow. The draft-scheme of the PWT-10 setup is shown in Fig.2.1.1.1.

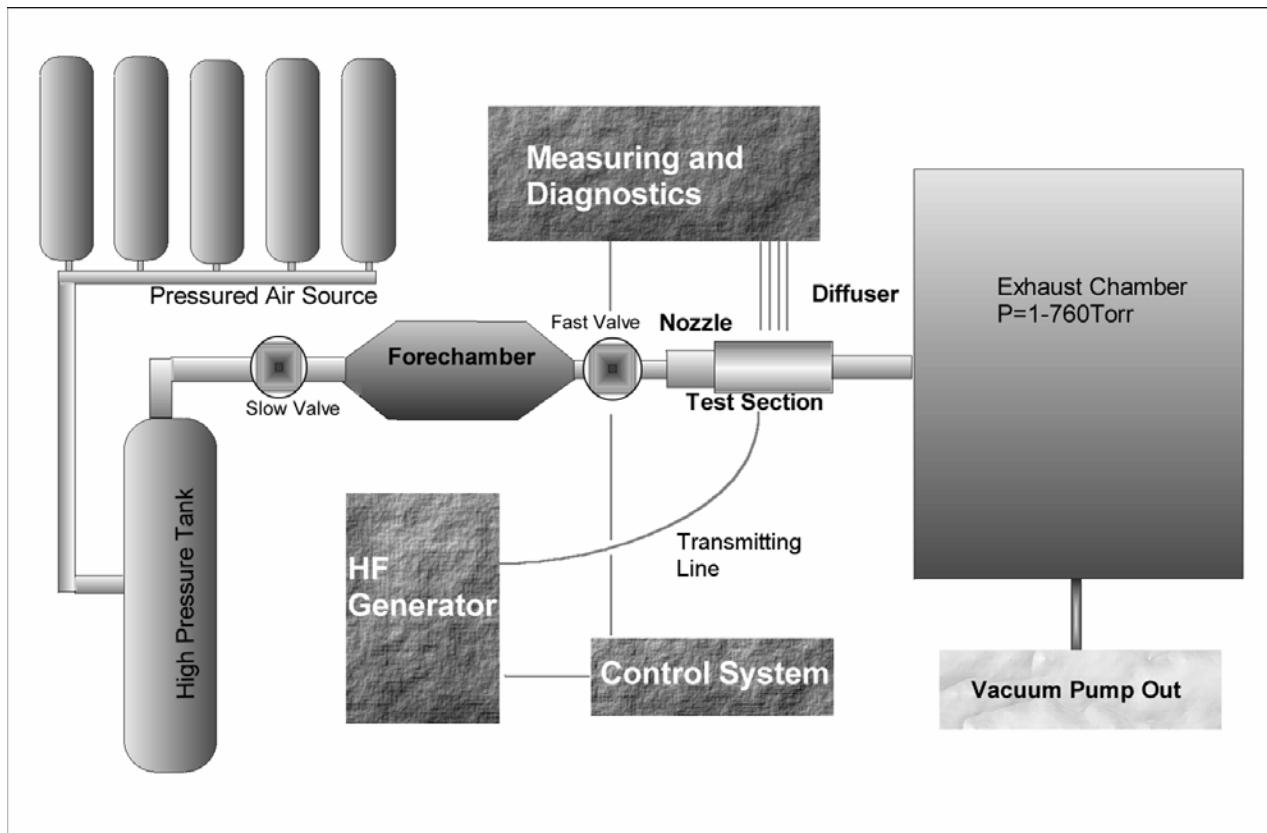


Fig.2.1.1.1 Layout of experimental setup.

The gas-dynamic duct contains the following main components.

- High-pressure tank;

- Fast valve with electromagnetic drive;
- Supersonic nozzle;
- Test section;
- Diffuser;
- Low-pressure tank.

High-pressure tank has volume 0.1m^3 and working pressure 1-5atm. It is connected to the fore-chamber of the test section by a fast valve and stainless steel tube and with suppliers of pressured air. Key component of the setup is the fast valve with cross-section 50mm and electromagnetic control. Two parallel lines can provide a pressured air: balloon's line and compressor's one. Compressor gives maximal pressure up to 5atm. Balloon contains pressured air at pressure up to 150atm. Pressure reductor is used on this line. The valve is used at non-standard configuration with a response time about 10ms. An adjusting tube is needed to provide a homogeneous distribution of gas velocity on a cross-section. Its input cross-section has diameter 50mm and rectangular output has dimensions $20 \times 50\text{mm}$. A general photo of the PWT-10 facility is shown in Fig.2.1.1.2.

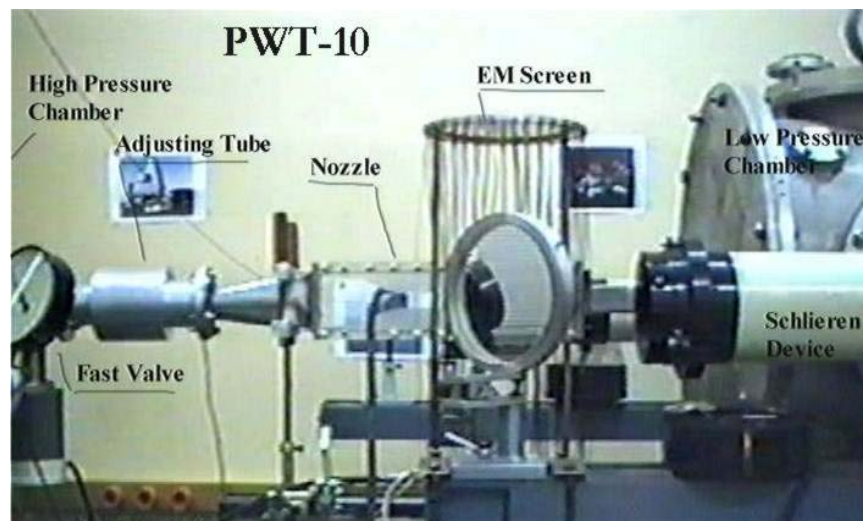


Fig.2.1.1.2. Photo of PWT-10 facility (2002).

A plain nozzle is utilized for Mach number $M=2$ airflow generation. Dielectric test section has a rectangular cross-section with dimensions $20 \times 50\text{mm}$. Vertical (long) walls are made from quartz glass. Horizontal walls are made from organic glass. TS has length about 200mm. Simple diffuser is used between TS and vacuum chamber. Vacuum chamber has volume about 0.63m^3 . Summarizing above, the experimental facility PWT-10 has the following characteristics in supersonic operation mode:

:

❑ Cross-section of airflow	20×50mm,
❑ Length of test section	200mm,
❑ Typical gas flow rate through duct	0.1kg/sec,
❑ Maximal gas flow rate	0.2kg/sec,
❑ Time duration of steady stage	0.2÷0.5sec,
❑ Mach number	1.7÷1.99,
❑ Static pressure in airflow	100÷350Torr,
❑ Reynolds number	$Re=(4\div 10) \times 10^6 \times L$,
❑ Boundary layer thickness	$\delta=0.5\div 1\text{mm}$.

The photo of the test section for supersonic operation mode is presented in Fig.2.1.1.3.

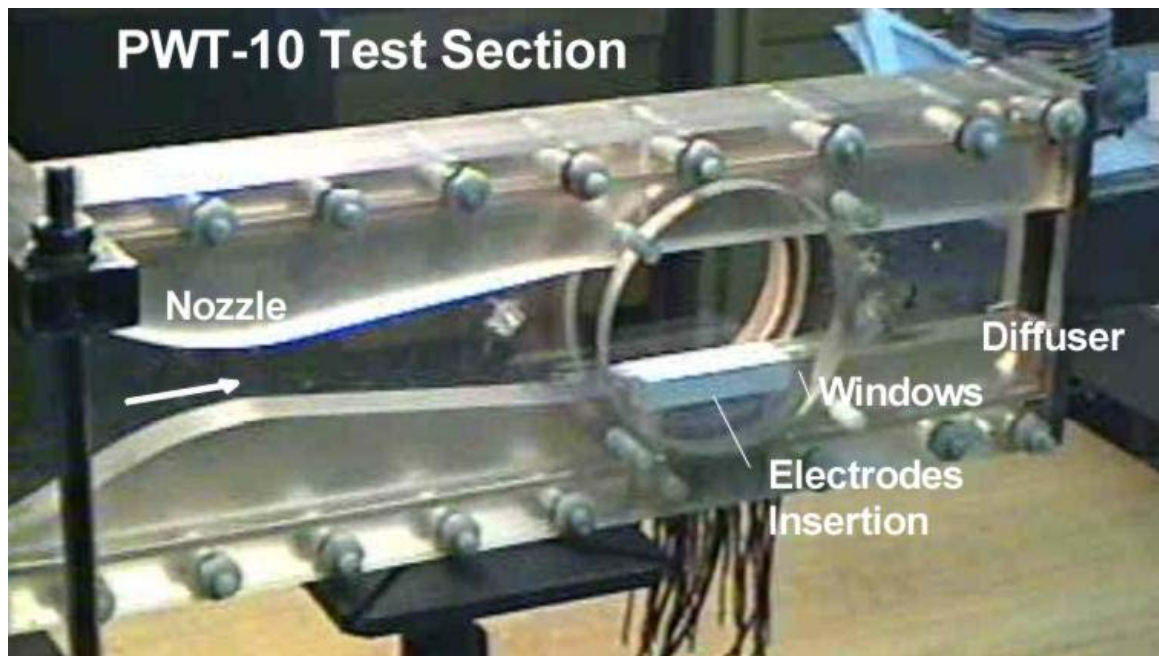


Fig.2.1.1.3. Photo of PWT-10 dielectric test section (2002).

Subsonic operation mode can be realized easily in described test section at ratio between pressure in fore-chamber and vacuum chamber less than 4. The second way is to use the special subsonic test section. It is differed from the supersonic one by wider size of cross-section and another profile of the main nozzle. Subsonic operation mode characteristics are the following ones:

❑ Cross-section of airflow	up to 40×50mm,
❑ Length of test section	200mm,
❑ Typical gas expense through duct	up to 0.3kg/sec,
❑ Time duration of steady stage	0.3÷1.0sec,

- Mach number $0.02 \div 0.85$,
- Static pressure in airflow $300 \div 750 \text{ Torr}$,
- Reynolds number $Re = (0.1 \div 8) \times 10^6 \times L$,
- Boundary layer thickness $\delta = 0.2 \div 1.5 \text{ mm}$.

The test section of PWT-10 was equipped by the electrode system, spectroscopic windows, Schlieren system, different sensors, including the set of pressure transducers of scanner assembly. The supersonic operation mode is realized in the test section, which has the typical pressure transducers' arrangement shown in Fig.2.1.1.4. The arrangement is adjusted every time for the specific aims of the each test.

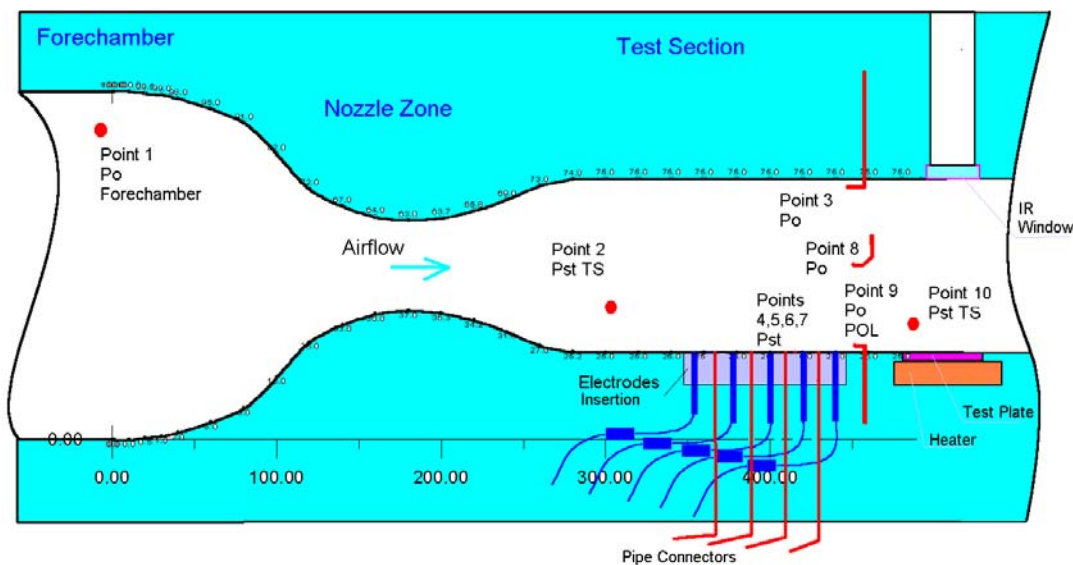


Fig.2.1.1.4. Supersonic test section equipment.

The facility PWT-10 was deeply modified to the installation PWT-50. The objective of this modification was in to diminish an influence of the lateral walls BL on the results of measurements. The cross-section of the test section was increased up to $A=72 \times 72 \text{ mm}$. A principal scheme of the facility PWT-50 is shown in Fig.2.1.1.5.

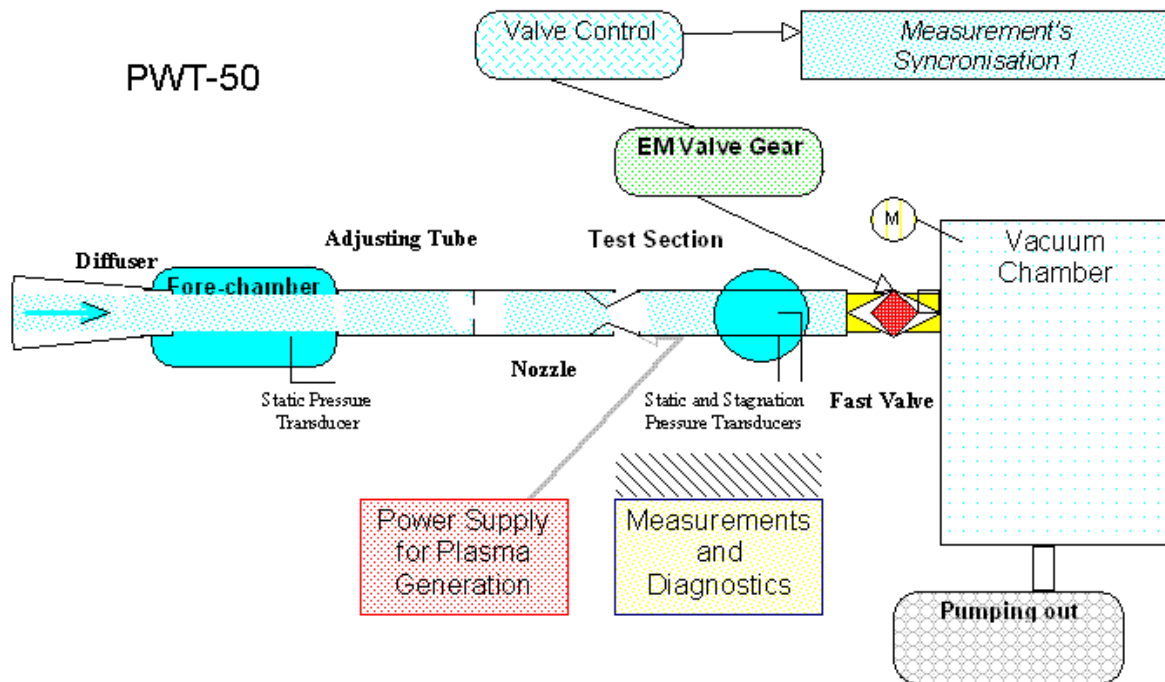


Fig.2.1.1.5. Layout of facility PWT-50.

The modified facility PWT-50 is characterized by the following parameters in subsonic operation mode:

- | | |
|--|--|
| □ Cross-section of airflow in test section | 72×72 / 57×72mm, |
| □ Length of test section | 400mm, |
| □ Typical gas flow rate through duct | 0.1kg/sec, |
| □ Maximal gas flow rate | 0.5kg/sec, |
| □ Time duration of steady stage | 0.5÷1sec, |
| □ Mach number | 0.03÷0.4, |
| □ Static pressure in airflow | 400÷750Torr, |
| □ Reynolds number | $Re=(0.2\div1) \times 10^6 \times L$, |
| □ Boundary layer thickness | $\delta=0.5\div1$ mm. |

The photo of PWT-50 facility with subsonic test section is shown in Fig.2.1.1.6. The experiments were done with the DBD plasma panel in different configurations. The description of the experimental models and power supplies is presented below.

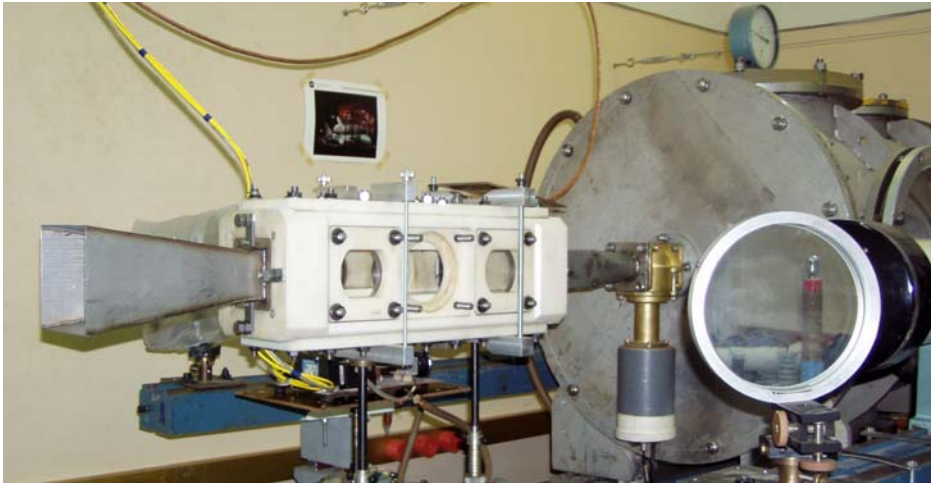


Fig.2.1.1.6. Photo of PWT-50 with subsonic test section.

The alteration of the flow velocity was executed by means of adjustment of the initial gas pressure in the low pressure tank. An appropriate dependence of the flow speed on the pressure is shown in Fig.2.1.1.7.

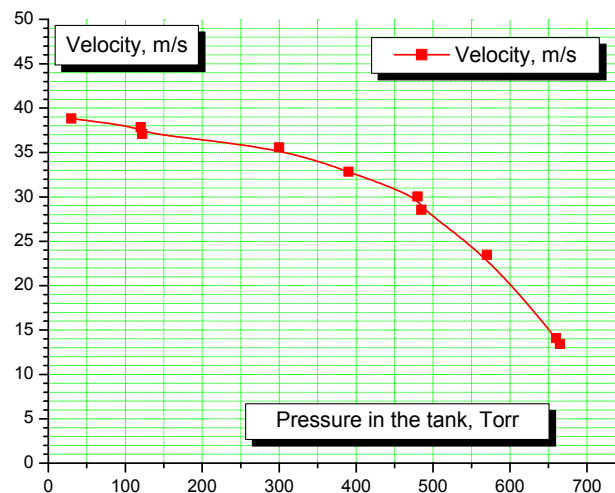


Fig.2.1.1.7. Flow velocity in subsonic test section of PWT-50 vs pressure in the tank.

Methods of Measurements.

The test sections of the pulse wind tunnels PWT-10 and PWT-50 were equipped by the following devices for a measurements and diagnostics:

- Pressure sensors “Honeywell™” for measurements of airflow parameters in a test section.

Response time of them is less than 1ms. Static pressure is measured in several points

along the test section near the wall. The sensor of stagnation pressure connected with Pitot pipe, which can moved across the cross section.

- Electronic pressure scanner ESP-32 for 32 channels of the pressure measurements and PCMCi interface. The characteristic response time is down to 0.3ms for the each channel.
- Data acquisition system on base of “National Instruments”[®] equipment.
- Fast digital video camera with PC control.
- Fast digital line-scan camera with PC control.
- Spectroscopic system of “LOT-ORIELTM”: quartz fiber optic transmitting line, polychromator, CCD-camera, special board and PC computer with the original software.
- Schlieren-system, allowing to visualize the flow with separation under investigation of the needed phase of a process;
- Schlieren system on base of double laser beam sensoring;
- Electrical current and voltage sensors, including symmetric dividers, current shunt, filters and digital oscilloscopes “Tektronix TDS-210” and HP-5062. They are connected with computer by GPIB serial interface.
- Synchronization system on base of pulse generators and fiber optic transmitting lines.

The special attention is paid for the following experimental parameters measurements:

- Bulk flow parameters, including level of turbulence;
- Shocks position monitoring;
- Boundary layer thickness and condition on the DBD plasma panel;
- Position of separation line on a contoured plate;
- Level of pressure pulsation near the surface;
- Plasma parameters.

The boundary layer thickness is estimated on the base of data of well-tuned Schlieren visualization (see the next section). A visualization of the separation is being done on base of processing images from the Schlieren device. Level of the pressure pulsation is measured by the fast-response small pressure sensor “KuliteTM”.

Following plasma parameters were measured by the appropriate methods:

- Input electric power was recalculated on the base of voltage-current measurements (see sections 2.1.5, 2.2.2 and 2.3.3). “PSpiceTM” software is utilized for the scheme simulation.

- Plasma temperature (T_e , T_v , and T_g) is measured by optical spectroscopy with exploiting of original processing software.
- Plasma radiation distribution is visualized by fast video-camera and line-scan camera with high spatial resolution. Original software for the image processing is used.
- A thickness of the plasma layer is measured on self-radiation visualization by video-camera with a special lens.

Two methods are mainly exploited for the registration of the flow structure, namely, the Schlieren shadow method and measuring of the pressure distribution. Several methods give the additional information: Preston tube data downstream plasma area, pressure distribution measurements in test section, monitoring of separation line.

A few original methods were designed specifically for these experiments. Some of them were tested last time. The level of flow disturbances in separation zone is recorded by means of diode-laser based Schlieren technique.

2.1.2. Schemes of Electric Discharges Tested.

Several standard aerodynamic situations were explored. Among of them the following ones are described in this Report:

- Transversal surface quasi-DC discharge in supersonic duct;
- Quasi-DC filamentary discharge near backwise wall step;
- Surface distributive dielectric barrier discharge (DBD) on plane plate in high-speed flow.

Rough schemes of the test section arrangement in these cases are presented in Fig.2.1.2.1. The first situation was studied in details during the first year of the project mainly and reported in the Section 2.2. The results of the experiments for the second configuration were published during last three years. But some new data was obtained recently. These data are also presented in section 2.2. In the third configuration the thin plain/contoured plate with DBD plasma panel was installed in the test section, perpendicular to optical windows. Appropriate data are presented in the Section 2.3.

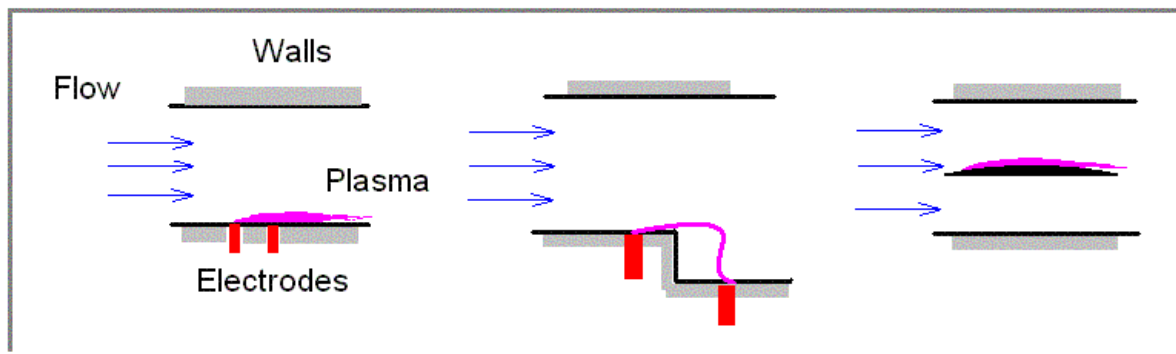


Fig.2.1.2.1. Layout of standard aerodynamic configurations.

In the first and the second configurations the High Frequency filamentary discharge and quasi-DC discharge were utilized. In the third position the DBD plasma was excited near the model's surface.

HF Filamentary Discharge.

The general layout of the high frequency (HF) plasma generator's power supply is shown in Fig.2.1.2.2. Main energetic parts and optional parts can be marked out. The main parts are High Frequency Generator, Tuning Circuits with Transmitting Line and Resonant Transformer.

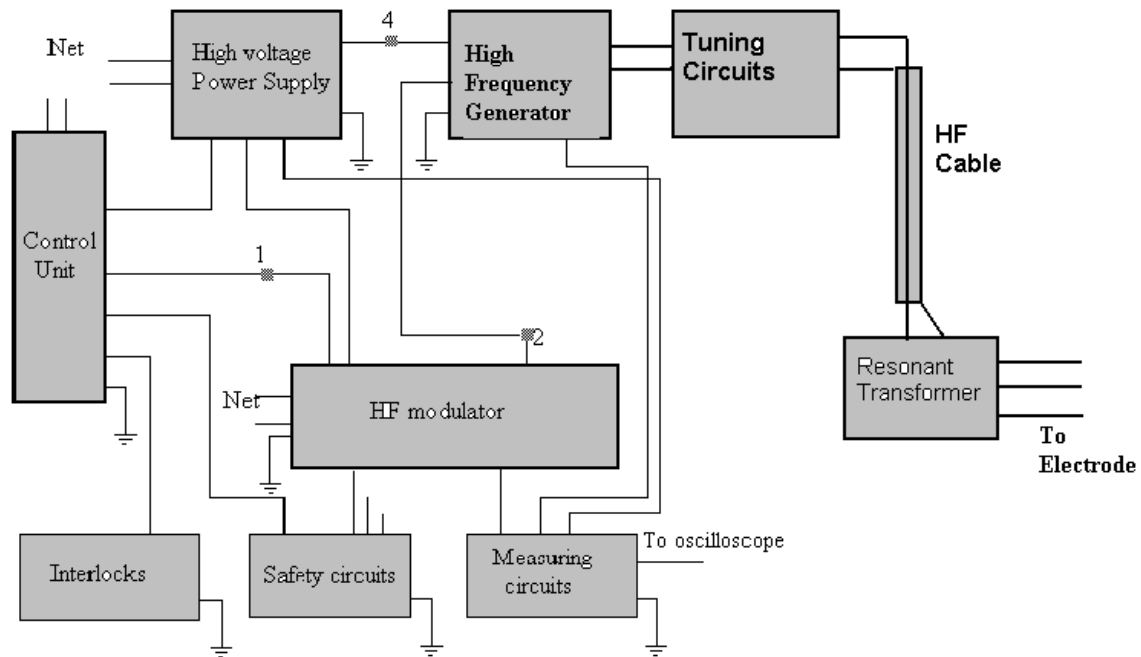


Fig.2.1.2.2.General Layout of HF Power Supply and Connections

A standard HF generator of 27.4MHz of frequency and output power up to 4kW has been used for the HF discharge excitation. Self-excited oscillator consists of powerful triode GU-58B and resonance cathode circuit. Variable capacity de-couples self-excited oscillator and output circuit. A modulation of HF power is used for the proper synchronization of plasma object and measuring system as well as to avoid a transformation of the discharge to torch type. The modulation has to occur at frequency about 100Hz, pulse duration $\geq 1\text{ms}$ and depth up to 100%. Electronic modulator is designed on a scheme of a cathode current interruption. Transmitting line has been modified by means of installation special cones on the both ends of the transmitting cable.

The first scheme of the electrodes configuration is shown in Fig.2.1.2.3. Such a type of electrodes system was applied for excitation of distributive surface discharge in experiments on plasma influence on parameters of viscous friction and generation of artificial separation

zones. The high frequency power generator was used as a primary source of the resonant contours supplying with the following parameters.

- | | |
|--|--------------|
| □ Frequency of wave | 27.4 MHz; |
| □ Typical output voltage | 5-7kV; |
| □ Maximal output power of HF generator | up to 4kW; |
| □ Amplitude modulation | up to 100Hz; |
| □ Type of transmitting line | cable. |

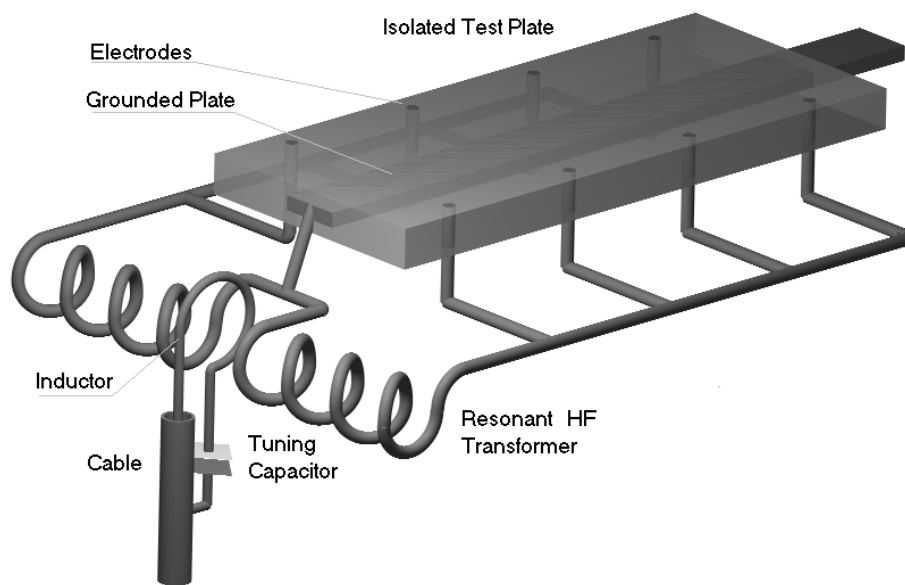


Fig.2.1.2.3. Generalized scheme of the electrodes system.

The HF generator is equipped by the elements of tuning and adjustment with the transmitting line. The transmitting line is special HF cable of relatively large cross-section of central wire. It is loaded by the resonant contour. The resonant inductor (contour) contains the capacitor and actual inductor. The last is one/two turns coil made from copper tube to diminish the skin-effect. The inductor is coupled inductively with the coil, which consists of two symmetric parts. This dual coil supplies two lines of electrodes with a single isolated grounded electrode. The wires inductivities divide the individual electrodes electrically. Note, that 1uH inductivity (less than 1m of direct wire length) is equivalent to resistivity $R_L=170\Omega$.

The HF voltage was applied between the distributed electrodes and isolated grounded plate transversally in respect of approach airflow. The equivalent length of the coil is less than $\lambda/4$ even if the system is loaded by the plasma. It means that the voltage between two lines of

electrodes is summarized and redoubled at no-load operation. Such an effect might stabilize the discharge structure.

The second electrodes configuration scheme is presented in Fig.2.1.2.4. This is actually a single-electrode scheme.

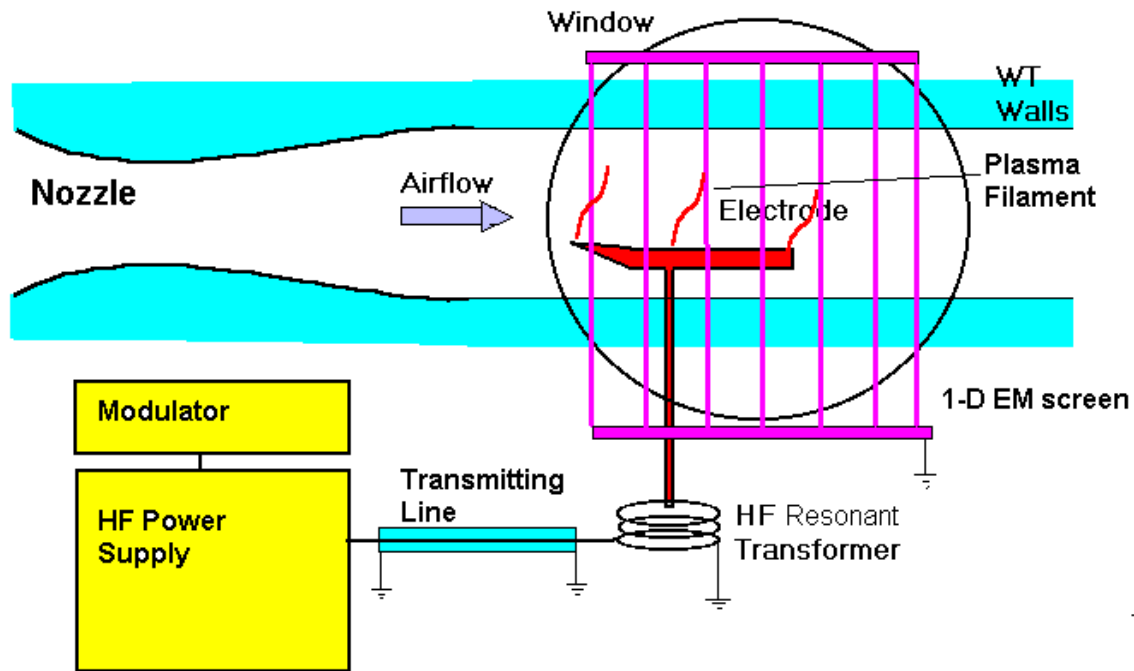


Fig.2.1.2.4. Principal scheme of the experiment with HF discharge excitation by single electrode.

A HF resonant transformer produces the high voltage for initiation of the discharge. Transmitting line (long cable and tuning elements) has a resonant characteristic. The system has a falling volt-ampere characteristic that stabilizes the discharge current. One dimensional copper screen is used to decrease an EM noise.

The standard electrode is a copper cylinder with a sharp fore part and blunted base part. A nose part of the electrode was slightly bent up. The length of electrode was about 50mm. It was connected with HF transformer in first 1/3 part of the length. It was located inside a test section at 10mm above a lower wall of WT.

Two systems for synchronization of PWT-10 operation and measuring devices have been used. The first system gives a signal when the main valve opens. It uses a relay contacts and pulse generator, which applies for needed delays. The second system has been used for a more exact synchronization with the streamer appearance. It consists of a well-collimated optical sensor (on a base of photo-multi-amplifier), threshold pulse generator and a pulse generator for a time delay. The photo sensor was collimated on the area 10-20mm above the middle

point of the electrode. The threshold scheme allows us to define exact time of the most powerful streamers' existing.

The HF discharge configuration and structure depend strongly on static pressure. Tuning of the transmission line has less influence on the discharge type but has to be done for an enough input power. Without HF power modulation the discharge quickly transforms to an arc/torch. Low static pressure $P_{st} < 100 \text{ Torr}$ leads to a glow HF discharge form. The torch type (single-electrode arc), streamer type (short length streamer corona), filamentary type and theirs combination can be observed at middle range of static pressure. The plasma filaments sometimes start not from metallic surface but from plasma of torch discharge downstream. We will describe only filamentary type of HF discharge as the most prospective.

A typical photo of plasma filament in high-speed airflow is shown in Fig.2.1.2.5. The plasma filaments propagate from electrode into the flow and grow to about 5cm before being swept downstream. Shadow-graphs show the remnants of streamers degenerating into turbulent patches as they are swept away. Observation of photos, shadow photos and time resolved luminosity show that the only one plasma filament exists in a field at standard mode.

Several important notes regarding the construction of the electrodes system and the method of power supplying have to be done. We were exploring the HF type of the discharge due to two main reasons. The first of them is that the capacitive HF discharge, as a rule, can be characterized by the large level of local reduced electric field E/N , i.e. the HF plasma is non-equilibrium and more active in terms of plasma chemistry. The second reason is that the electrodes for the HF discharge excitation can be isolated from the gas, prospectively. It is important for the further development to avoid the surface material and electrodes erosion.

The HF discharge can exist in different forms in dependence on external conditions. The general understanding now is that at high-speed (Mach number in a range $0.1 < M < 10$) and high-density airflow (pressure $0.1 < P < 10 \text{ Bar}$) the conventional types of electrical discharges are transformed to filamentary form. The individual plasma channels move in airflow with the velocity, which is close to airflow velocity. At the same time the filaments' penetration speed at the discharge initial breakdown is much more.

The process of HF discharge channel appearance and propagation looks as follows. At the positive half-period of the applied voltage a streamer is appeared at point of electrode. This streamer leaves a trace of excited and ionized gas after itself. Under the next positive half-periods the waves of ionization and excitation are propagated along this trace. These waves can be treated as the secondary streamers. Their difference from the streamer in its

classic foundation is that they propagate in previously disturbed, ionized media. The secondary streamers form brighter main channel of the discharge, which develops with velocity less than the streamer's one sufficiently. This process of HF discharge developing resembles the development of long spark. The role of leader is played by the main channel of HF discharge and the streamers in the vicinity of the main channel form the streamer zone, as in the case of long spark.

At the condition of high-speed flow the displacement of plasma filament and, sequentially, root part of the filament downstream takes place. The length of plasma channel grows up. Luminosity rises. Secondary streamers generation from the old filament ahead of airflow occurs as well as the turbulization of root part downstream. Finally the displacement of root part of filament to the next electrode below takes place. At this time the voltage on the first electrode jumps and the next plasma filament is generated.

Sample of the HF single electrode filamentary discharge appearance is presented in Fig.2.1.2.5. Here a frame of video-record and the Schlieren photo are shown. Well seen that such a low-energetic plasma filament disturbs the flow locally.

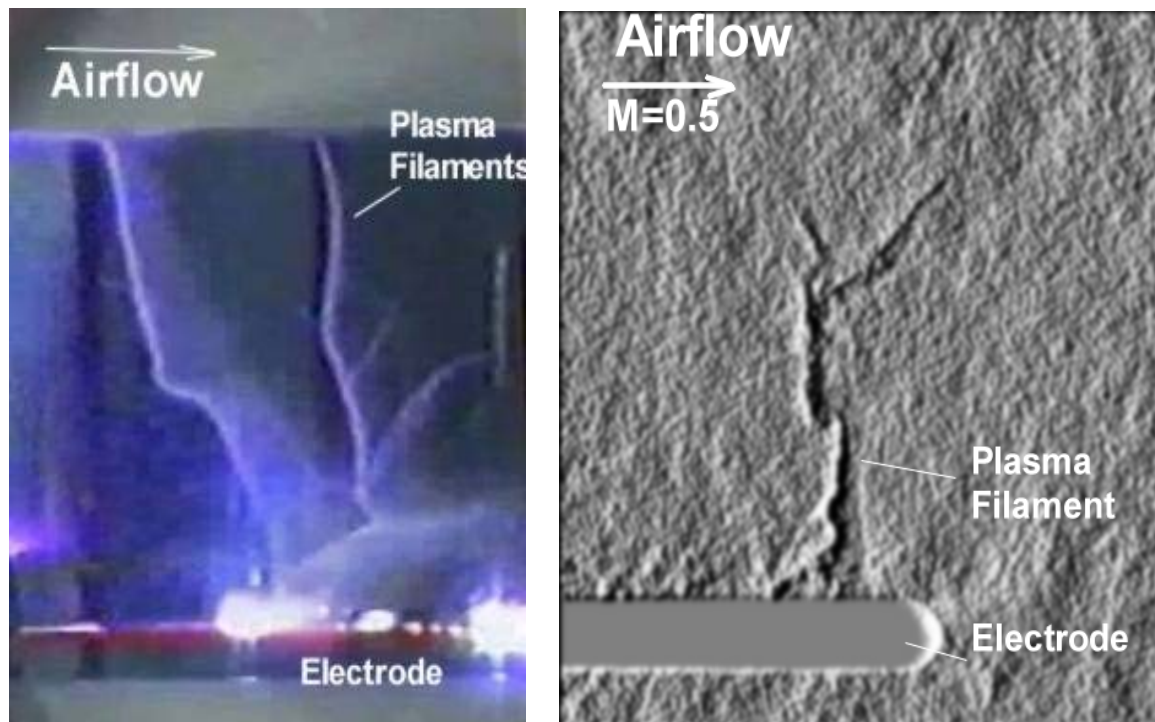


Fig.2.1.2.5. Single-Electrode HF Discharge Appearance in High-Speed Flow.

Video-record and Schlieren photo.

The HF plasma filaments move together with the airflow downstream. When the root part of the individual plasma channel goes away from the electrode the generation of new one occurs on the tip of the electrode. The next plasma filament repeats the way of the previous

one. In such a method the burst of plasma filaments takes place. A frequency of the process is corresponded to a characteristic gasdynamic time on the length of the electrode $F_{pl} \approx l_{el}/V$. Such a process is well seen in oscillogram in Fig.2.1.2.6. The plasma luminosity recorded by collimated photo-sensor is presented. Here the frequency of plasma filaments' appearance is about $F_{pl} \approx 10\text{kHz}$.

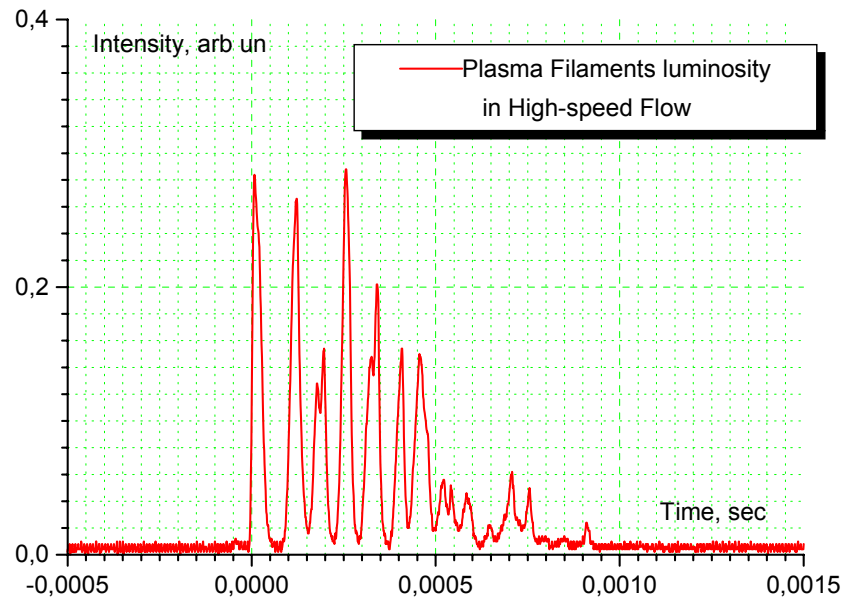


Fig.2.1.2.6. Radiation of burst of HF plasma filaments.

Though the single-electrode HF discharge is investigated for a rather long period of time, many aspects of this phenomenon are faint up to now. Among the types of single-electrode HF discharge only the HF torch discharge is investigated relatively well and has its mathematical model. As for the type of single-electrode discharge, which was named HF streamer (or – flash, spark) discharge, it has no self-consistent physical model. The reasons for such situation arise from very complicated sequence of processes, which underlie the mechanism of HF plasma channel propagation. Another reason for difficulties in a single-electrode HF discharge physics comprehension is that HF channel growth takes place under the voltage amplitude which is sufficiently less than that needed for conventional pulse discharge of the same channel length. High frequency allows to reduce noticeably the “burning” voltage, but at the cost of noticeable decreasing of general velocity of channel growth. Thus, the range of HF channel growth in air spans from 10^4cm/s to 10^7cm/s (carrying frequency 10 – 50MHz) in contrast with DC pulse discharge, which has the lower limit in channel propagation of order of 10^7cm/s .

For general characterization of the channel parameters (especially for the root domain) several scales of time for HF pulse duration of conditional HF voltage level can be (also conditionally) outlined:

- Several microseconds, up to $10\mu\text{s}$ – highly non-equilibrium plasma without noticeable gas heating.
- From $10\mu\text{s}$ to $300\mu\text{s}$ - non-equilibrium plasma with noticeable gas heating.
- Over 1ms – thermal plasma in a channel.

Taking into account that the condition of the HF discharge generation is high-speed airflow and that the electrodes typical dimension is a few centimeters we can consider that the time scale of the phenomena is $10\text{-}100\mu\text{s}$. Thus the HF plasma channel is non-homogeneous object.

The study of the HF discharge behavior in high-speed flow has given an important information for the further development. From the other side in that case the HF filaments propagate into the flow perpendicularly to the surface and cannot be applied for the BL modification. As the result the idea of HF multi-filamentary near-surface discharge excitation was transformed to application of dielectric barrier surface discharge as a more suitable for the objectives of this work (see section 2.3).

Reference to Subsection: S. Leonov, V. Bityurin, Y. Kolesnichenko “Dynamics of a Single-Electrode HF Plasma Filament in Supersonic Airflow”, AIAA-2001-0493, 39-th Aerospace Meeting, 8-11 January, 2001, Reno, NV.

Surface Discharge of Relaxation Type.

The second base for the consideration is quasi-DC surface discharge of relaxation type. The typical photo of such a discharge appearance is presented in Fig.2.1.2.7. The detailed information is put to the section 2.2.1.

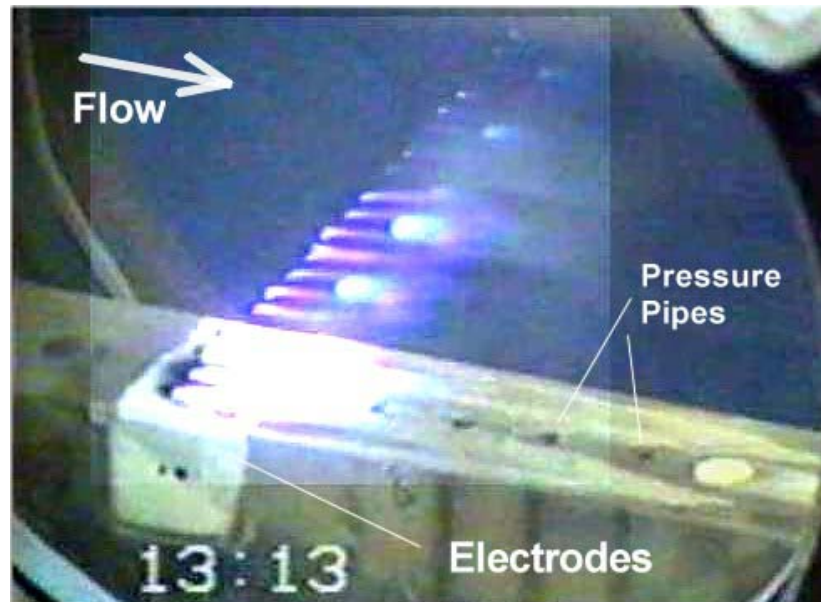


Fig.2.1.2.7. Quasi-DC surface discharge appearance under supersonic flow.

Plasma generation occurs by means of surface multi-electrode distributive electric discharge at two different modes: longitudinal and transversal. It provides energy release to airflow as well as change of gas-kinetic and electro-magnetic properties of the medium. The behavior and properties of the electric discharge in airflow are sharply different from ones in static ambience. The experimental data on plasma generation near the body's surface and influence on parameters and volume of stabilized separation zone downstream of wall step have been reported recently [2-4]. Some data on the surface discharge in free stream was presented in paper [1].

Original power supply was used for plasma generation. The anodes had individual excitation to provide similar conditions for each one. The positive ("hot") electrodes have been located upstream in respect of grounded electrodes at distance 10mm for the longitudinal operation mode. One of the peculiarities of this mode of the discharge is that the current connects from the anodes to the ground with separate "cords" along the velocity vector. Current sharing between the electrodes pairs has been measured as negligible. In the case of transversal discharge a relaxation type of the plasma generation process took place. An initial plasma filament is being blow down, breaking and starting again in about 10 μ s.

The time behavior of voltage-current-radiation characteristics of two modes is sufficiently different too. Longitudinal discharge, as a rule, has a low level of the parameters' amplitude modulation, typically on the level a few percent in the gap voltage. Oppositely this the transversal discharge is characterized by large level of modulation of the main parameters, including gap voltage, resistivity, radiation and the position of downstream edge. Large level of fluctuations in discharge parameters can be related to the filamentary plasma instability, which is due to interaction with high-speed airflow. A very close correlation between the voltage and radiation modulation has been observed and published recently [4].

Special attention has been paid to the problem of effective method of electric energy input to the plasma. In terms of this viewpoint the transversal mode of the surface discharge is more effective than longitudinal one.

Two different electrodes arrangements of quasi-DC surface discharge have been applied: on the plane wall and upstream the backwise wall step. They are discussed in section 2.2 both.

References to subsection.

1. S. Leonov, V. Bityurin, K. Savelkin, D. Yarantsev "Effect of Electrical Discharge on Separation Processes and Shocks Position in Supersonic Airflow." 40th AIAA Aerospace Sciences Meeting & Exhibit, 13-17 January 2002 / Reno, NV, AIAA 2002-0355.
2. S. Leonov, V. Bityurin, A. Klimov, Yu. Kolesnichenko, A. Yuriev "Influence of Structural Electric Discharges on Parameters of Streamlined Bodies in Airflow", AIAA-2001-3057, AIAA 32nd Plasmadynamic and Laser Conference, June, 2001, Anaheim, CA.
3. S. Leonov, V. Bityurin, N. Savischenko, A. Yuriev, "Influence of Surface Electrical Discharge on Friction of Plate in Transonic Airflow". AIAA-2001-0640, 39th AIAA Aerospace Meeting and Exhibit, 8-11 January, 2001, Reno, NV.
4. S. Leonov, V. Bityurin, K. Savelkin, D. Yarantsev "The Features of Electro-Discharge Plasma Control of High-Speed Gas Flows." 33th AIAA Plasmadynamics and Lasers Conference, 20-23 May 2002 / Maui, Hawaii, AIAA 2002-2180.

Dielectric Barrier Discharge (Surface type).

In this work the quasi-continuous multi-trace surface barrier discharge is used for the plasma excitation. Two modifications of the electrodes arrangement were tested: symmetric and non-symmetric. There was found out that the structure of such a discharge is non-uniform in micro-scale. The Fig.2.1.2.8 shows the fine structure of plasma near surface in case of non-symmetric (A) and symmetric (B) base electrodes location. The size of electrode trace is 1mm and camera shutter is 30mcs. At good temporal and spatial resolution it looks like a multi-filamentary structure.

In the first case the gas obtains an additional directed impulse, in the second case the boundary layer is affected by periodic pressing forces. Directed flow generation near the surface due to non-symmetric discharge is well seen in sequence of Schlieren images. Resulting velocity can be calculated on the base of position of disturbances correlation (see section 2.3.6).

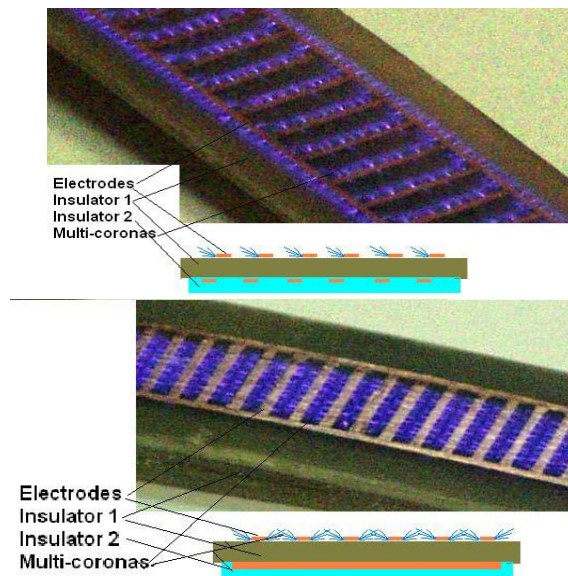
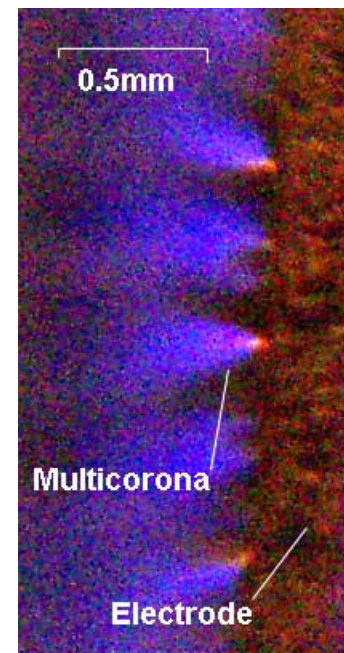


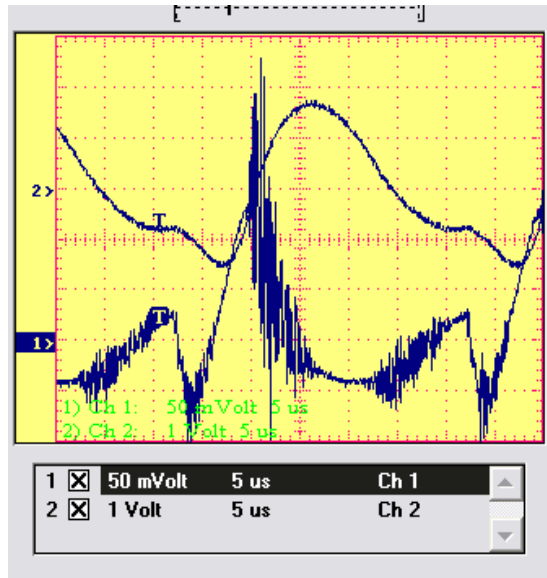
Fig.2.1.2.8. Non-symmetric (A) and symmetric (B) DBD appearance.

Fig.2.1.2.9. Photo of the multi-corona mode of SDBD.



The efforts to recognize a fine structure of DBD were done on the base of micro-photographs observations. The Fig.2.1.2.9 shows a sample of such a photo, which was done by means of extra lens application. As the result the enhanced spatial resolution was obtained, not worse than $\delta=0.2\text{mm}$. In this case the exposure was 1/30sec. Well seen that the discharge has a fixed spots of the coronas affixment. These spots locate just on the edge of the electrode and often have a high temperature due to a large current density. The diameter of such a spot is about 25mcm, the current through the spot is about 1mA, and thus the current density can be in a range $100\text{A}/\text{cm}^2$. These spots are

stable in position from run to run as well as the distance between them. When the saturation effect of spots number takes place (see below) the distance between them is measured in



range of half from insulator thickness δ , approximately, i.e. about $\Delta z \approx \delta/\epsilon$, where ϵ is the permittivity of insulator. The Fig.2.1.2.10 shows a typical volt-ampere record for such a discharge.

Fig.2.1.2.10. DBD regime at compensation of resonant frequency shift. Ch1 – current 2A/V (inverted), Ch2 – voltage 2kV/V.

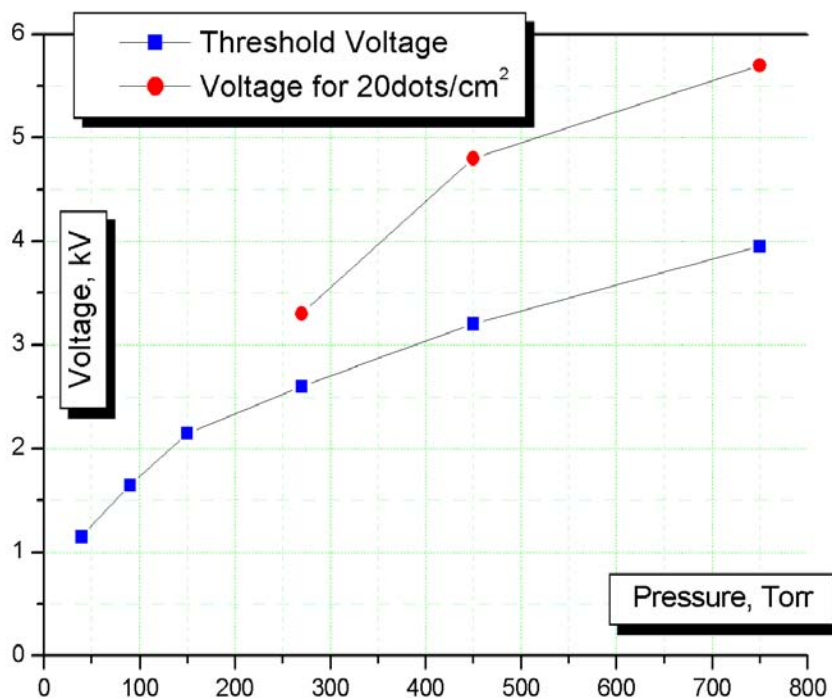


Fig.2.1.2.12.

Breakdown and characteristic voltage of DBD. Sinusoidal feeding $f=70\text{kHz}$. Dielectric thickness $d=1\text{mm}$.

The surface type of DBD discharge modifies the parameters and appearance at reducing pressure. A special observations were fulfilled to clear up the DBD properties in a range of pressure $P=90\text{-}750\text{Torr}$, namely, the breakdown voltage and the DBD plasma geometry. The photographs in Fig.2.1.2.11 present images' gallery of the DBD discharge appearance at different pressure. The top pictures were recorded from the direction perpendicular to the DBD panel surface. The bottom images were made under the condition

where the line of sight almost slides along the surface to recognize the plasma thickness. The neighbor electrodes were removed to give plasma an ability of free expansion on the surface. It was well seen that at the pressure reducing a homogeneous share of the DBD increased as well as the plasma layer became thicker.

The voltage of DBD initiation and the voltage when numbers of individual coronas achieved the value $N \approx 20 \text{ spots/cm}^2$ were recorded. The Fig.2.1.2.12 demonstrates a dependence of those (breakdown and characteristic) voltages on air pressure.

References to subsection. S. Leonov, A. Kuryachii, D. Yarantsev, A. Yuriev, "Study of Friction and Separation Control by Surface Plasma." AIAA-2004-0512.

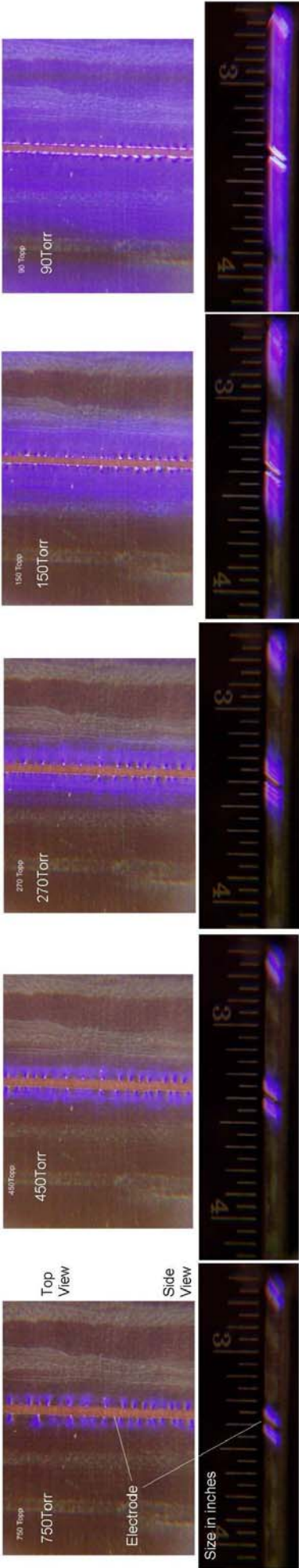


Fig.2.1.2.11. DBD appearance at reduced pressure.

2.1.3. Schlieren Shadow System.

Very often plasma generation occurs on a non-homogeneous manner. The HF and quasi-DC plasma filaments have a specific appearance at relatively high static pressure $P_{st}=100-750\text{Torr}$. The typical size of the plasma structure at the initial stage is in a range 0.1-1mm and velocity of the movement is about the velocity of airflow. The characteristic speeds of the plasma filaments span in the following ranges:

- Velocity of penetration (Y component) 10^6-10^9cm/s ;
- Velocity of movement (X component) 10^4-10^5cm/s , almost equal to V;
- Velocity of radial expansion 10^3-5*10^3cm/s .

At the same time the level of airflow disturbances in an external airflow can be relatively large in respect of integral phase change on a light beam way. Mentioned above the shadow-type of device for the tiny plasma objects visualization in supersonic airflow might possess the following characteristics:

- Exposure time no more than $1\mu\text{s}$ due to the plasma movement speed is equal 0.1-1mm/ μs and no more than 1ms for steady-stage flow structure recognition.
- Spatial resolution should be not worse than 0.3mm due to the typical radial dimension of the plasma filament is supposed in range 0.1-1mm. The typical boundary layer thickness is 0.1-1.0mm.
- Accuracy in synchronization of the plasma process with the image recording should be not worse than $5\mu\text{s}$ due to the residence time of the plasma filament in the area of the interaction is 10-30 μs .

The schemes of a direct shadow device under the different options and a Schlieren scheme have been analyzed for the visualization of such plasma objects. The generalized layout of the shadow device is shown in Fig.2.1.3.1. It contains two long-focused collimators, illuminator, two mirrors and registration system on base of CCD camera. The optical filters (aperture and wavelength band) have been applied for the plasma radiation rejection. The second lens is used to adjust the shadow picture independently in respect of sensitivity and resolution.

As a light source the short-pulse globular flash lamp is utilized. A few tests have been done with a surface spark at discharge duration not more than $1\mu\text{s}$. Some tests have been done

with continuous type of illuminator and “shutter ” option of the CCD-camera operation mode.

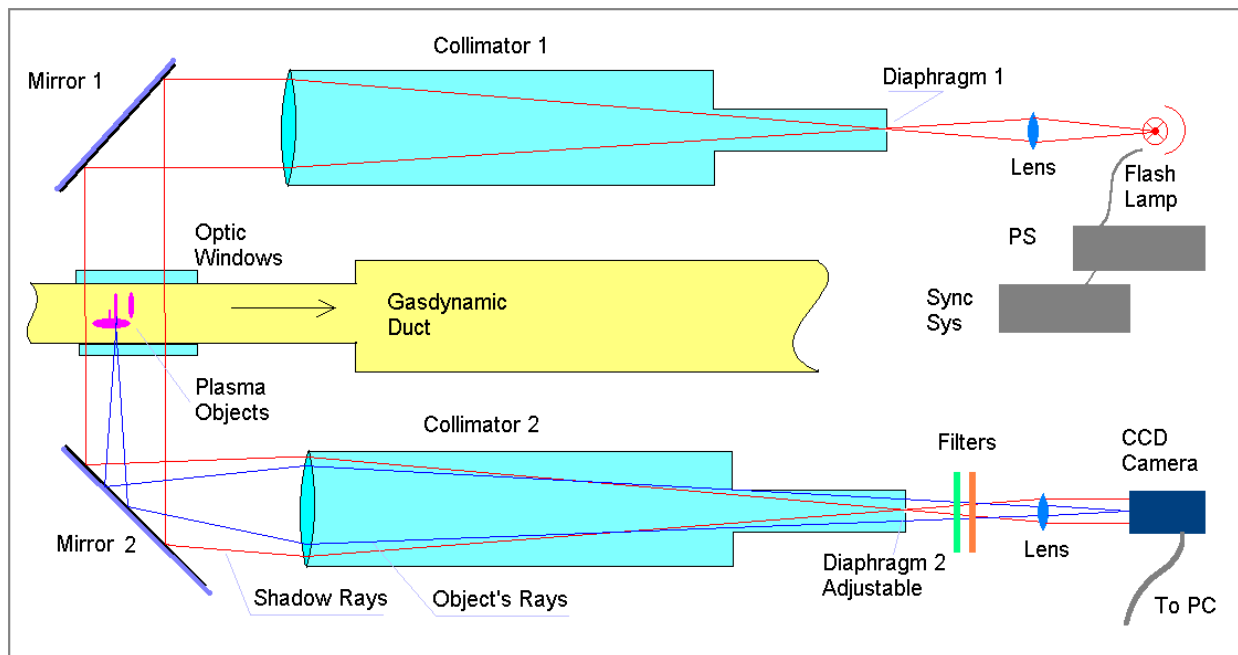


Fig.2.1.3.1. Generalized layout of the shadow device.

Different schemes of a registration system have been tested. Finally the layout was chosen, which has name “Tepler’s shadow scheme”. It contains the adjustable diaphragm (movable knife) and additional lens, which allows us to focus the image on various planes in respect of plasma object position.

The optical scheme simulation has been fulfilled. As the object of visualization the filament with a circular cross-section and thin contract layer are used. The radius of the filament simulated was $r=0.5\text{mm}$ and the specific refraction index was $N=n/n_0=1,0001$. The position of the focused plane $Y=y/r$ was varied ($Y=0$ in Fig.2.1.3.2). A negative value is correlated to the plane position closer to flash lamp. The sample of resulting intensity distribution in the shadow image in dependence on the effective position of the system focus is shown in Fig.2.1.3.2. Well seen that the optical scheme can be adjusted effectively on the different (required) parameters of the object visualization.

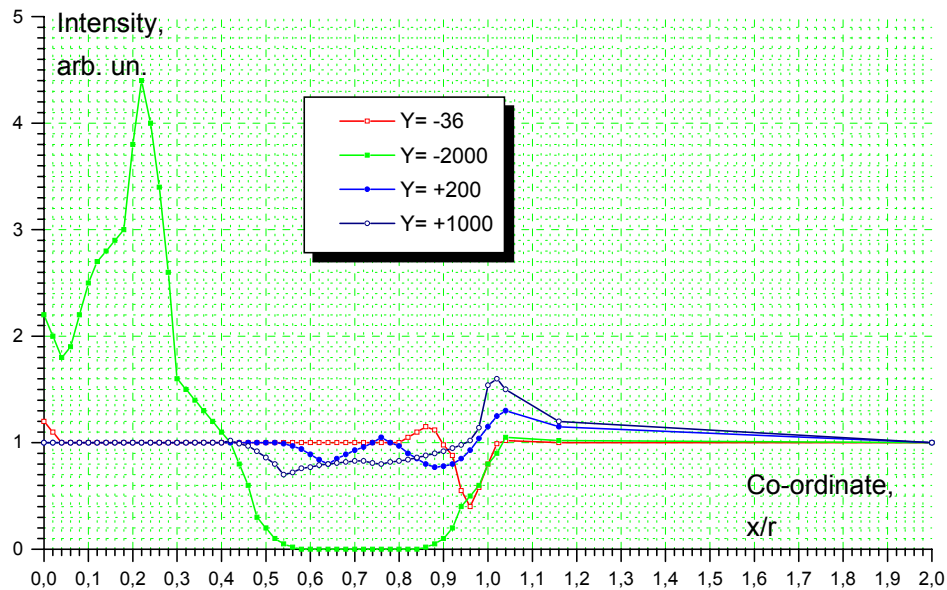


Fig.2.1.3.2. Shadow image intensity distribution in dependence on tuning of the focus plane.

On the base of the calculations the optical scheme has been optimized for specific conditions of a thin plasma layer and filamentary discharge. The analysis of a parasitic turbulence influence has been executed.

The visualization device of that type has been used for the flow bulk structure exploration. The final scheme of optical system for Schlieren video/photo records is presented in Fig.2.1.3.3. Light from the continuously radiating/pulsing light source is focused at the collimator's entrance on circular diaphragm. Then, collimating light is reflected by the mirror and passes through the flow channel windows. The second mirror directs light to the second collimator. There is a diaphragm with a revolvable slit at the exit of the second collimator. Such a slit allows us to gather more light in one defined direction and to see structures oriented along this direction more clearly as a result (for example shock waves). An aperture diaphragm follows the slit diaphragm. This diaphragm cuts the light, which is emitted by the object itself (discharge light). Then different filters are used to avoid chromatic aberrations. At last, light is focused on the CCD matrix. It must be mentioned that focus of optical system is allocated behind the object. This is made for increasing of sensitivity.

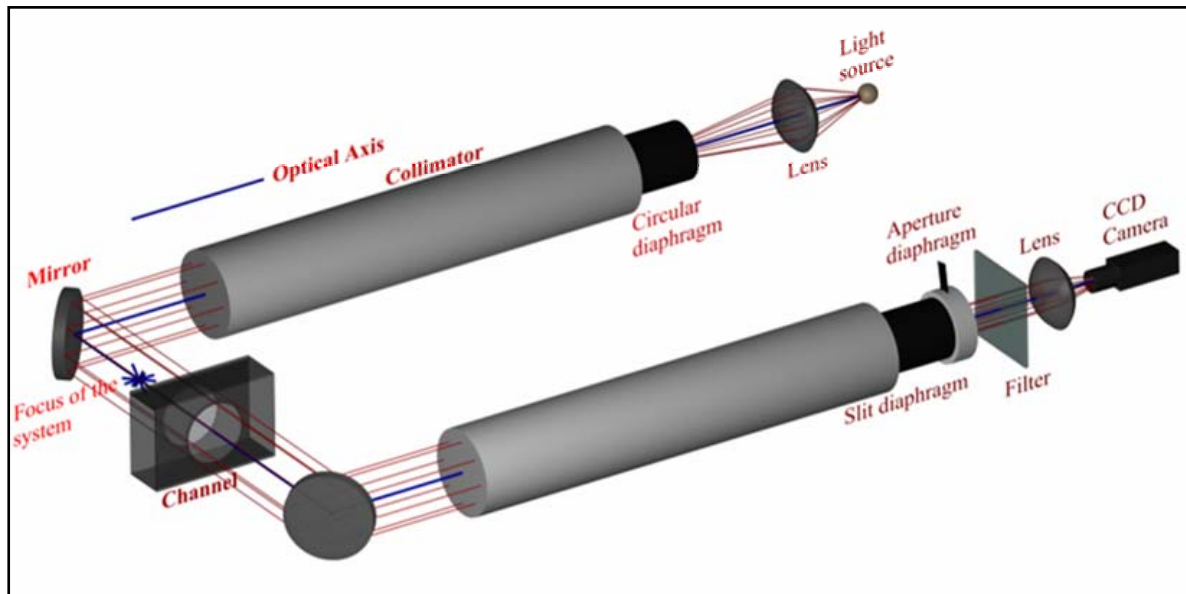


Fig.2.1.3.3. Scheme of the Schlieren device for the flow bulk structure visualization.

The Schlieren (Tepler's scheme) method is used in our experiments due to its high illumination in comparison with focus (direct-shadow) method. Recently the Schlieren device was modified. During previous efforts it was utilized in two main modes: either multi-frames record with continuous type of light source (minimal exposure was defined by shutter of video camera down to 30mcs) or single-frame mode with flash lamp (exposure about 1mcs). Digital video camera "Pulnix-6710" was exploited with typical frame-rate 120fr/sec and frame size 480*640 pixels. In the last experiments a multi-flash lamp was used as a light source and the "Basler-A504K" video camera with frame-rate up to 2000fr/sec. The comparison of previous and new system performance is shown in Table 2.1.3.

Table 2.1.3. Comparison of Schlieren devices performance.

Parameter	Previous edition Multi-frame	Previous edition Single-frame	Modified one
Type of camera	Pulnix-6710	Pulnix-6710	Basler-A504K
Type of light source	continuous	Flash-lamp	Multi-flash lamp
Max frame-rate, fr/sec	350	single	2000
Minimal exposure, mcs	30	1	1
Typical frame-rate, fr/sec	120	single	100-400
Typical exposure, mcs	1000-4000	1	1
Frame size, pxs	640*480	640*480	1280*1024

Reference to subsection. Leonov S.B., Kharitonov A.I., Sharov Yu.L. “Visualization of a Filamentary Plasma Objects in Supersonic Airflow.” Proceedings of IEEE-28th ICOPS-13th PP, PPPS-2001, June 17-22, 2001, Las-Vegas, NV, P3A01, p.377.

2.1.4. Spectroscopic Measurements. Method of the Spectrum Fitting.

As it might be considered contact methods are non-applicable for the measurements of the plasma parameters in the case of filamentary discharges due to unpredictable position of an individual filament and perturbation of the plasma properties by a probe. Among of non-contact methods the optical spectroscopy is the most popular.

There are a number of spectroscopic methods of the gas temperature determination in electrical discharges. They can be divided on the laser (active) methods and self-emission (passive) methods. The laser methods are an subject of special interest and not available in this work. Among the passive methods the following ones could be named.

Self-emission method. Generally, the gas temperature in air plasma can be determined from the plasma emission of molecular nitrogen. The gas temperature is typically determined from the contour analyses of the emission bands in the well-known, N_2 2nd positive ($C^3\Pi - B^3\Pi$, 337,1nm) system. The N_2 2nd positive system has large oscillator strength and is easily recognized in nitrogen discharges making it the preferred system for temperature determination. The plasma emission under atmospheric pressure was found in [3] to be dominated by continuum radiation and emission from other species, which obscured large portions of the N_2 2nd positive emission. In spite of these difficulties, the gas temperature could be determined from a fit of partially resolved N_2^+ 1st ($B^2\Sigma^+ - X^2\Sigma^+$, 391,4nm) negative vibrational transitions. This method is based on the assumption of the Boltzman population of the rotational levels of molecules N_2^+ in the excited electronic state and on the correspondence of the measured rotational temperature to the gas temperature. The estimation [4] gives the following relationship: $\tau_c \gg \tau_{rt}$, where τ_c – the life time of the exited electronic state ($B^2\Sigma^+$), τ_{rt} – the time of the rotational relaxation of nitrogen molecules at atmospheric pressure and temperature 300K. The rotational temperature can be determined by fitting of the experimental spectrum with calculated one. Parameters of the calculation are the apparatus function, and rotational temperature.

Determination of electron temperature and density by spectroscopic methods. Recombination of positive ions and electrons is resulted in radiation of continual spectrum. Photon with frequency ν is emitted by atom if this atom has captured electron with mass of m and velocity of v on electronic level n . The frequency is determined by the following equation:

$$h\nu = h\nu_i + \frac{1}{2}mv^2, \quad (1)$$

here, ν_i – the frequency of the electronic level n . Free electrons have continual spectrum of energy, so emitted optical spectrum is continual. Intensity of this spectrum depends on concentration and velocity distribution of the free electrons, concentration of the positive ions and relation between recombination rate coefficient and velocity ν . The dependence between spectral intensity and factors mentioned above is the following [4]:

$$\frac{I(\nu)d\nu}{h\nu} = \nu q(\nu, \nu_i) N_+ N_- F(\nu) d\nu, \quad (2)$$

where $\nu q(\nu, \nu_i)$ - recombination coefficient; N_+ and N_- - concentrations of the positive ions and electrons; $F(\nu)d\nu$ – the part of the electrons, which have velocities in the range of $\nu \div \nu + d\nu$. In a case of Maxwell-Boltzmann distribution

$$F(\nu)d\nu = \frac{4}{\alpha^3 \sqrt{\pi}} \exp\left(-\frac{\nu^2}{\alpha^2}\right) \nu^2 d\nu, \quad (3)$$

where, $(m\alpha^2)/2 = kT_e$, k – Boltzmann's constant, T_e – electronic temperature. If $N_+ = N_-$, then from (1-3):

$$\frac{I(\nu)d\nu}{h\nu} = \nu q(\nu, \nu_i) \frac{N_-^2 \cdot 4}{\alpha^3 \sqrt{\pi}} \exp\left(-\frac{\nu^2}{\alpha^2}\right) \nu^2 d\nu. \quad (4)$$

As it was shown in [2]:

$$\nu q(\nu, \nu_i) = \frac{K}{\nu^2 \sqrt{\nu - \nu_i}}, \quad (5)$$

So, from (4-5):

$$\lambda I(\lambda) = \frac{KN_-^2}{T_e^{3/2}} \exp\left(-\frac{E}{kT_e}\right), \quad (6)$$

where, E – kinetic energy of the electron which gives radiation with wavelength λ at recombination. We can write this equation in the following form:

$$\ln[\lambda I(\lambda)] - \ln \frac{KN_-^2}{T_e^{3/2}} = -\frac{E}{kT_e}. \quad (7)$$

If we know intensity of the radiation in the unit interval for two wavelengths λ_1 and λ_2 , we can write:

$$\ln \frac{\lambda_1 I(\lambda_1)}{\lambda_2 I(\lambda_2)} = \frac{E_2 - E_1}{kT_e}. \quad (8)$$

As $E = (mv^2)/2 = h(\nu - \nu_i)$, $E_2 - E_1 = h(\nu_2 - \nu_1)$, then

$$\ln \frac{\lambda_1 I(\lambda_1)}{\lambda_2 I(\lambda_2)} = \frac{hc}{kT_e} \left(\frac{1}{\lambda_2} - \frac{1}{\lambda_1} \right) \quad \text{or} \quad T_e = \frac{\frac{hc}{k} \left(\frac{1}{\lambda_2} - \frac{1}{\lambda_1} \right)}{\ln \frac{\lambda_1 I(\lambda_1)}{\lambda_2 I(\lambda_2)}}. \quad (9)$$

We can determine temperature of the electrons from the last equation if we know relative intensities of the continual recombination spectrum for two wavelengths. It has to be mentioned that continual recombination spectrum is obscured on the most part of the visible spectrum. There are only several windows where it can be observed.

The distinct atomic lines observed in emission from dense low-temperature plasma are reasonably well represented by a Lorentzian line shape. This is due to the Stark broadening, arising from perturbations of the atomic system by electrons and ions, is dominant broadening mechanism. Analysis of Stark broadened profiles is a useful technique for determination the electron number densities within the plasma, because the Stark widths give a direct measure of the electron density [5].

Method of spectrum fitting. The described method is based on a comparison of experimental data with theoretically based spectrum. The $N_2 \text{ C}^3\Pi_u (v'=0) \rightarrow B^3\Pi_g (v''=0)$ band was selected by several reasons. First of all it is observed in the emission of the most type of electrical discharges in air, that allows us to compare gas temperatures in these cases on the base of one band. Besides it, this band has a relatively higher intensity than the other bands of N_2 second positive system. And, finally, there is no influence of CN violet band that arises at the presence of the hydrocarbons on this range of wavelengths ($< 3400\text{\AA}$). A description of diatomic molecules' spectral terms may be found in [6].

The emission coefficient ε_{ul} of a transition from upper state $u = (n'v'J'i'p')$ to a lower state $l = (n''v''J''i''p'')$ (denoted in short $u \rightarrow l$) is given by the expression:

$$\varepsilon_{ul} = N_u hc \sigma_{ul} A_{ul} = \frac{64\pi^4 c}{3 \times 4\pi\epsilon_0} \sigma_{ul}^4 \frac{N_u}{g_u} S_{(n''v''J''i''p'')}^{(n'v'J'i'p')} \quad (10)$$

where h , c , ϵ_0 are the conventional physical constants, v and J are the vibrational and rotational quantum numbers respectively, the subscript I denotes one component of the multiplet, p is the parity, N is the density of molecules in the upper state, g_u is the statistical weight of the upper electronic level, σ_{ul} is the wavenumber of the emitted spectral line, A_{ul} is the transition probability and $S(\dots)$ is the total line strength. This last quantity can be split into

two factors: the rotational intensity factor (also called the Holn-London factor) and the second, which depends only on the particular electronic transition.

Taking into account the consideration above, the intensity of an individual spectral line of a rotational band structure depends on the rotational line strength $S_{(J''p'')^{J'p'}}^{(J'p')^{J''p''}}$ for that particular line, the population of molecules in the initial state, the wavenumber of the rotational transition and a factor C_{ul} that is the same for all lines of the same band. We may write the emission coefficient $\epsilon_{J'p',J''p''}$ of a particular line of rotational fine structure of the band (v',v'') as

$$\epsilon_{J'p',J''p''} = C_{ul} S_{(J''p'')^{J'p'}}^{(J'p')^{J''p''}} \sigma_{ul}^4 \exp\left(\frac{-F_{v'i'}(J',p')}{k_B T_{rot}}\right) \quad (11),$$

where $F_{v'i'}(J',p')$ is the rotational energy of the initial level and T_{rot} is the rotational temperature. This expression may be used if a thermal equilibrium exists among rotational states. Kovacs [7] has given the formulas of rotational line strength calculation for all type of transitions and couplings.

The N₂ second positive bands naturally appear in various types of discharges. The lifetime of the N₂ ($C^3\Pi_u$, $v'=0$) state is $3.668 \cdot 10^{-8}$ sec and excited molecule has no time to live region where it was excited. Therefore, even though the chemical processes in the plasma are unknown, they are often used as a thermometer to estimate the gas temperature in the corresponding emission region. The second positive bands correspond to transitions between $C^3\Pi_u$ and $B^3\Pi_g$ electronic states. These are triplet states, thus for each J there are three rotational levels $J-1$, J and $J+1$ (denoted by $I = 1, 2$ and 3 respectively). Kovacs [7] gave formulae for triplet rotational energy levels corresponding to three rotational quantum numbers $J-1, J, J+1$:

$$T_{v1}(J) \equiv T_{vJ-1}(J) = B_v \left(J(J+1) - [Y_1 + 4J(J+1)]^{1/2} - \frac{2 Y_2 - 2J(J+1)}{3 Y_1 + 4J(J+1)} \right); \quad (J \geq 2)$$

$$T_{v2}(J) \equiv T_{vJ}(J) = B_v \left(J(J+1) + \frac{4 Y_2 - 2J(J+1)}{3 Y_1 + 4J(J+1)} \right); \quad (J \geq 1)$$

$$T_{v3}(J) \equiv T_{vJ+1}(J) = B_v \left(J(J+1) - [Y_1 + 4J(J+1)]^{1/2} - \frac{2 Y_2 - 2J(J+1)}{3 Y_1 + 4J(J+1)} \right); \quad (J \geq 0)$$

where $Y = A/B_v$; $\Lambda = 1$; $Y_1 = \Lambda^2 Y(Y-4)+4/3$; $Y_2 = \Lambda^2 Y(Y-1)+4/9$. For the band (0,0), simplifying the notations, the discrete line components are given by

$$\begin{aligned} P_i(J'') &= \sigma_0 + F_i'(J''-1) - F_i''(J''); \\ Q_i(J'') &= \sigma_0 + F_i'(J'') - F_i''(J''); \\ R_i(J'') &= \sigma_0 + F_i'(J''+1) - F_i''(J''). \end{aligned} \quad (i = 1,2,3)$$

for the principal branch and

$$\begin{aligned} P_{ij}(J'') &= \sigma_0 + F_i'(J''-1) - F_j''(J''); \\ Q_{ij}(J'') &= \sigma_0 + F_i'(J'') - F_j''(J''); \\ R_{ij}(J'') &= \sigma_0 + F_i'(J''+1) - F_j''(J''). \end{aligned} \quad (I,j = 1,2,3; I \neq j)$$

for the secondary branches. In these expressions J'' is the rotational quantum number of the lower level and the wavenumber σ is replaced by the branch name (P, Q or R). σ_0 is the initial position of the (0,0) band of the Second positive system.

Table 2.1.4.1. Molecular constants according to Herzberg [8].

Constants	$C^3\Pi_u$	$B^3\Pi_g$
T_e (cm ⁻¹)	89136,88	59619,3
ω_e (cm ⁻¹)	2047,17	1733,39
$\chi_e\omega_e$ (cm ⁻¹)	28,445	14,122
$\gamma_e\omega_e$ (cm ⁻¹)	2,0883	0,0569
B_e (cm ⁻¹)	1,8247	1,6374
D_e (cm ⁻¹)		$5,9 \cdot 10^{-6}$
α_e (cm ⁻¹)	0,01868	0,0179
γ_e (cm ⁻¹)	-0,00228	-0,00007
r_e (Å)	1,1486	1,2126
A	39,2	42,24

Using tables 1 and 2 we may find wavelengths and rotational line strength expressed by Kovacs in the intermediate coupling regime [7]. On the base of these results we can numerically calculate the (0,0) Second positive band spectrum emitted by an N₂ molecule at a given temperature T_{rot} . Our calculations show that branches with significant (relative) intensity are essentially the Pi and Ri principal branches, whereas the intensities of the Pij, Qij, Rij and Qi branches are weak (Figure 2.1.4.1b).

Table 2.1.4.2. Further molecular constants according to Herzberg [8].

Constants	$C^3\Pi_u$	$B^3\Pi_g$
B_v (cm ⁻¹)	1,81536	1,62845
D_v (cm ⁻¹)	$5,9 \cdot 10^{-6}$	5,9
Y1	381,2391	570,3985
Y2	444,2417	646,4371
Y	21,59351	25,93878

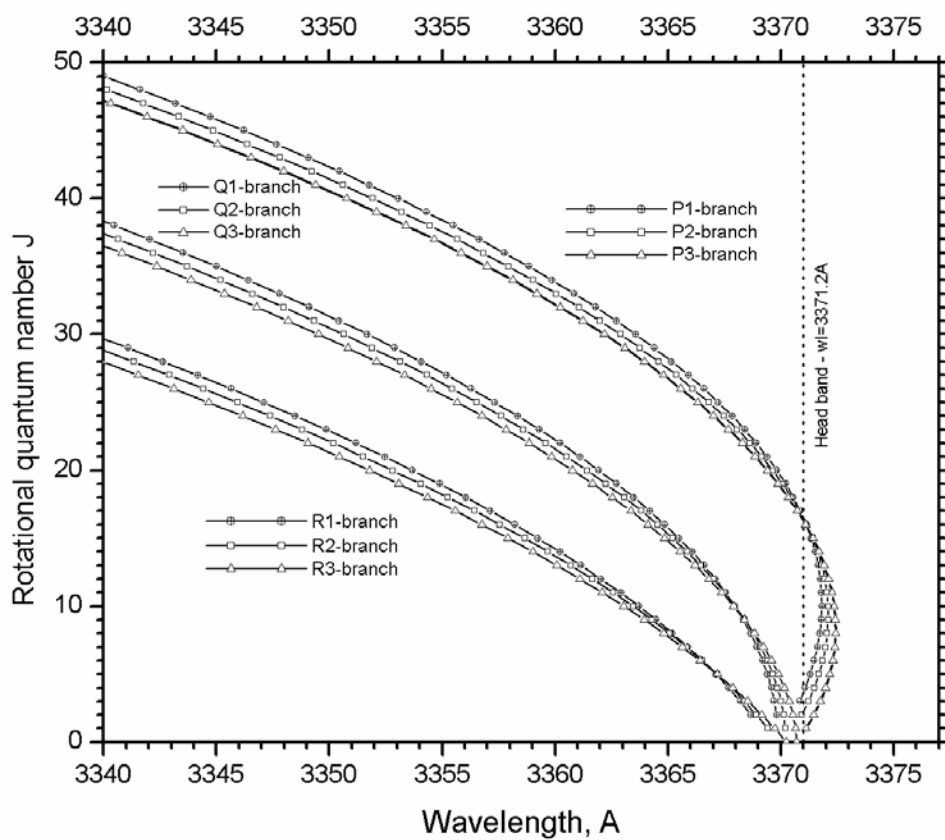
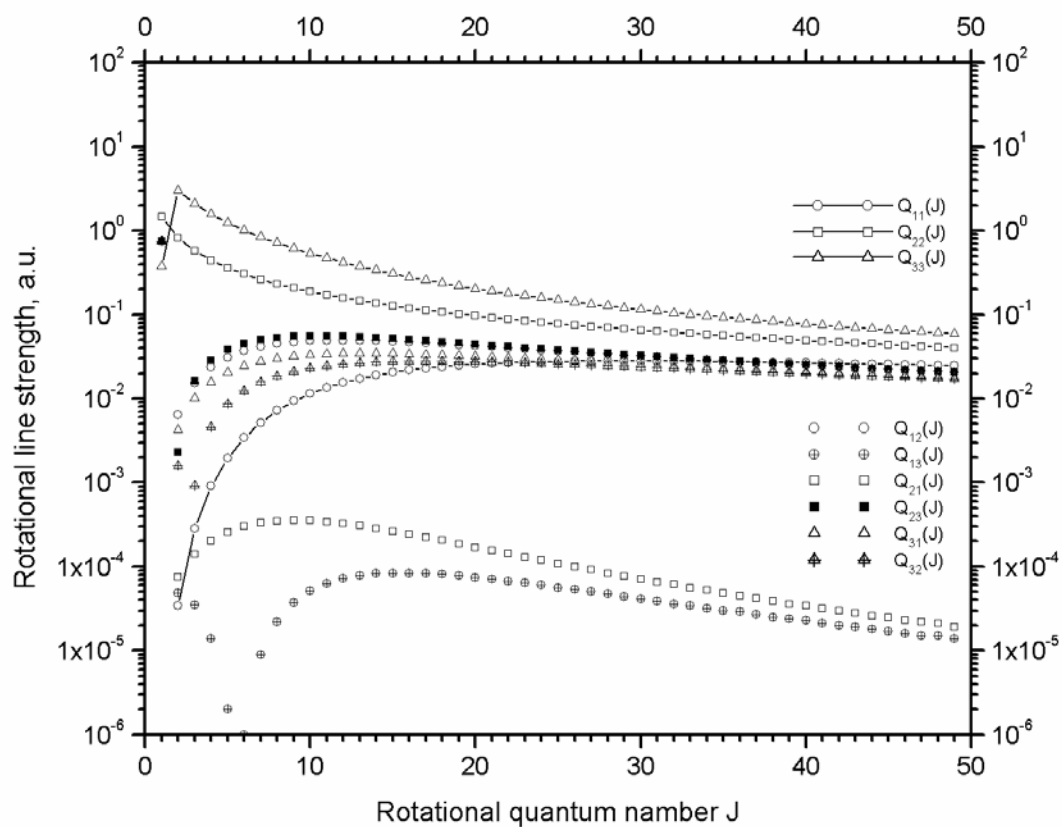


Fig.2.1.4.1(a) Fortrat graph.



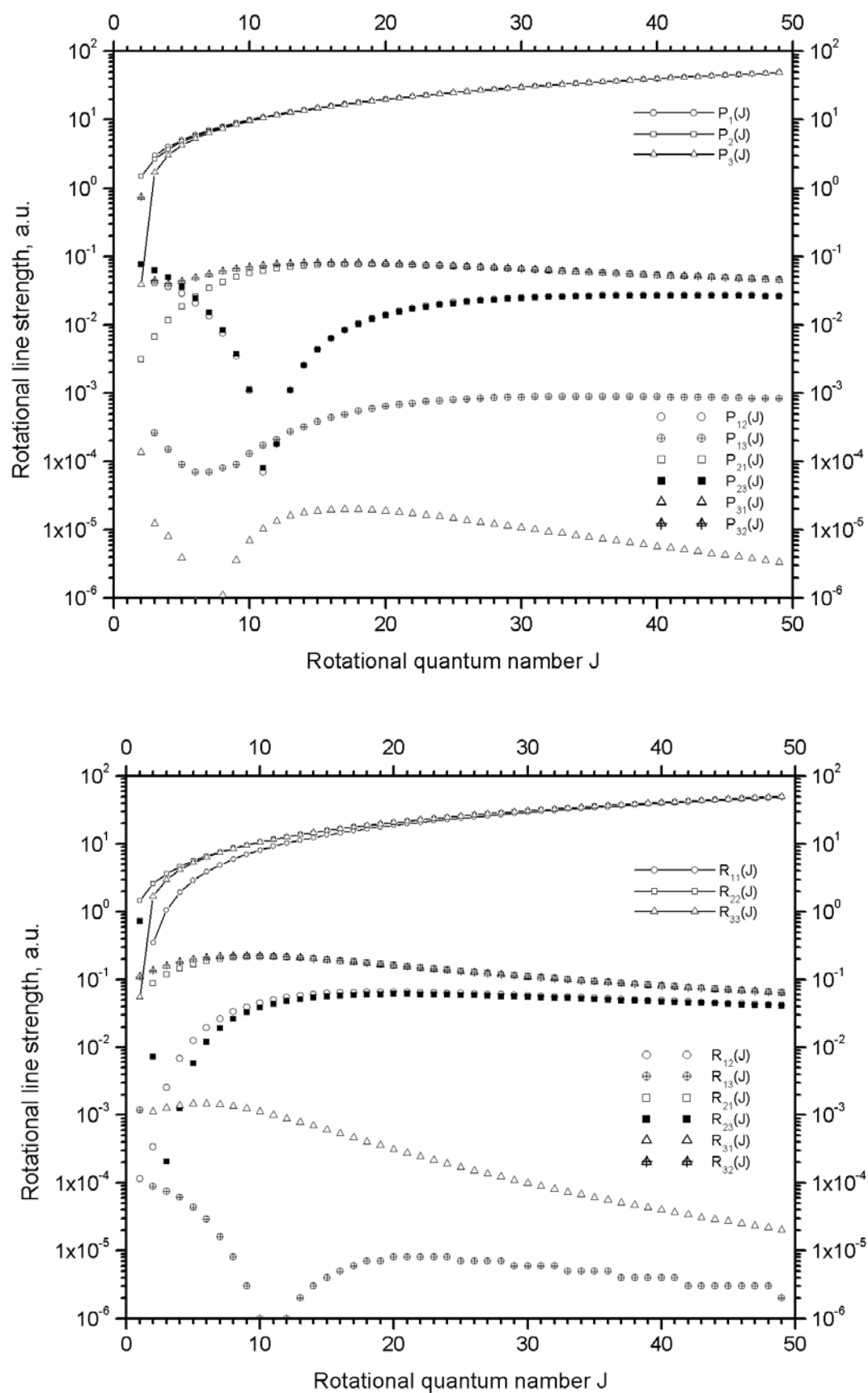


Fig.2.1.4.1. (b). The rotational lines strength.

The main branch profile can be compared with the help of the Fortrat graph plot for the (0,0) Second positive spectrum (Figure 2.1.4.1(a)).

Calculation of the (0,0) Second positive band of N₂. The spectral line profile obtained with a spectral apparatus is not the true line profile. Even a spectral line of infinitesimal width is broadened by the following reasons:

- Transfer of the slit image to the grating occurs without changing of the slit size;
- Pixel of the camera has a finite size;
- There is some inaccuracy of the monochromator optic system;
- Diffraction occurs on the monochromator slit and apertures.

The line profile obtained for monochromatic light, called the apparatus profile, is generally well approximated by a Lorencian or Gaussian functions with a full width at half maximum $\Delta\lambda_{app}$. In the temperature range 300-7000 K, broadening of spectral lines results mainly from the convolution of the emission profile with this apparatus function. Convolution integral is defined by the following expression [9]:

$$F(\lambda) = \int_{\lambda_0 - \Delta\lambda}^{\lambda_0 + \Delta\lambda} P(\lambda) \cdot \frac{\Delta\lambda}{(\lambda_0 - \lambda)^2 + (\Delta\lambda/2)^2} \cdot d\lambda ;$$

where $P(\lambda)$ – nonconvoluted theoretical spectrum, $F(\lambda)$ – real spectrum, $\Delta\lambda$ - ap. function.

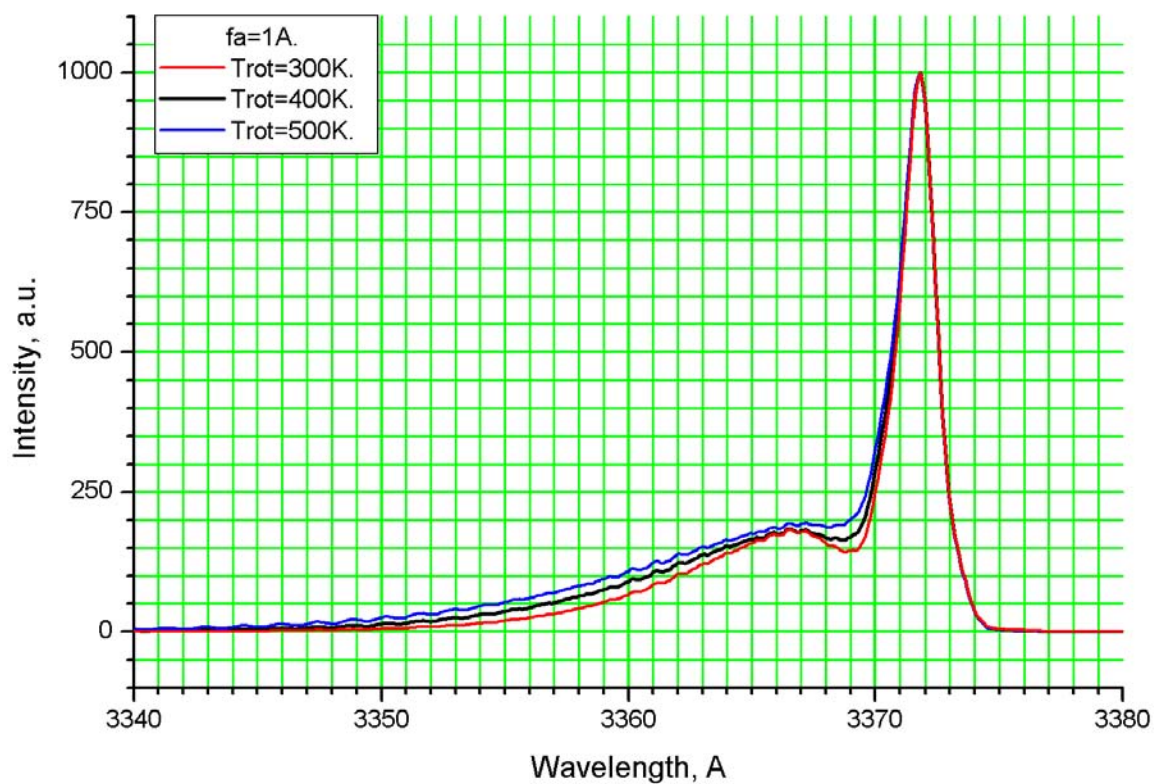
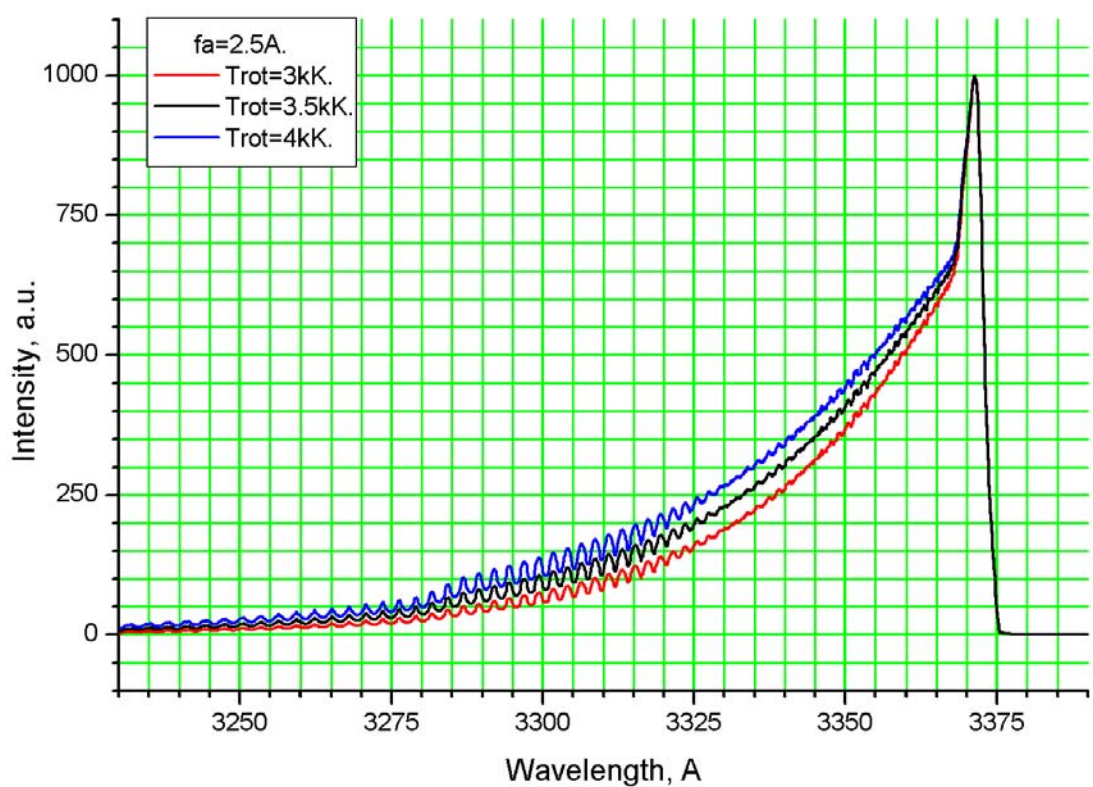


Fig.2.1.4.2. N2 Second positive band spectra.

Using the physical parameters of the (0,0) Second positive system spectrum, we calculated theoretical spectra in the wavelength range from 3200Å ($J=75$) to 3380Å (the (0,0) head band is at $\lambda = 3371.8\text{Å}$), for various temperatures and apparatus functions. For lower temperatures (a few hundreds of Kelvin's degree) the wide slit, like 30mkm (corresponds to the $\Delta\lambda_{\text{app}} = 2,5\text{Å}$) may be applied. However, for the same apparatus function and temperatures higher than 3000K, the shape of the spectrum depends on the temperature lighter (Fig.2.1.4.2).

Determination of the temperature. We observe a superposition of small-J R lines and high-J P lines in the (0,0) Second positive band spectrum. Due to this particularity, the shape of N2 spectrum is very sensitive to the rotational temperature T_{rot} . In our experiments the following procedure was applied.

- (1) The measured spectrum was corrected for the continuous background, which was assumed to be linear in the studied spectral range.
- (2) The experimental spectrum intensity was normalized with respect to the head band peak value, which was set to 1000.
- (3) The apparatus function $\Delta\lambda_{\text{app}}$ was estimated from the profile of a well-isolated line in the spectrum (Fig.2.1.4.3), or from the previously measured profile of Hg line for different slit widths (Fig.2.1.4.4). $\Delta\lambda_{\text{app}}$ can be estimated also from the shape of the band head because it is influenced by temperature slightly.

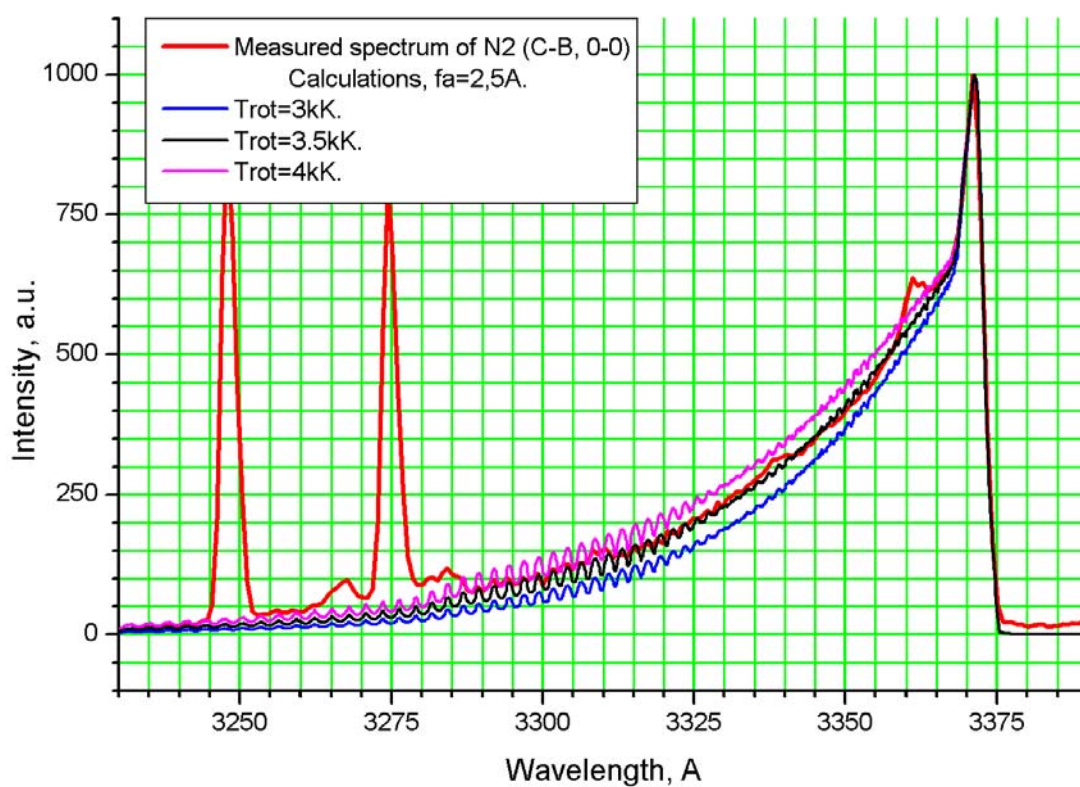


Fig.2.1.4.3. Fitting of the synthetic spectra and experimental one.

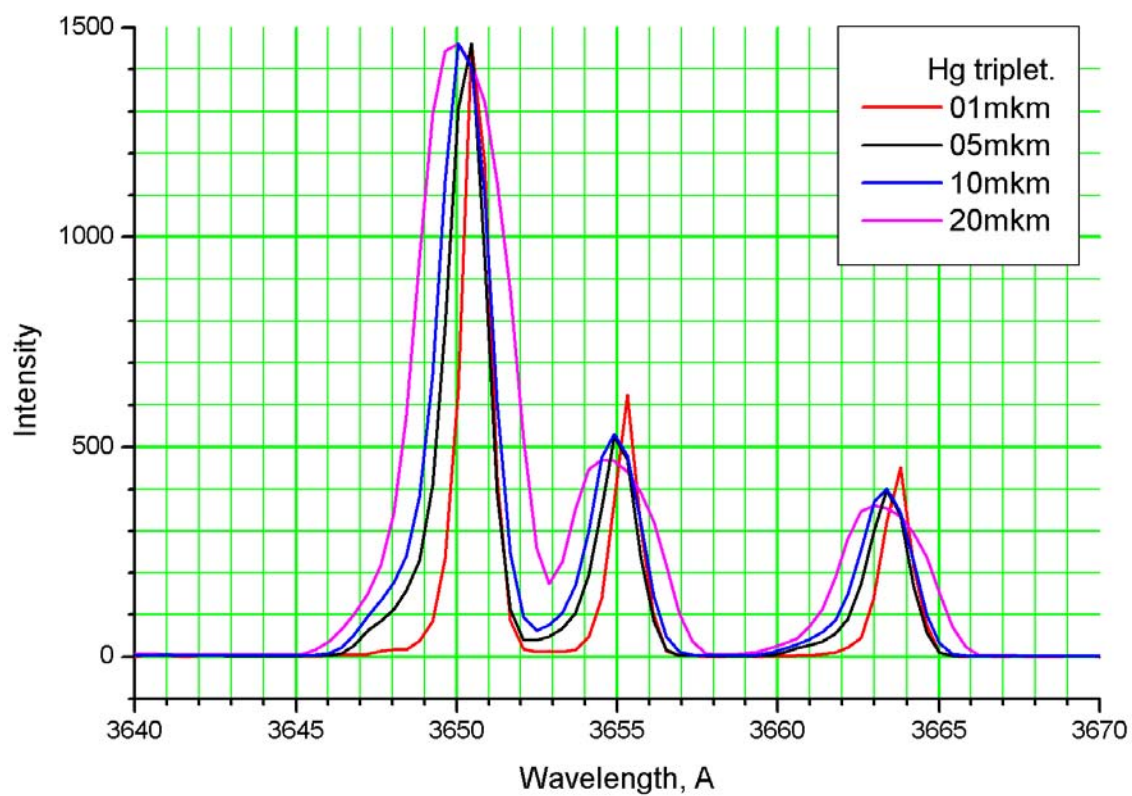


Fig.2.1.4.4. Hg line profile for different slit widths.

Spectroscopic scheme. As it was mentioned above the spectroscopy of the second positive system of molecular nitrogen and CN molecular spectrum were chosen as a main method of gas temperature measurements. The optical spectra were registered by means of a spectrograph Lot-ORIEL connected with a CCD camera with spectral resolution of about 0.04nm/pixel. The device spread function was 0.12-0.15nm. So, a partially resolved molecular spectrum can be obtained in experiment. The spectra registration in pressure range from 100Torr to 350Torr with different pulse duration and repetition rate was made. For the determination of gas temperature in a discharge the method of optical emission spectrum shape fitting has been adopted.

Schematic diagram of the experimental imaging system is shown in Fig.2.1.4.5. Radiation from the discharge area is registered by CCD camera at resolution 640(H) on 200(V) at frame rate 240 frames per second. For another thing light emission passes through quartz lens to monochromator. Then light is divided in two rays. The first beam is the broad part of the spectrum that is registered by CCD matrix. The second ray passes to the photoamplifier and the magnitude of the signal is saved in computer's memory. Images that were captured by CCD camera (Pulnix-6710) are saved in computer's memory. Using the fast CCD camera we can understand from which point of the discharge the light emission is captured.

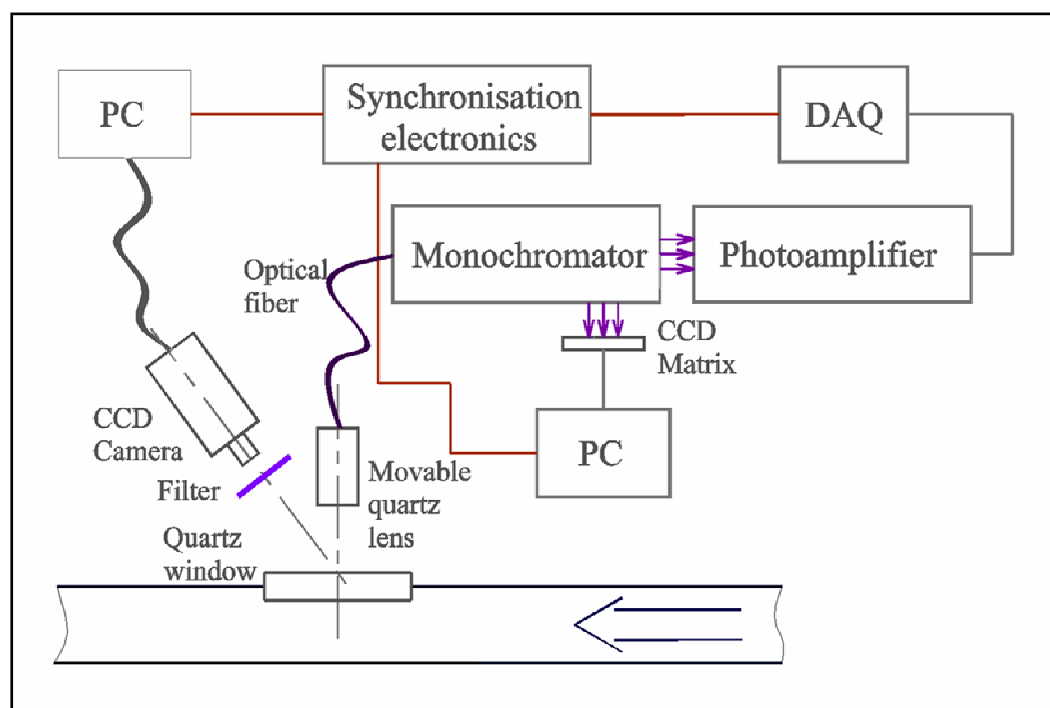
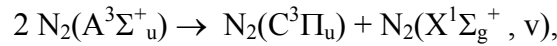


Fig.2.1.4.5. Principal scheme of spectroscopic observations.

Vibrational temperature. The correct determination of vibrational temperature T_V of the ground state demands as a necessary condition an occupying the upper electronic state ($C^3\Pi_u$) by the direct electron impact from the main state ($X^1\Sigma_g^+$). Alternative to the direct electron impact channel of an occupying a $C^3\Pi_u$ state is the process



with the velocity constant $k^* \approx 7.7 \cdot 10^{-11} \text{ cm}^3/\text{s}$. Comparison of the population fluxes of a $C^3\Pi_u$ level via the both channels under average concentration of electrons in the discharge and reduced electric field in the plasma should be done. This gives a basis to consider the population of ($C^3\Pi_u$) level by the direct electron impact to be the main mechanism.

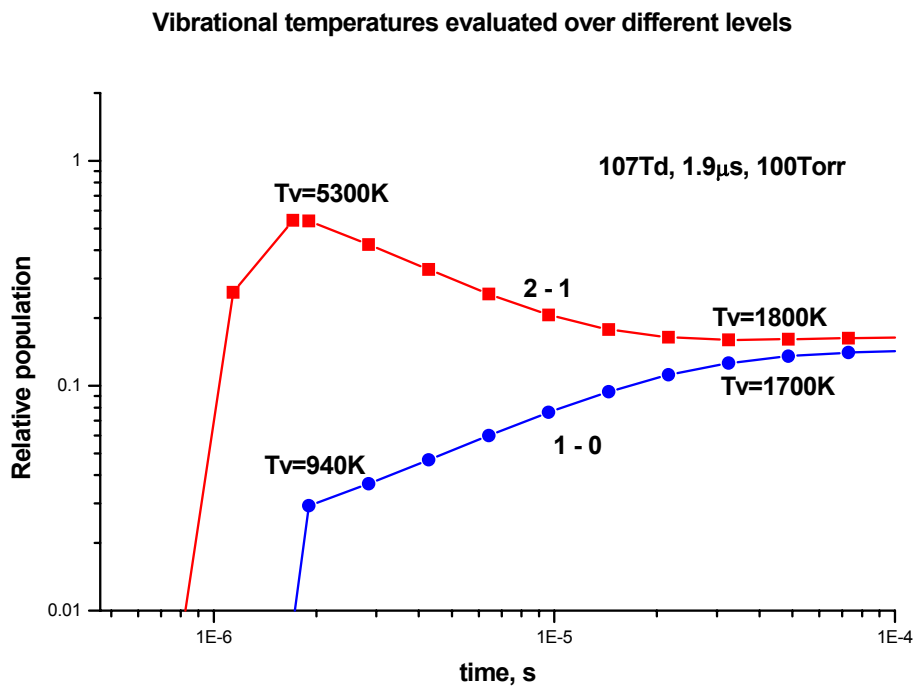


Fig.2.1.4.6. Vibrational temperatures evaluation on levels.

For the situation of a short-impulse discharge (which is equivalent to the early phases of HF channel development, or its spatial domains which are close to channel head) it should be taken into account that characteristic time of distribution function relaxation over vibrational levels is sufficiently larger than that for translational and rotational ones. This situation is illustrated by Fig.2.1.4.6, where distribution function over vibrational levels of nitrogen molecules is shown for different points of time. The characteristic relaxation time is of order of several times of VV exchange at the lower levels, it is about $30\mu\text{s}$ at 100Torr air pressure (Fig.2.1.4.7). It is seen that for the first 20 - $30\mu\text{s}$ after the short (about $2\mu\text{s}$) electric

discharge the distribution function (evaluated via vibrational temperatures of the first and second levels) is highly non-equilibrium, and only after 30 μ s it converges to an equilibrium value. As the spectrum can be obtained only by the end of electric pulse, when distribution function is the most non-equilibrium due to electron excitation of vibrational levels, the above mentioned method for vibrational temperature determination is not valid in general and corrections are to be made to have more adequate result. This situation is characteristic to relatively low levels of vibrational excitation, so only the first vibrational level population can be determined with eligible reliability.

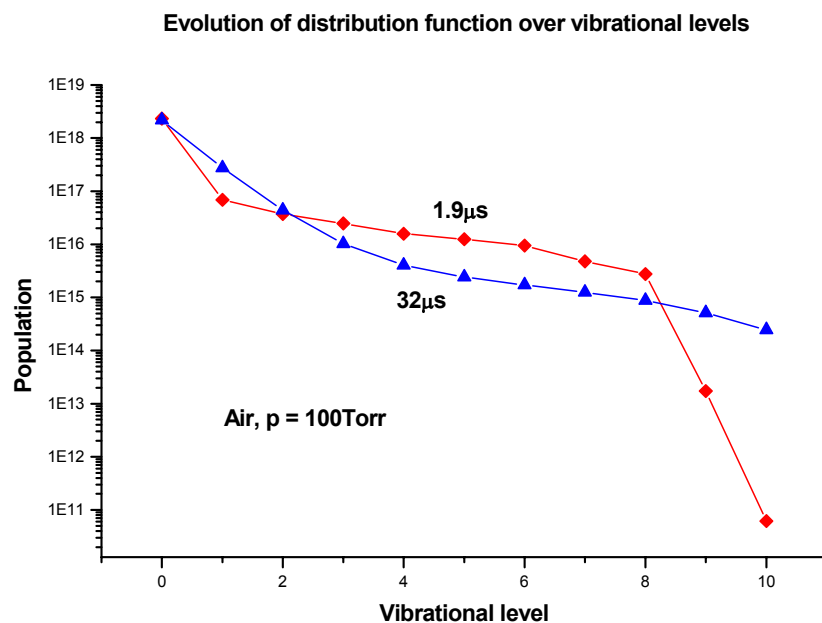


Fig.2.1.4.7. Evolution of distribution function on vibrational level.

For determination of vibrational temperature in both situations of stationary and impulse discharges the program is developed. It allows by processing of the sequence $\Delta v = -3$ (transitions 0-3, 1-4 and 2-5) and $\Delta v = -2$ (transitions 0-2, 1-3 and 2-4) of the second positive nitrogen system spectrum to define vibrational temperature of the ground state in steady-state situation and the relative population of the level $v=1$ of the nitrogen ground state $X^1\Sigma_g^+$ in situation of short-impulse discharge.

Nevertheless, determination of gas and vibrational temperatures remains one of the most delicate and debatable procedures in gas discharge physics and demands additional investigation in every case under consideration.

References to section 2.1.4.

1. Elliot S., Glumac N., *Campbell D. Carter, Molecular filtered Rayleigh scattering applied to combustion*, Meas. Sci. Technol. 12 (2001), 452-466.
2. Egon P. Hassel and Sven Linow, *Laser diagnostics for studies of turbulent combustion*, Meas. Sci. Technol. 11(2000), R37–R57.
3. Williamson M. James and DeJoseph Jr. A. Charles, *Determination of the Gas Temperature in an Open-Air, Atmospheric Plasma Torch from the Resolved Plasma Emission*, Innovative Scientific Solutions, Inc., Dayton, OH.
4. Edels H., *The Determination of the Temperatures of an Electrical Discharge in Gas*, Techn. rep. ERA, ref L/T 230, 1950.
5. Jong-Uk Kim, Clemens N.T., and Varghese P.L. *Experimental study of an underexpanded pulsed plasma-jet*. Paper AIAA-99-0452.
6. Herzberg Gerhard 1971 *The spectra and structure of simple free radicals*, Cornell University Press Ithaca and London.
7. Kovacs I 1969 *Rotational Structure in the Spectra of Diatomic Molecules* (Budapest: Akademiai Kiado)
8. K.P. Huber and G. Herzberg 1979 *Molecular Spectra and Molecular Structure IV. Constants of Diatomic Molecules*.
9. F. Garcia-Vicente, J.M. Delgado and C. Rodriguez, *Exact analytical solution of the convolution integral equation for a general profile fitting function and Gaussian detector kernel*. Phys. Med. Bol. 45 (2000) 645-650.
10. S. Pellerin, K. Musiol, O. Motret, B. Pokrzywka and J. Chapelle, “*Application of the (0,0) Swan band spectrum for temperature measurements*”. J. Phys. D: Appl. Phys. 29 (1996).
11. U. Kogelschatz, “*Fundamentals and Applications of Dielectric-Barrier Discharges*”. ABB Corporate Research Ltd, 5405 Baden, Switzerland.
12. E. Baselyan, Yu. Rayzer, “*Spark Discharge*”, Moscow, MIPT, 1997.

2.1.5. Gasdynamic and Electrical Measurements.

Measurement of the bulk parameters was carried out using a Data Acquisition system based on “National Instruments™” ADC DAQ-Card AI-16E-4 & 5 channels SCXI - block of pre-processing of a signal. In the test section of a wind tunnel the gauge of absolute pressure “HoneyWell™” is installed, reference of base pressure is deduced in a point of measurements of this gauge, and thus, the checking of reference of the base pressure gauge is made. Flow control gauges P_0' and P_{st} of the “HoneyWell” differential type are used for calculations of the aerodynamic characteristics of a flow (Mach number, high-speed pressure). Their reference pressure is observed and calculated on calibration curves according to the indications of the gauge of absolute pressure “HoneyWell™”.

During processing the acquired information, all measured values are transformed to absolute physical values (stagnation pressure P_0 was iterated, in view of the amendments to P_0' due to losses in supersonic jump on a receiving pipe), the values of the characteristics of a flow and aerodynamic factors are calculated. The estimation of parameters changes is carried out on the formalized statistical technique with use of pre-defined threshold probability (80% as a rule).

The multiducer ESP-32 (32-channel differential pressure transducer) is used to register a pressure distribution on the model surface and in the duct. Signal from ESP through the isolated amplifier SC-1121 in SCXI conditioning system goes on DAQ-Card AI-16E-4 and is stored as data files in computer. The original address line driver for ESP with optical isolated outputs is used to form ESP addressing. These signals also are measured to verify process of data flow and for sequential channel separation. A fully symmetrical LPT-LPT cable handshaking can be used to synchronize a data acquisition time. Some measurements are performed under very noisy conditions. Partially this problem was solved by using non-grounded isolated power suppliers.

The main software was developed on National Instruments LabView© program language. Data acquisition, sequential representation, treatment and calculation are performed using original programs. The acquired data are viewed, primary filtered (with using build-in digital Median or Butterworth filters), qualified and estimated. On this stage, the interference of electrical noise was excluded.

Flow parameters are calculated from data on P_0 , P_{st} and fore-chamber temperature T , as follows below.

$$M = \sqrt{\frac{2}{\gamma-1} \left[\left(\frac{P_0}{P_{st}} \right)^{\frac{\gamma-1}{\gamma}} - 1 \right]} \quad V = M \cdot \sqrt{\gamma \cdot R \cdot T_{st}} \quad T_{st} = T_0 \cdot \left(\frac{1}{1 + \frac{\gamma-1}{2} \cdot M^2} \right)$$

$$\frac{P_0'}{P_0} = \left[\frac{(\gamma+1) \cdot M^2}{2 + (\gamma-1) \cdot M^2} \right]^{\frac{\gamma}{\gamma-1}} \times \left[\frac{(\gamma+1)}{2 \cdot \gamma \cdot M^2 - (\gamma-1)} \right]^{\frac{1}{\gamma-1}} \quad q = \frac{\gamma}{2} \cdot M^2 \cdot P_{st}$$

where are: $-P_0$ – stagnation pressure; $-P_{st}$ – static pressure; $-M$ – Mach number of airflow; $-\gamma$ – adiabatic factor; T_{st} and T_0 – static and total temperatures; $-q$ – airflow specific force; P_0' – pressure behind plain SW.

In the last experimental series the subsonic flow mode was realized in test section of PWT-50 facility. A flow parameters were measured by set of pressure transducers with electronic commutator ESP-32. In that configuration seven measuring channels were operated as it is shown in scheme Fig.2.1.5.1. Three central pipes of total pressure measurements were movable to be able to measure the pressure redistribution.

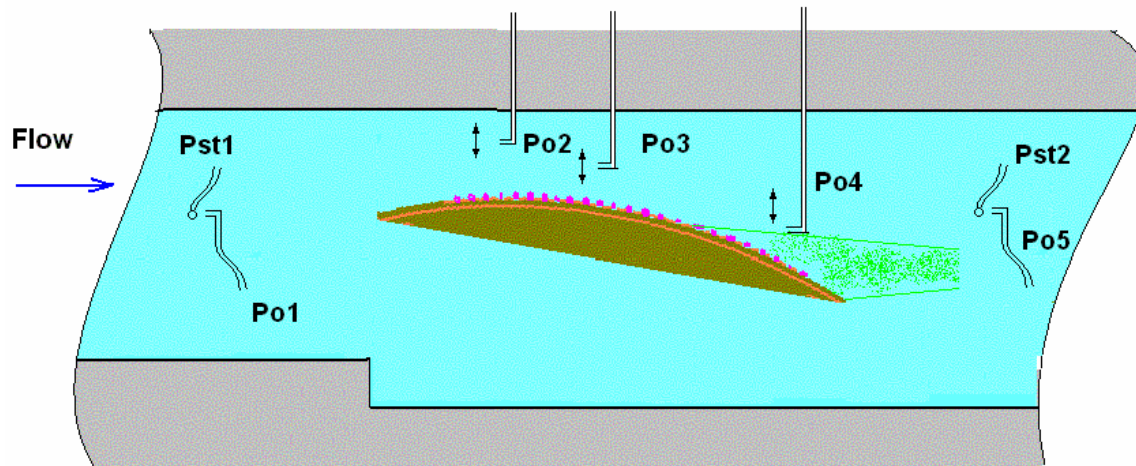


Fig.2.1.5.1. Pressure sensors location.

A sample of the pressure record is presented in Fig.2.1.5.2. In this case the Pitot pipe Po4 was located near the edge of separation area thus the pressure was about static one there.

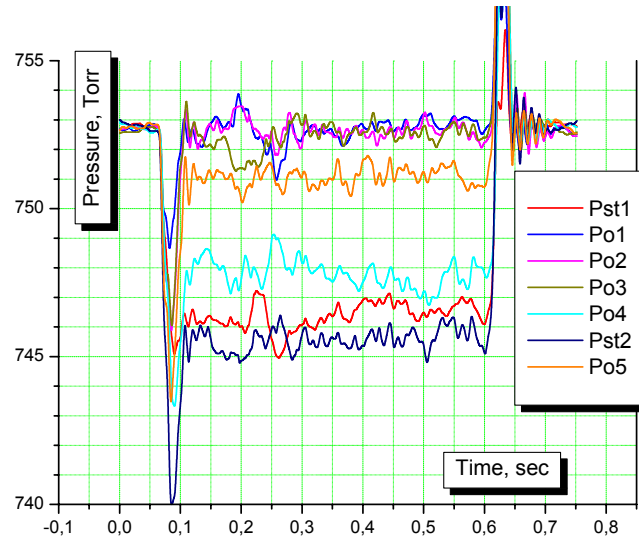


Fig.2.1.5.2. Sample of the pressure record in test section.

The flow velocity was calculated on the base of Bernoulli's law:

$$\frac{p_0}{p_{st}} = \left(1 + \frac{\gamma - 1}{2} M^2 \right)^{\frac{\gamma}{\gamma - 1}},$$

which can be transformed to “simple math” under the suggestion of subsonic flow rate:

$$M = \sqrt{\frac{2}{\gamma} \times \frac{\Delta P}{P_{aver}}};$$

where P_{aver} – is an average pressure (about 1Bar in our case), and ΔP – is the difference between stagnation and static pressure.

Two different methods were applied for skin friction factor measurements: direct measurements of tangential strength of isolated plate, stagnation and static pressure measurements near the wall. Those methods are conventional and have been used before. They posses some disadvantages and are difficult for a proper experimental realization.

At the basic type of the discharge supply (quasi-DC mode) it is possible to measure the input power by means of measuring of voltage on the discharge gap. Variants of the sensors arrangement are shown in Fig.2.1.5.3.

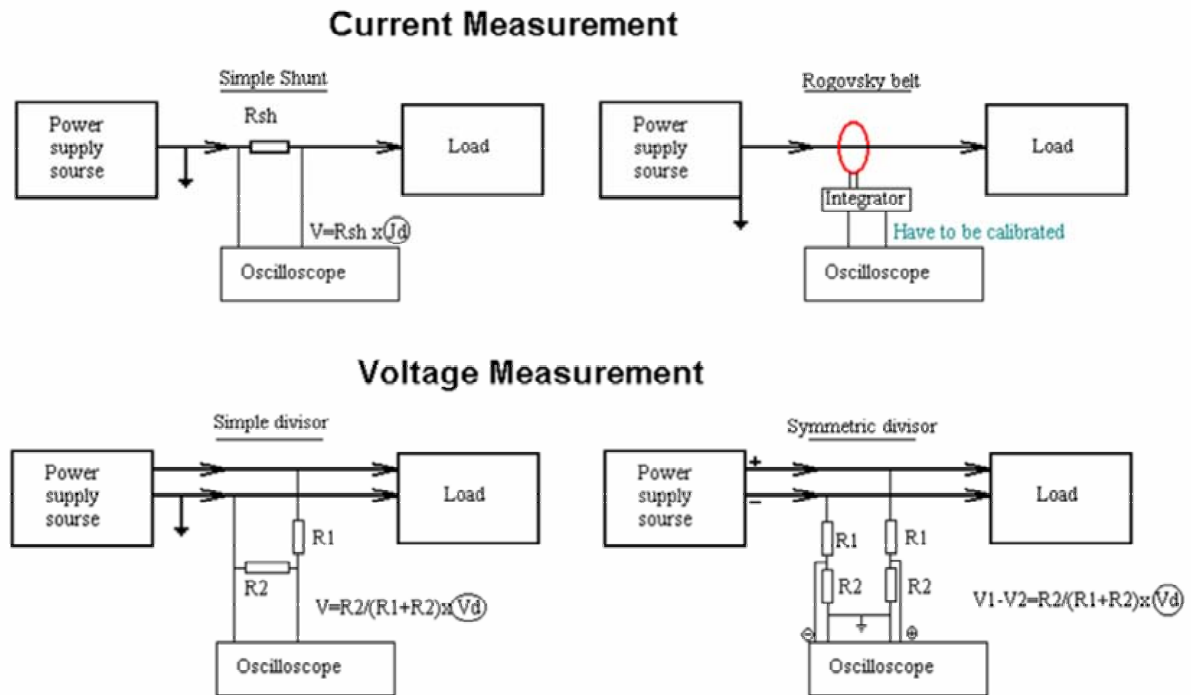


Fig.2.1.5.3. Sensors arrangement

The input power can be calculated in accordance with a simple formula:

$$W_{pl} = N \times U_{pl} \times (U_{ps} - U_{pl}) / R_b;$$

where W_{pl} - input power to a plasma volume, U_{pl} -voltage on a plasma gap; U_{ps} -voltage of power supply; N -number of ballast resistors; R_b -resistivity of ballast. It is easy to recognize that the maximal input power is achieved at gap voltage in a half of input voltage. At eight electrodes and 5kV of the capacitance voltage the maximal value of the input power depends on the ballast resistance in accordance with the following formulae:

$$W_{plmax} = 50 / R_b (\text{kW}).$$

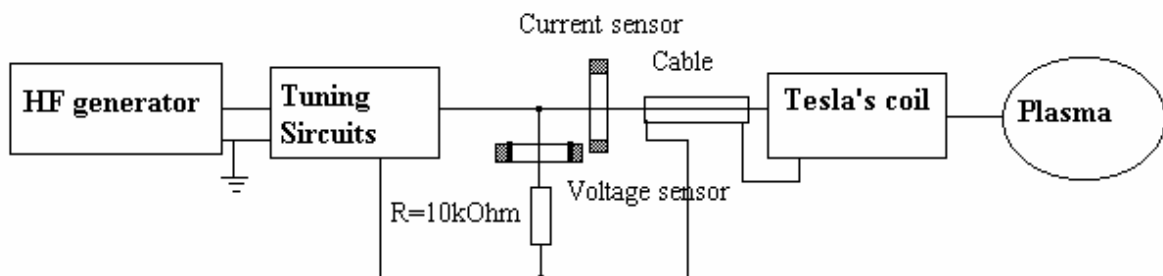


Fig.2.1.5.4. Principal scheme of the input power measurements.

In a case of HF feeding the input power and electrode voltage were measured during the experiments. A main method of input power measurement is the calculations on base of

Voltage-Current-Phase measurements: $W_m = I_{ef} \times V_{ef} \times \cos\varphi$. A principal layout of these measurements is presented in Fig.2.1.5.4. It has been verified during last works.

For the measurements a current transformer (Rogovsky coil) is the most expediently to use. It is not tied galvanically with power circuits, which is useful for a EM noise rejection procedure. As a current sensor a Rogovsky belt (thoroidal) can be used with air core and screened turns. As a voltage sensor a Rogovsky belt can be used with ferrite core and screened turns. A load of about 10kOhm allows measuring current instead of voltage. The measurements of power require a measuring of phase difference. Values of current and voltage in contour change not so dramatically at change of load. The phase difference is close to 90 degrees.

In the case of middle frequency power supply the gap voltage and current have to be measured independently. At such a time scale the plasma is not a linear load. The instant input power is calculated in accordance with the simple formulae:

$$W_{pl} = N \times U_{pl} \times I_{pl};$$

but the mean input power will be defined by means of automatic procedure of integration.

The electrical measurements in the case of dielectric barrier discharge require more complex methodic, which is considered in section 2.3.3 in details.

2.2. Experimental Results on Quasi-DC Surface Plasma Effect.

General Notes.

These efforts were fulfilled due to two main ideas: flow control in ducts and diffusers/inlets adjustment.

Duct-driven flow control. The scheme of the plasma-induced flow modification method is shown in Fig.2.2.1. An idea of the method is that the surface-generated plasma provides the energy release under the predefined location and creates a “smooth” plasma layer near the duct surface. In dependence with the input power such a layer generation can lead to boundary layer modification, local BL separation or extensive (global) separation. Shock waves structure accompanies these processes. Flow parameters such as Mach number, pressure and shocks position can be changed controllably, as well as their distribution in cross-section. The effect of instabilities damping and obstacles’ screening has been also described and published recently (see references below).

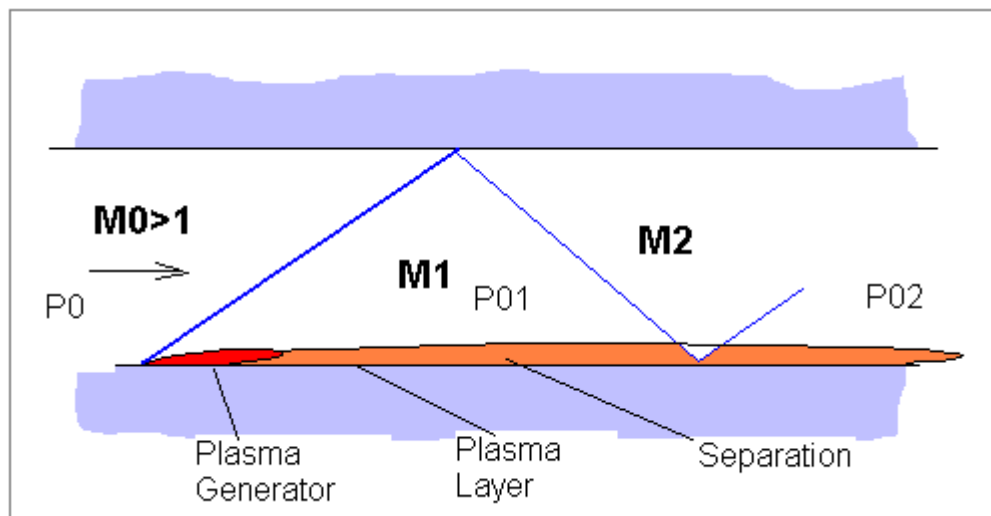


Fig.2.2.1. Scheme of the flow modification by the surface plasma.

The scheme of the model experiments is corresponded with Fig.2.2.1 directly. The effect of the obstacle’s drag reduction has been explored for the case of 10% elliptic half-profile.

Inlet’s shocks control. The idea is described in Fig.2.2.2. The generation of the plasma layer just upstream the inlet edge can prevent undesired shock reflection. The surface plasma generation could be useful to change the position of the second shock upstream and stabilize the location of the third shock reflection near the edge of the inlet.

The scheme of the model experiments is corresponded to Fig.2.2.2. The change of the shock position and angle on the artificial wedge and the duct bulk parameters are studied under the surface plasma effect.

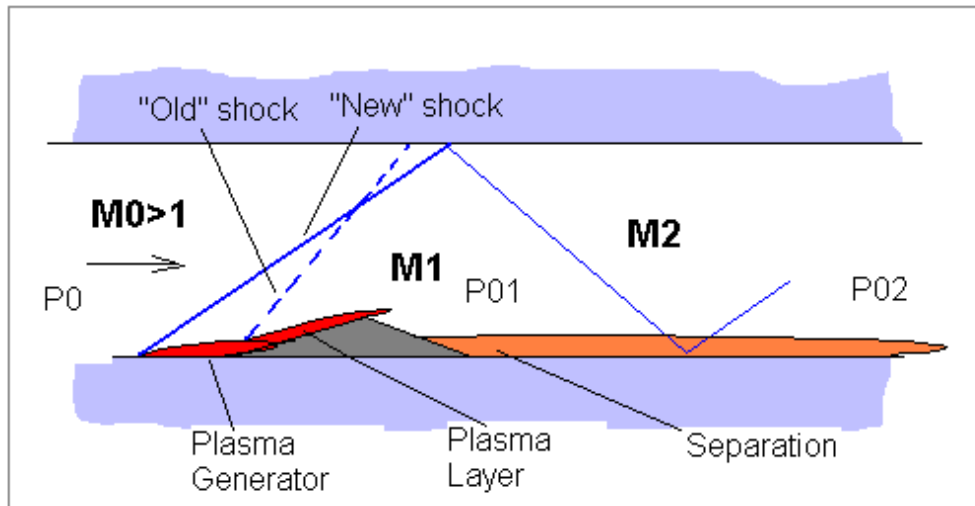


Fig.6.1.2. Model experiment arrangement on inlet control.

It is clear that addition of large amount of the thermal energy might lead to modification of the wave structure in duct-driven flows. From the other side such an addition can change the parameters of whole flow significantly and not to the desired direction. Thus, the efficiency of the plasma effect is very important at the diminishing of the possible penalties. The optimization of such an influence is urgently considered necessary.

References to Section 2.2.

1. S. Leonov, V. Bityurin, K. Savelkin, D. Yarantsev "The Features of Electro-Discharge Plasma Control of High-Speed Gas Flows." AIAA-2002-2180, 33-th Plasmadynamic and Laser Conference, 20-24 May, 2002, Maui, HI.
2. S. Leonov, V. Bityurin, A. Klimov "Effectiveness of Plasma Method of Flow/Flight Control." Proceedings of the Symposium on Thermal-Chemical Processes, St-Petersburg, "Leninets", July, 2002.
3. S. Leonov, V. Bityurin, K. Savelkin, D. Yarantsev "Effect of Electrical Discharge on Separation Processes and Shocks Position in Supersonic Airflow." 40th AIAA Aerospace Sciences Meeting & Exhibit, 13-17 January 2002 / Reno, NV, AIAA 2002-0355.

4. S. Leonov, V. Biturin, N. Savischenko, A. Yuriev, "Study of Surface Electrical Discharge Influence on Friction of Plate in Transonic Airflow". AIAA-2001-0640, 39th AIAA Aerospace Meeting and Exhibit, 8-11 January, Reno, NV, 2001.
5. S. Leonov, V. Biturin, A. Klimov, Yu. Kolesnichenko, A. Yuriev "Influence of Structural Electric Discharges on Parameters of Streamlined Bodies in Airflow." 32th AIAA Plasmadynamics and Lasers Conference and 4th Weakly Ionized Gases Workshop 11-14 June 2001 / Anaheim, CA, AIAA-2001-3057.
6. S. Macheret, M. Schneider, R. Miles "Nonequilibrium Magnetohydrodynamic Control of Turbojet and Ram/Scramjet Inlets", AIAA-2002-2251, 33th Plasmadynamic and Laser Conference, 20-24 May, 2002, Maui, HI.
7. S. Leonov, V. Biturin, A. Bocharov, E. Gubanov, Yu. Kolesnichenko, K. Savelkin, A. Yuriev, N. Savischenko "Discharge plasma influence on flow characteristics near wall step in a high-speed duct." The 3rd Workshop on Magneto-Plasma Aerodynamics in Aerospace Applications, Proceedings, Moscow, IVTAN, 24-26 April, 2001.
8. Kazakov A., Kogan M., Kuriachi A., Influence on the friction of local heat addition to the turbulent boundary layer. Mech. Of Fluids and Gases, N1, 1997. // Kurjachi A. P., Boundary layer transition by means of electrodynamics method. Prikl. Math. I Mech., vol.49, issue 1, 1985. // A.V. Kazakov, A.P. Kuryachii, Electrogasdynamic influence on the development of the small disturbances in a boundary layer in the thin profile Izv. AN USSR, Mekhanika zhidkosti i gaza, 1, 1986
9. S. Leonov, V. Nebolsin, V. Shilov "Effectiveness of plasma jet Effect on Bodies in an Airflow", Proceedings of Workshop "Perspectives of MHD and Plasma Technologies in Aerospace Applications", Moscow, IVTAN, 1999, pp. 58-65.
10. G. Candler, D. Kelley "Effect of Internal Energy Excitation on Supersonic Blunt-Body Drag", Proceedings of Workshop "Perspectives of MHD and Plasma Technologies in Aerospace Applications", Moscow, IVTAN, 1999, pp. 53-57.
11. S. Leonov, V. Biturin, K. Savelkin, D. Yarantsev D. VanWie "Hydrocarbon Fuel Ignition in Separation Zone of High Speed Duct by Discharge Plasma." The 4th Workshop on Magneto-Plasma Aerodynamics in Aerospace Applications, Proceedings, Moscow, IVTAN, April, 2002.
12. S. Leonov, V. Biturin "Hypersonic/Supersonic Flow Control by Electro-Discharge Plasma Application." 11th AIAA/AAAF International Symposium Space Planes and

Hypersonic Systems and Technologies, Orléans, 29 September – 4 October, 2002, AIAA-2002-5209.

13. S. Leonov, V. Bityurin, K. Savelkin, D. Yarantsev "PROGRESS in INVESTIGATION for PLASMA CONTROL of DUCT-DRIVEN FLOWS." AIAA-2003-0699 41th AIAA Aerospace Meeting and Exhibit, 6-10 January, Reno, NV, 2003.
14. S. Leonov, V. Bityurin, K. Savelkin, D. Yarantsev, Plasma-Induced Ignition and Plasma-Assisted Combustion of Fuel in High Speed Flow. Proceedings of the 5th Workshop "PA and MHD in Aerospace Applications", 7-10 April, 2003, Moscow, IVTAN.
15. S. Leonov, V. Bityurin, D. Yarantsev "The Effect of Plasma-Induced Separation", AIAA-2003-3853, 34-th Plasmadynamic and Laser Conference, 23-26 June 2003 / Orlando, FL.
16. S. Leonov, A. Kuryachii, D. Yarantsev, A. Yuriev, "Study of Friction and Separation Control by Surface Plasma." Paper AIAA-2004-0512, 42th AIAA Aerospace Sciences Meeting & Exhibit, 05-08 January 2004 / Reno, NV.
17. S. Leonov "Near-Surface Plasma Effects in High-Speed Flows", Russian School-Workshop "MPA in Aerospace Applications", 20-21 April 2004, IVTAN, Moscow.
18. S. Leonov, K. Savelkin, D. Yarantsev "Electrical Discharge Effect on Structure and Parameters of Supersonic Airflow". Proceedings of the Symposium on Thermal-Chemical Processes and Plasma Applications in Aerodynamics, St-Petersburg, "Leninets", 12-14 July, 2004.

2.2.1. Design of Quasi-DC Surface Plasma Generator.

Typically, a quasi-continuous multi-electrode surface discharge was used for the plasma excitation. The electric energy release to the plasma volume was occurred over a width of the discharge plate of 10-20mm. The electrodes have been flush mounted on an insert made of a dielectric thermo-resistive material. The discharge was excited in two main modes: longitudinal and transversal, although the most data are related to the last one. The draw of the electrodes arrangement is shown in Fig.2.2.1.1. The anodes-cathodes location is imaged as for longitudinal mode here.

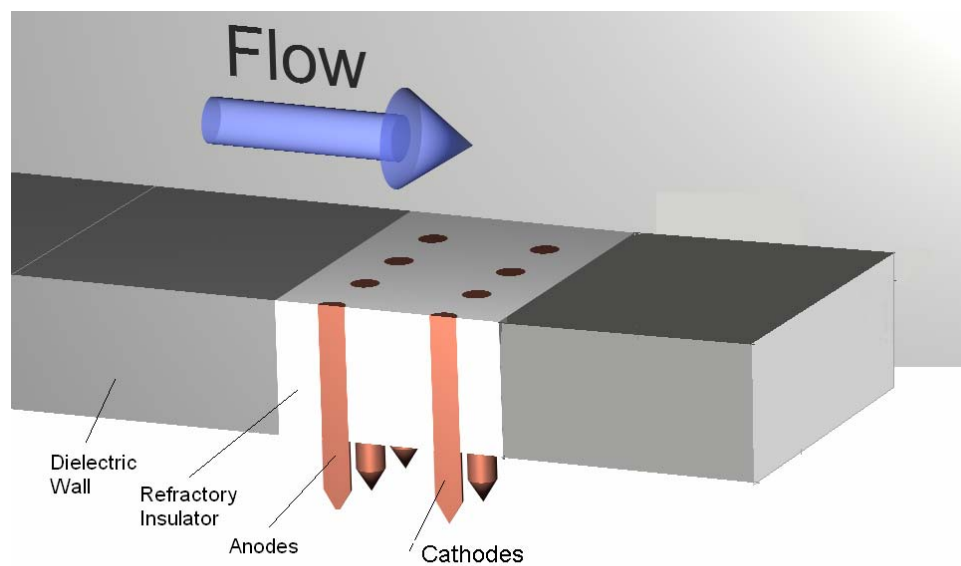


Fig.2.2.1.1. Scheme of the surface discharge lay-out.

The surface discharge can be characterized roughly by the following parameters:

- ◇ type of plasma – quasi-DC multi-electrode surface discharge,
- ◇ typical electric current through an individual electrode $I_d \approx 1-5A$,
- ◇ typical total input electric power $W = 1-4kW$,
- ◇ reduced electric field up to $E/n=40Td$,
- ◇ duration of plasma pulse between 50 and 100ms.

The discharge appearance in two modes and the principal scheme of the supply are shown in Fig.2.1.1.2a,b. The positive (“hot”) electrodes have been located upstream in respect of grounded electrodes at distance 10mm for the longitudinal operation mode. One of the peculiarities of this mode of the discharge is that the current connects from the anodes to the ground by separate “cords” along the velocity vector. Current sharing between the electrodes

pairs has been measured as negligible. In the case of transversal discharge a relaxation type of the plasma generation process took place. An initial plasma filament is being blow down, breaking and starting again in about 10 μ s (see below).

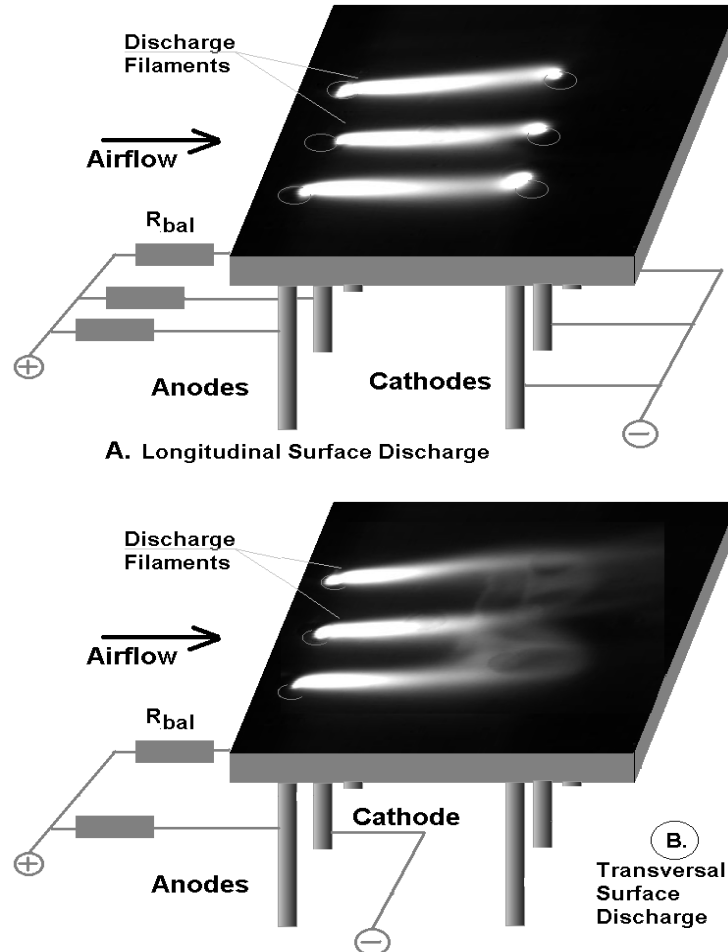


Fig.2.2.1.2. Longitudinal (a) and transversal (b) discharges appearance. Layout of binding.

Original power supply was used for plasma generation. An appropriate principal scheme for the four channels is presented in Fig.2.2.1.3. The anodes had individual high-voltage excitation to provide similar conditions for each one. The pulse scheme provides high-voltage pulses for breakdown and to avoid an occasional discharge termination. The plasma loads in the scheme are simulated by resistance $R(I)$ which value depends on current flowed through.

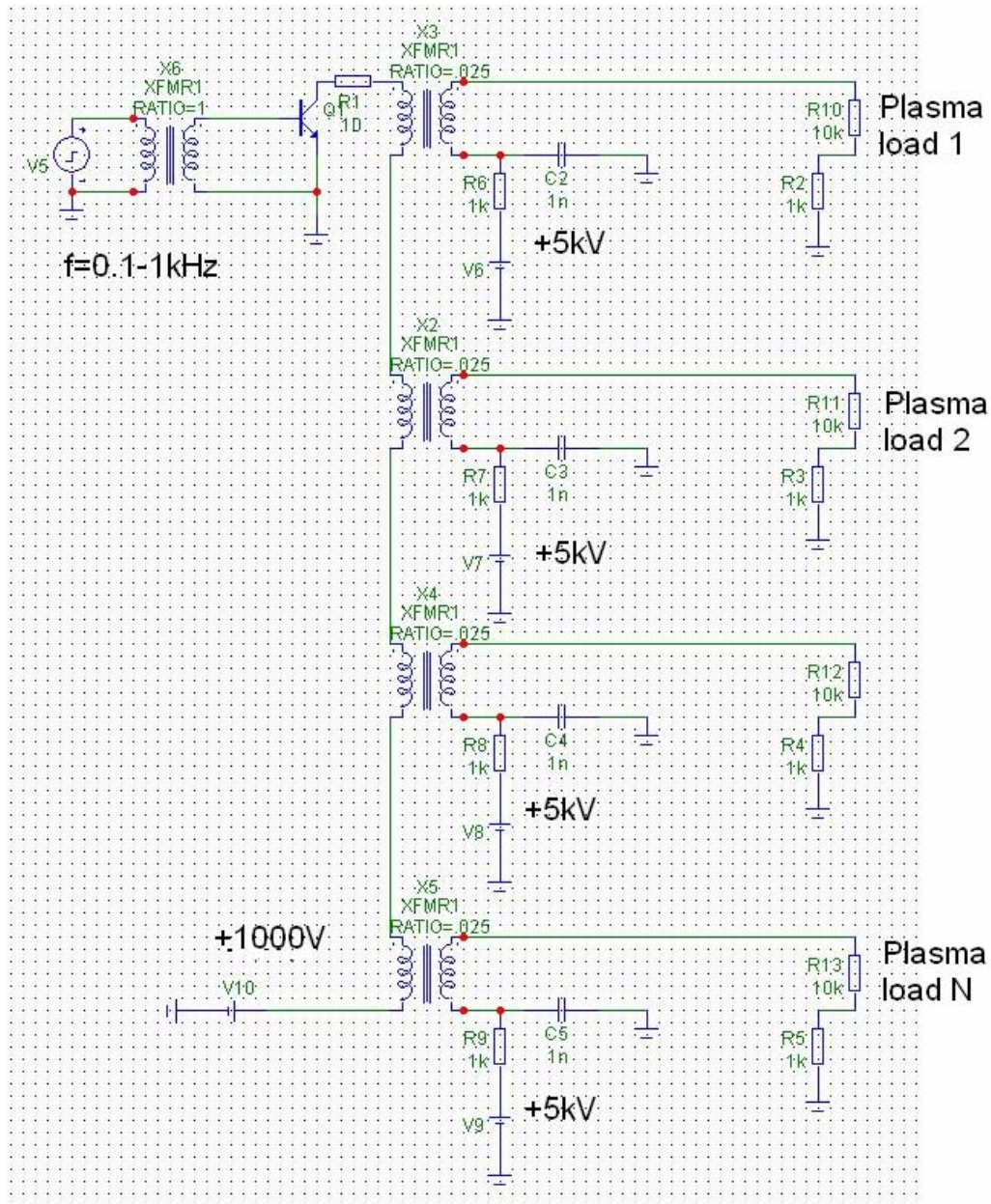


Fig.2.2.1.3. Principal electric scheme of the surface discharge excitation.

The time behavior of voltage-current-radiation characteristics in two modes is sufficiently different too. Longitudinal discharge, as a rule, has a low level of the parameters' amplitude modulation, typically on the level a few percent in the gap voltage. A sample of voltage, current and integral radiation oscillogram for the longitudinal discharge is presented in Fig.2.2.1.3.

Oppositely that the transversal discharge is characterized by large level of modulation of the main parameters, including gap voltage, resistivity, radiation and the position of downstream edge. The appropriate oscillograms are shown in Fig.2.2.1.4.

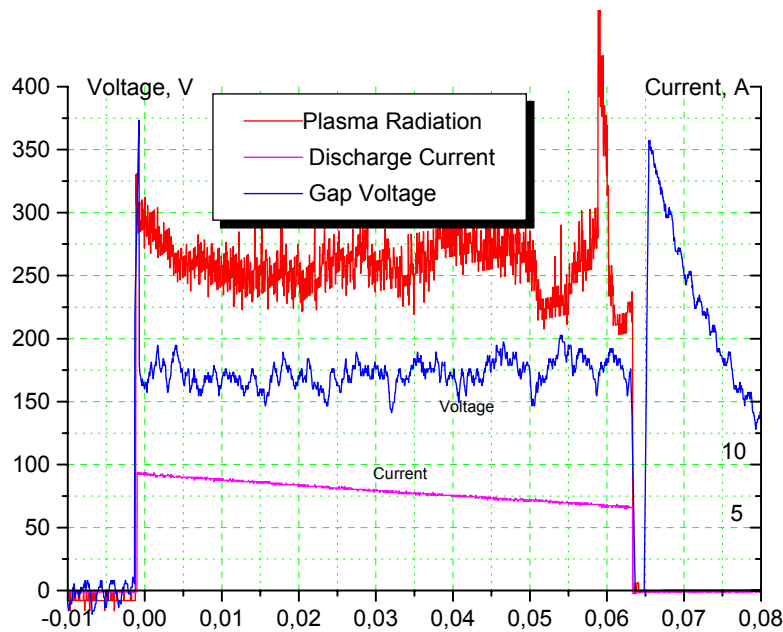


Fig.2.2.1.3. Oscillograms of processes in longitudinal surface discharge.

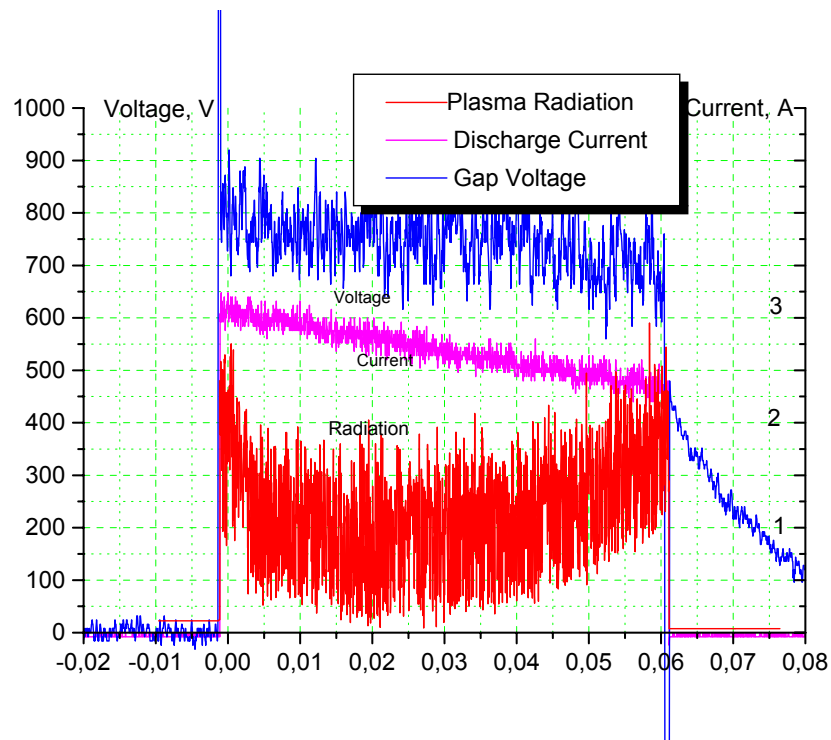


Fig.2.2.1.4. Oscillograms of processes in transversal surface discharge.

Well seen that the gap voltage value is much greater in the case of transversal discharge than at longitudinal one. It is quite reasonable due to the efficient length of the plasma filament is larger. As the result the less current and numbers of electrodes gives the same input power for the transversal mode. The transversal discharge occurs more effective to

change the structure of airflow. That is why the transversal type of the surface discharge has been chosen for the further experiments.

A large level of fluctuations in discharge parameters can be explained by the filamentary plasma instability, which is due to interaction with high-speed airflow. A very close correlation between the voltage and radiation modulation has been observed experimentally. A detail oscillogram of the signals is shown in Fig.2.2.1.5.

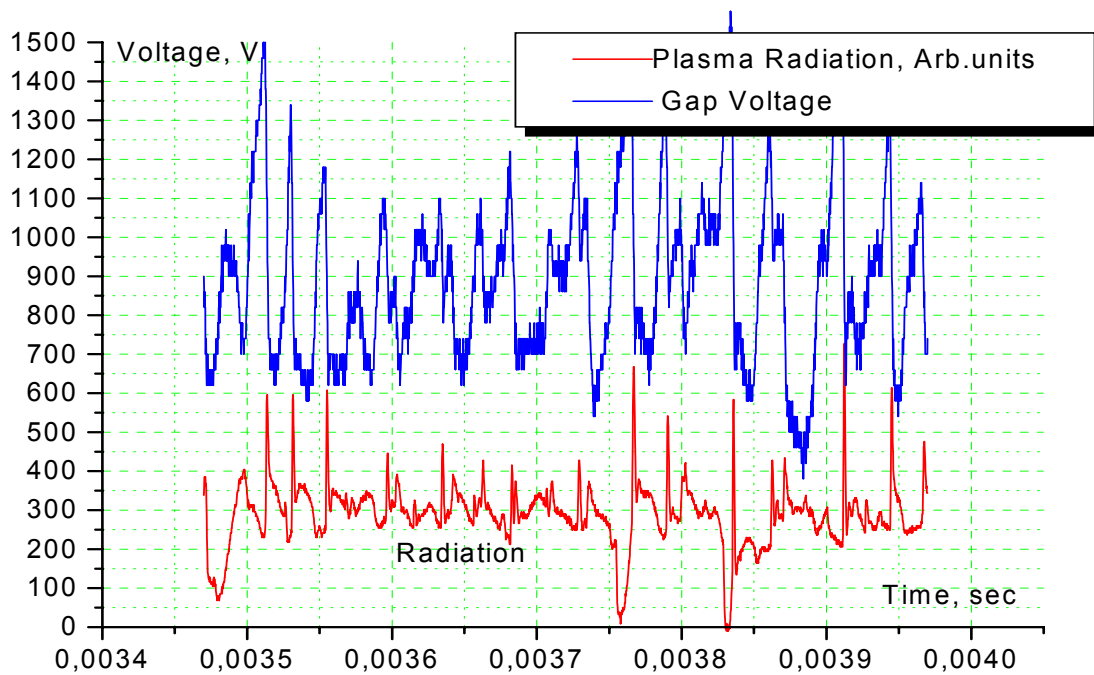


Fig.2.2.1.5. Detailed correlation between voltage and plasma radiation at instability.

Two regimes of the discharge renovation are possible: when the plasma is distinguished, and repetitive mode with sequential runs of individual plasma filaments. A typical Fourier spectrum of the voltage modulation is shown in Fig.2.2.1.6. The maximal amplitude occurs near the frequency $f=20\text{kHz}$. Under the conditions of the experiment the value of the relaxation time is well correlated with the characteristic length of the plasma channel about 2cm. The frequency of such a relaxation process is defined by the flow local velocity and can be tuned by the level of voltage and inter-electrode gap.

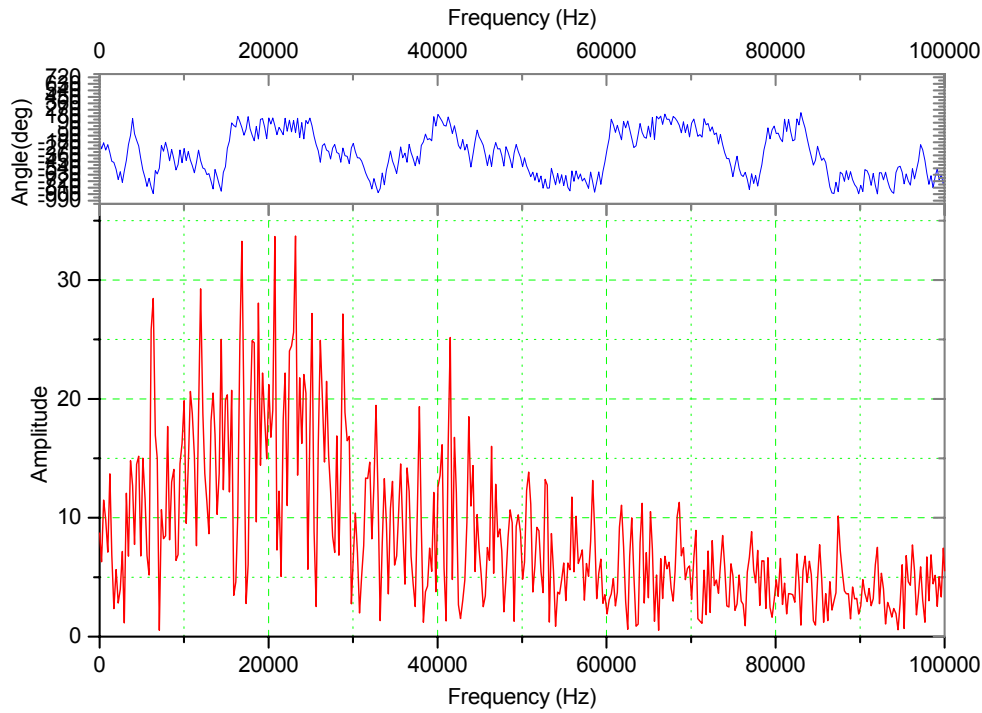


Fig.2.2.1.6. Fourier spectrum of the gap voltage variation in transversal surface discharge.

A special attention has been paid to the problem of effective method of electric energy deposition to the plasma. As it has been told above the transversal mode of the surface discharge is more effective than longitudinal one. The next chart in Fig.2.2.1.7 presents volt-ampere characteristic of such discharge at different static pressure in the test section.

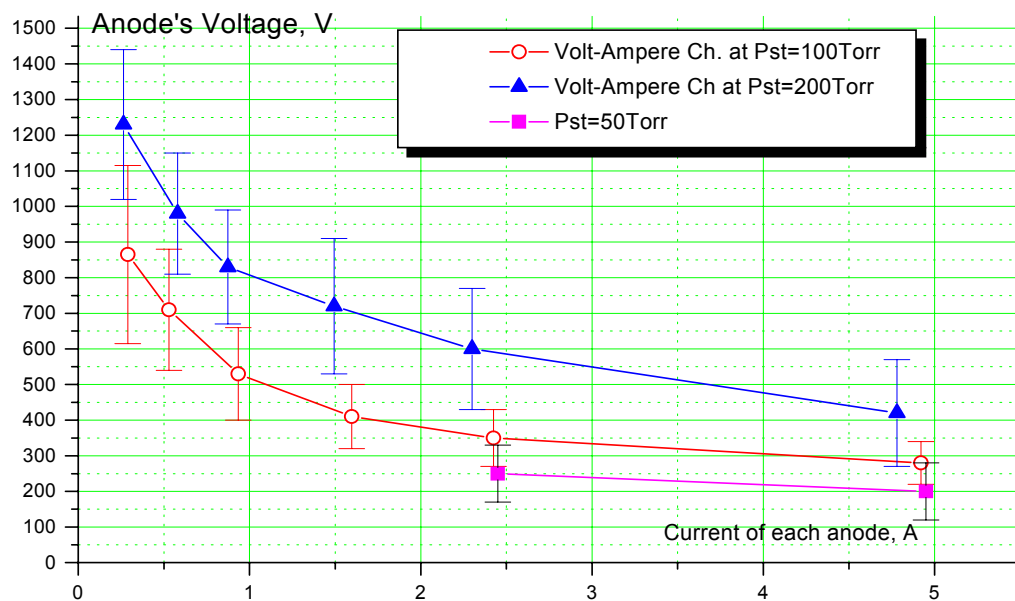


Fig.2.2.1.7. Transversal surface discharge volt-ampere characteristics at two anodes, $M=1.9$, inter-electrodes gap 7mm.

The current-power characteristic of the transversal surface discharge is presented in Fig.2.2.1.8. The edges in power input, when the BL separation without reattachment took place, are pictured in the next figure for two values of static pressure (see below).

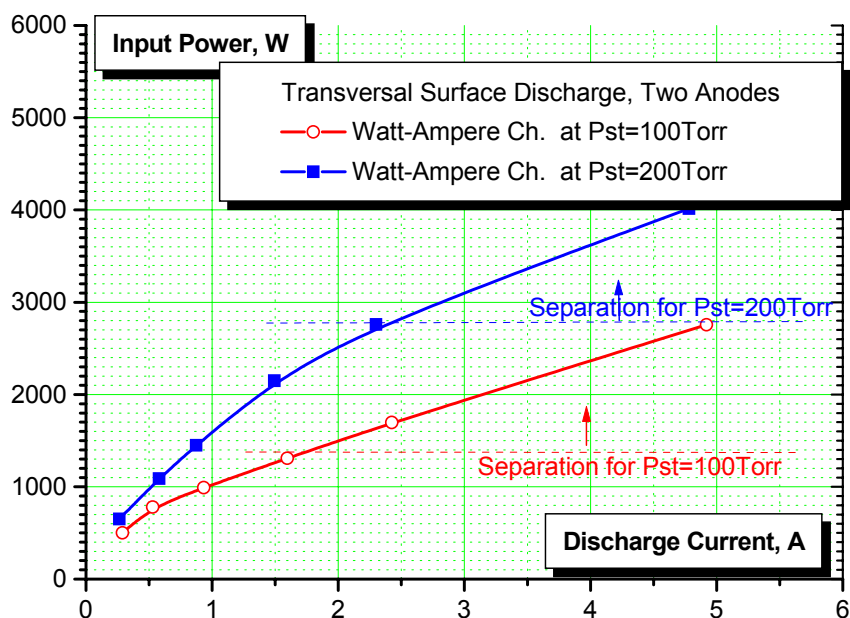


Fig.2.2.1.8. Transversal surface discharge characteristics at two anodes,
M=1.9, inter-electrodes gap 7mm.

2.2.2. Measurements of Filamentary Plasma Parameters.

Emission spectrums of the surface discharge were measured by LOT-Oriel MS 257 spectrograph with spectroscopic CCD camera Andor DU420. A main scheme of measurements was described in section 2.1.4. The modification is shown in Fig.2.2.2.1. Duration of the discharge was 70ms and exposure time of the spectroscopic camera was 50ms. Synchronization was the following: exposure period starts by trigger2 after the discharge having been switched on by trigger1.

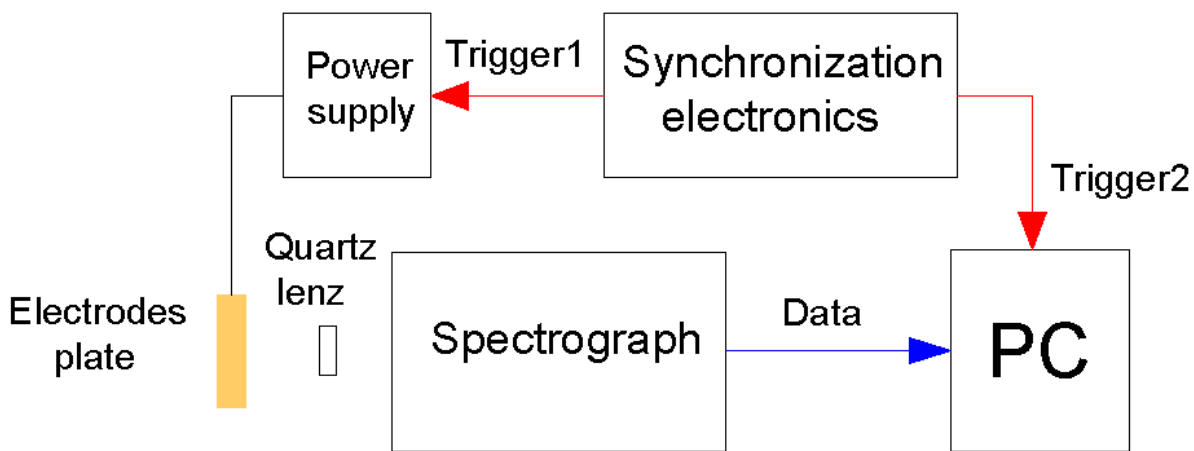


Fig.2.2.2.1. Scheme of spectroscopic measurements

The filamentary plasma of transversal surface discharge has a high temperature (more than 3kK in our conditions) so, as was mentioned above, accuracy of the temperature measurements is about 10% in this case. When the spectrum is unresolved the regular error of the temperature determination can be estimated as 200-300K for $T_g = 3\text{kK}$ and 500-800K for $T_g = 5\text{kK}$.

A minimal dispersion of the monochromator we used in experiments is 1.6 nm/mm. A pixel size of the spectroscopic camera is 26 μm , summary dispersion is of 0.4 Å/pixel. Each separate line must be described by three points at least. Therefore, the minimal instrumental function half-width is $f_a = 0,8\text{Å}$. At such condition we can resolve rotational lines of N₂ the second positive system partly and, as a result, increase the precision of temperature measurements in comparison with unresolved case.

In the experiments described the maximal rotational temperature of the gas was measured by two molecular bands: second positive system of neutral nitrogen N₂ and violet system of neutral cyan CN. The most tests were done at 100Torr and 200Torr of static pressure and initial Mach number of the flow $M = 1.99\text{-}1.9$.

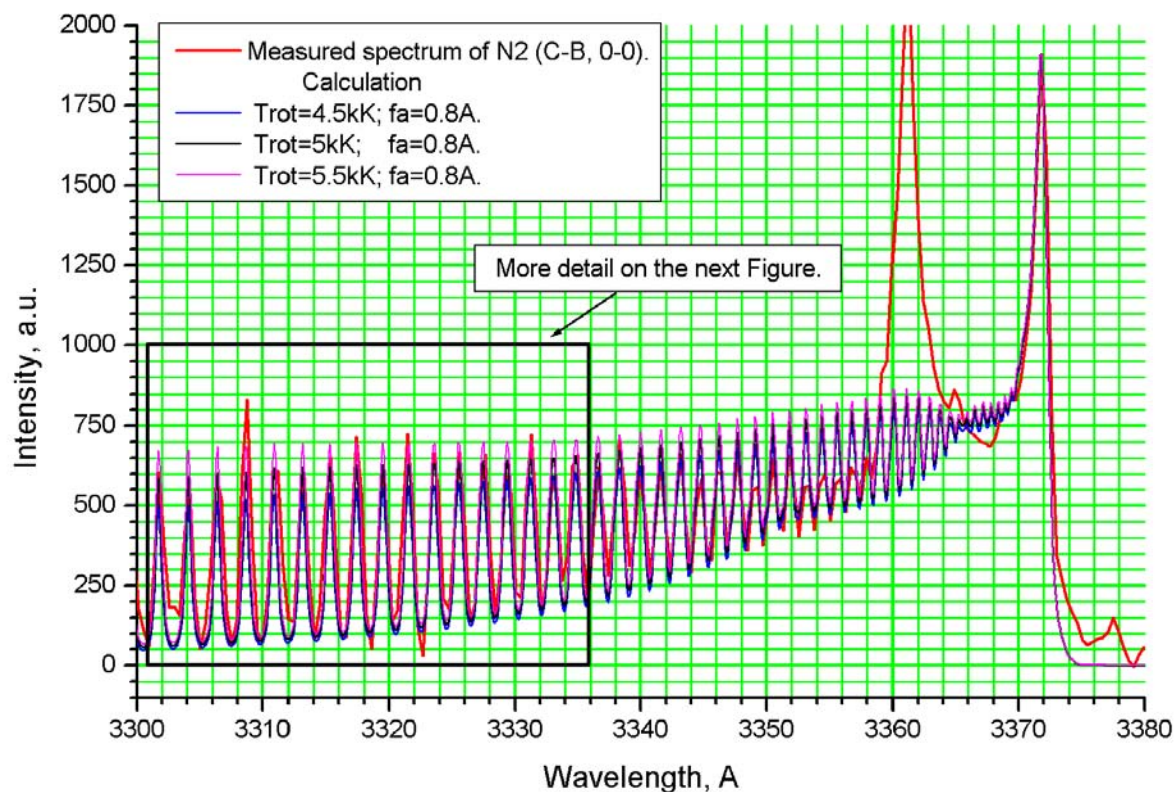


Fig.2.2.2.2. Fitting of the synthetic spectrum and experimental one for the filamentary surface discharge.

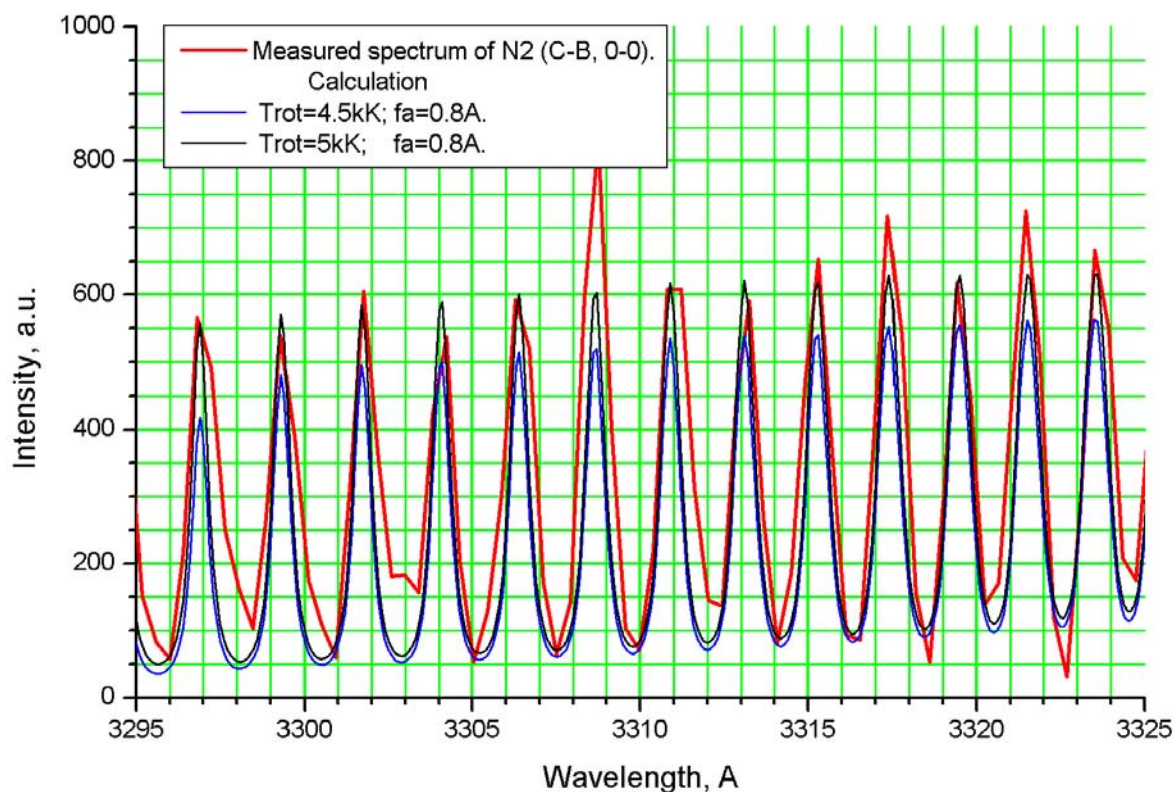


Fig.2.2.2.3. Zoomed part of the Fig.2.2.2.2.

A sample of the N₂ spectrum fitting is presented in Figs.2.2.2.2 and 2.2.2.3 for the surface discharge through two anodes with current $I_{pl}=2.3A$ of each at static pressure $P_{st}=100Torr$. It is seen that the experimental spectrum is the most close to synthetic one with the temperature about $T_g=5kK$.

A small addition of CO₂ to working gas was used for the CN spectrum generation. The method of processing is found on accurate fitting of experimental and calculated spectra at rotational and vibrational temperatures variation. A sample of the spectra fitting is presented in Fig.2.2.2.4.

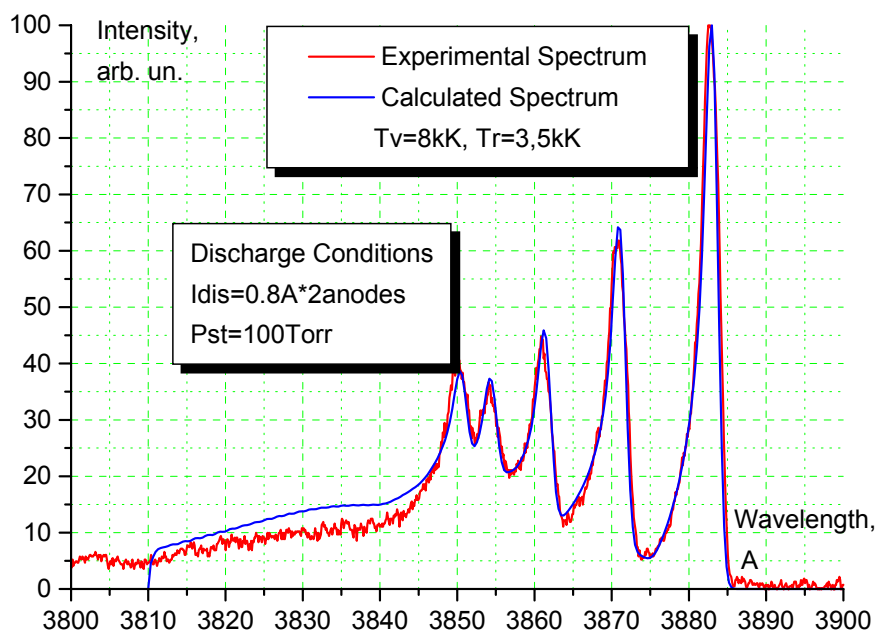


Fig.2.2.2.4. Sample of CN spectra fitting.

It should be noted that the large excess of the vibrational temperature over the rotational one is not a rule. When the current and pressure are increased the rotational temperature increases too. In the most cases such an excess is negligible in comparison with the average level of the temperature.

The results of the rotational temperature measurements are summarized in Table 2.2.2.

Table 2.2.2.

Pressure	Molecule measured	$I_{pl}=0.8A$	$I_{pl}=2.3A$	$I_{pl}=4.3A$
100 Torr	N2	$T_r=4.5\pm0.5\kappa K$	$T_r=5\pm0.5\kappa K$	$T_r=9\pm1\kappa K$
100 Torr	CN	$T_r=3.8\pm0.5\kappa K$		$T_r=7\pm1\kappa K$
200 Torr	CN	$T_r=3.0\pm0.5\kappa K$		$T_r=4.5\pm0.5\kappa K$

The plasma temperature was measured in the region of the discharge cords using spectroscopic techniques and was 3-5 kK depending on the experimental conditions. Increasing the input power leads to slow rise of the maximal temperature. At the same time the temperature values are unexpected high when the power deposition exceeds some critical level. The explanation could be in fact that in that case the most part of the plasma is located inside of artificial separation zone (see below).

Plasma temperatures within the discharge were measured using optic spectroscopy, although it should be noted that the correct interpretation of plasma spectrum is difficult and presents uncertainties due to the strong non-homogeneity of the discharge structure. The alteration between values measured by different molecules could be considered as the result of their different location and origination.

The thermodynamic approach allows relating the power input W_{pl} , the plasma temperature $T+\Delta T$, the thickness of the plasma layer δ_{pl} and the discharge hot area thickness δ_{dis} (Z is the duct width):

$$W_{pl} \cong G_{pl} c_p \Delta T, \text{ where } G_{pl} = \rho_{\infty} M_{\infty} c_{\infty} Z \delta_{dis};$$

$$\text{Thus, } \delta_{pl} = \delta_{dis} \left(1 + \frac{\Delta T}{T} \right)^{1/\gamma}.$$

The correlation of the data of observations and pressure measurements gives the following result at power input a few kW and the static pressure about 100Torr: typical Mach number in the plasma overlayer is $M=0.7-0.95$ (the modes with $M>1$ are experienced too), mean gas temperature $T=700-800K$, gas expense through the discharge area about $G_{pl}=2g/sec$, stagnation pressure in the layer drops at the discharge switching on typically from 400Torr down to 140Torr. The problem of contradiction between measurements and calculations can be resolved by suggestion of the local separation in area of the discharge generation as well as by the idea of strong non-homogeneous distribution of the plasma parameters.

2.2.3. Dynamics of Filamentary Plasma Inflow.

As it was mentioned above the transversal electric discharge is the system of relaxation type when the individual plasma filaments move in airflow from electrodes area downstream. This movement continues up to moment when the gap voltage achieves some limit. The old plasma filament breaks and a new one starts again.

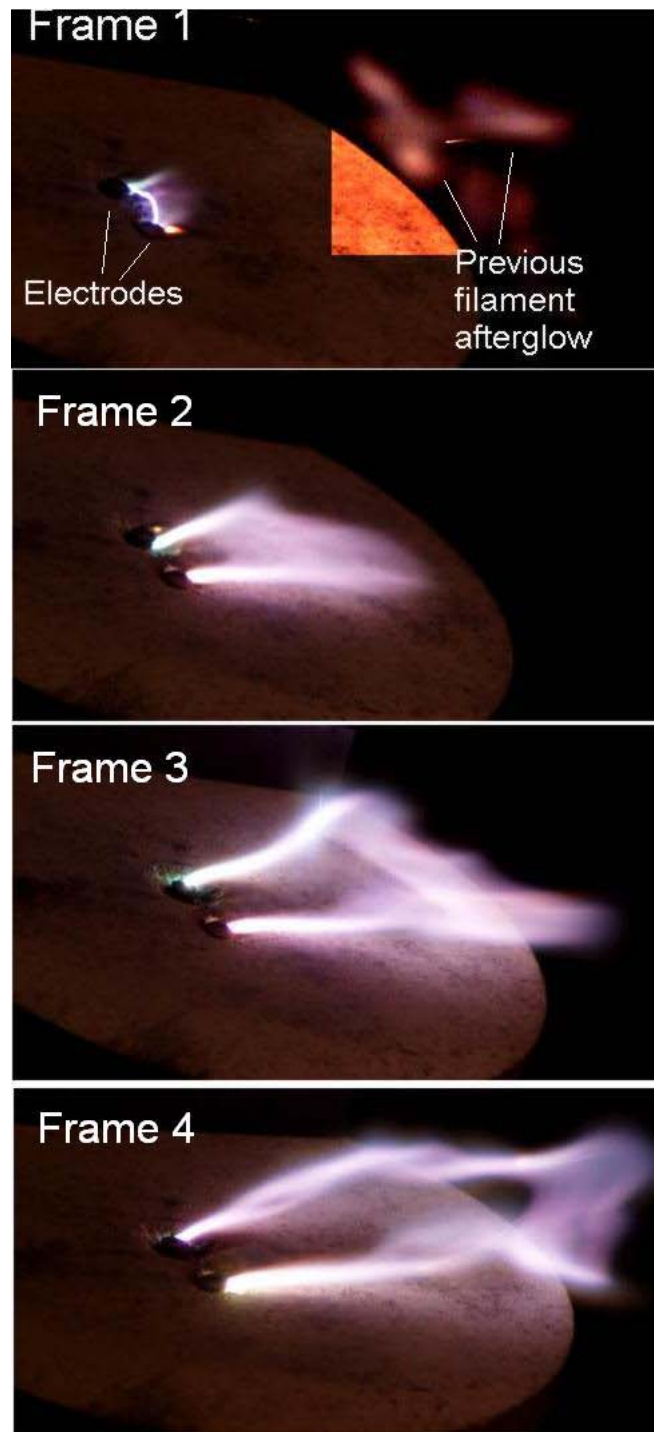


Fig.2.2.3.1. Dynamics of individual plasma filament inflow.

Such a dynamics is illustrated by frames sequence presented in Fig.2.2.3.1. It was recorded under subsonic conditions but quite reflect all features of the relaxation process.

A different technique was applied to study of the plasma filament behavior in supersonic flow. The electrical current was modulated by AC component with the frequency 100kHz (that is corresponds to 200kHz of the radiation intensity modulation). Frame duration of the camera in “short shutter” operation mode was 30mcs. Under these parameters six maximums of plasma luminosity have to be recorded. Samples of such records are shown in Fig.2.2.3.2 for two electrodes configuration and for three electrodes arrangement.

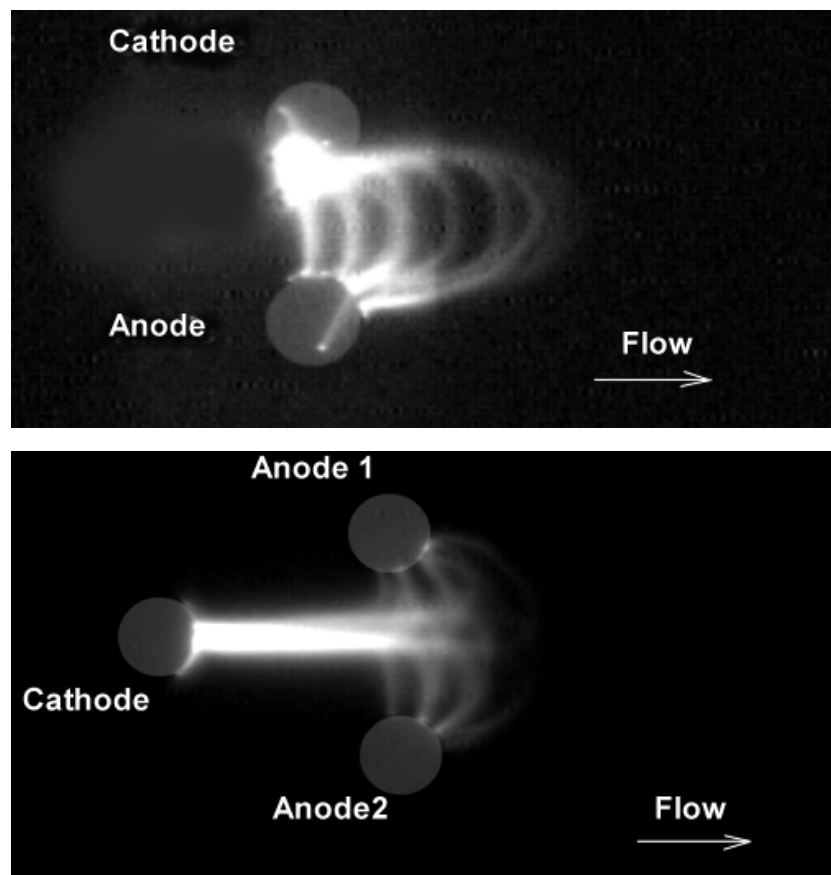


Fig. 2.2.3.2. Image acquisition with current modulation.

This technique allowed us to measure the plasma filament movement velocity inflow. The value was in a range $V=400-450\text{m/s}$, i.e. equal to flow speed practically.

2.2.4. Simplified Physical Model of Interaction.

The model of the phenomena includes three important items:

- Discharge structure and parameters in airflow near the surface;
- Plasma layer generation process;
- Interaction of the plasma layer with the supersonic flow.

The discharge structure in airflow depends on the type of discharge sufficiently. The transversal quasi-DC discharge has been described above phenomenologically. The discharge engenders energy release to airflow as well as change of gas-kinetic and electro-magnetic properties of the medium. The behavior and properties of the electric discharge in airflow are sharply different from ones in static ambience. In the case of transversal discharge a relaxation type of the plasma generation process took place. An initial plasma filament is being blow down, breaking and starting again in about 10-20mcs. The transversal discharge is characterized by large level of modulation of the main parameters, including gap voltage, resistivity, radiation and the position of downstream visible edge of the plasma. The appropriate oscillograms are shown in Fig.2.2.4.1 with high temporal resolution.

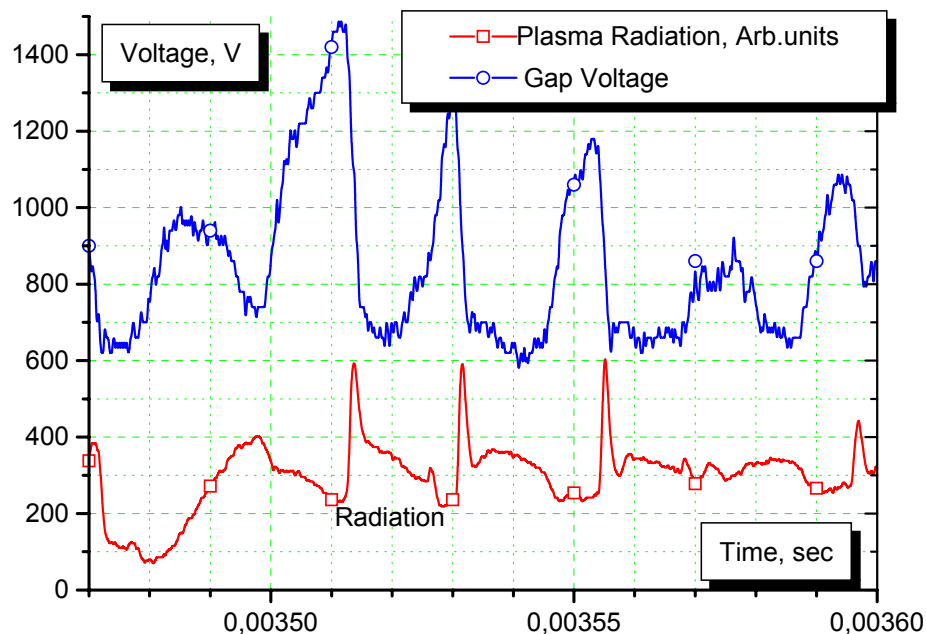


Fig.2.2.4.1. Detailed correlation between voltage and plasma radiation at instability.

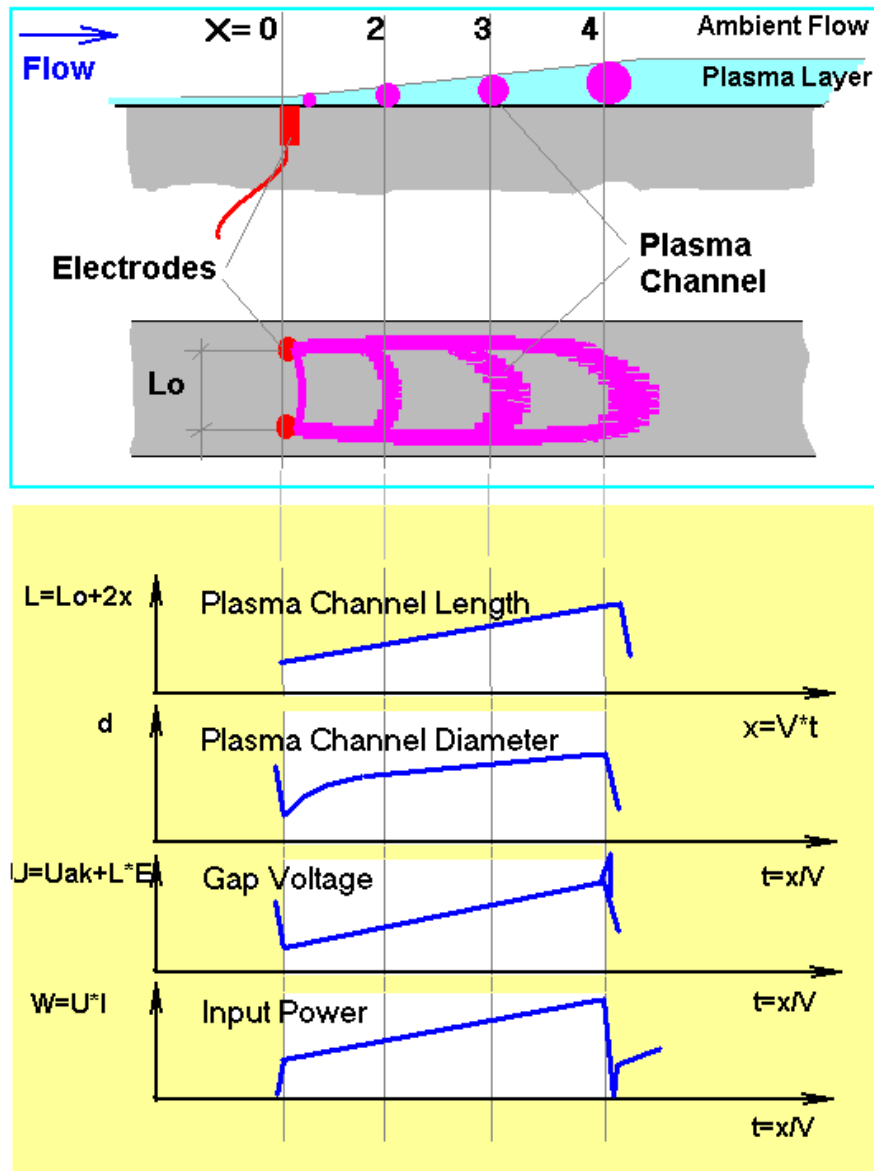


Fig.2.2.4.2. Scheme of the model consideration.

Large level of fluctuations in discharge parameters can be related to the filamentary plasma instability, which **is** (arises) due to interaction with high-speed airflow. A very close correlation between the voltage and radiation modulation has been observed. The frequency of such a relaxation process is defined by the flow local velocity and can be tuned. In our specific conditions the maximal amplitude in an oscillation spectrum occurs near the frequency 30-50kHz. Under the conditions of the experiment such a value is well correlated with the characteristic length of the plasma channel (x_{\max}) about 2cm. The process is drawn in Fig.2.2.4.2.

An initial breakdown between the flush-mounted electrodes takes place under the flow conditions ($P_{st}=100\text{Torr}$) at the electric field strength about $E=3\text{kV/cm}$. The first and

sequential breakdowns happen, as a rule, inside the boundary layer due to a lower value of the gas density there. The gas temperature inside the plasma channel starts to rise and the channel swells up itself volumetrically. This time the plasma filament comes into the main flow-field and blew down with the flow speed. The plasma filament's expansion is continued simultaneously with its lengthening. The filament's shape looks like an increasing loop. The gap's voltage increases in accordance with the filament's length up to the level when the new breakdown is realized in the position much closer to the electrodes. Such a relaxation type of process is repeated with the frequency, which can be referred to a gas-dynamic time. The external shape of the generated on such manner plasma layer looks like a near-surface wedge, which is streamlined by the main flow, as it can be seen in photo and Schlieren photo in Fig.2.2.4.3 if the temporal resolution is not high enough to recognize the fast oscillations. More exactly, such a wedge forces out the main flow from the surface.

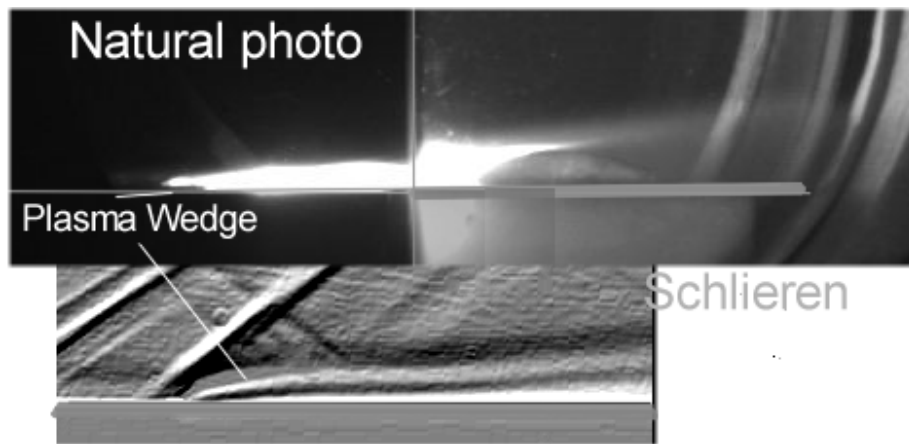


Fig.2.2.4.3. Plasma "wedge" generation.

Plasma layer generation process can be described roughly as following. For the estimations three assumptions are done:

- The gas is weakly ionized, equilibrium and ideal;
- Plasma channel expands isobarically (2-D volumetric expansion);
- The local energy input is proportional to the length of the plasma channel at the constant electrical current.

Energy release to the plasma filament increase the temperature of the gas:

$$W = \frac{\partial m}{\partial t} c_p \Delta T = G1 \times \frac{R}{\mu} \times \frac{\gamma}{\gamma - 1} \times \Delta T ,$$

where W- is the local power input, m- is the gas mass in the plasma channel, G1- is the mass flow rate through the plasma layer, ΔT- is the temperature increase.

The isobaric conditions give the relation between the temperature and the filament's volume:

$$\frac{m}{\mu} R \Delta T = p \Delta V, \text{ where } \Delta V = \frac{\pi}{2} \times y \times \Delta y \times z,$$

where y-is the plasma layer thickness.

Simple transformations give the following expression for the plasma wedge angle θ :

$$tg^2(\theta) = \left(\frac{\partial y}{\partial x} \right)^2 = \frac{\gamma - 1}{\gamma} \times \frac{2}{\pi \times z} \times \frac{1}{p \times v} \times \frac{W}{x},$$

where v-is the flow velocity, z-is the plasma layer depth.

The relation between local power input and the coordinate y can be found from the expression on the average power W_{av} :

$$W_{av} = \frac{1}{\tau} \times \int_0^{x_{max}} W(x) \frac{\partial x}{v},$$

where τ - is the period of the plasma filaments oscillations and $W(x)$ - is the local power input:

$$W(x) = E \times I \times (L_0 + 2 \times x),$$

L_0 - is the inter-electrodes gap.

Utilizing these expressions it is possible to find out the plasma wedge expansion angle through the integral (bulk) characteristics:

$$tg^2 \theta = \left(\frac{\partial y}{\partial x} \right)^2 = \frac{\gamma - 1}{\gamma} \times \frac{1}{\pi \times z} \times \frac{4}{x_{max}} \times \frac{W_{av}}{p \times v}.$$

Remarkably, that the angle of the plasma wedge doesn't depend on the initial mass flow rate through the plasma area (thickness of an initial plasma channel y_0). In frames of the model the temperature of the gas could be estimated as following:

$$T_{max} = T_{st0} \times \left(\frac{x_{max}}{y_0} \right)^2 \times tg^2 \theta.$$

Using the typical values of the experimental parameters (namely: $W_{av}=1kW$, $z=20mm$, $x_{max}=15mm$, $v=550m/s$, $T_{st0}=200K$, $y_0=y_{bl}=1mm$, $p=100Torr$) and adiabatic factor for $T=3000K$ the estimations give the following results:

$$\alpha \approx 15^\circ \quad \text{and} \quad T \approx 2950\text{K}.$$

The direct measurements provide very close result for the plasma wedge angle and a bit more value of the gas temperature (see sections below) that can be explained by the specific method of the measurements and by plasma non-homogeneity. Some difference in value of the angle (12° experimental and 15° calculated) could be explained by the energy loss. Well known that the plasma of molecular gases has got a large vibrational excitation and relaxation time is rather large in comparison with gasdynamic time.

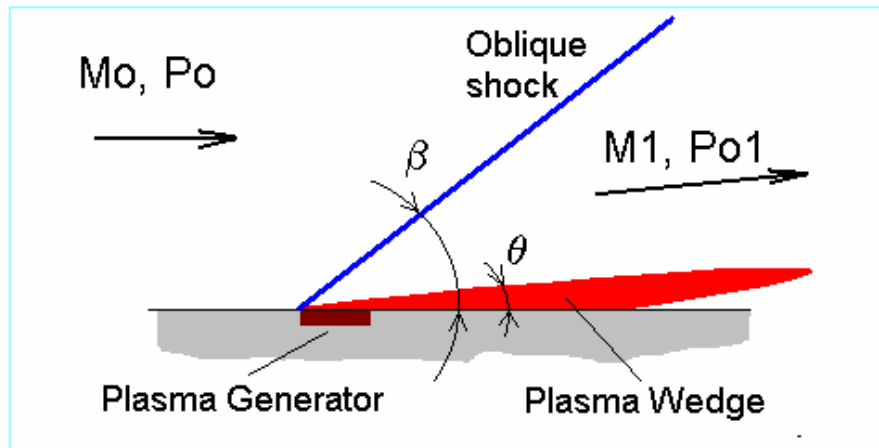


Fig.2.2.4.4. Scheme of oblique shock generation.

The interaction of the plasma near-surface layer with the main flow occurs on the following manner (Fig.2.2.4.4.). We will consider that the plasma effective “wedge” acts as a solid “wedge”, although the actual process of the interaction is much more complex. Nevertheless the effective angle of oblique shock wave (β) associated with the plasma generation can be related to the effective angle of the plasma wedge (θ), i.e., finally, to input power.

In accordance with such an approach the angle of the oblique shock can be expressed in terms of:

$$\operatorname{tg}(\beta - \theta) = \frac{2 + (\gamma - 1) \times M^2 \sin^2 \beta}{(\gamma + 1) \times M^2 \sin \beta \times \cos \beta}.$$

If the effective angle of the plasma wedge is quite small, the expression can be simplified up to:

$$\operatorname{tg}(\beta - \theta) \approx \frac{1}{\sqrt{M^2 - 1}},$$

and increase of the static pressure can be calculated through the following formulae:

$$\Delta P_{st} \approx \operatorname{tg}(\theta) \times \frac{1}{\sqrt{M^2 - 1}} \times (\rho v^2).$$

As the result we can bind the angle of the oblique shock with the input power to the surface plasma. It has to be considered that such a simple model can be applied successfully for the prediction of the surface plasma effect, including the thermal chocking.

2.2.5. The Effect of Plasma-Induced Separation.

The principal scheme of the discharge excitation is presented in Fig.2.2.5.1. It should be remarked that the secondary separation takes place downstream at enough high level of the power input (see below). Plasma generation occurs by means of surface multi-electrode distributive electric discharge at transversal mode. The transversal discharge is characterized by large level of modulation of the main parameters, including gap voltage, resistivity, radiation and the position of downstream visible edge of the plasma. Transversal discharge appears to be more effective to change the structure of airflow.

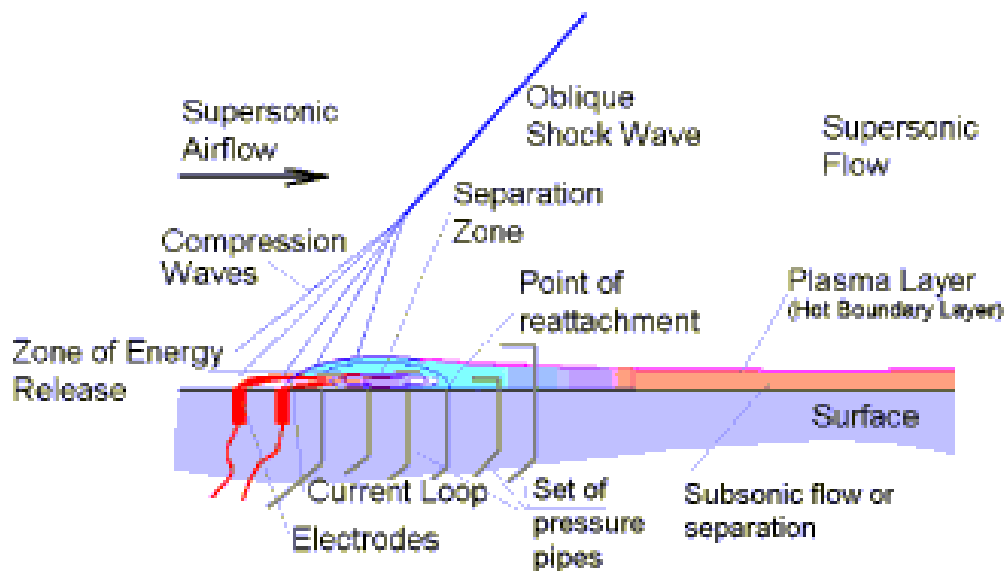


Fig.2.2.5.1. Scheme of Surface Discharge Excitation.

The plasma generation near the surface of the duct creates the layer of hot air downstream the electrodes area. In dependence on conditions such a hot layer appears in different configurations and is a cause of different sequences in flow structure. A typical Schlieren image of the surface plasma-airflow interaction is shown in Fig.2.2.5.2. Mainly two methods have been exploited for the observations of the flow structure: namely the Schlieren shadow method and measuring of the pressure distribution. The plasma overlayer and an appropriate oblique shock wave are seen. An essentially subsonic area or huge separation zone is generated near the surface downstream the plasma area.

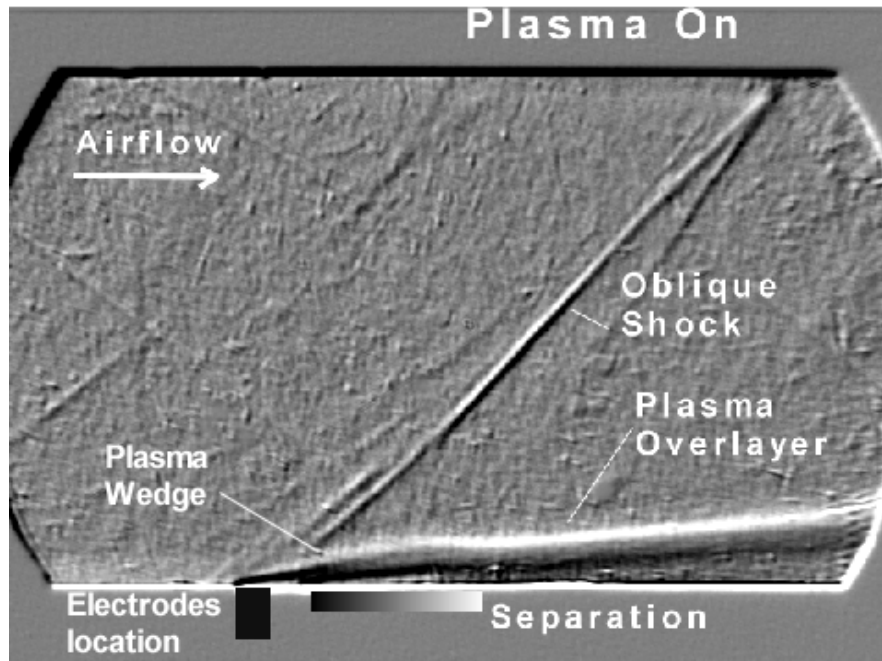


Fig.2.2.5.2. Standard Schlieren photo of surface plasma interaction with duct-driven supersonic flow. Exposure 30us.

Three different situations can be described:

- low-power plasma (input power below 1kW for pressure about 100Torr) leads to subsonic layer generation;
- low-power plasma (input power 1-2kW) leads to subsonic layer generation with local separation;
- high-power plasma deposition (more then 2kW or 10% of the flow enthalpy) leads to global separation processes, and it is presented in Fig.2.2.5.2.

The processed Schlieren photos of three standard situations are shown in Fig.2.2.5.3. The first photo in Fig.2.2.5.3 is related to undisturbed airflow. The weak shock waves are generated due to wall irregularities and local separation areas between nozzle and the duct. In the second case there was the surface discharge generation at relatively low level of power input (less than 5% of the flow power). A new oblique shock wave generation and a small separation area just in plasma region could be seen. New shock has practically the Mach angle and changes the Mach number in whole duct negligibly. But the position of the shock can be localized accurately. This case is appropriated to increase of the stagnation pressure downstream the plasma area.

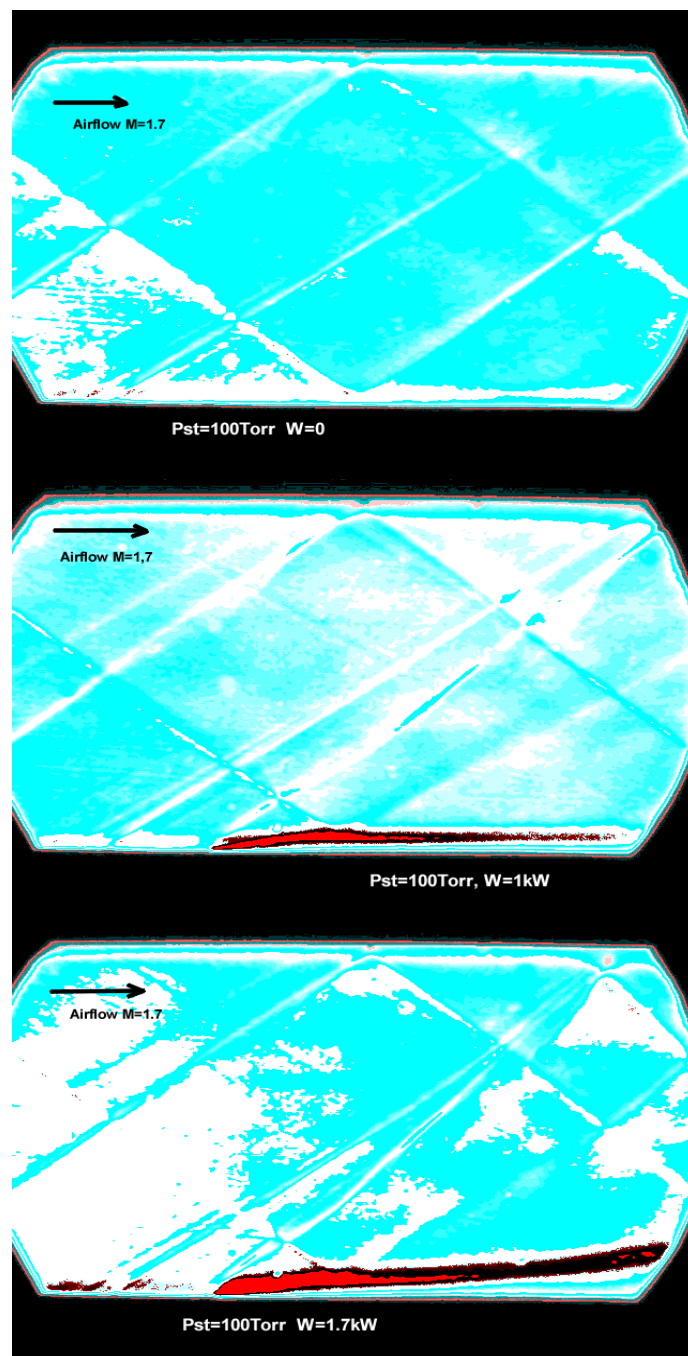


Fig.2.2.5.3. Processed Schlieren photos of plasma-airflow interaction at different power input.

Exposure 30us.

At higher level of the power input to the plasma the result can be characterized by two important features. The amplitude of the plasma-induced shock wave increases sufficiently, up to direct shock generation and the thermal choking of the duct. The second peculiarity is that the boundary layer is separated without sequential reattachment. In this case Mach number in whole duct can be changed significantly. Accurate analysis of the pressure measurements data leads to conclusion that it is a typical situation when the full pressure near

the wall is decreased and the static pressure is constant practically or increases, when the global separation takes place. At the same time the stagnation pressure at the axes increases slightly. The difference between the cases is well recognized: in case of large power input the “stagnation” pressure near the bottom wall occurs lower than “static” pressure. It means that a circulative flow near the wall with reverse direction of the flow velocity vector is observed. The situations with and without the global separation are presented in Fig.2.2.5.4. In the first case the mean power input was $W=1\text{kW}$, in the second case it was $W=1.7\text{kW}$ correspondingly.

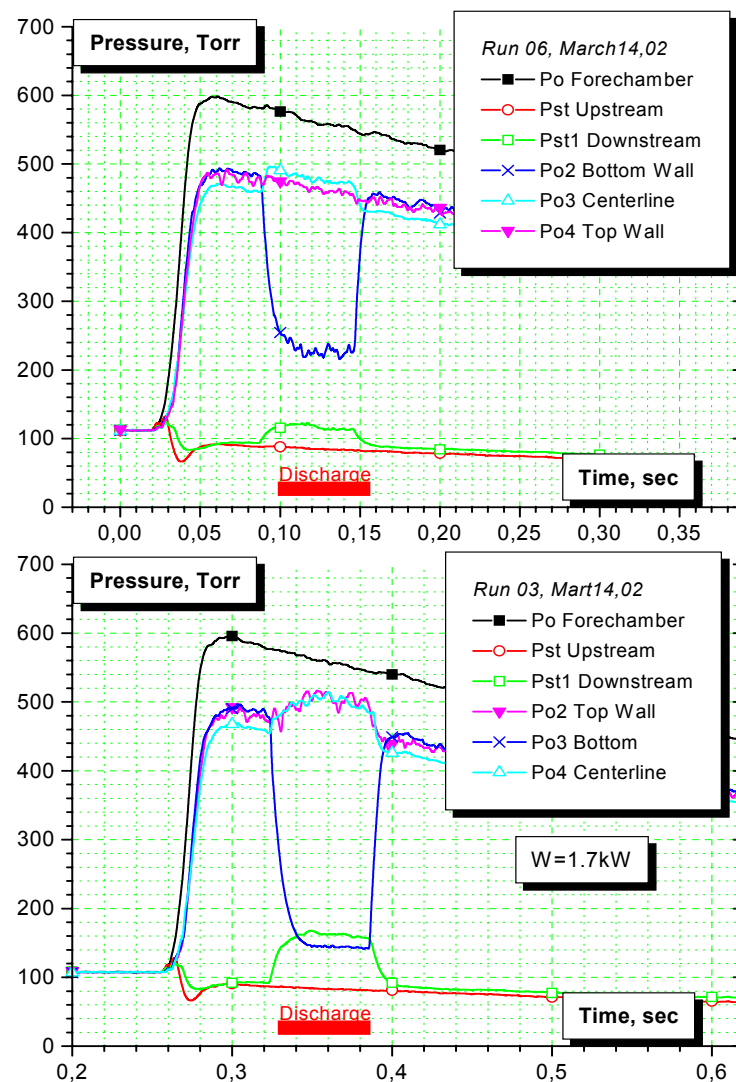


Fig.2.2.5.4. Pressure redistribution at surface plasma generation.

All intermediate regimes of the interaction have been obtained experimentally. At input power more than 4-5kW the choking of the duct takes place under the standard conditions of the experiment. A new oblique shock wave generation is observed in all cases. New shock has practically the Mach angle at low power of the plasma and changes the Mach number in whole duct negligibly. Increasing the power there is possible to change the Mach number of the flow downstream and the angle of the oblique shock. The position of the shock is localized by the place of plasma generation. The stagnation pressure downstream the plasma area decreases that is become apparent in increasing of Po' downstream, which is measured by the Pitot gage.

The angle of the oblique shock wave due to plasma generation depends on the level of the energy release. We can compare this angle with the calculated data obtained on the base of proposed above model. The result of such a comparison is presented in Table 2.2.5.1. The angles should be referred to Fig.2.2.4.4, “exp” means experimental, “calc” means calculated.

Table 2.2.5.1. Dependence of oblique shock angle on the input power of the electric discharge (in degrees).

Power, kW	Solid Wedge,	0	1	1,7	2,4
θ , exp	14°	0	12		
θ , calc	14	0	14	18	21
β , exp	45	31	43	46	50
β , calc	45	31	45	49	52

Well seen that the oblique shock angle grows with the plasma power and that the experimental values a bit less than calculated ones. Now we are explaining this difference by the power losses due to vibrational reservoir of molecular gas.

It is clear that the presence of shock wave with non-Mach angle has to be reflected in Mach number modification in whole duct. The result of measurements is shown in Fig.2.2.5.5. The Mach number has been recalculated on base of pressure measurements in three sequential sections of the duct: upstream and downstream the plasma generator place.

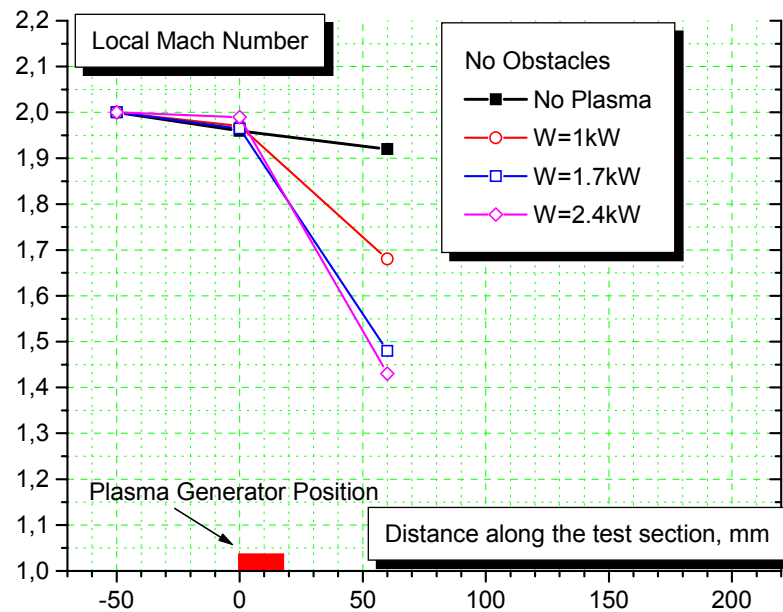


Fig.2.2.5.5. Mach number modification under the surface plasma generation.

It has to be noted that the plasma effect doesn't entail any other harmful sequences like a turbulence or instabilities generation. Quite the contrary, the gasdynamic instabilities damping takes place.

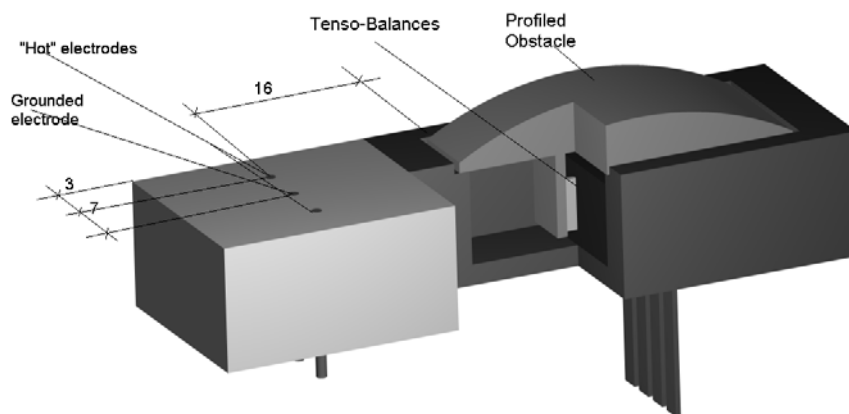


Fig.2.2.5.6. Arrangement of the bottom wall of the TS.

In this series of measurements the test section has been equipped by a flush-mounted balance's plate. The scheme is shown in Fig.2.2.5.6, where the profiled 10% or 17% obstacle is drawn.

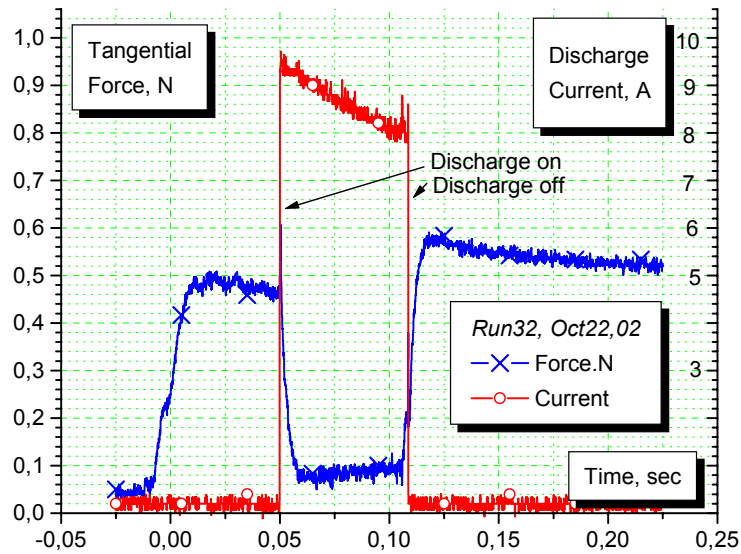


Fig.2.2.5.7. Drag force reduction on surface obstacle under plasma generation.

The generation of the plasma overlayer has to lead to a “screening” effect in respect of surface obstacles. This phenomenon has been examined by the profiled surface-mounted body with a small value of drag factor, which has been installed on a micro-bridge balance with a response time about 5ms. The body is characterized by 10% profile (3mm thickness at 30mm of the length) and effective drag factor $c_d \approx 0.2$. The sample of the tangential force measurement is presented in Fig.2.2.5.7. A small positive drift of the signal is explained by the thermal decompensation of the balance’s bridge. It is easy to recognize a good correlation between the electric current of the plasma and the force reduction. In some cases the drag reduction reached up to 95% of the initial force.

The typical Schlieren photo of such an effect is shown in Fig.2.2.5.8. The separation area due to surface plasma generation covers the obstacle and decreases dynamic pressure on its surface. This process is confirmed by the pressure measurements, which are presented in Fig.2.2.5.9.

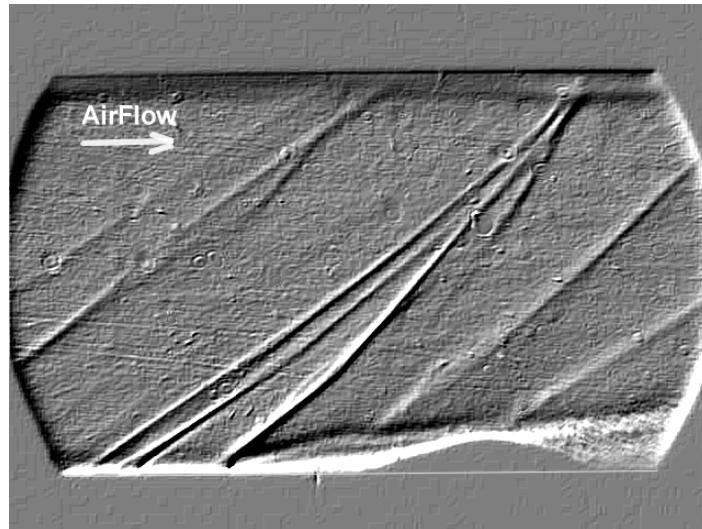


Fig.2.2.5.8. Schlieren picture of the obstacle-plasma interaction.

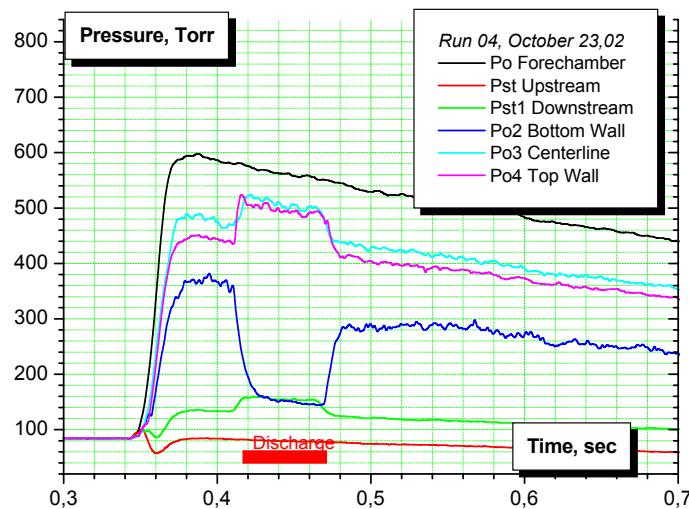


Fig.2.2.5.9. Pressure redistribution near obstacle under the plasma generation.

The dependence of the effect on the input power is shown in Fig.2.2.5.10. A subsequent increasing of the power leads to the duct choking. It is seen that all data can be divided on two groups by the level of effect. At power deposition level in $W > 1.7\text{kW}$ the plasma influence grows rapidly. It could be supposed logically that the reason is in flow mode transformation to separation type. The energetic efficiency of the drag reduction on such a manner is rather small, about 20%, that is in accordance with our conception for well-streamlined bodies [see Section 1.3.3].

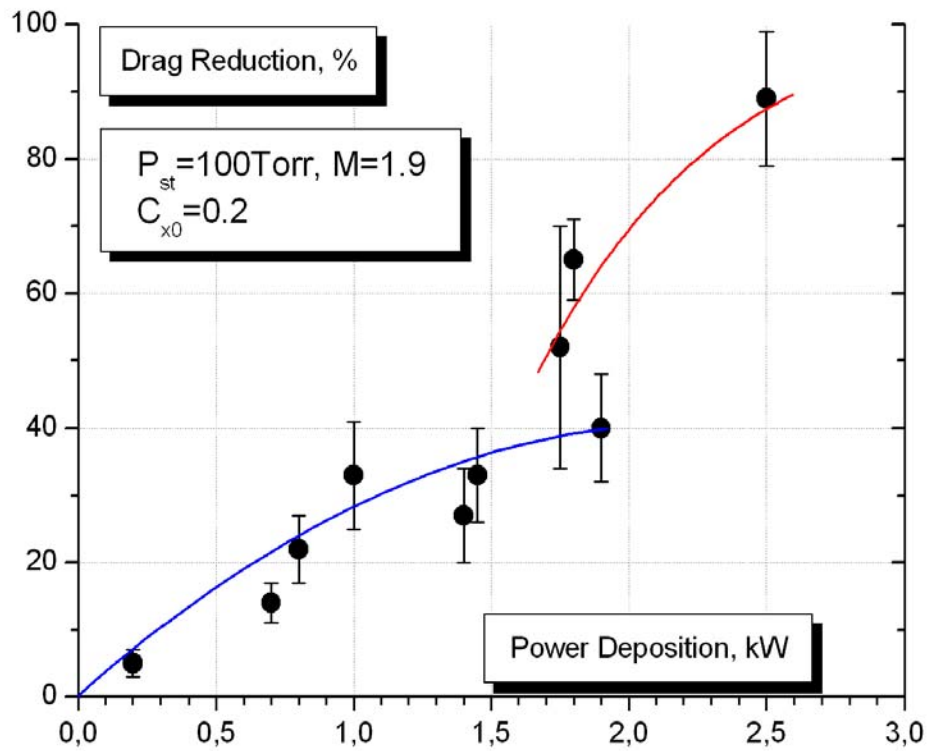


Fig.2.2.5.10. Drag reduction vs input power to surface discharge.

Energy release or plasma formation near surfaces in high-speed airflow influences on a near-wall layer itself, in particular, leads to a local/global separation, oblique shock and the plasma overlayer generation. These aerodynamic structures can be applied instead of mechanical arrangements, especially, under non-optimal operation mode of the duct-driven flows and combustors.

2.2.6. Duct-Driven Flow Control.

The experimental scheme presented in section 2.2.5 has been applied to verify the plasma layer ability for the oblique shocks control (change the position and angle). Small model obstacles with 10% and 17% of thickness (3 and 5mm correspondingly) have been installed into the duct to simulate the inlet's configuration. The second model was blunter. They were positioned 16mm downstream the electrodes area on the bottom wall of the duct. The oblique shock falls on the top wall of the duct in about 28 and 52mm downstream the obstacle fore-edge zone correspondingly.

The typical Schlieren photos of the fore-generated plasma effect on the shocks position are shown in Fig.2.2.6.1 for the different level of the power input.

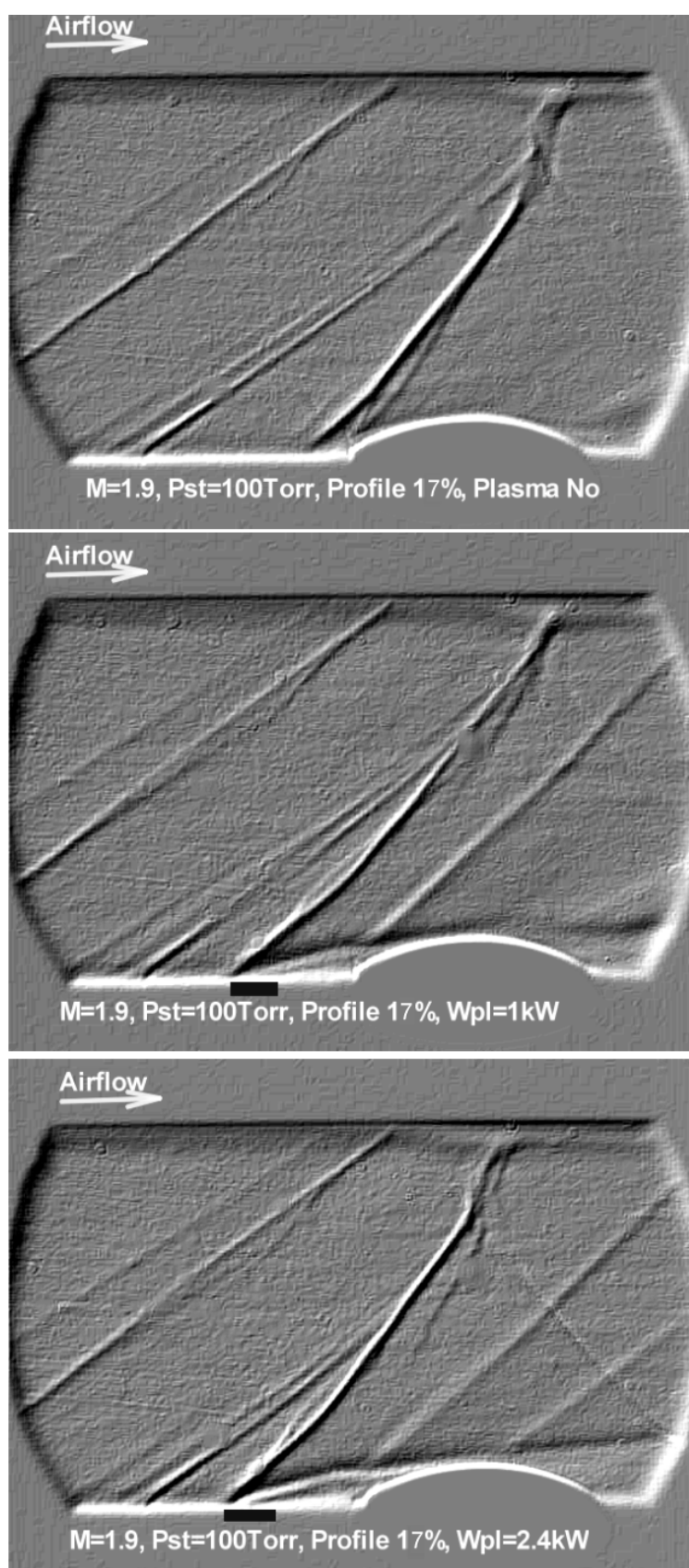


Fig.2.2.6.1. Schlieren images of plasma –flow interaction under the different power deposition.

The Fig.2.2.6.2 presents the result of the shock position control experiment for two obstacles. As it could be noted the plasma effect is relatively more intensive for a small obstacle. Under the large level of the input power the shocks position and configuration are defined only by the plasma. At such power input the global separation in the duct occurs.

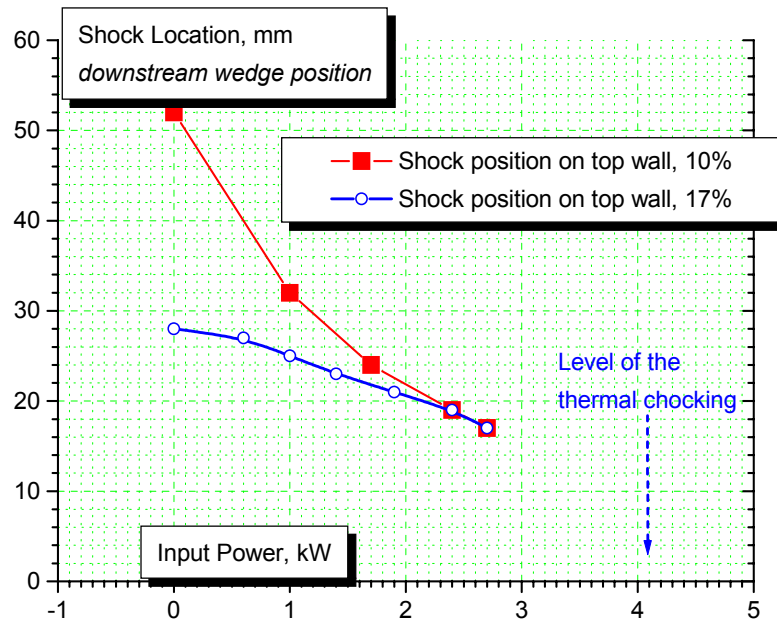


Fig.2.2.6.2. Shock wave position on the top wall of the duct vs power input.

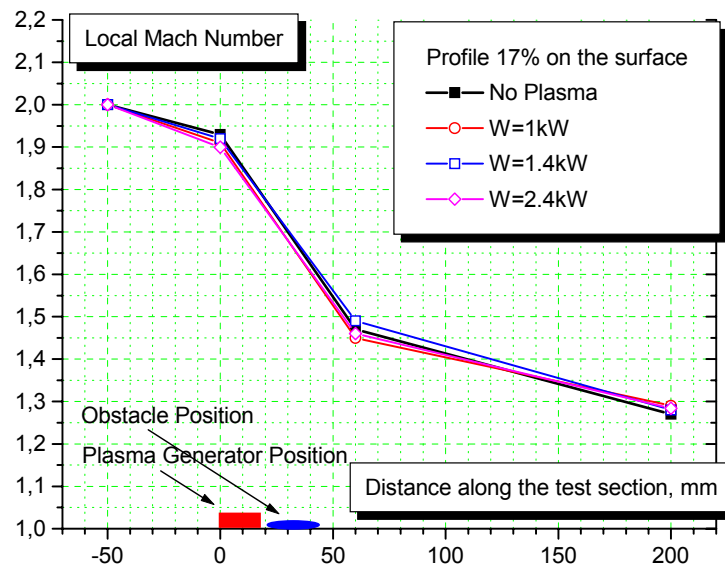


Fig.2.2.6.3. Mach number modification under the plasma effect.

At the same time the plasma generation influence on the flow Mach number in whole duct is not strong in comparison with the case when the obstacle is installed. It is correct if the power level is much less then the choking level. The Mach number dependence on the input power is demonstrated in Fig.2.2.6.3. The difference with a free discharge is well visible (see Fig.2.2.5.5 for the comparison). Actually in this conditions the pressure losses increase with the power rising.

Detail measurements of pressure distribution downstream the plasma show that in some important cases instead of braking of the flow we can observe the flow enhancement in terms of total pressure recovery factor. The shock changes its position and the visible amplitude is decreased. It is easy to see how the plasma excitation transforms the airflow structure not only near the surface but also in whole duct. The result of the measured total pressure recovery factor in dependence on conditions is shown in Table 2.2.5. The measurements have been done in 200mm downstream the plasma generation region in comparison with the pressure just upstream the plasma generation place. The conditions were chosen when the Mach number fell from about 1.96 down to about 1.44. It is seen that the result at plasma effect is better than in case of 17% solid profile.

Table 2.2.5. Total pressure recovery factor. $Po2/Po$
($Mo=1.94-1.98$, $M2=1.42-1.45$).

Power, kW	0	1	1.4	1.7	2.4	2.7
Wedge	0.77					
Plasma		0.86 M2=1.7		0.8	0.81	0.8
Wedge+ Plasma		0.71	0.71		0.8	0.81

A similar gasdynamic configuration has been utilized in model test to explore the surface plasma effect on oblique shock reflection. A small wedge was fixed on the top wall of the duct for the falling shock wave generation. Schlieren photos for that test are presented in Fig.2.2.6.4.

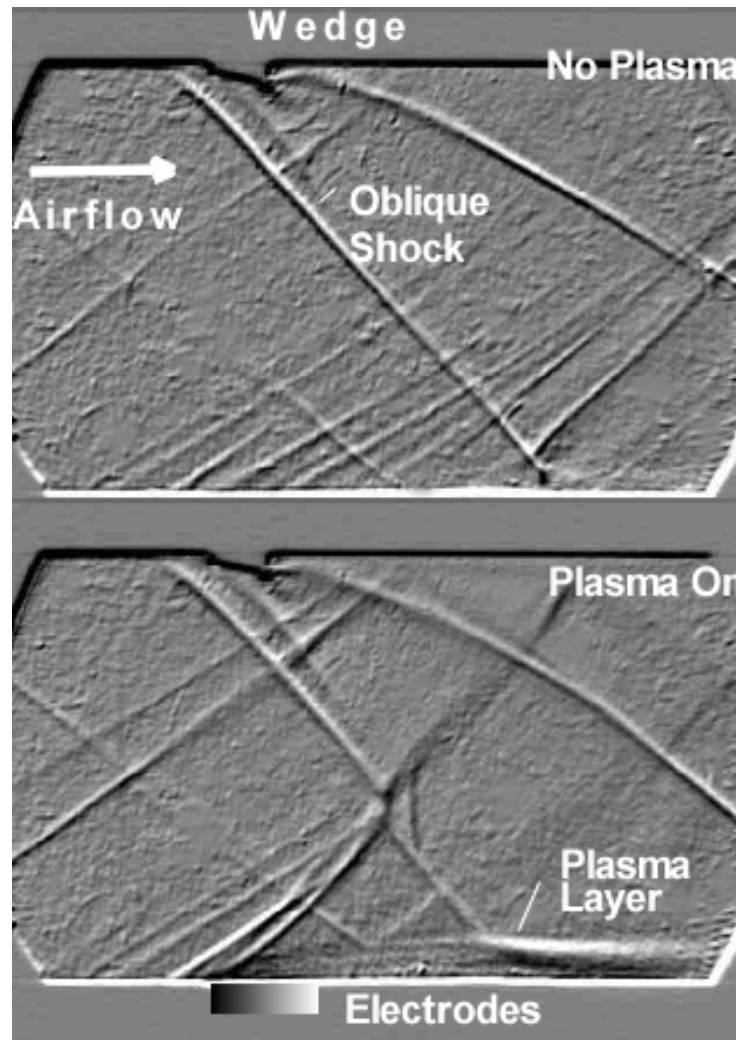


Fig.2.2.6.4. Schlieren photos of the external shock interaction with the plasma overlayer.

What is important in these images? It is the decrease the amplitude of the oblique wave reflected from bottom wall. Seen that the plasma overlayer change shape itself like a “smooth” surface, so the reflection occurs in a form of series of weak compression waves. The next picture in Fig.2.2.6.5 presents the pressure redistribution data under such an effect.

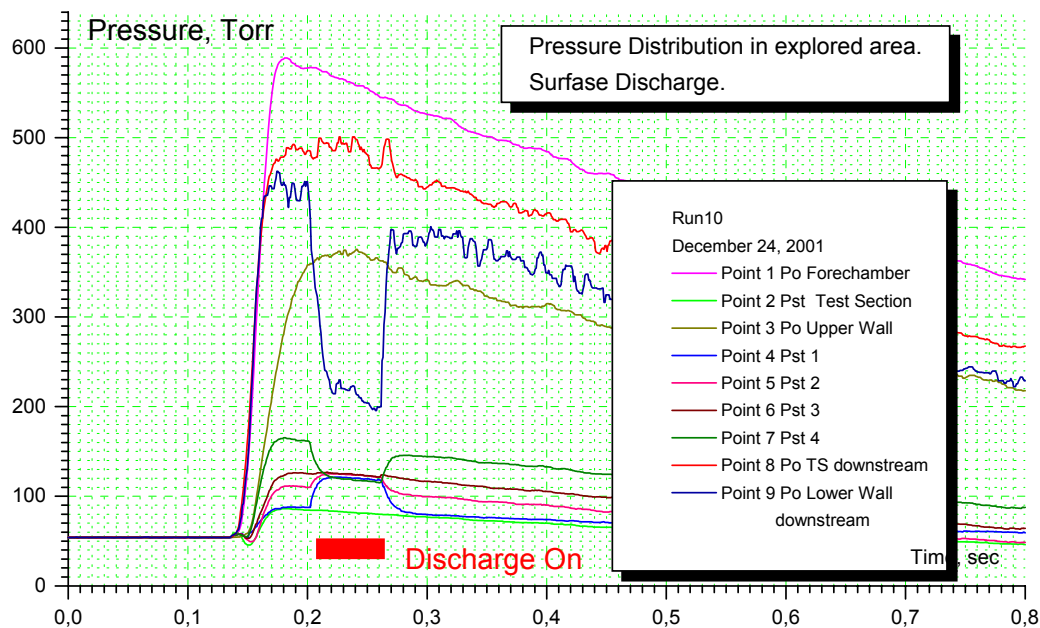


Fig.2.2.6.5. Pressure redistribution at plasma overlayer interaction with external oblique shock wave.

The measuring points should be referred to the scheme in section 2.1.1. Following important details could be considered in Fig.2.2.6.5. An initial distribution of the static pressure in the area of the shock wave falling on the wall goes to plain one at plasma generation; total pressure in the overlayer decreases significantly; total pressure in core of the flow increases slightly. It means that the pressure losses in such a situation is less downstream the interaction area at surface plasma generation.

2.2.7. Separation Control by Filamentary Plasma.

The scheme of the test arrangement is shown in Fig.2.2.7.1. The discharge insertion was mounted upstream the fixed separation zone. The test objective was in control of flow structure and parameters just in that area.

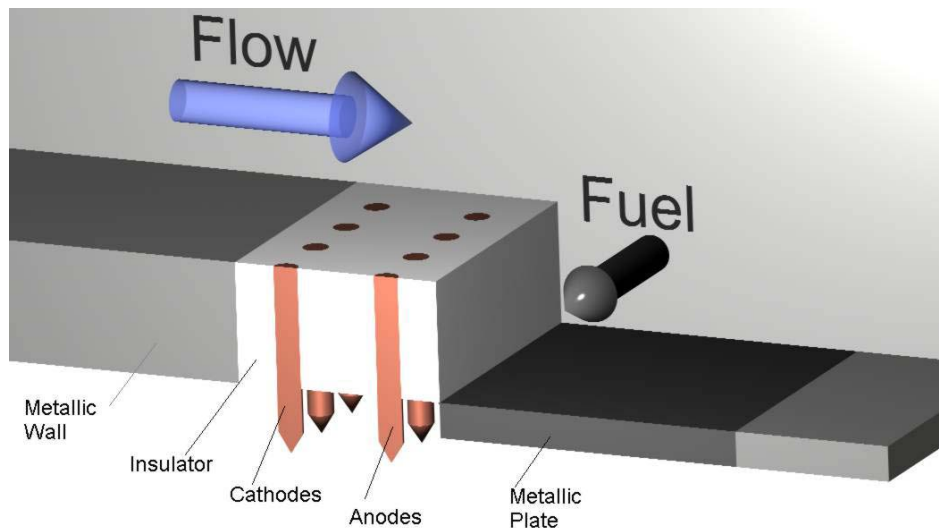


Fig.2.2.7.1. The scheme of the test arrangement.

The scheme of the discharge excitation is shown in Fig.2.2.7.2.

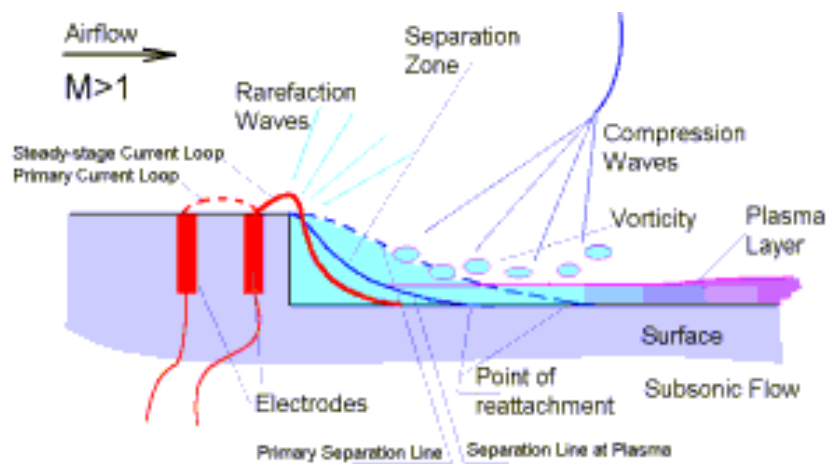


Fig.2.2.7.2. Test arrangement under the fixed separation zone.

Two different modes of the discharge operation have been found in case of separation zone. At the first mode the discharge is excited between electrodes. At the second mode the discharge current is being connected to the metallic wall in separation zone. We are talking

about the second mode in this section as the most prospective for an application. Electric energy input to the plasma volume reached up to 2kW at the transversal direction of plate about 20mm and axial distance between the electrodes about 10mm.

Spectrums of the filamentary discharge under the condition of separation zone were measured for different pressures. It is pointed out that gas temperature depends on the static pressure in separated zone: an increase of the pressure leads to the growth of the rotational temperature in plasma filament, see Table 2.2.7. It reflects the decrease of the filaments' diameter.

Table 2.2.7. Plasma temperature in fixed separation zone behind backwise wallstep.

Pressure in the separation zone.	Temperature of the gas.
100 Torr	$5 \pm 0,1$ kK
220 Torr	$5,5 \pm 0,1$ kK
500 Torr	$6 \pm 0,1$ kK

The discharge voltage is not proportional to the discharge gap. The fast video shows that the length of plasma “cords” is much more in the case of the second discharge mode, which is reflected in the gap voltage increasing. Another difference is that the discharge in separation zone is generally more stable. The photo of the discharge appearance in the separation zone at the second mode is presented in Fig.2.2.7.3.

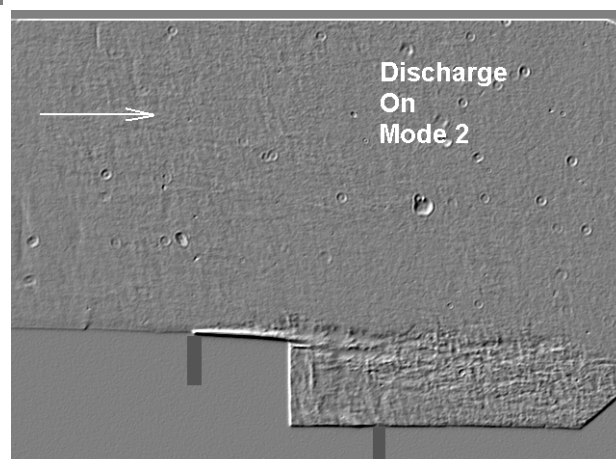
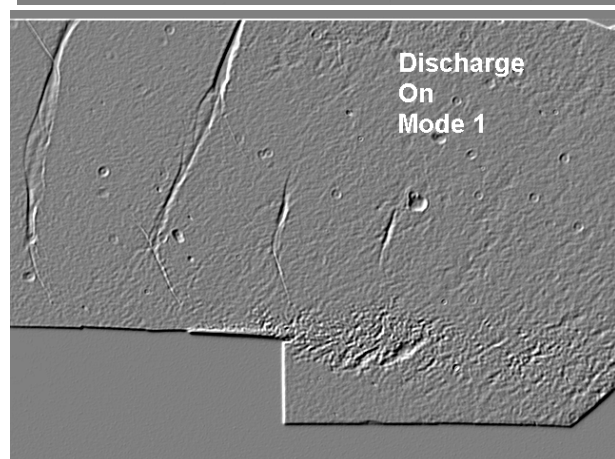
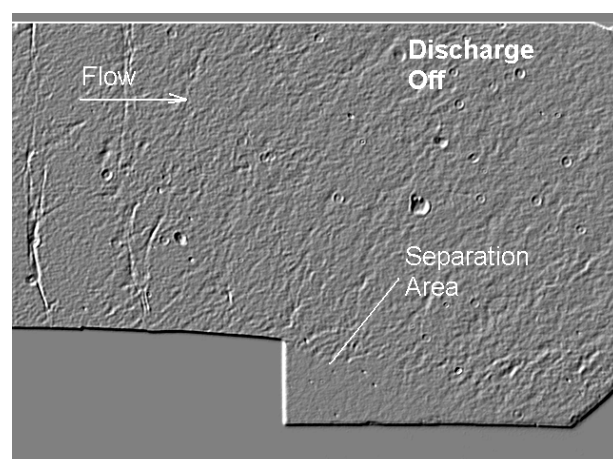
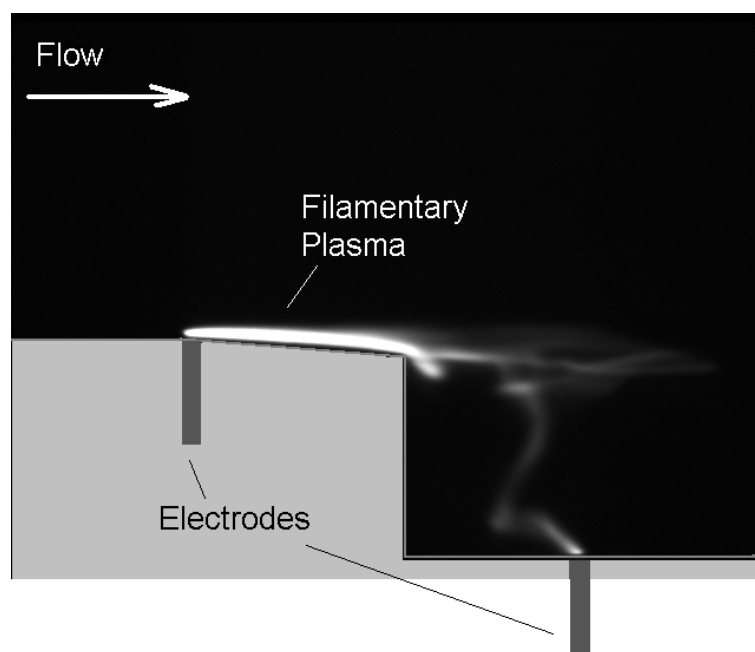


Fig.2.2.7.3. Surface discharge appearance in separation zone.

Fig.2.2.7.4. Schlieren photos of the discharge effect on separation zone parameters.

The samples of Schlieren photos are presented in Fig.2.2.7.4 for three cases: when the discharge was switched off and for two different modes of the discharge connection. In the second case the effect is much stronger.

Plasma excitation near and inside the separation zone effects on static pressure distribution in this zone. The Fig.2.2.7.5 shows the diagram of the pressure redistribution in all points at the different conditions. At observation of them it can be considered that for explored conditions the result is the same: plasma excitation leads to increase the static pressure near wall step approximately on 15-20%. Generally, this statement is correct for the standard and the second mode of the discharge spacing both but in the second case the effect is larger. It can be noted that the pressure distribution in a separation zone is changed significantly. The pressure gradient occurs much lower than in the case without plasma. Such an effect can lead to increasing of gas exchange between the separation zone and the main flow. The fuel ignition allows increase the level of input power and the appropriate effect.

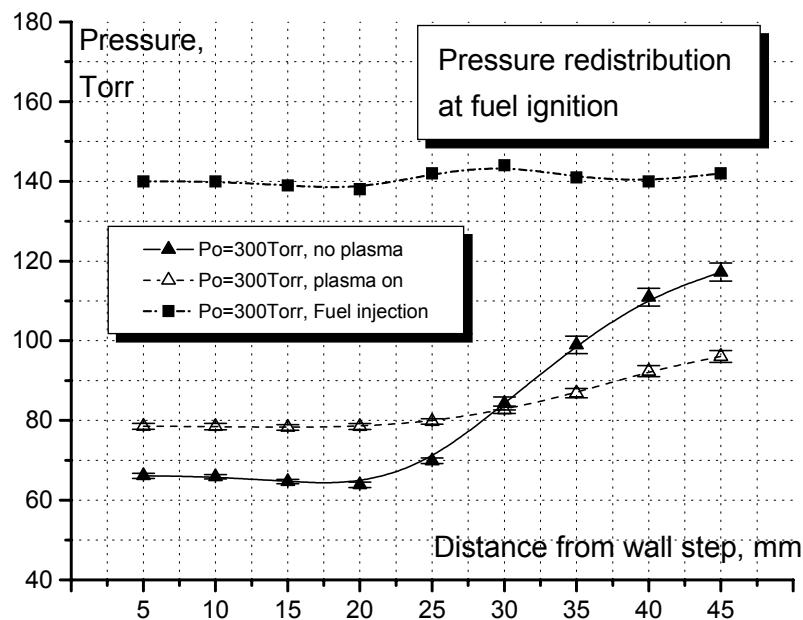


Fig.2.2.7.5. Pressure redistribution due to plasma and fuel ignition effect.

The fuel ignition allows increase the level of input heat power to separation zone. Pulse type of the fuel injector with electromagnetic control was used during the test. The following injector parameters are typical: type of fuel – liquid hydrocarbon mixture on base of isooctane's; type of injection – high pressure spraying to separation zone; fuel expense - $G_f = 10 \div 100 \text{ mg/pulse} = 2 \div 5 \text{ g/sec}$. Such a portion requires stoichiometric amount of air in a range $100\text{-}1500 \text{ cm}^3$ at the atmospheric pressure. At the parameters of the test duct this air portion flows through the separation zone during several milliseconds in dependence on the conditions. The test sequence was the following: wind tunnel start (duration of steady stage 150ms approximately), 50ms pause, discharge start (duration 50-70ms), 20ms pause, fuel injection during 2-20 ms. The third curve in Fig.2.2.7.5 shows the result appeared in pressure redistribution.

The fuel combustion essentially effects on pressure distribution in the duct, especially in the separation zone. Note, that the level of the pressure inside the separation zone at combustion is equal to the static pressure upstream the backstep. Three important things should be considered. The first one is that the flow regime upstream of the energy release area is not changed (Mach number about $M=1.2$). The second statement is that the large additional energy release to the area took place, much more than due to the plasma generation. The comparison with the results of CDF simulation allows us to estimate the power release with the combustion of about $W_{\text{comb}}=25 \text{ kW}$. It means that the combustion completeness lies in a range $\eta=0.2\text{-}0.6$ in this operation mode. The third statement is that the combustion process was stopped at the discharge switching off. It could be explained by the low gas temperature in flow without plasma generation.

2.2.8. Transonic Effects.

The experiments on transonic flow control and boundary layer control have been conducted in transonic wind tunnel under the following parameters: total pressure about 1Bar, Mach number 0.5-0.98, test section 200*300mm, surface discharge up to 15kW of input power. The model arrangement is presented in Fig.2.2.8.1.

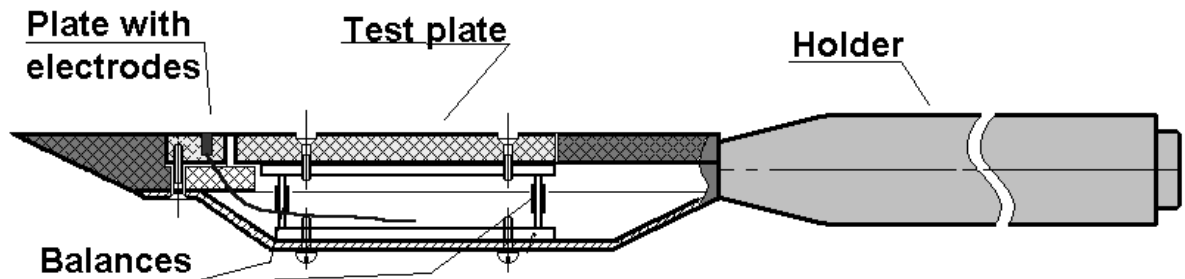


Fig.2.2.8.1. AD model. Test plate plain and profiled 100*120mm.
Balances and pressure distribution measurements.

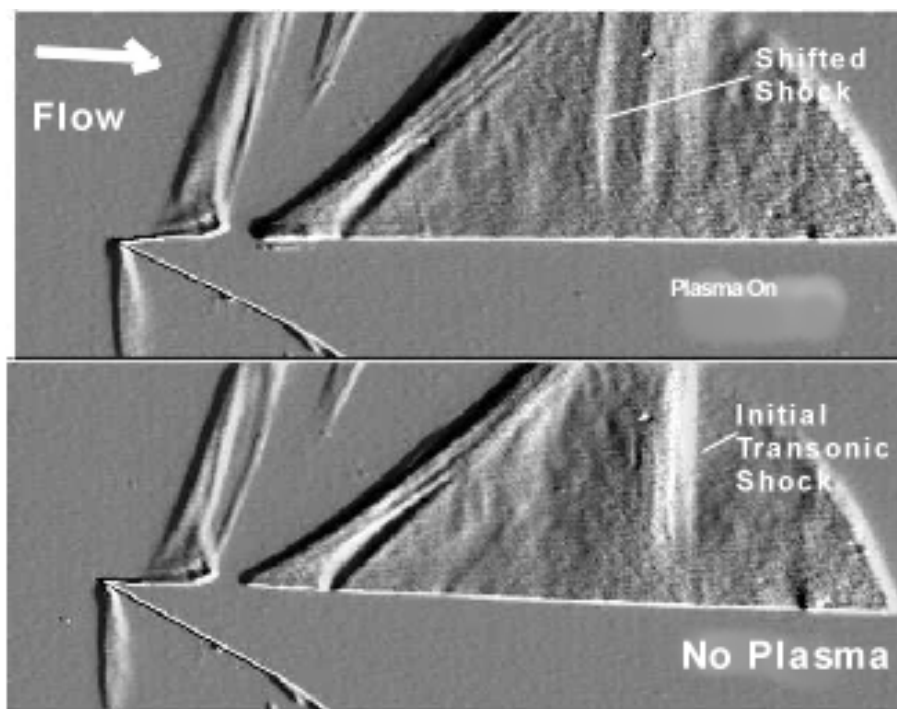


Fig.2.2.8.2. Schlieren photos of surface plasma effect on the direct shock position above the plain plate at transonic airflow.

The generation of an electric discharge near the surface allows shifting a position of direct transonic shock upstream and decrease it amplitude sufficiently. The mechanism of

such a shifting is the following: energy input to a near-surface layer increase a sonic velocity there. It means that an effective Mach number of the flow falls and the shock moves upstream. A sample of such a case is presented in Fig.2.2.8.2 by processed Schlieren photos.

At this case the visible splitting of a main shock takes place. Actually, we see two shocks: first (“old”) shock is from a part of model, which is without plasma generator; second shock is from a test plate and plasma excited area. Thus, the plasma influences on whole supersonic zone by decreasing of effective Mach number inside of it. “Lambda”-shock has been stabilized by means of artificial obstacle. The effective power deposition in this case is more due to increase of power input and more time of a heated gas presence inside of an interaction area. As the result the intensity of a direct shock near the surface drops. A similar result and change of wave structure of airflow has been obtained when a special cavity on the surface has been applied for the discharge stabilization.

The experiment on boundary layer control was conducted in transonic wind tunnel at Mach number $M=0.7-0.9$ (see Fig.2.2.8.1). In dependence on Mach number a Reynolds number (on length 1m) was in range $1-1.5 \times 10^7$. A friction drag factor of the plate was about $c_f=6 \times 10^{-3}$, which is correlated with turbulent boundary layer. During the test a balance measurements of friction drag (tangential force), pressure distribution and optical observations (natural, shadow and Schlieren) were fulfilled. Shadow photos show a structure of airflow and a separation line location. Quasi-continuous multi-electrode surface discharge was used for a plasma excitation.

Typical balances signal for a plain test plate is shown in Fig.2.2.8.3. Plasma switching on was 1.5sec of duration. Well seen that the tangential force reduction was about $\Delta F_{fr}=0.4N$ or in a range 10%. In case when an artificial separation has been applied and/or profiled test plate the tangential force reduction was much more, up to 100%.

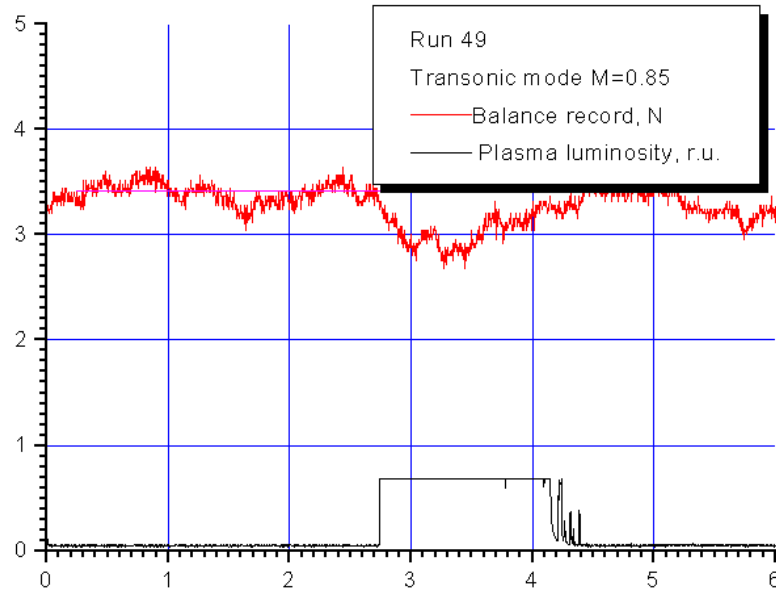


Fig.2.2.8.3. Sample of the balances record (tangential force) at surface plasma excitation upstream plain test plate.

The analysis of pressure distribution data allows dividing the balance's measurements on the viscous friction effect, including transition, and plasma influence through the separation. Sample of such a distribution for profiled plate with the obstacle is presented in Fig.2.2.8.4. One can see that static pressure along the test plate is changed slightly. At the same time the total pressure of flow near the surface drops.

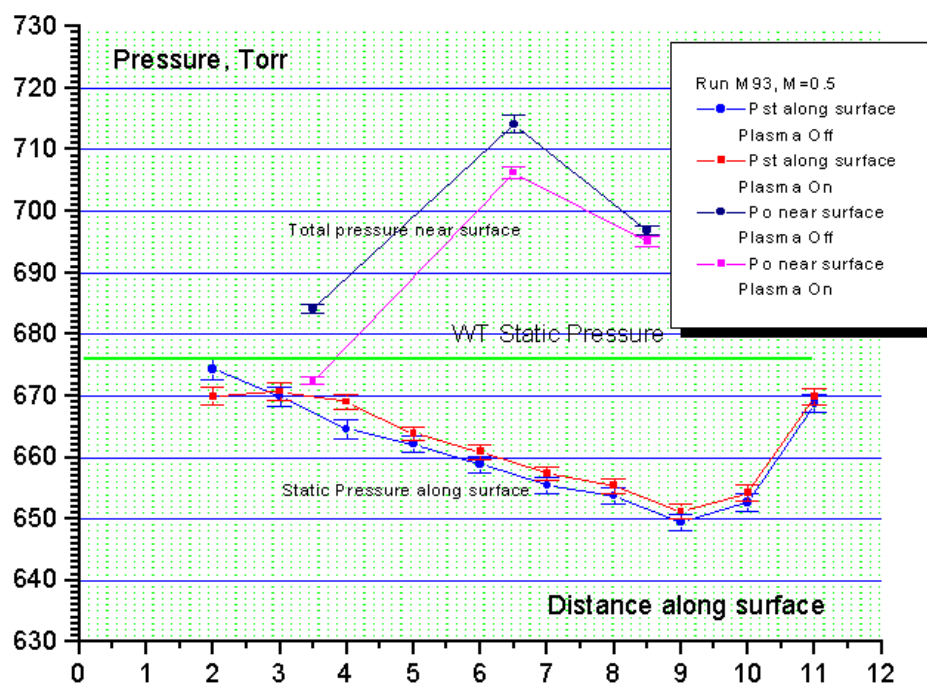


Fig.2.2.8.4. Pressure distribution along the test plate and upstream surface plasma effect.

The plasma effect on the tangential force in subsonic and transonic airflow depends on input power. The input power to the electric discharge alternates not only with the parameters of the power supply but also on conditions of the plasma excitation. Observations of the discharge luminosity show that plasma in high-speed airflow is non-homogeneous. Utilizing of cavities and obstacles of the different type gives additional method of plasma control in airflow, including control of input power. The Fig.2.2.8.5 summarizes the series of experiments on plasma control of boundary layer. Amplitude of the tangential force (drag force) was in a range $1 \div 8\text{N}$.

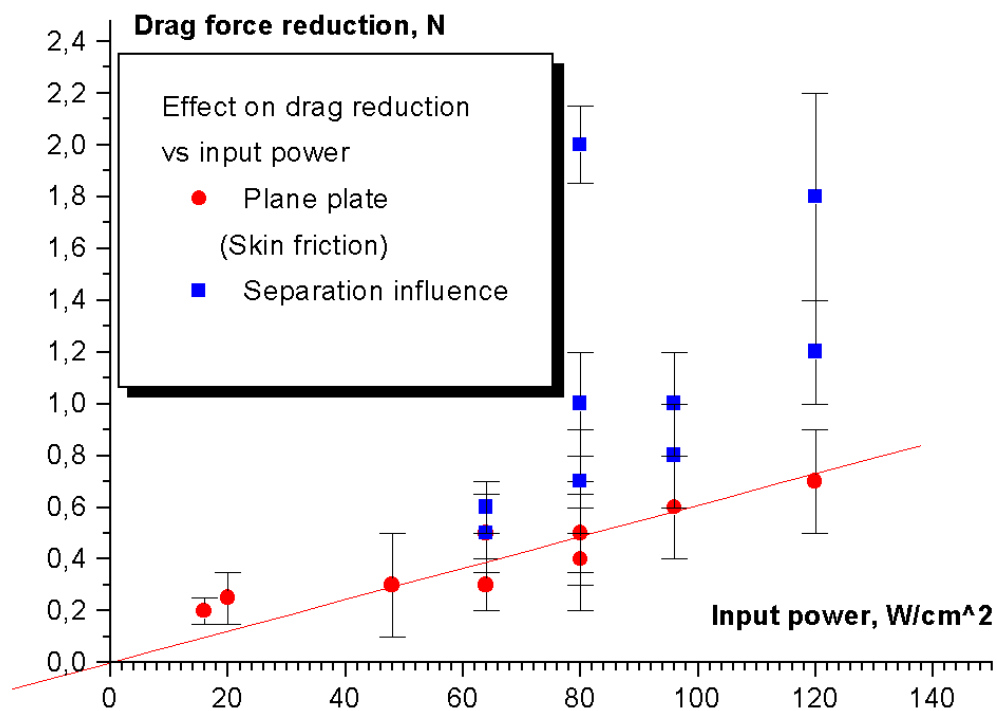


Fig.2.2.8.5. Two modes of plasma control of boundary layer.

Dependence of plasma effect on the input power.

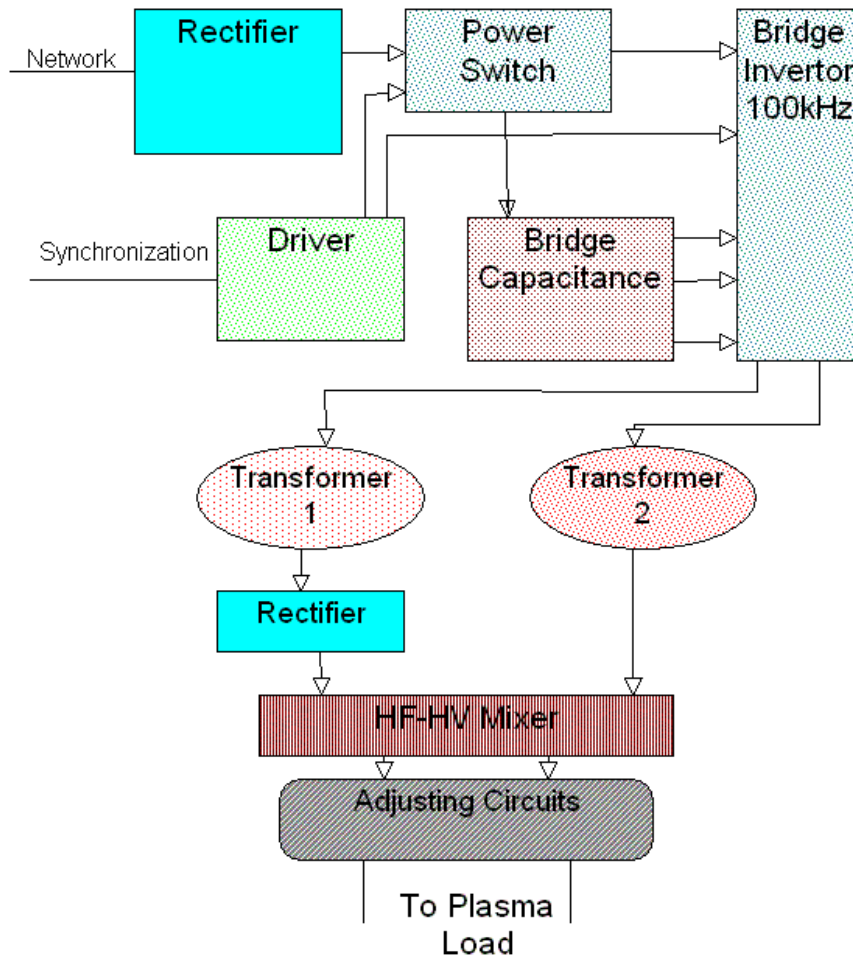


Fig.2.3.1.1. General layout of power supply.

The general block-layout of the power supply is presented in Fig.2.3.1.1. The power supply for the surface discharge consists of two main circuits: MFD power generation and HV-DC power generation.

More specifically the supply unit for barrier and combined discharge consists of the following parts:

- General rectifier from power net;
- Intermediate capacitances (not shown);
- Power Switch (modulator-regulator);
- Working capacitance;
- 100kHz inverter;
- HV power transformers;
- Secondary rectifier;

- Mixer;
- Additional circuits and feedbacks.

This power supply unit is a current type of electrical source with the sharply fall volt-ampere characteristic. The general operation mode is understandable from layout in Fig.2.3.1.1 and current-voltage graphs in Fig.2.3.1.2.

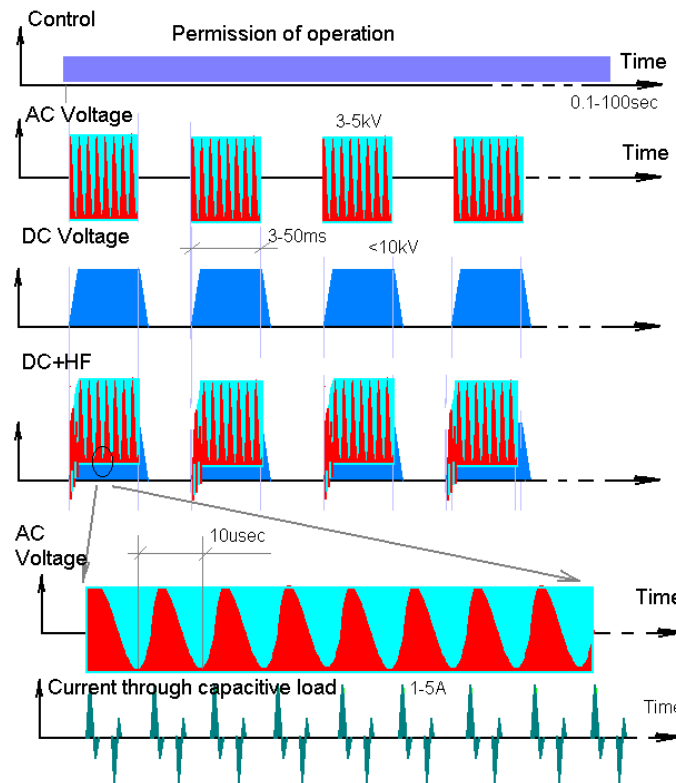


Fig.2.3.1.2. Operational diagram of HV-HF combined power supply.

On the Figure the generation of HF + quasi DC discharge pulses process is shown. In the first graph the initial pulses for HF modulator are presented. The modulator produces the powerful pulse with amplitude is not less than 3kV. The next graph presents the voltage of high voltage electrical source. The DC voltage is decreased at the discharge operation because load. The next graph shows the mixer output voltage. The output current shape and amplitude depend on characteristics of the plasma load. Under the short gap and low pressure the current shape repeats the voltage time trend. In case of insulated electrodes (when one or two electrodes are covered by insulator) the current pulses' shape and voltage pulse are strongly differed from each other.

It has to be noted that combined HV-HF self-maintained discharge includes advantages of the capacitive type HF discharge and of the continuous current DC discharge.

In dependence on electrodes configuration and gas parameters the different plasma parameters could be obtained, as a rule, non-equilibrium. As a result, in combined discharge the additional mechanisms for effective control of plasma thermal and chemical processes (such as gas dissociation, secondary emission and gas heating inside the cathode layer) can be realized. Under some specific electrodes configuration the combined type of the discharge can be generated. In such a case the ionisation of the gas in thin layer is being made due to barrier discharge but the main power input can be supplied by flush-mounted metallic or ceramic additional electrodes.

After an experimental verification of several plasma generators the basic electrodes configuration for the aerodynamic test has been chosen. It is a multi-trace plasma panel of barrier type. Appropriate sketch drawings of the electrodes systems are shown in Fig.2.3.1.3. The plasma panel consists of grounded electrode (entire plain copper film), insulating plate from polymer composite material or ceramics, and a grid of thin flush-mounted conductors above. An upper surface can be covered by a thin layer of insulating material for a low static pressure operation.

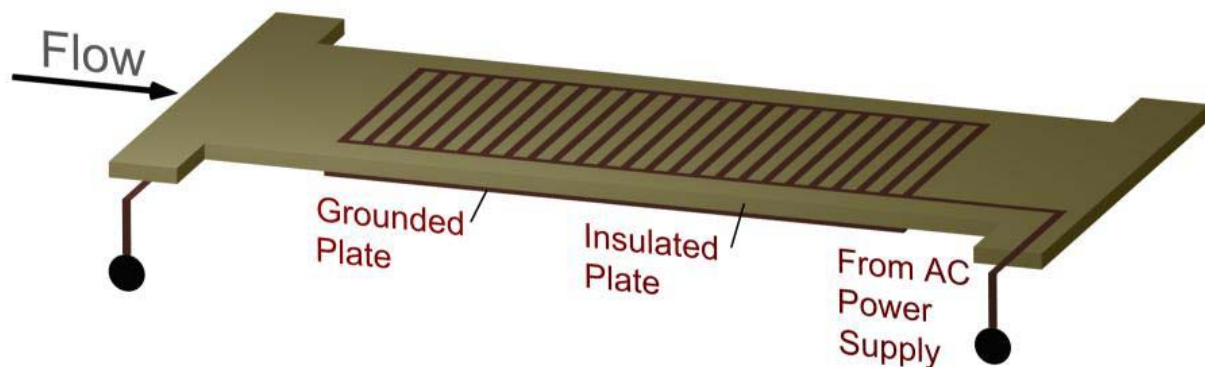


Fig.2.3.1.3. Basic design of multi-trace plasma panel.

This type of electrodes system has been designed to apply for excitation of distributive surface discharge in experiments on plasma influence on parameters of viscous friction and generation of artificial separation zones. The technical parameters could be announced as

following ones:

- | | |
|-----------------------------|-----------------------------|
| □ Flat area of plasma panel | >5cm ² ; |
| □ Insulator thickness | 0.5mm and 1mm; |
| □ Upper conductor wideness | 0.07-0.1mm; |
| □ Electric capacitance | 40-100pF/up to 300pF; |
| □ Pulse Frequency | 100 kHz; |
| □ Pulse polarity | bipolar; |
| □ HF Voltage amplitude | up to 5kV |
| □ Rate of the voltage rise | up to 10 ¹⁰ V/s; |
| □ Maximal mean output power | up to 5kW/m ² ; |
| □ Amplitude modulation | 0-1kHz; |
| □ Type of transmitting line | cable. |

The HF voltage is applied between the distributed electrodes and isolated grounded plate transversally in respect of approach airflow. As it has been observed the primary corona and capacitive effect stabilize the discharge structure. Several important explanations regarding the construction of the electrodes system and the method of power supplying have to be notified. We have explored the HF type of the discharge due to two main reasons. The first of them is that the capacitive HF discharge, as a rule, can be characterized by the large level of local reduced electric field E/N , i.e. the HF plasma is non-equilibrium and more active in terms of plasma chemistry. The second reason is that the electrodes for the HF discharge excitation can be isolated from the gas. It is important for the further development to avoid the surface material and electrodes erosion. The HF discharge can exist in different forms in dependence on external conditions. The general understanding now is that the conventional types of electrical discharges are transformed to non-uniform phase under high-speed (Mach number in a range $0.1 < M < 10$) and high-density airflow (pressure $0.1 < P < 10$ Bar). The individual plasma channels, if they exist during relatively long time $t > d/V$, move in airflow with the velocity, which is close to airflow velocity. At the same time the filaments' penetration speed at the discharge initial breakdown is rather high.

A typical photo of the dielectric discharge operation in ambient air is presented in Fig.2.3.1.4 below. To recognize the electrodes arrangement the Fig.2.3.1.4a is shown as an insertion.

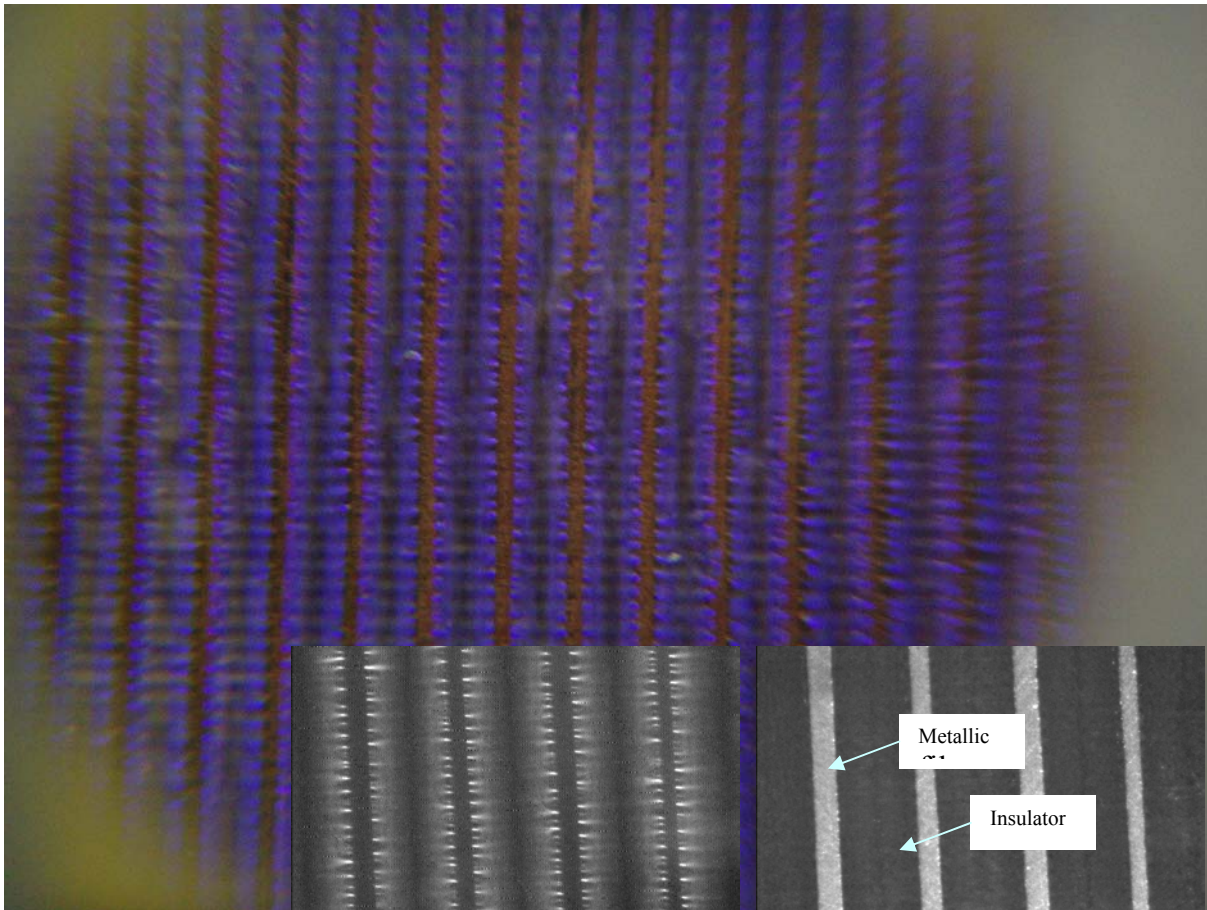


Fig.2.3.1.4. Multi-trace barrier discharge appearance at ambient air.

As it was found the structure of such a discharge is non-uniform in micro-scale. At good temporal and spatial resolution it looks like a multi-filamentary structure but not like a homogeneous corona. At reduced pressure the homogeneous plasma is appeared in combination with multi-coronas (see section 2.1.2).

The observation of the Fig.2.3.1.4 shows that the DBD plasma occupies not whole surface of the available sheet. An optimization of the electrodes configuration is possible to minimize a “dark” space. At lower air pressure this panel works better and the plasma covers more part of the surface.

The discharge has a fixed spots of the coronas location. They tire to the edge of the electrode and often have a high temperature due to a large current density. The diameter of such a spot is about 25mcm, the current through the spot is about 1mA, and thus the current density can be in a range $100\text{A}/\text{cm}^2$. These spots are stable in position from run to run as well as the distance between them. When the saturation effect of spots number takes place the distance between them is measured in range of half from insulator thickness δ , approximately, i.e. about $\Delta z \approx \delta/\epsilon$, where ϵ is the permittivity of insulator.

To ascertain a question on how many individual coronas exist simultaneously the image records with different exposures were done. All other parameters of the discharge excitation were the same. The samples of such records are shown in Fig.2.3.1.5. In the second case the exposure was 5 times less than in the first shoot. It is easy to recognize that the number of individual plasma spots is the same in both images. Moreover, some peculiarities in their distribution occur the same in microscale. A shorter exposure gives the same picture.

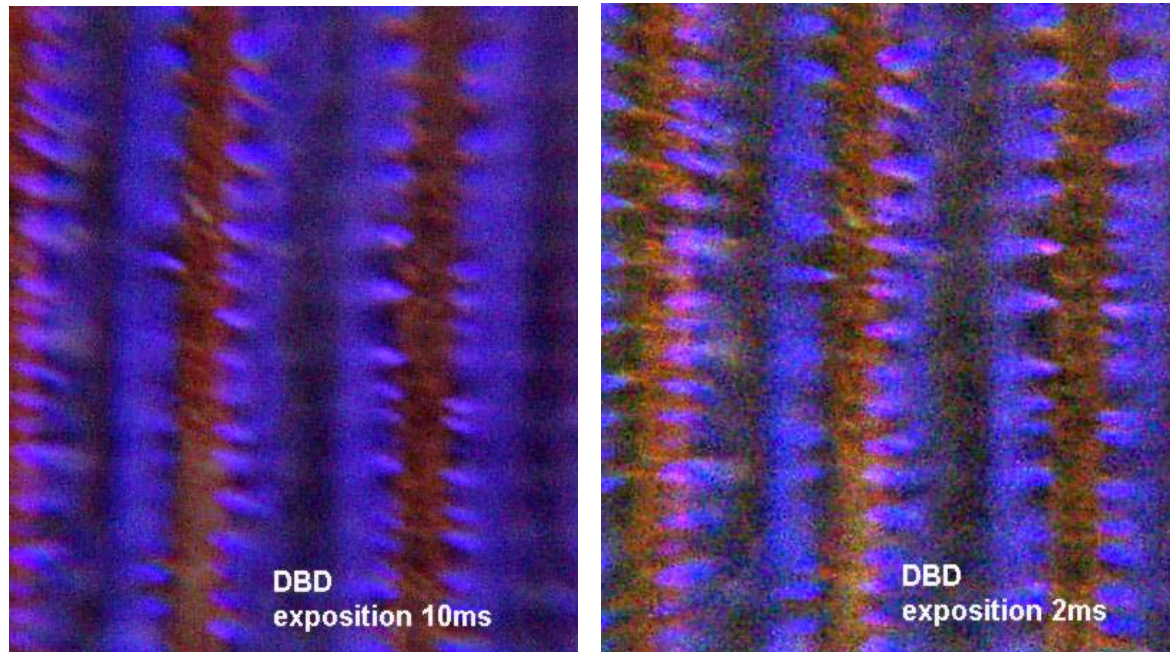


Fig.2.3.1.5. Photos of DBD with different exposition at atmospheric pressure.

The fact above means that DBD plate contains the same number of individual coronas during the period of time longer than period of supplying voltage. This number was 100-150 spots/cm² at the condition of experiment and such an electrodes arrangement. From the other hand the number of plasma spots hardly depends on the supplying voltage, mainly, on the amplitude and frequency. The figures (Fig.2.3.1.6 a-d) below illustrate how the DBD structure depends on the parameters of supplying power. Here the oscillograms of voltage-current and appropriate photos are presented for some operation modes. The power supply has a resonant characteristic at frequency about 45kHz, which is presented in section 2.3.2 in details.

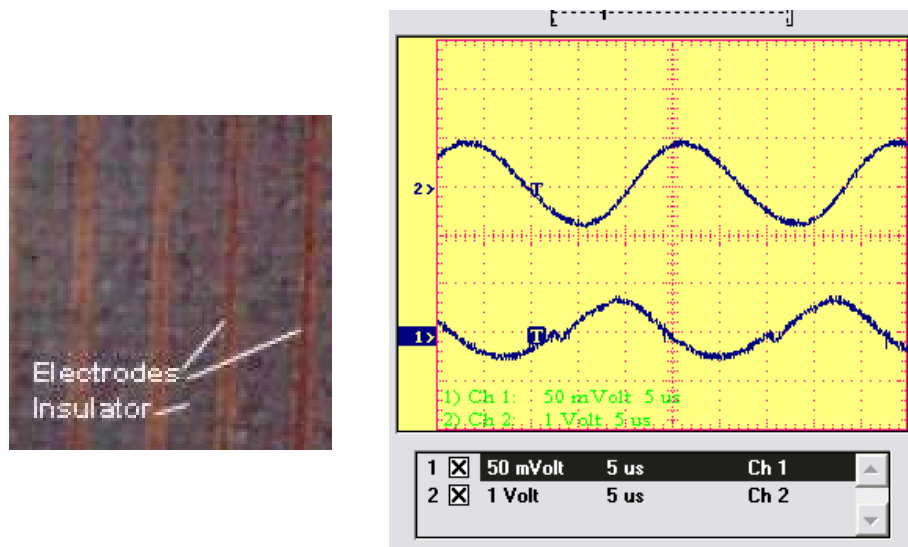


Fig.2.3.1.6a. DBD regime below breakdown.

Ch1 – current 2A/V (inverted), Ch2 – voltage 2kV/V.

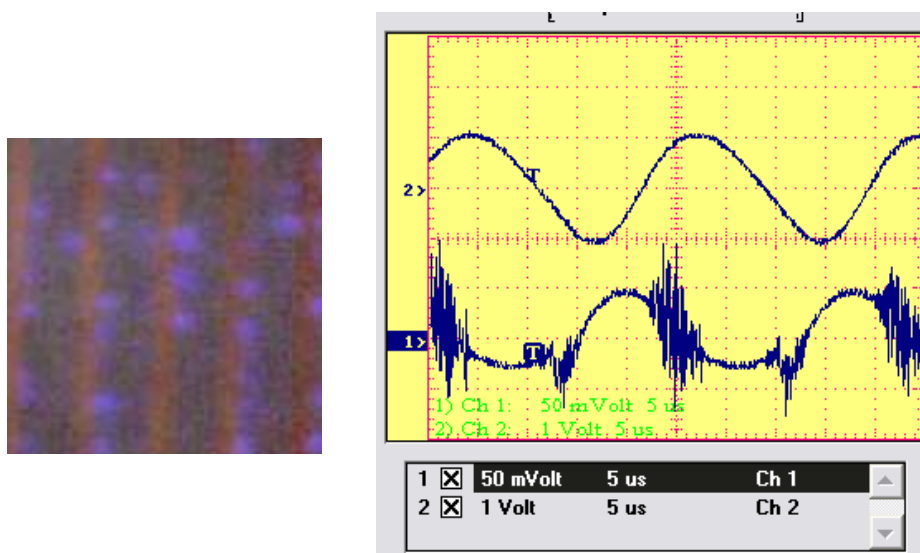


Fig.2.3.1.6b. DBD regime with weak plasma generation.

Ch1 – current 2A/V (inverted), Ch2 – voltage 2kV/V.

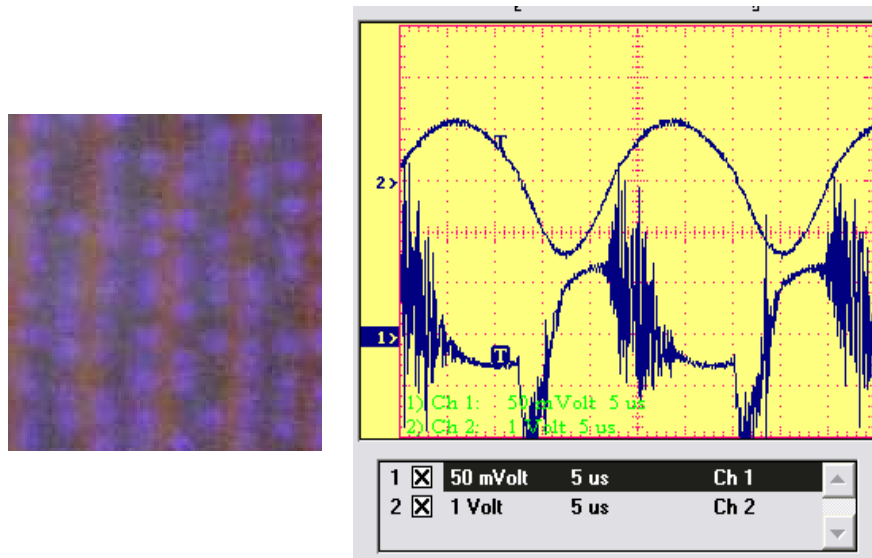


Fig.2.1.3.6c. DBD regular regime.

Ch1 – current 2A/V (inverted), Ch2 – voltage 2kV/V.

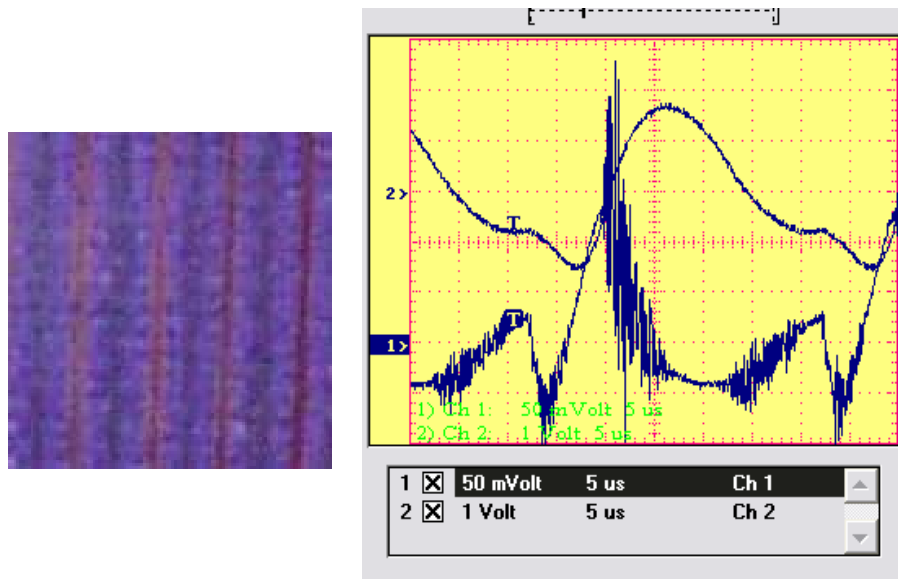


Fig.2.3.1.6d. DBD regime at compensation of resonant frequency shift.

Ch1 – current 2A/V (inverted), Ch2 – voltage 2kV/V.

Some important comments should be done about the series Fig.2.3.1.6. The first one (Fig.2.3.1.6a) reflects the situation before an electrical breakdown. The voltage and the current have almost sinusoidal shape with phase shift $\pi/2$. Small irregularity in the current record is due to loss compensation by pulse source. Well seen that the losses are negligible in this case. The second images are related to situation with a weak DBD discharge (not many plasma points). The discharge current looks like a noise due to parasitic vibration in measuring circuits. In the third case the active losses are so much that the voltage has non-

symmetric shape and resonant frequency of the system is decreased. To enhance the mode a compensation regime can be applied (Fig.2.3.1.6d). In this case an input power is increased in several times and plasma covers the DBD plate quite continuously. Moreover, the plasma generation occurs during the most part of the period. This operation mode can be characterized by the large level of specific power deposition $W=10-20\text{W}/\text{cm}^2$. The methodic of measurements is described in section 2.3.3.

The resulting plasma occupation dependence on applied voltage is presented in Fig.2.3.1.7. It is easy to see that the voltage threshold takes place as well as the effect of saturation of plasma spots number. The level of saturation is defined by the type and thickness of insulator (electric field distribution). The increase of the voltage in this area leads to extra growth of input power. It occurs due to increase of power deposition to each individual corona but not by increase of coronas number as it was in previous zone.

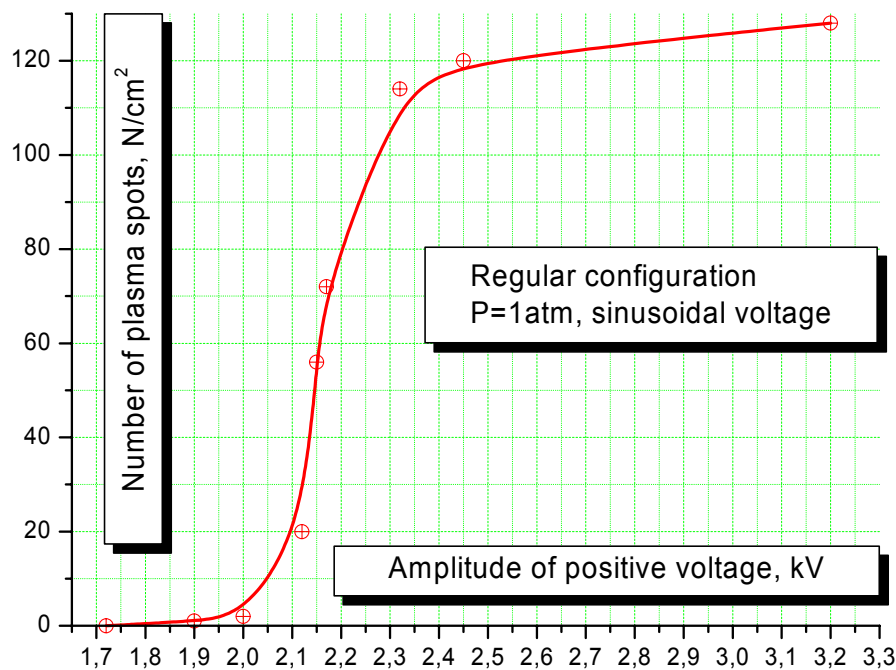


Fig.2.3.1.7. Multi-coronas number vs applied voltage.

The DBD discharge properties in airflow were the same as in ambient air. At least we didn't find any difference. It is quite understandable due to very short time of individual streamers generation $t < 0.1\text{mcs} \ll t_{\text{gd}}$ that is much less than characteristic gasdynamic time.

Schlieren photos of the surface discharge generation in ambient air are shown in Fig.2.3.1.8. These photos have been obtained at the discharge duration about 1ms and

exposure time 30mcs. A grid of air density perturbations due to the non-uniform discharge generation is well seen.

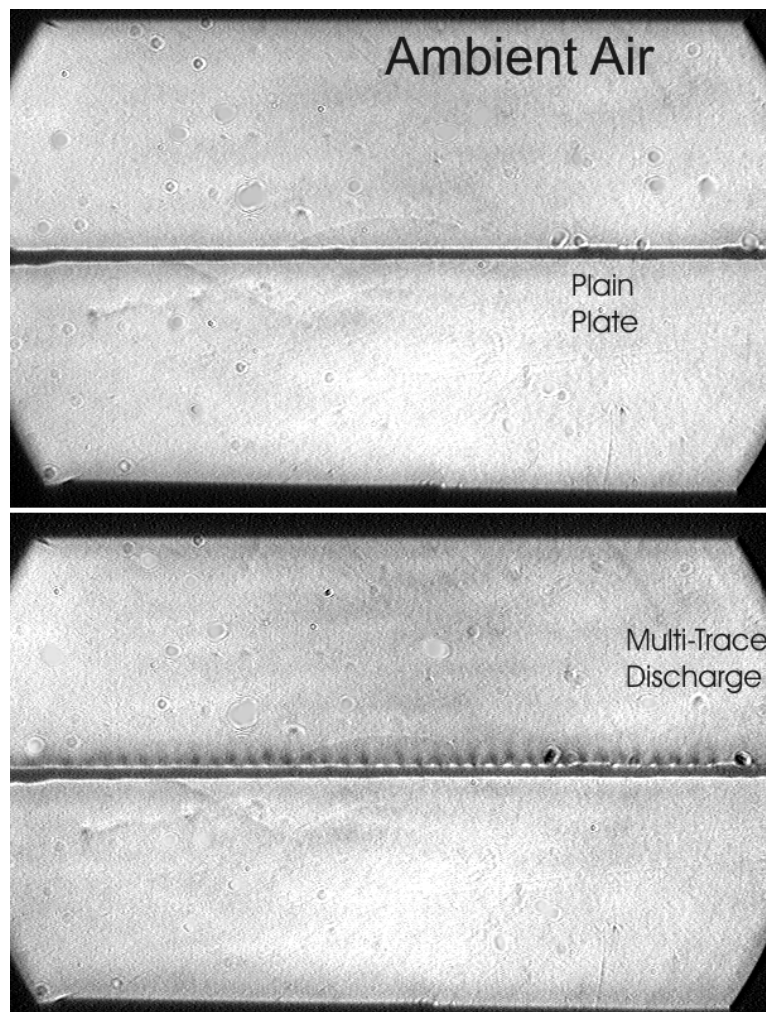


Fig.2.3.1.8. Short-time Schlieren photos of the surface discharge generation in ambient air.

Besides differentiation that was named above discharge configurations differ from each other in another way, namely, symmetric mode of barrier discharge and non-symmetric one. Difference between them is the following. Non-symmetric mode of the barrier discharge was obtained by making grounded electrode as a grid and shifting this grid with respect to potential one, Fig.2.3.1.9.

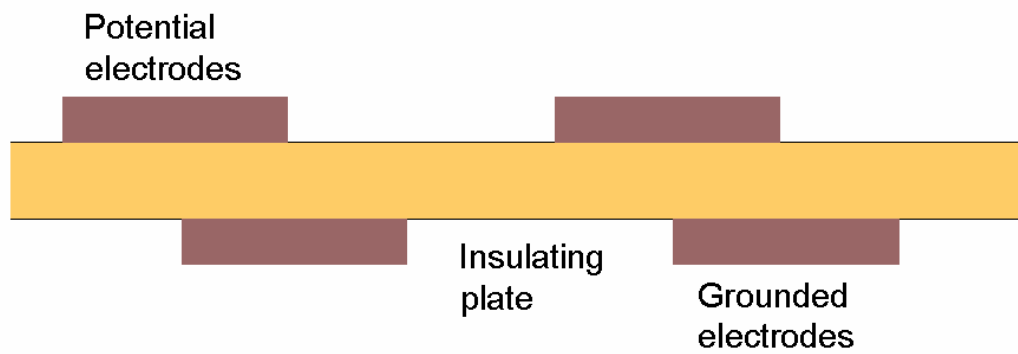


Fig.2.3.1.9. Design of the non-symmetric plasma panel.

Those two modifications of the electrodes arrangement have been tested in ambient air and flow. The Fig.2.3.1.10 shows the fine structure of plasma near surface in case of non-symmetric (A) and symmetric (B) back electrodes location. The size of electrode trace is 1mm and camera shutter is 30mcs.

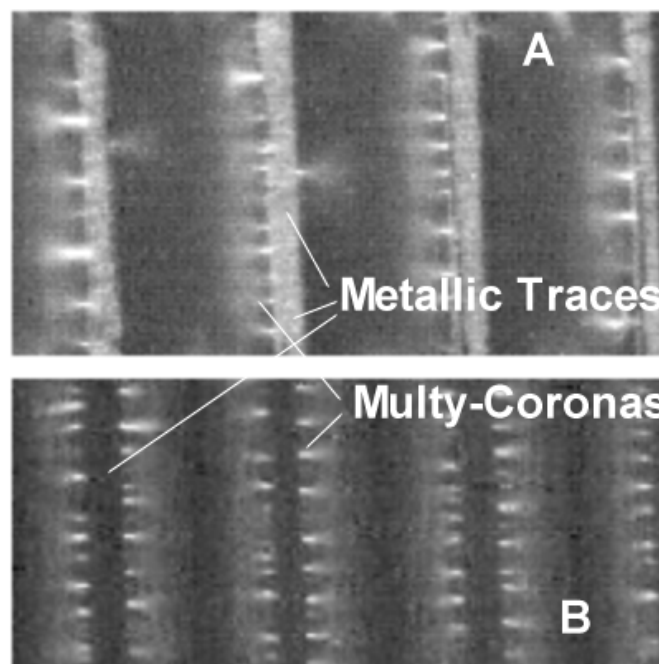


Fig.2.3.1.10. Non-symmetric (A) and symmetric (B) barrier discharge appearance.

In the first case the gas obtains an additional directed impulse, in the second case the boundary layer is affected by periodic pressing forces. Directed flow generation near the surface due to non-symmetric discharge is seen in sequence of Schlieren images, which is presented in the Fig.2.3.1.11 (see section 2.3.6 for details).

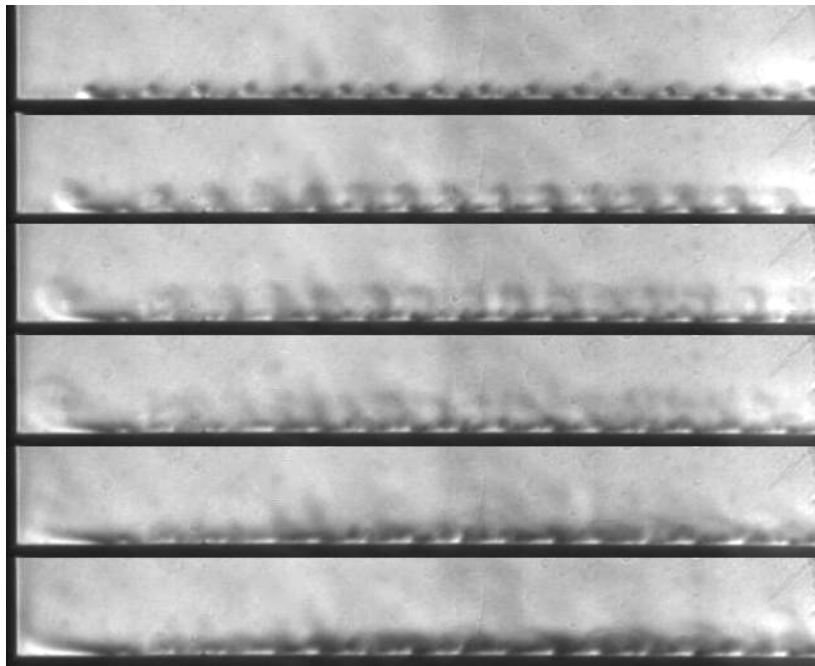


Fig.2.3.1.11. Development of the non-symmetric barrier discharge.

It is well seen that non-symmetric barrier discharge generates directed flow that disturbs an air. The Schlieren photos allow considering the area of energy release as a place near metallic trace edge. The plasma-induced flow velocity is slightly increased downstream.

The location of the heating points and the increasing of the heating layer thickness downstream are well visible in processed Schlieren photos. The sample is presented in Fig.2.3.1.12.

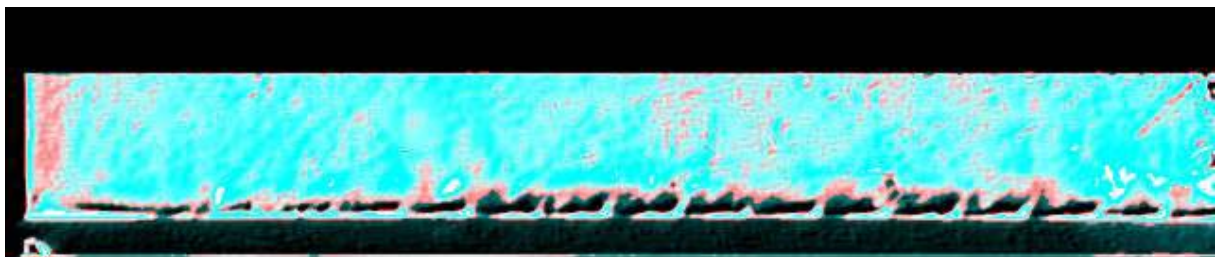


Fig.2.3.1.12. Sample of processed Schlieren photo of the DBD discharge in ambient air.

Induced flow from left to right.

2.3.2. Scheme Simulation.

Two different schemes of the DBD supplying were used: direct feeding with triangle shape of the pulses and resonance scheme. The second power source is built on the resonant scheme and differs from the previous one by more effective adjustment with the plasma panel in particular test. The first device allows obtaining a large peak power. The second power supply demonstrates a good adjustment and relatively low level of EM noise.

The draft scheme of the resonant power supply is shown in Fig.2.3.2.1. A plasma load is simulated here by means of two switches controlled externally.

The power supply is characterized by the following technical parameters:

- Type of power supply resonant, with external control of frequency;
- Output AC (sine);
- Output AC voltage ($I=0$) up to 7kV;
- Output AC current ($V<4kV$) up to 0.3A;
- Maximal output pulse current ($t<1mcs$) up to 5A;
- Typical output power (optimal adjustment) 1kW;
- DC shift (not shown in the scheme) -10kV÷+10kV;
- Main frequency of oscillations (tunable) 10kHz÷1MHz.

The equivalent scheme computational analysis was executed on the base of PSpice™ software. The most difficult problem was a plasma load simulation. Here it was done roughly by voltage controlled breakdown devices with a different level of switching on and switching off threshold. The effect of small time delay of breakdown was simulated by integral circuit.

Some results of the scheme simulation are shown in Figs.2.3.2.2-4. The Fig.2.3.2.2 presents the result of transitional analysis at $F=100kHz$. Well seen that the time delay of working cycle is about 100mcs. The plasma current, which is presented in Fig.2.3.2.3, exists during small period of time as it was measured experimentally under a bit different conditions. The regimes with plasma current oscillations were found as well. The details are shown in Fig.2.3.2.4.

A preliminary experimental testing of the scheme was done with a load of resistive type. The results were very similar as due to simulations.

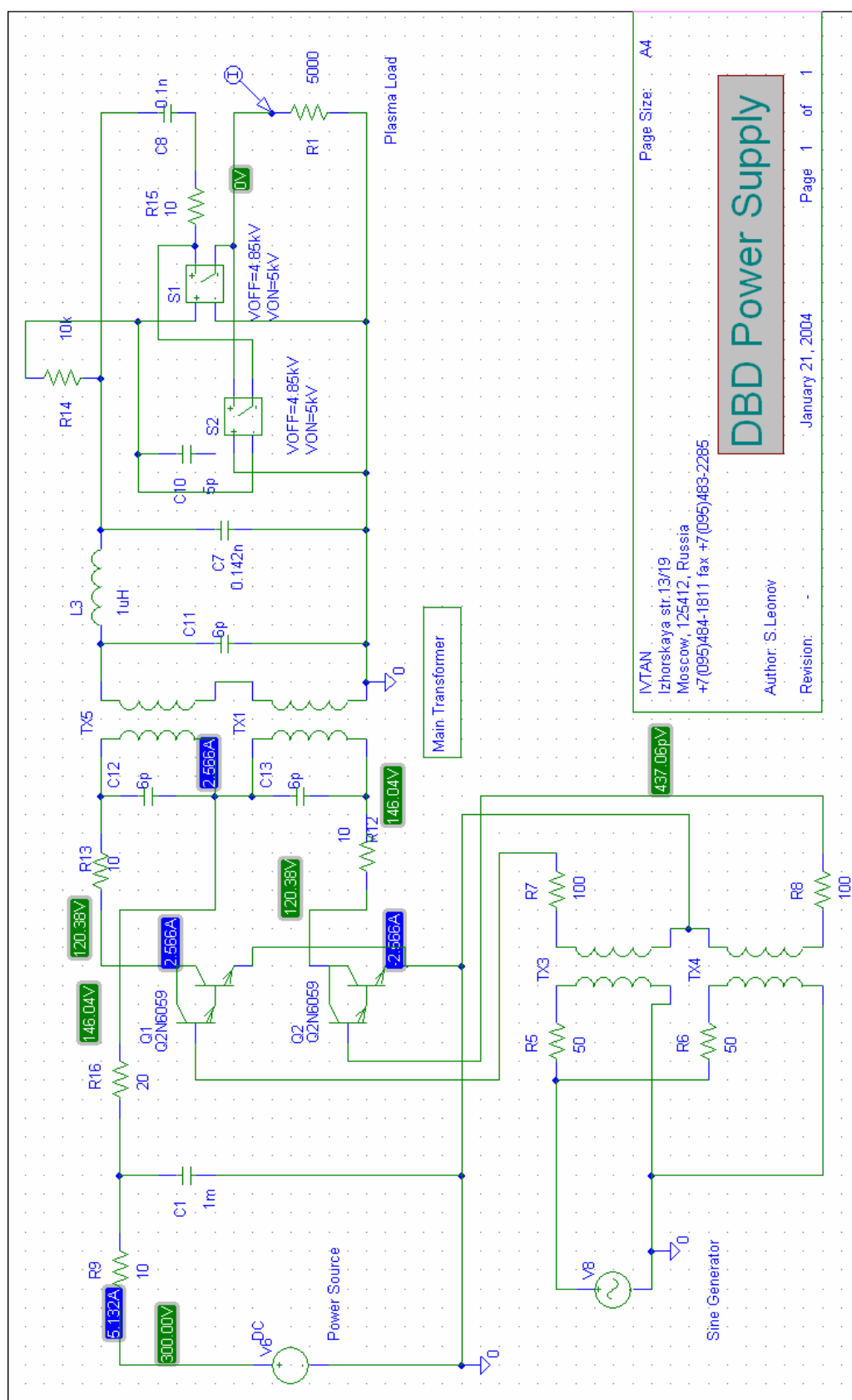


Fig.2.3.2.1. Draft scheme of resonant power supply.

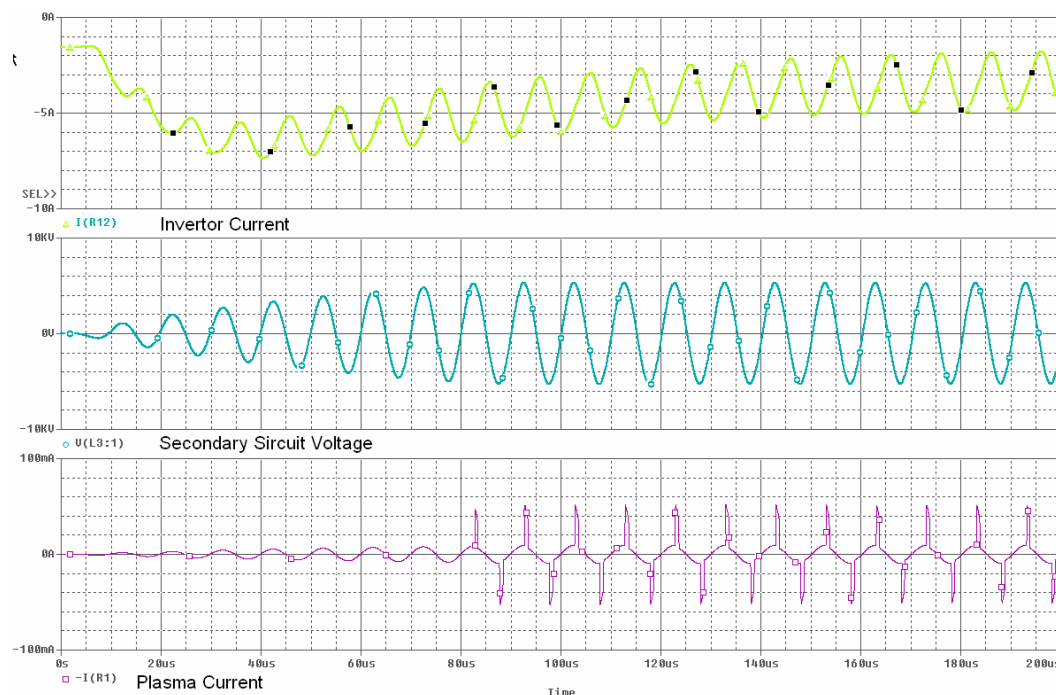


Fig.2.3.2.2. Result of equivalent scheme simulation. Transitional analysis.

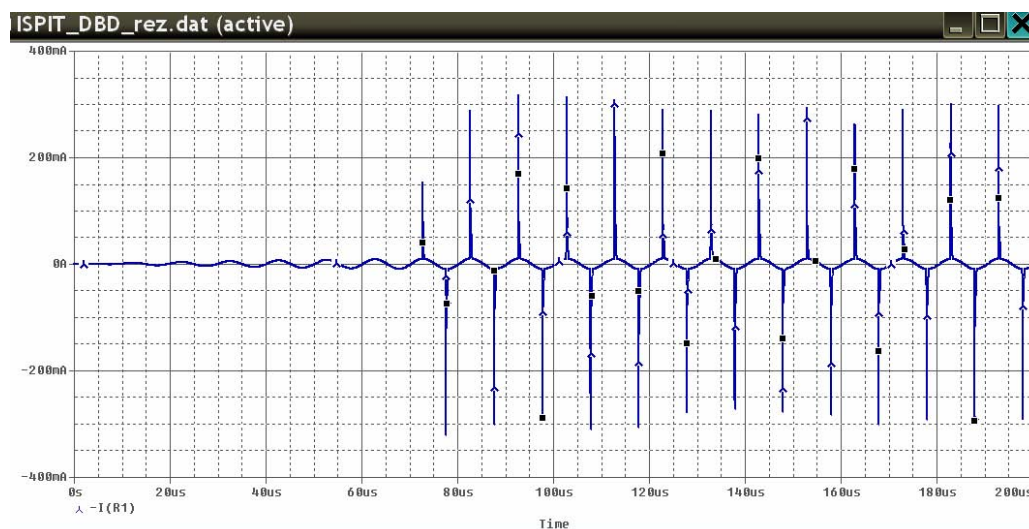


Fig.2.3.2.3. Result of equivalent scheme simulation. Plasma current.

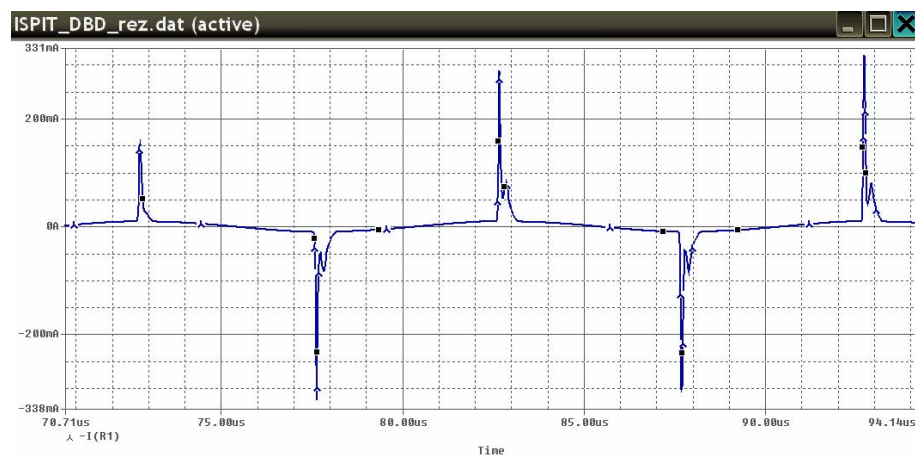


Fig.2.3.2.4. Result of equivalent scheme simulation. Plasma current (details).

2.3.3. Measurements of Electric Parameters.

Special voltage and current sensors were used for the regular measurements. Standard high-voltage high-frequency divider and current sensor of “Tektronix” have been utilized for the verification of the measurements. Typical Volt-Ampere records (oscillograms) are shown below. The record when a standard inductive-less resistance was connected as the load is presented in Fig.2.3.3.1. Well seen that the current and voltage are repeated by each other. Some difference in waveform can be explained by the inductivity of admitting wires. A constant positive shift of the voltage in $U \approx 450V$ occurs due to HF-DC mixing in power supply.

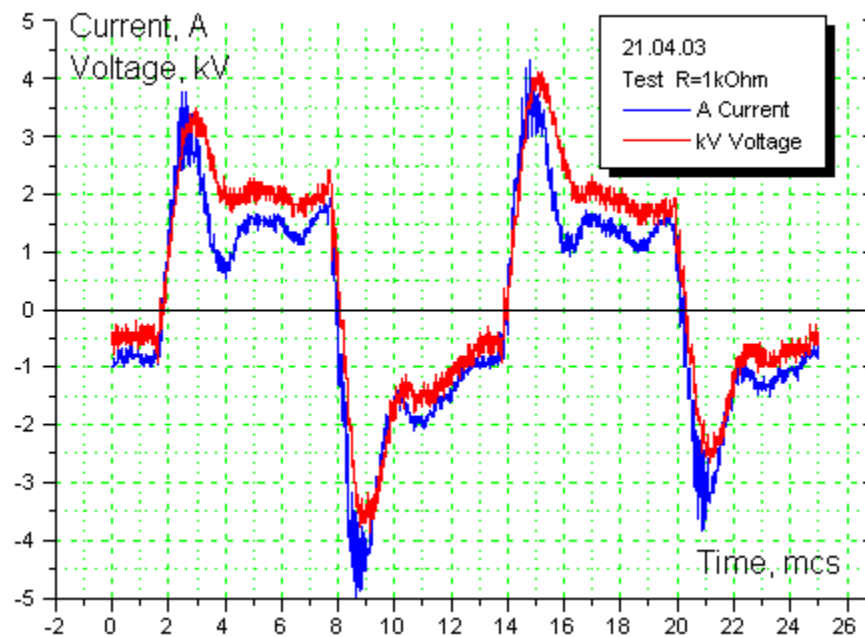


Fig.2.3.3.1. Test Volt-Ampere record on active load.

A sample of the Volt-Ampere record for the plasma panel is presented in Fig.2.3.3.2. A simplified analysis allowed obtaining the value of input power. It was about $W_{pl} \approx 100W$ for the conditions of measurements and electrodes configuration. An appropriate power density was about $w \approx 20W/cm^2$. The Fig.2.3.3.3 demonstrates the procedure of plasma current extraction from the experimental data. Here the measured current is compared with the calculated current through the initial panel capacitance (voltage derivative multiplied of the

capacitance value). It is easy to recognize two moments of the discharge breakdown. The estimated mean value of the important composition is:

$$I_p^2 = (I_t - I_{C1})^2 = (I_t - C1 \times \frac{dU_d}{dt})^2 \approx 0.1(A^2).$$

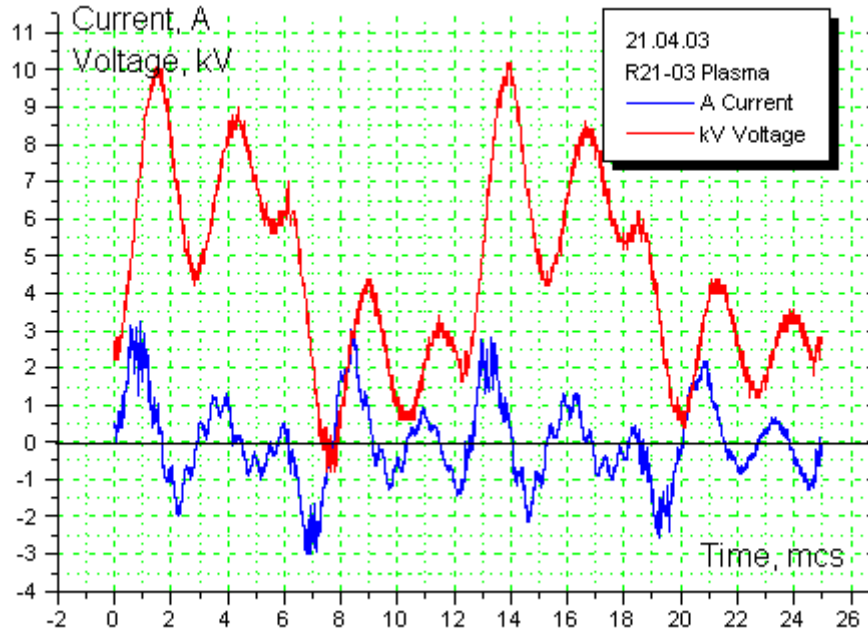


Fig.2.3.3.2. Volt-Ampere record on plasma load (barrier discharge).

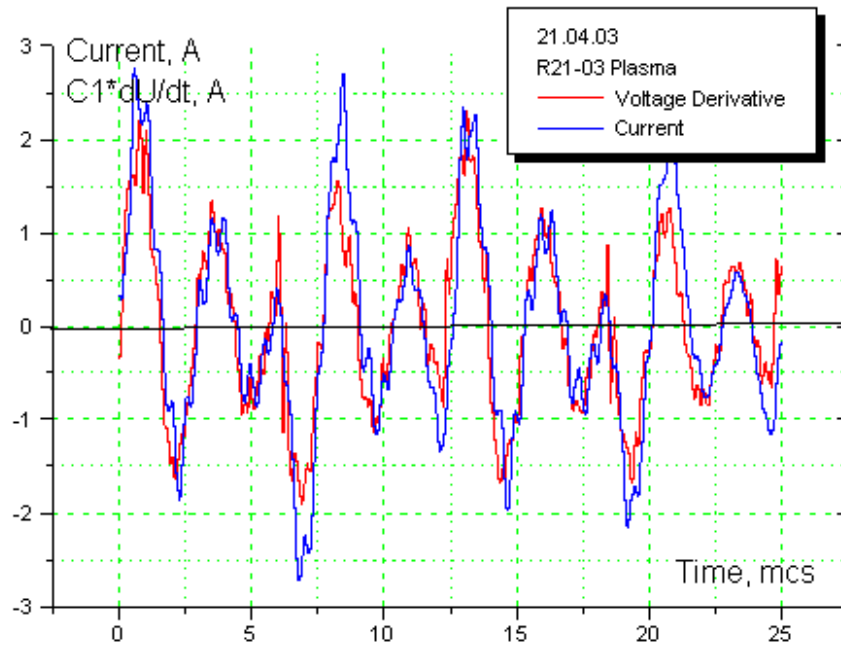


Fig.2.3.3.3. Comparison of current and voltage derivative for the plasma panel.

To recognize definitely the time of the discharge operation the correlation of the current and the plasma radiation has been considered. A sample of such a correlation is shown in Fig.2.3.3.4. Well seen that sometimes the plasma can be excited several times per period due to voltage oscillations in supplying circuits.

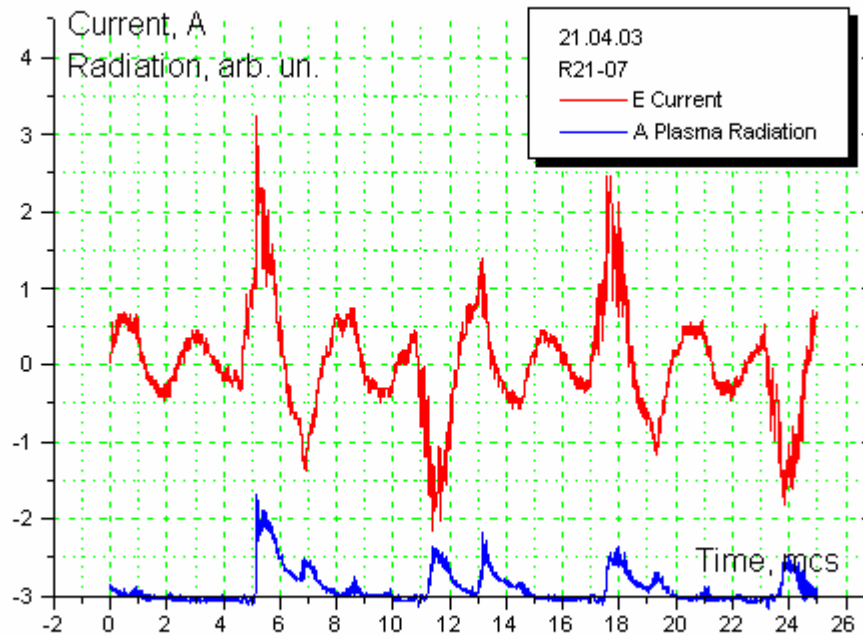


Fig.2.3.3.4. Current-Radiation record on plasma load.

The measurements of the input power have been verified on the base of analysis of equivalent scheme of the plasma generator. A simplified equivalent scheme is presented in Fig.2.3.3.5. Here the “Gen” is a generator of the voltage of complicated wave-form, R1 is inner resistivity of the power supply, L1 is wires inductivity, C1 is initial capacity of the plasma panel, R2 is active resistivity of the plasma, C2 is additional capacity due to the plasma generation.

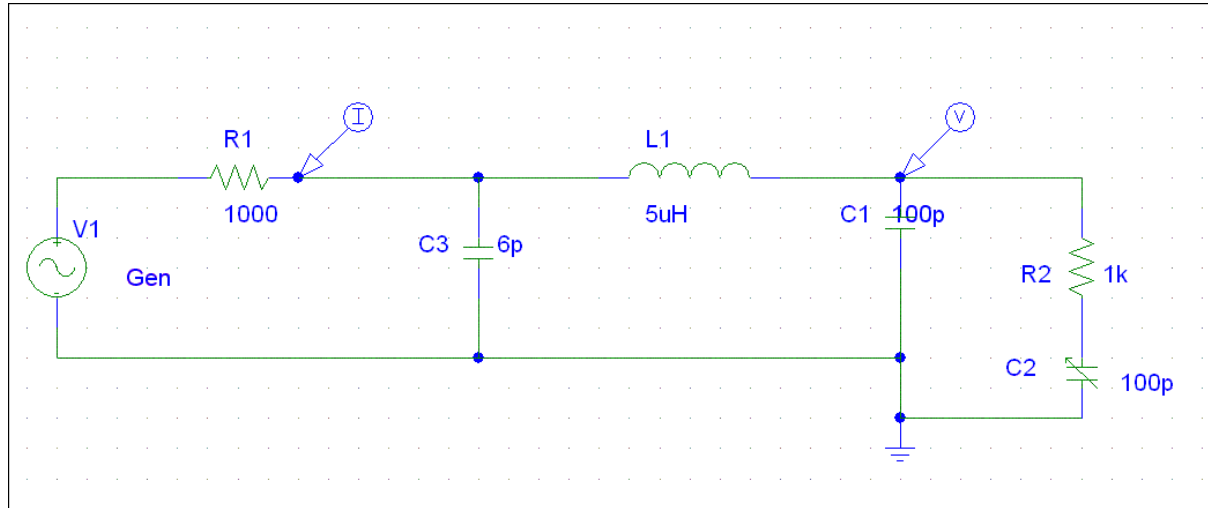


Fig.2.3.3.5. Simplified equivalent scheme of the barrier discharge.

We can measure the gap voltage U_d and total current through the circuit I_t . At the same time the input power is defined by the voltage and the current through plasma itself: U_{pl} and I_{pl} :

$$W_{pl} = U_{pl} \times I_{pl} = (U_d - U_{C2}) \times (I_t - I_{C1}) ;$$

where unknown parameters can be recalculated by the following expressions:

$$I_{C1} = C1 \times \frac{dU_d}{dt} ; \quad \text{and} \quad U_{C2}(t) = \frac{1}{C2} \times \int_0^t (I_t - I_{C1}) dt .$$

The most correct method of the input power recalculation is a full circuit simulation by means of appropriate software. A preliminary scheme's adjustment efforts have been done on the base of scheme simulation technique. The PSpice™ software has been utilized. The result of the scheme's simulation can be summarized as follows:

- Each value of the plasma load requires the individual tuning of the system, especially transmitting line. By the other words, the scheme can be tuned on the predefined level of the voltage and power output. Specific type of electrode system required an individual tuning of the output circuits as well as transmitting line.
- The output voltage at off-load operation mode can reach the value up to 20kV. Such a level is enough for the initial discharge breakdown at the most conditions.
- The power-load characteristic of the system is of the resonant type. The maximal value of the output power depends on the scheme parameters. It means that the power stabilization operation mode is possible.

2.3.4. Measurements of Barrier Discharge Plasma Parameters.

Some data on the rotational plasma temperature measurements have been reported in [1,6]. Spectroscopy of the second positive system of molecular nitrogen and CN molecular spectrum were chosen as a method of gas temperature measurements. The optical spectrums were registered by means of a spectrograph Lot-ORIEL connected with a CCD camera at spectral resolution about 0.04nm/pixel. The device spread function was 0.12-0.15nm. So, a partially resolved molecular spectrum was obtained in experiment. For the determination of gas temperature in a discharge area the method of optical emission spectrum shape fitting has been adopted.

Survey spectrums of barrier discharge in ambient air and in airflow, in air with addition of CO₂ and in air with addition of Ar were obtained experimentally. No differences between these three cases were pointed out except the appearance of Ar lines in the discharge at Ar-air mixture. Besides it intensity of the spectrum of the discharge at Ar addition is higher than intensity of the discharge without Ar. Such a spectrum for the discharge at ambient air is shown in Fig.2.3.4.1. It is well seen that excitation of C³Π^u(v'=0,1,2,3) states of N₂ molecules rather efficient. The spectrum with Ar addition is shown in Fig.2.3.4.2.

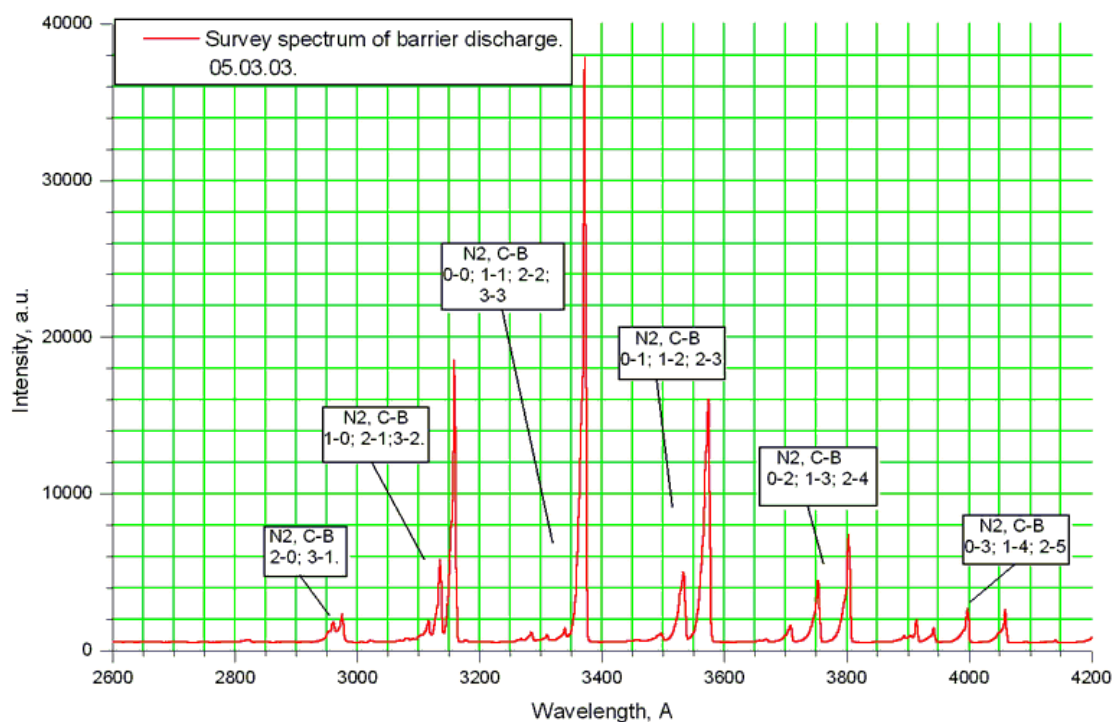


Fig.2.3.4.1. Survey spectrum of the barrier discharge at ambient air.

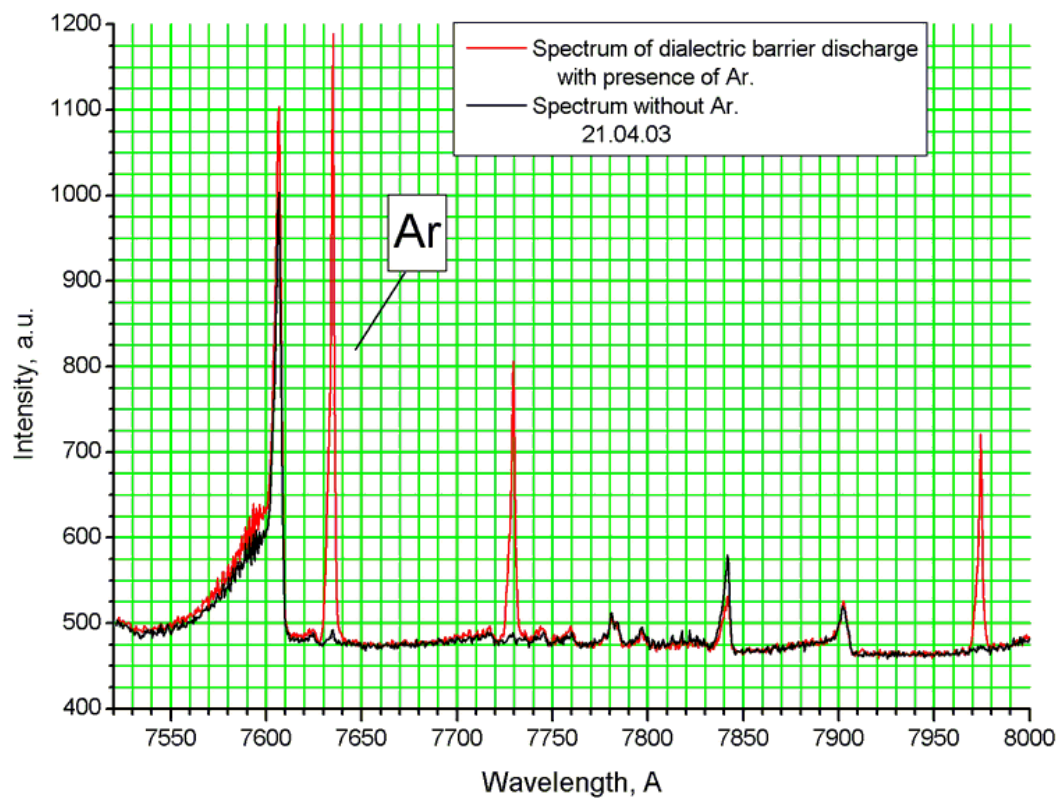


Fig.2.3.4.2. Spectrum of barrier discharge in air with and without addition of Ar.

Measurement of Rotational (Translational) Temperature.

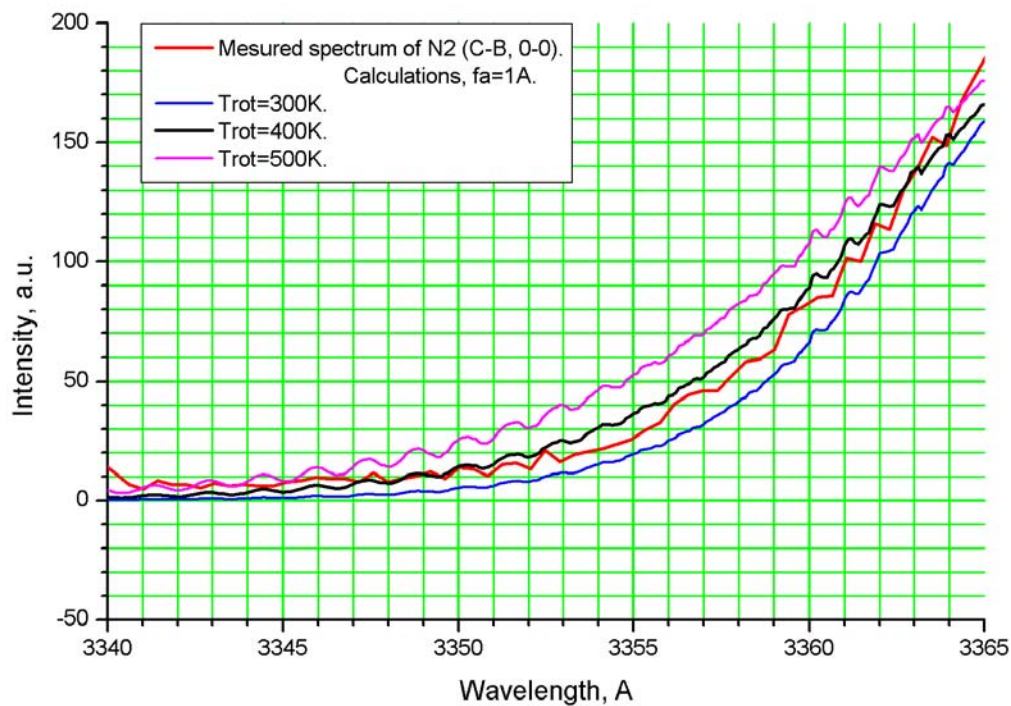


Fig.2.3.4.3. Fitting of the synthetic spectrum and experimental one for the DBD.

Plasma temperature has been measured in region of DBD multi-coronas at mean power deposition in a range $5\text{-}20\text{W}/\text{cm}^2$. Example of the fitting of the calculated spectrum and experimental one is presented in Fig.2.3.4.3. The result of formal procedure gives that the translational temperature is $T_{tr}=360\pm 20\text{K}$. The result coincides well to [7, 8].

A barrier discharge had been studied by spectroscopic methods to find out its ability to heat the gas. Spectrum of the discharge was registered at the following conditions:

- 1) Plasma panel in the ambient air at the 200 ms from the start of discharge.
- 2) Plasma panel in high-speed airflow.
- 3) Plasma panel in ambient air; two moments of the discharge: 0ms and 330ms.

Corresponding spectrums are presented in the Fig.2.3.4.4.

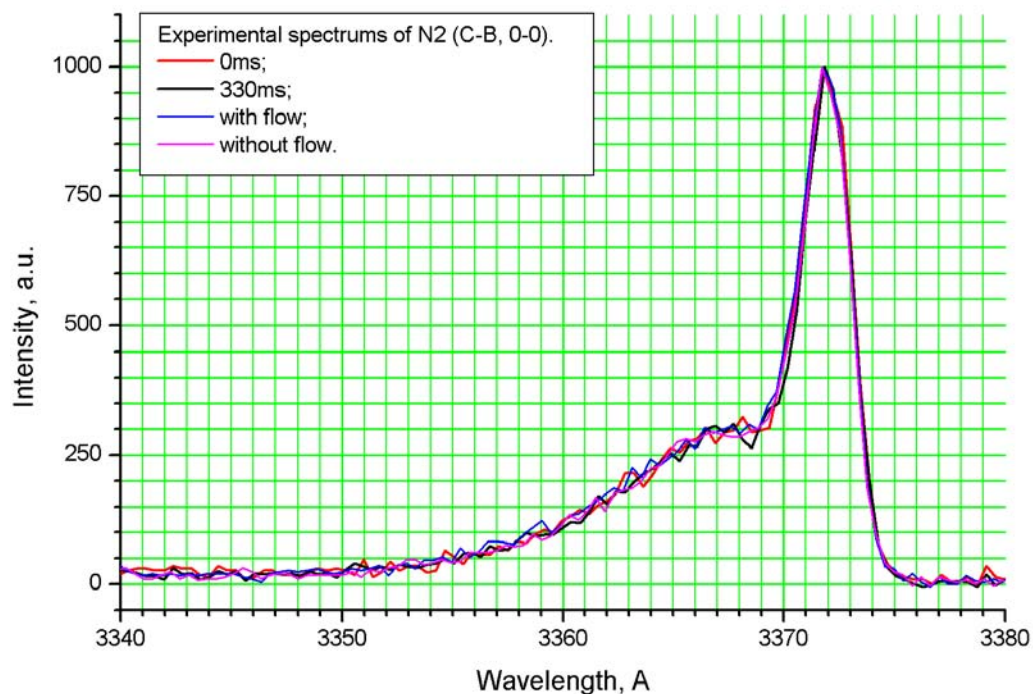


Fig.2.3.4.4. Spectrums of the DBD at different conditions.

Well seen that all these spectrums correspond to the same temperature. It means that gas heating occurs very quickly and each separate plasma streamer processes a new portion of medium. If it was not so, temperature of the gas should been reduced after the air inflow and increased during the discharge.

Measurement of Vibrational Temperature.

The most intense bands in the spectrum of DBD relate to the N₂ second positive system. Rotational temperature of DBD was determined from the (0-0) transition of N₂ spectrum. Here we are interested in the $3650\text{ Å} \div 3850\text{ Å}$ spectral range, covering the 0-2, 1-3 and 2-4

head bands (at 3804 Å, 3754 Å and 3709 Å, respectively). These bands were chosen due to the relatively narrow spectral range they are situated in that is result in small spectral intensity disturbances, which are caused by dependence of CCD matrix quantum efficiency from wavelength.

The intensity of band head of vibrational band structure depends on the vibrational dimensionless Franck-Condon $q_{v'v''}$ factor for that particular band, the population of the molecules in the initial state, the wavenumber of the vibrational transition σ_{ul} and a factor C_{ul} that is the same for all vibrational bands of the same electronic transition. We may write the vibrational emission coefficient of the particular band for a given electronic transition ($C^3\Pi_u - B^3\Pi_g$) as:

$$\varepsilon_{v''}^{v'} = 10^{-7} \times C_{ul} \times \sigma_{ul}^4 \times q_{v'v''} \times \exp\left(-1,42141 \times \frac{F_{v'}}{T_{vib}}\right), \quad [1]$$

where $F_{v'}$ – vibrational energy of the initial level, and T_{vib} is the vibrational temperature. This equation may be used if a thermal equilibrium exists among vibrational states. Dimensions of equation components are the following: $[\sigma_{ul}] = \text{cm}^{-1}$; $[F_{v'}] = \text{cm}^{-1}$; $[T_{vib}] = \text{K}$. Constants for transitions under consideration are presented in Table 2.3.4.1.

Table 2.3.4.1. Spectroscopic constants and experimental intensities.

	Wavelength, nm	$\sigma_{ul}, \text{cm}^{-1}$	$q_{v'v''}$	$F_{v'}, \text{cm}^{-1}$	I, a.u.
0-2	3804	26289,92	0,145	1016,70	1000
1-3	3754	26636,70	0,202	2568,14	574,1
2-4	3709	26958,88	0,169	4244,46	158,4

Taking a logarithm from equation [1] we get a linear function $f(F_{v'})$:

$$\ln\left(\frac{I \times 10^7}{\sigma_{ul}^4 \times q_{v'v''}}\right) = \text{const} - \frac{1,42141}{T_{vib}} \times F_{v'}, \quad [2]$$

So, we can calculate T_{vib} if we know several points (I, $F_{v'}$). Spectrum of the 0-2, 1-3 and 2-4 transitions is presented in the Fig. 2.3.4.5.

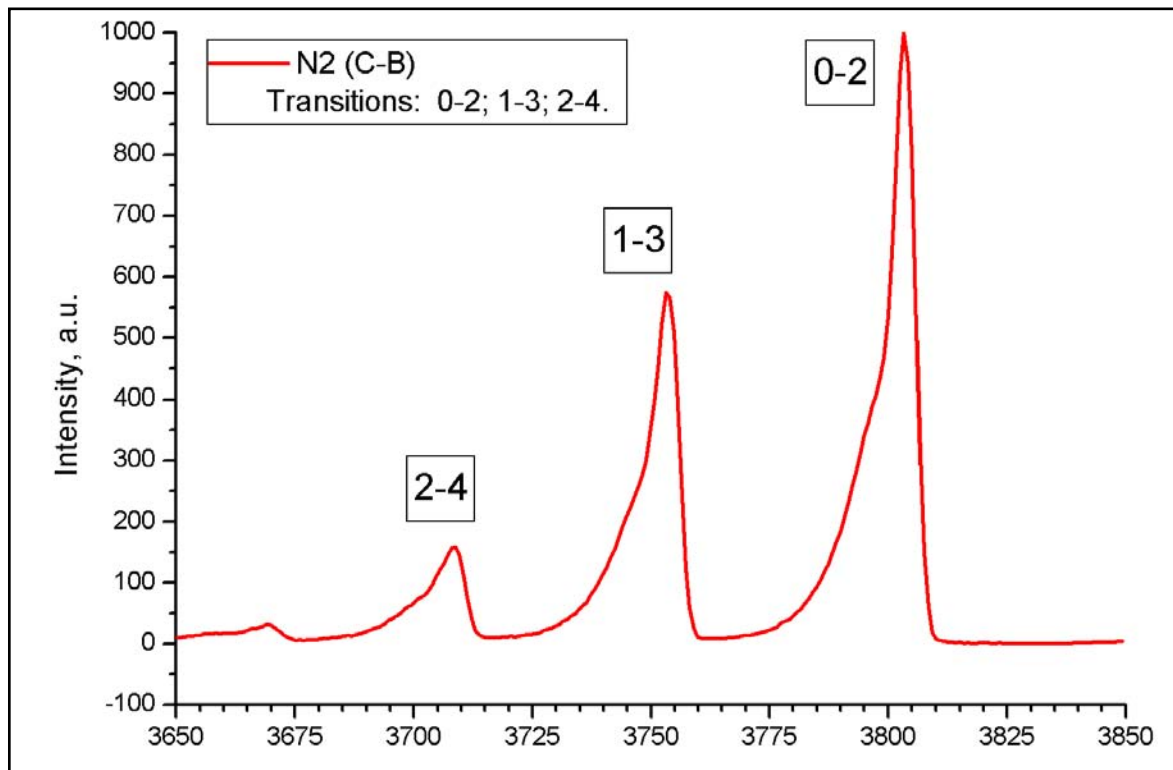


Fig. 2.3.4.5. Experimental spectrum N2 for vibrational temperature measurements.

Vibrational temperature calculation by the method described above has given a value $T_v = 2200 \pm 150 \text{ K}$.

Electron temperature measurements.

Method of electrostatic probe and spectroscopic methods are the most widely used methods of electron temperature measurements in the plasma. Application of the probe is complicated in our case by the small thickness of plasma layer on the surface of DBD plate (approximately several millimeters). Besides this, the method has its inherent disadvantages, for example its intrusive nature. At the same time DBD in our configuration is a suitable object for spectroscopic observations, because it can work in stationary mode that allows us to obtain relatively high intensity of signal. So, we have chosen spectroscopic method of electron temperature measurement because of these reasons.

Choice of the particular spectroscopic method is determined by the experimental conditions and by the spectral composition of the emission. Measurements were provided by means of the spectrograph LOT-Oriel that is constructed on the base of monochromator MS257 and spectroscopic camera Andor420DU. Minimal instrumental function of the spectrograph was 1.2 Å. Such a value complicates any calculations based on the line width

measurements. Survey spectrum of the DBD was presented in the previous reports, so only part of the spectrum that is interesting in respect to electron temperature measurement, i.e. that is reach by the atomic lines, is presented here in the Fig.2.3.4.6a, b.

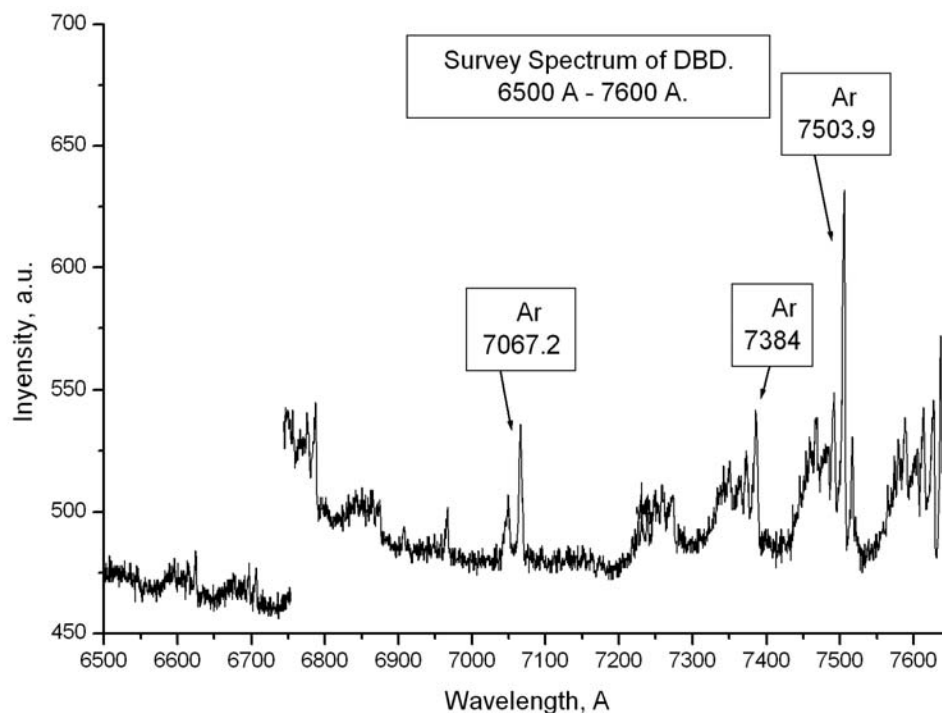


Fig.2.3.4.6a. Survey spectrum of the DBD. 650-770nm.

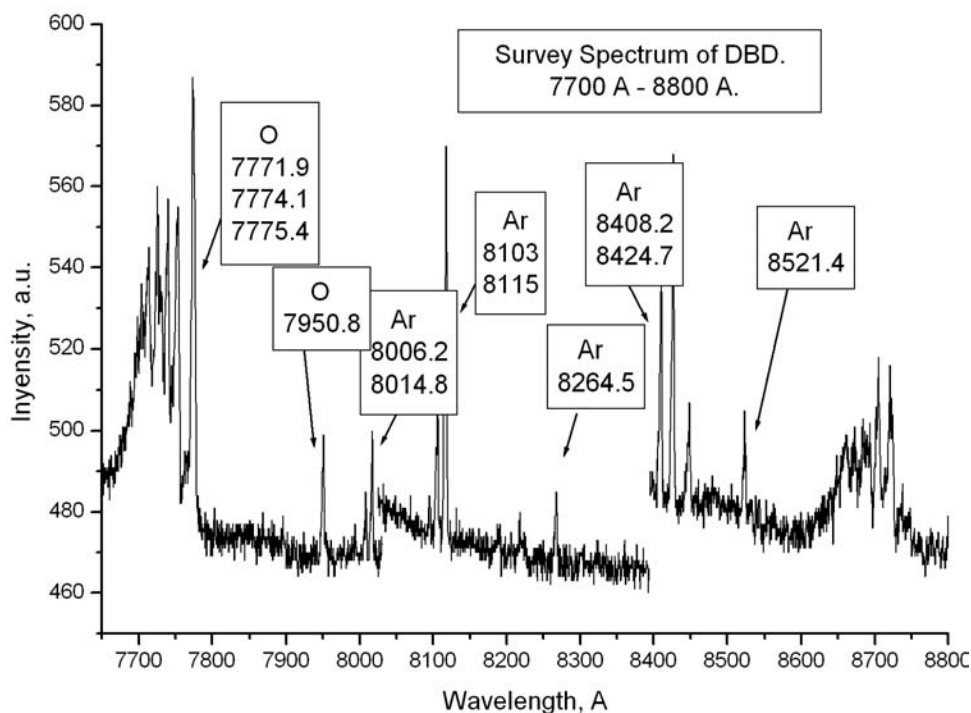


Fig.2.3.4.6b. Survey spectrum of the DBD. 770-880nm.

It is well seen that argon lines prevail among the atomic lines in the spectrum. So, evident choice in this case is the method of electron temperature measurements by the relative intensities of the lines that belong to the atoms of the same ionization degree (neutral atoms in our case). This method is based on the fact that densities of the different excited states are proportional to the product of the statistical weights and Boltzmann factors of these states [9]:

$$N_n \propto g_n \exp\left(-\frac{E_n}{kT_e}\right). \quad (3)$$

Full atomic line emission intensity of the transition $n \rightarrow m$ can be written in the following form:

$$I_{nm} = \frac{h\nu_{nm}}{4\pi} A_{nm} N_n. \quad (4)$$

So, temperature is inversely proportional to the logarithm of the ratio of the full line intensities that are generated at the transitions from the different upper states. Equations (3) and (4) cause quantitatively to the following equation for the temperature:

$$T_e [eV] = \frac{E'' - E'}{\ln\left(\frac{I' \cdot \lambda' \cdot A'' \cdot g''}{I'' \cdot \lambda'' \cdot A' \cdot g'}\right)}. \quad (5)$$

where I , λ , A , g – full intensity, wavelength, transition probability and statistical weight of lower state of transition; E – excitation energy.

This method of electron temperature measurement is often used for hydrogen lines [10] and for argon lines [11] in the wide range of plasma parameters as well as in the case of low electron temperature (several eV).

Two argon lines that lie within the short spectral interval have been chosen for measurements. Short spectral interval reduces mistake of the intensity measurements. Besides this, difference between the upper energy levels of these transitions is one of the biggest among the others, which influences very strong on the temperature measurement accuracy. Parameters of the transitions are presented in the Table 2.3.4.2.

Table 2.3.4.2. Parameters of the transitions.

Transition	$1s_2 - 2p_2$	$1s_5 - 2p_9$
Upper level energy	$E'' = 13.33 \text{ eV}$	$E' = 13.075 \text{ eV}$
Intensity	$I'' = 15$	$I' = 100$
Wavelength	$\lambda'' = 8264.53 \text{ \AA}$	$\lambda' = 8115.31 \text{ \AA}$

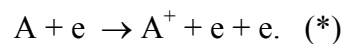
Probability	$A'' = 0.168 \cdot 10^8 \text{ s}^{-1}$	$A' = 0.366 \cdot 10^8 \text{ s}^{-1}$
Statistical weight	$g'' = 3$	$g' = 7$

The following result has been obtained after the substitution of the values from the Table 2.3.4.2 to the equation (5): $Te \approx 1 \text{ eV}$.

Calculations that were carried out by other lines of argon gave different results, so accuracy is estimated as 30%. The main source of calculation error is a small energy difference between upper levels of transitions that were observed in the spectrum in comparison with electron temperature.

It is need to note, that dependence of the states' excitation cross-sections on the electron energy was not taken into account. It was so because maximums of these dependences lie at the energy of the order of 20 eV (24 eV for $1s_2$ and 21 eV for $1s_5$). These energies are in the distribution tail area. Besides this, dependencies slightly differ from each other. So, inaccuracy that is generated by these assumptions during calculations is negligible.

As a result a conclusion could be made that above-mentioned electrode system generates non-equilibrium weakly-ionized plasma in a form of streamers. Such plasma is non-equilibrium by two means. Firstly there is large difference between electron temperature, vibrational temperature and gas temperature. Secondly plasma ionization degree is much lower than ionization degree, which corresponds to the equilibrium plasma at the same electron-temperature and much higher than ionization degree, which corresponds to transitional temperature ($T_e=1\text{-}3\text{eV}$, $T_v=2\text{-}3\text{kK}$, $T_g=300\text{-}400\text{K}$). Electron temperature differs from gas temperature because Joule heat of the current in weakly ionized plasma is too low to heat the gas. Equilibrium ionization degree is achieved due to compensation of forward and inverse processes. Main process of ionization is the following:



Processes of dissociative recombination and diffusion are much more quickly than recombination in triple collisions, which is an inverse process of (*). Quick loss of charged particles does not allow of ionization degree to rise to equilibrium level. Such a mechanism can explain rising of emission intensity at Ar addition. Indeed, ions of Ar are recombined in triple collisions mostly. This process is inverse with respect to ionization one, so the ionization degree of the plasma rises, which leads to the rise of emission intensity.

References to section 2.2.

1. S. Leonov, A. Kuryachii, D. Yarantsev, A. Yuriev, "Study of Friction and Separation Control by Surface Plasma." Paper AIAA-2004-0512, 42th AIAA Aerospace Sciences Meeting & Exhibit, 05-08 January 2004 / Reno, NV.
2. Valentin I Gibalov and Gerhard J Pietsch "The development of dielectric barrier discharges in gas gaps and on surfaces", J. Phys. D: Appl. Phys. **33** (2000) 2618–2636.
3. Pietsch G J and Gibalov V I Discharge phenomena on a dielectric surface with extended electrodes *Proc. 12th Int. Conf. on Gas Discharges and Their Applications* vol 2, 1997, pp 750–765.
4. Samoilovich V, Gibalov V and Kozlov K 1997 *Physical Chemistry of the Barrier Discharge* 2nd edn (Dusseldorf: DVS).
5. Muller S and Zahn R-J On various kinds of dielectric barrier discharges *Contrib. Plasma Phys.* **36** (1996) 697–709.
6. S. Leonov "Near-Surface Plasma Effects in High-Speed Flows", Russian School-Workshop "MPA in Aerospace Applications", 20-21 April 2004, IVTAN, Moscow.
7. S. Pellerin, K. Musiol, O. Motret, B. Pokrzywka and J. Chapelle, "Application of the (0,0) Swan band spectrum for temperature measurements". J. Phys. D: Appl. Phys. **29** (1996).
8. U. Kogelschatz, "Fundamentals and Applications of Dielectric-Barrier Discharges". ABB Corporate Research Ltd, 5405 Baden, Switzerland.
9. Hans R. Griem, *Plasma Spectroscopy*, MCGRAW-HILL BOOK COMPANY, 1964
10. V.P. Veremiyenko, U. Fantz, W.J. Coedheer, M.G. von Hellermann, G.J. van Rooij, R.P. Dahiya, and N.J. Lopez Cardozo, *Determination of Te and ne from atomic spectroscopy in low temperature (divertor) plasmas*. FOM Institute for Plasma Physics Rijnhuizen, Association Euratom-FOM, Trilateral Euregio Cluster, The Netherlands, www.rijnh.nl
11. D. Samsonov and J. Goree, *Line ratio Imaging of a Gas Discharge*, IEEE Transactions on Plasma Science, Vol. 27, NO. 1, February 1999.

2.3.5. Experimental Arrangement and the Test Parameters.

The test plate positioning in wind tunnel is shown schematically in Fig.2.3.5.1. Plain and profiled plates were tested under subsonic, transonic and supersonic flow condition. The following instrumentation was utilized for non-equilibrium plasma effect detecting: shadow visualization of boundary layer, Preston tube data downstream plasma area, pressure distribution measurements in test section, monitoring of transonic shocks position, monitoring of separation line.

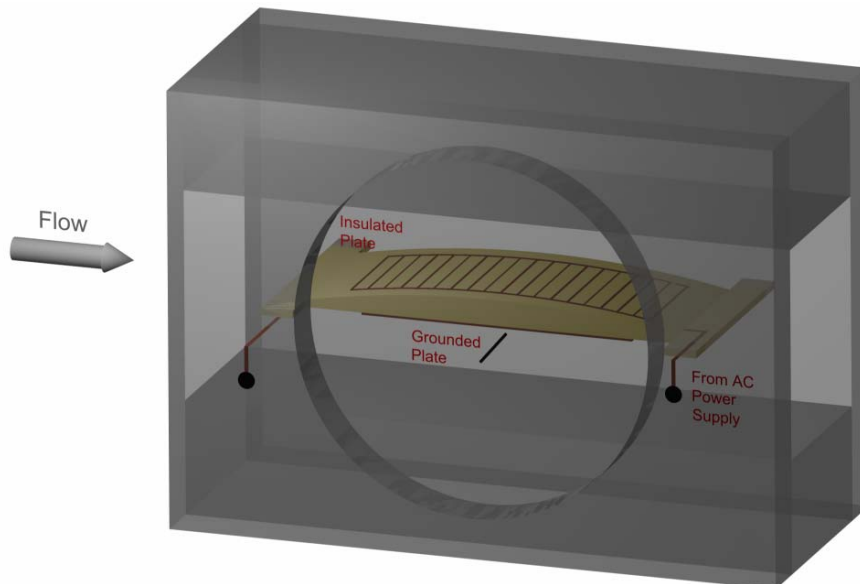


Fig.2.3.5.1. Test plate arrangement.

Specifically this test section is the most suitable for transonic flow mode investigations. But it can be utilized also for subsonic mode and supersonic mode with $M < 1.3$.

The design of the test models is shown in Fig.2.3.5.2. The first model was the plane plate from insulating material. It has thickness 1mm and dimensions 20mm*100mm. The second model was profiled with the same dimensions and maximal thickness about 5mm. The electrodes system was made from copper film at thickness about 0.05mm. The test parameters are presented in the table 2.3.5.1 below.

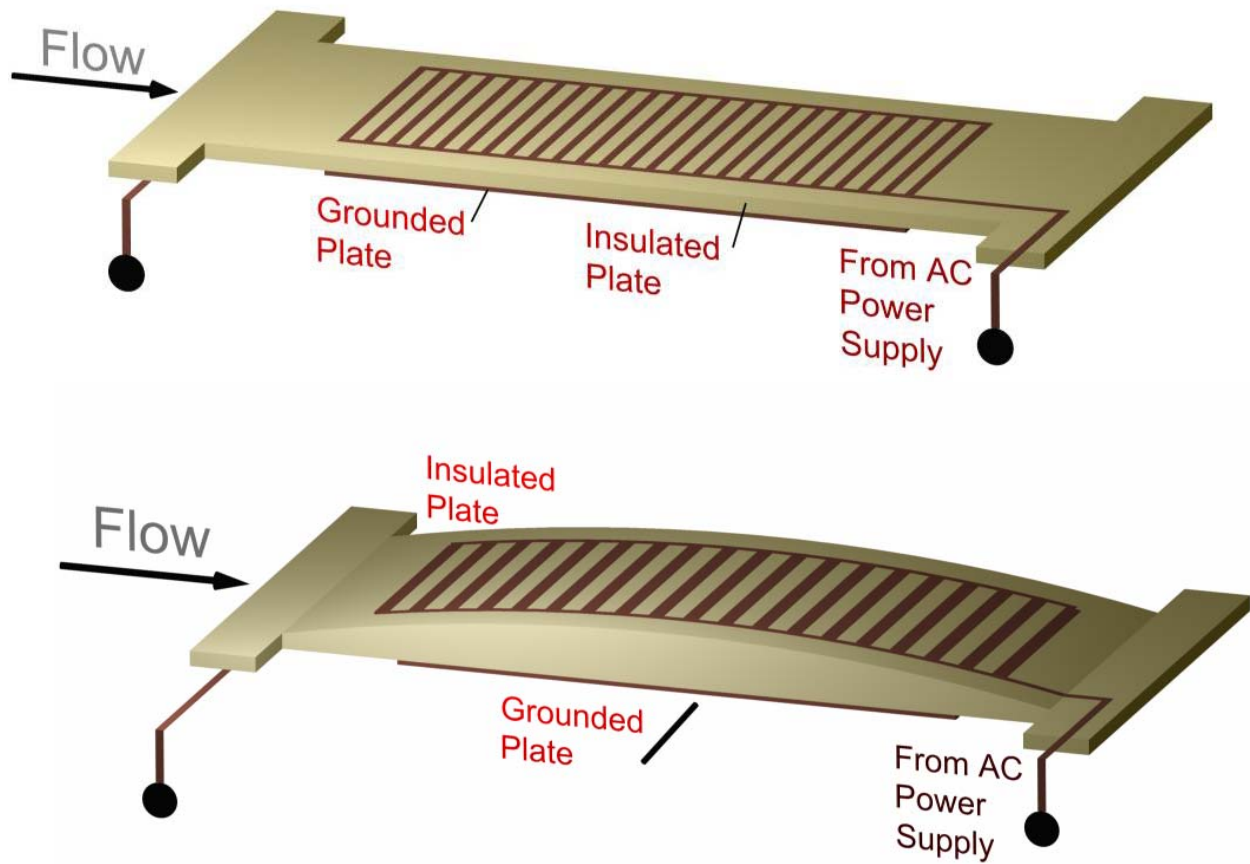


Fig.2.3.5.2. Aerodynamic models.

Different configurations of multi-trace plasma panel.

Table 2.3.5.1. Test parameters.

	Subsonic Mode	Transonic Mode	Supersonic Mode
Mach number	M=0.02-0.2	M=0.95-1.1	M=2 for plane plate M=1.2-1.3 for profiled plate
Reynolds number	$\approx 10^4$	$\approx 3 \cdot 10^5$	$\approx 5 \cdot 10^5$
Static pressure, Torr	100-750	100-500	100-250
Input power, W	50-100	50-100	50-100
Discharge duration, ms	10-1000	10-100	10-100
Applied voltage, kV	5kV AC +10kV DC	5kV AC +10kV DC	5kV AC +10kV DC
Discharge Mode	Symmetric and non-symmetric.	Symmetric and non-symmetric	Symmetric and non-symmetric

Three types of experiments were prepared. In the first case the sequences of the friction modification were explored. In the second case transonic effects were being found. In the third test an effect of separation control was studied.

During the first test it was intended to find a thin effect of DBD plane plate interaction with supersonic turbulent boundary layer. This test was performed under the conditions of short time wind tunnel PWT-10 of IVTAN. The scheme of the test is shown in Fig.2.3.5.3. Due to a negative result of this test the arrangement was modified. The aim was to recognize the plasma effect by observation of shock reflection from the BL. The scheme is shown in Fig.2.3.5.4.

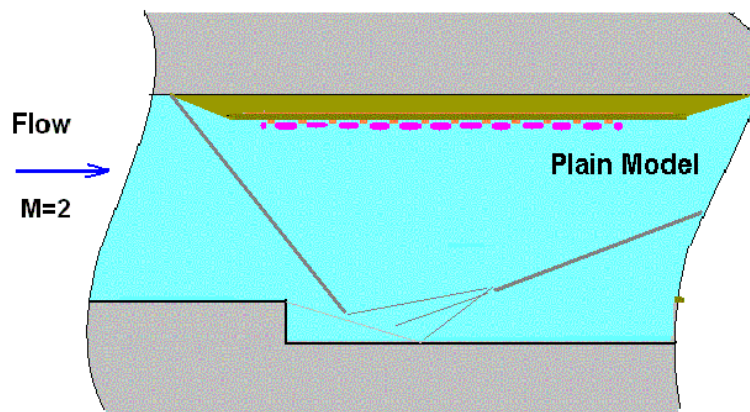


Fig.2.3.5.3. Scheme of the DBD test in supersonic flow.

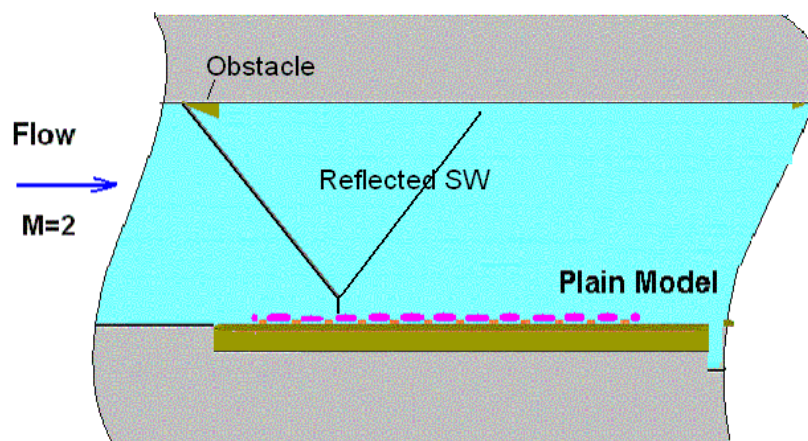


Fig.2.3.5.4. Modified scheme of the DBD test in supersonic flow.

To avoid an undesirable shocks reflection and the duct choking these configurations include the backwise wallstep. As a result in the first case the DBD plate locates in area of homogeneous supersonic flow. The following characteristics of the test were provided:

- Mach number of undisturbed flow $M=1.8-1.95$;

- static pressure $P_{st} \approx 100\text{-}250\text{Torr}$,
- Reynolds number about $Re = (0.2\text{-}0.5) \cdot 10^6$ (on the model length),
- duration of steady-stage operation up to 1sec,
- typical air mass flow-rate through the duct about $G \approx 0.1\text{kg/sec}$,
- typical input power $W = 10\text{-max W/cm}^2$.

The photo of plane DBD model installed is shown in Fig.2.3.5.6 in the test section of PWT-10.

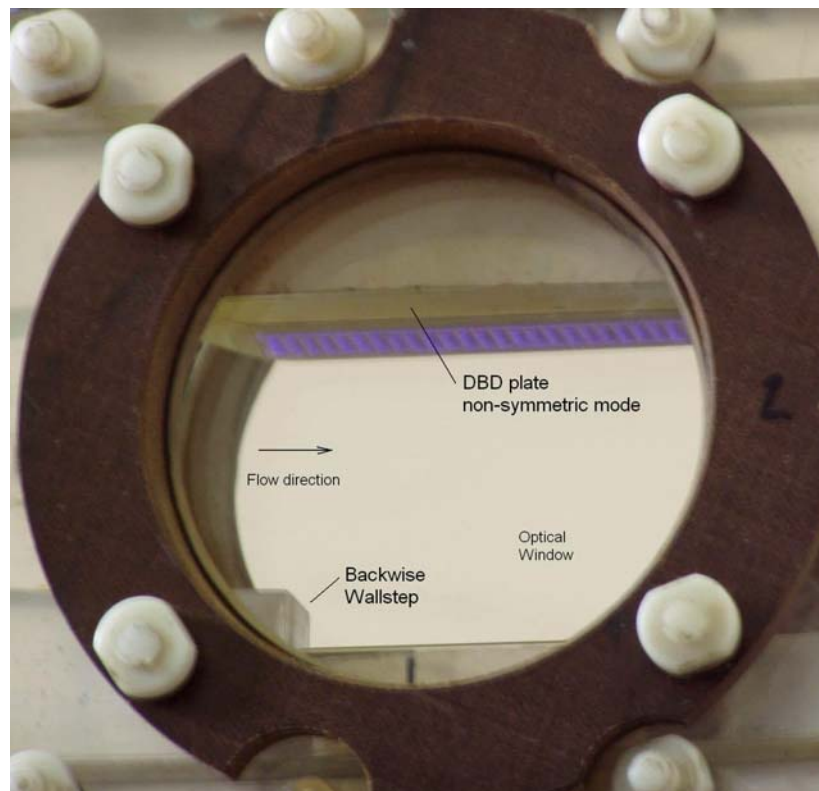


Fig.2.3.5.6. Photo of the test section for supersonic test.

The scheme of the second test is clear from the Fig.2.3.5.1. A shock configuration includes a plane transonic shock wave over the top side of the model. Such a situation (shock position) is sensitive to small modifications of the BL. The photo of profiled model's prototype is shown in Fig.2.3.5.7.

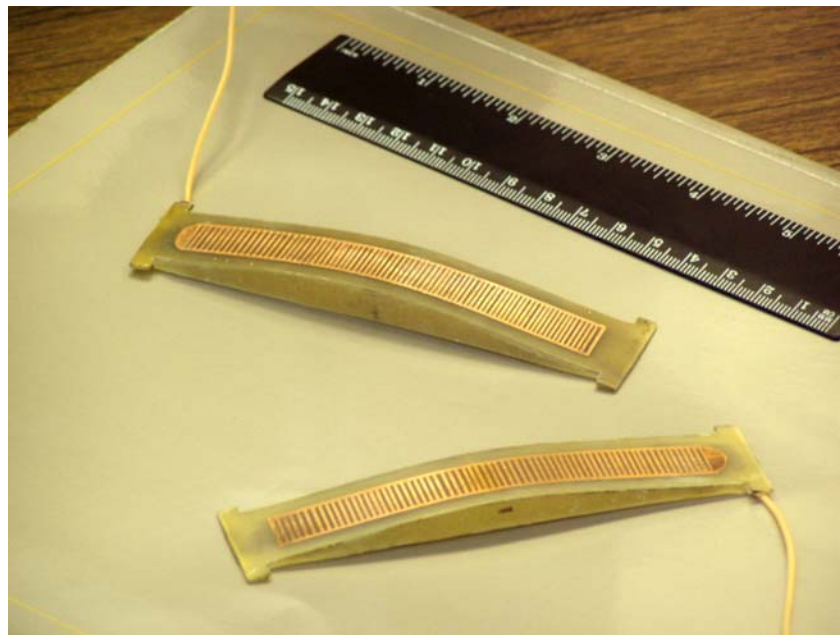


Fig.2.3.5.7. Photo of the profiled (5%) aerodynamic model with DBD plasma panel.

The third experiment was conducted in a short-duration blowdown wind tunnel PWT-50 of IVTAN with a closed-type of the test section. The scheme of the test is shown in Fig.2.3.5.8. The test was performed under subsonic flow and had to result in obtaining of data on separation control by DBD profiled panel.

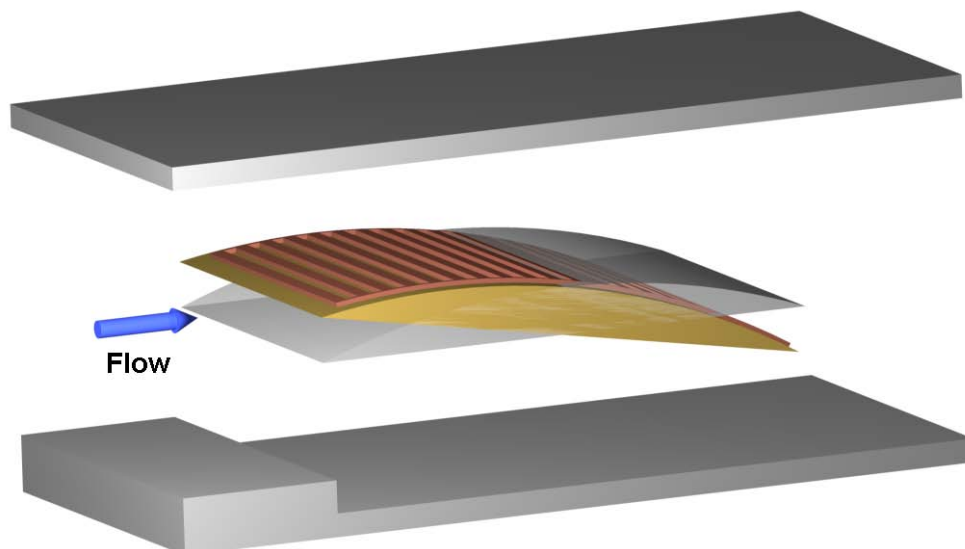


Fig.2.3.5.8. Test arrangement at inflow model installation (separation control experiment).

Incidence angle $\alpha=0\div12^\circ$.

Two orientations of DBD plate were investigated – the first one with the angle of attack $\alpha=0^\circ$ and the second one with $\alpha=12^\circ$.

The tests have been done at the following conditions:

- | | |
|--|--|
| ○ Velocity of undisturbed flow | $V=10 - 40\text{m/sec};$ |
| ○ static pressure | $P_{st}\approx 650\text{-}750\text{Torr},$ |
| ○ Reynolds number on the model length | $Re>10^6,$ |
| ○ duration of steady-stage operation | $0.5\text{-}1.0\text{sec},$ |
| ○ typical air mass flow-rate through the duct less/about | $G \approx 0.25\text{kg/sec},$ |
| ○ incidence angle of the model | $\alpha=0^\circ, 12^\circ,$ |
| ○ profiled model chord | $8\%,$ |
| ○ applied voltage of AC source | $3\text{-}6\text{kV},$ |
| ○ type of power supply (pulse shape) | sinusoidal and triangle, |
| ○ mean power deposition | $5\text{-}20\text{W/cm}^2,$ |
| ○ AC frequency | $f=45/100\text{kHz}.$ |

The photo of profiled model in the test section of PWT-50 is shown in Fig.2.3.5.9. The DBD is under operation there.

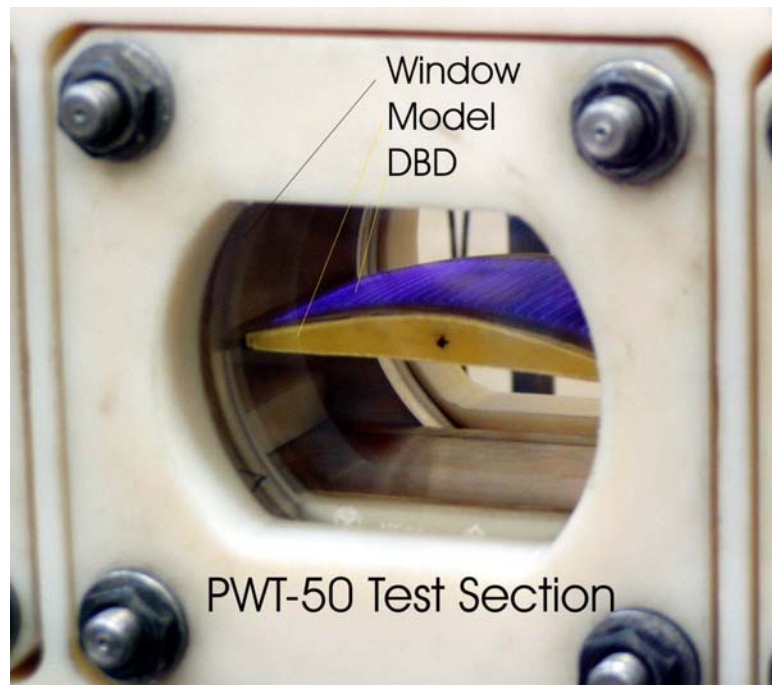


Fig.2.3.5.9. Photo of the model in test section under DBD operation.

Some results on supersonic flow adjustment in configuration with DBD plane plate and backwise wallstep are presented in this section. The analysis of flow structure was performed on the base of Schlieren images and pressure distribution records.

By the idea of flow adjustment the nose shock from the DBD plate has to drop not just on the opposite wall but on the separation zone downstream wallstep. The model position was chosen in accordance with this requirement. The typical Schlieren image with the flow structure reconstruction is shown in Fig.2.3.5.10.

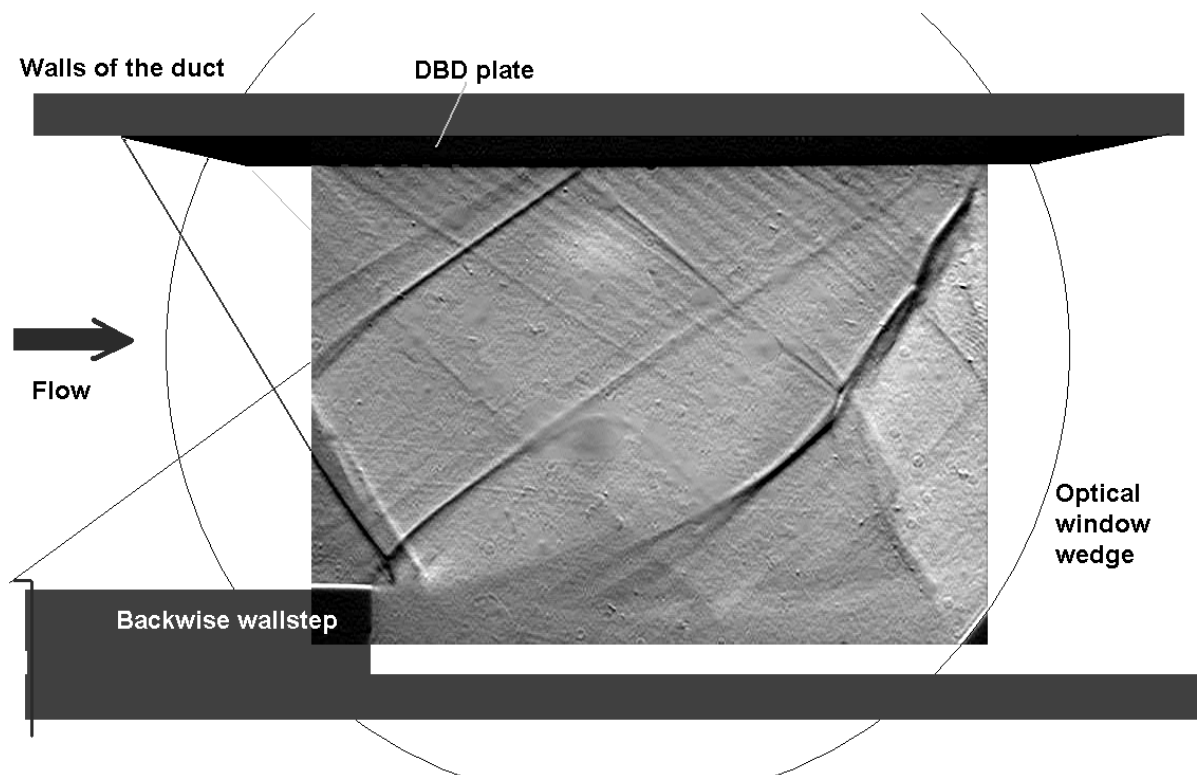


Fig.2.3.5.10. Typical flow structure by Schlieren photo before adjustment.

An appropriate pressure distribution record is shown in Fig.2.3.5.11. It should be noted that in this case the flow structure is not quite good for the test. It is seen that not whole plate is located in homogeneous supersonic area due to strong reflection of shock wave and not reattached separated zone. The stagnation pressure near the base wall is too low. This operation mode is characterized by large level of losses.

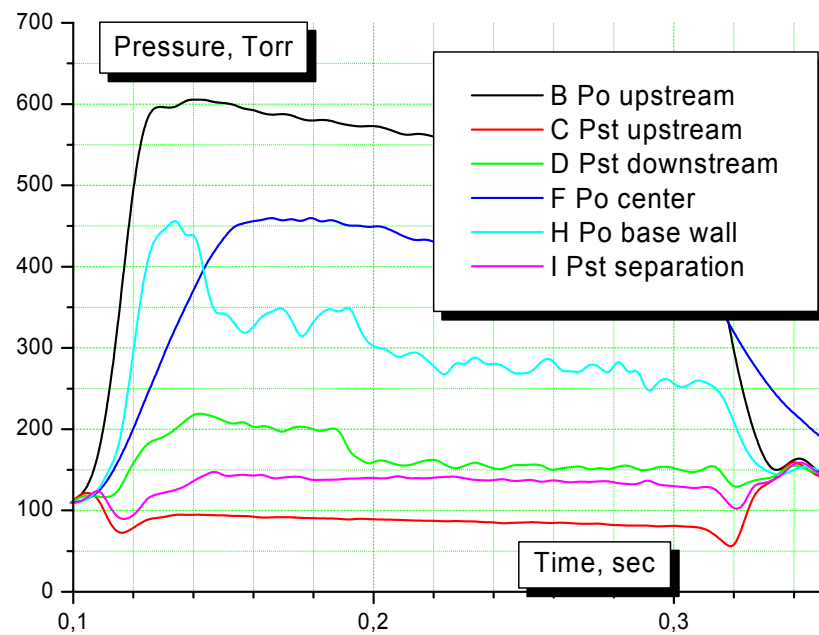


Fig.2.3.5.11. Pressure distribution before adjustment.

The procedure of adjustment includes a trowelling of transition between the model and the wall and a small shift of the model downstream. The results in flow structure and pressure distribution are presented in Fig.2.3.5.12 and Fig.2.3.5.13 correspondingly. Such a flow structure is much more convenient for the experiment's results analysis.



Fig.2.3.5.12. Flow structure by Schlieren photo after adjustment.

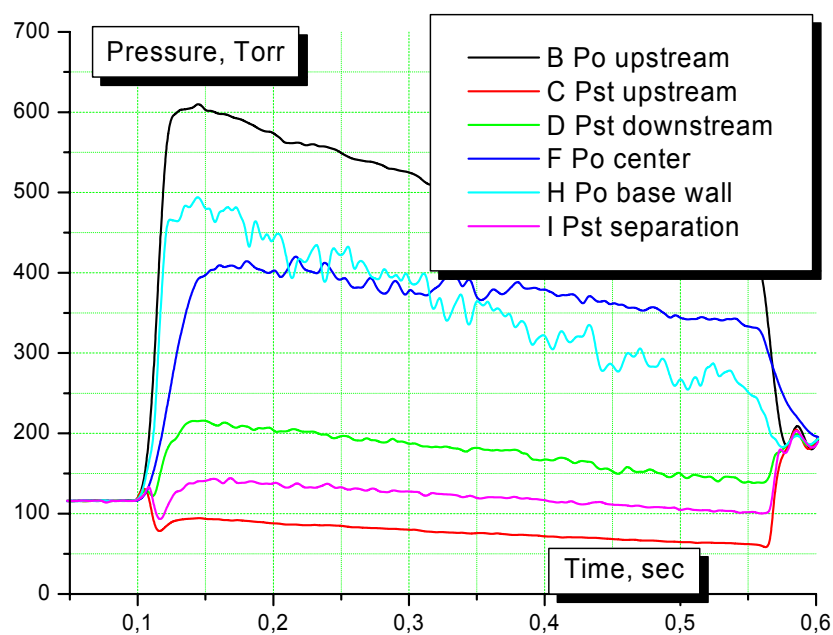


Fig.2.3.5.13. Pressure distribution after adjustment.

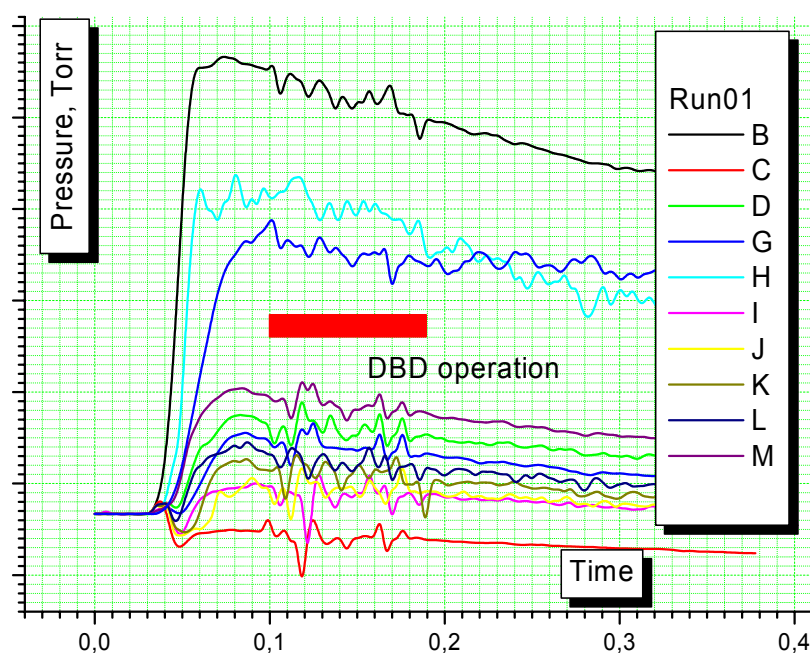


Fig.2.3.5.14. Pressure distribution under DBD operation.

The preliminary runs were done. A sample of pressure measurements at the DBD operation is shown in Fig.2.3.5.14. Some problems with EM noise are visible. They were solved partly by formalized procedure of the noise rejection.

2.3.6. Plasma-Induced Flow.

At the non-symmetric configuration of DBD electrodes a directed air movement along the DBD plate was registered. A plane plate with non-symmetric configuration was utilized in the test. The supplying power has following parameters: bipolar pulses of triangle shape with frequency 100kHz and amplitude up to 5kV. The upper electrode have width $\Delta x=1\text{mm}$ with inter-electrodes period 3mm and insulator thickness 0.5mm. Base electrodes were shifted on 1mm in respect of upper ones. A mean input power was about $W=10\text{W}/\text{cm}^2$. This section is devoted to description of experiments on measurements of the plasma-induced “wind” in dependence on conditions.

The velocity of the plasma-induced flow was measured by means of analysis of Schlieren images and Schlieren streak video scanning. The first method was used in previous efforts and gives a not satisfied accuracy due to too slow frame rate of video recorder. The sample of three first frames is shown in Fig.2.3.6.1. They were recorded for the described above DBD configuration in ambient air at atmospheric pressure.

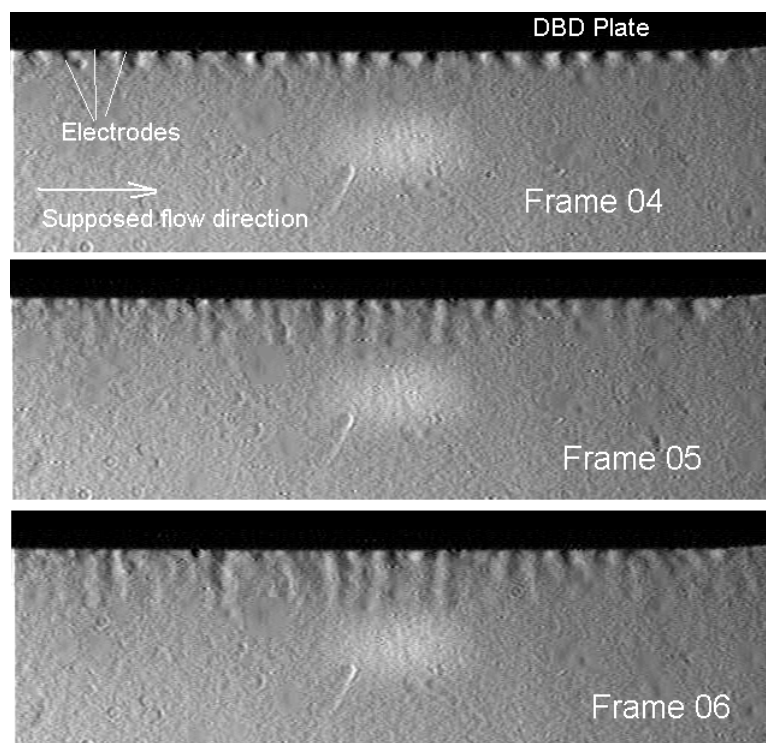


Fig.2.3.6.1. Sequence of frames. Schlieren photos. Exposure 0.5ms, frame rate 240fr/sec.

Thermal irregularities are seen well due to the DBD operation. A movement of them reflects the generation of plasma-induced movement of medium near the surface. To

recognize such a flow exactly the line-scan camera “AVIVA” was utilized. It possesses a frequency of scanning up to $f=50\text{kHz}$. The projection of image is adjusted in desired position as it shown in Fig.2.3.6.2. As a result the Schlieren image can be recorded from any cross-section with a large speed of scanning. A horizontal axis is corresponded to X space line and the vertical axis is corresponded to T - time axis.

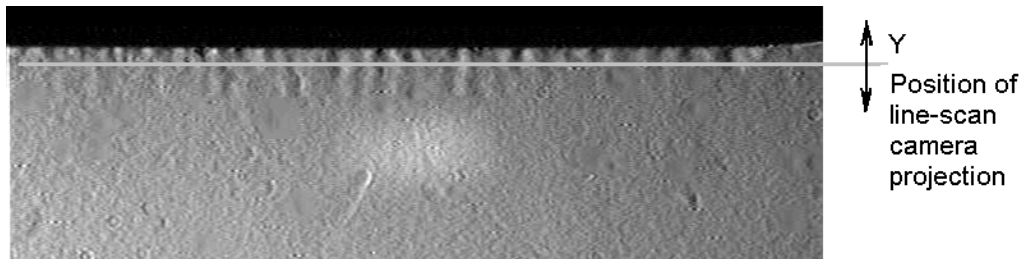


Fig.2.3.6.2.

Samples of record by this method are shown in Fig.2.3.6.3. The frames appropriate to records of hot air jet in transversal and longitudinal directions of projection accordingly. In the second case an oblique lines are seen well. They are a consequence of gas density irregularities movement in mixing layer. The angle of these lines reflects the velocity of appropriate flow $angle=A \cdot dx/dt$, where A is a factor of lens's amplification and scan speed.

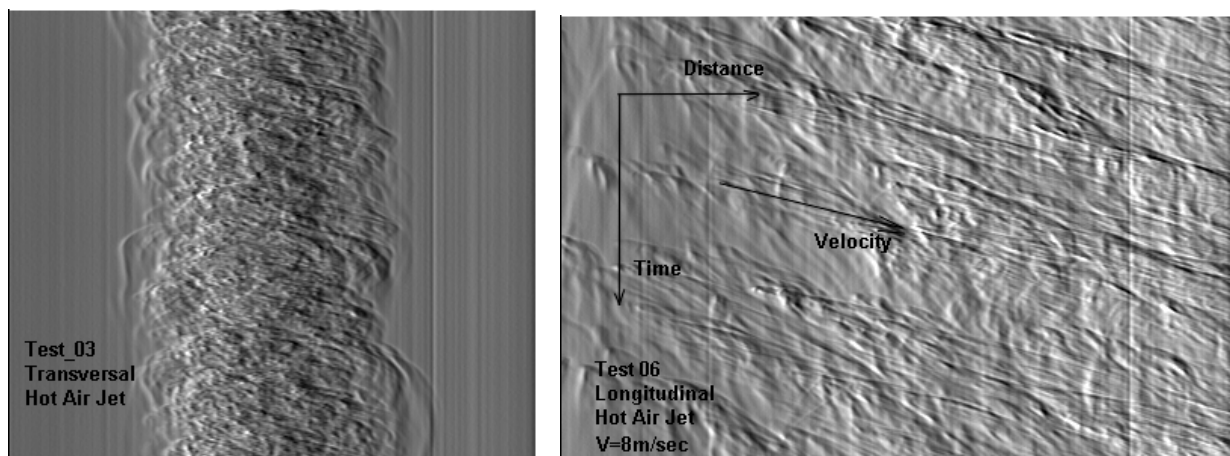


Fig.2.3.6.3. Schlieren streak scanning methodic test with hot air jet.

Some results of DBD scanning by methodic mentioned above are presented in Figs.2.3.6.4 and 5. The Fig.2.3.6.4 shows the streak record at atmospheric pressure. Two photos are differed by the distance Y from the DBD plate (see Fig.2.3.6.2). In the first case the distance was $Y=1\text{mm}$, in the second case it was $Y=3\text{mm}$ that is compatible with inter-electrodes space period. The contrast of the images hardly differs each from other that is explainable under observation of full Schlieren photos (see Fig.2.3.6.1). At the same time the measured flow velocity was practically constant in a range $0.5\text{-}5\text{mm}$ from the surface. The

time of induced flow acceleration (achievement of constant speed) was a few milliseconds. The value of this speed is practically independent on the position along the DBD plate.

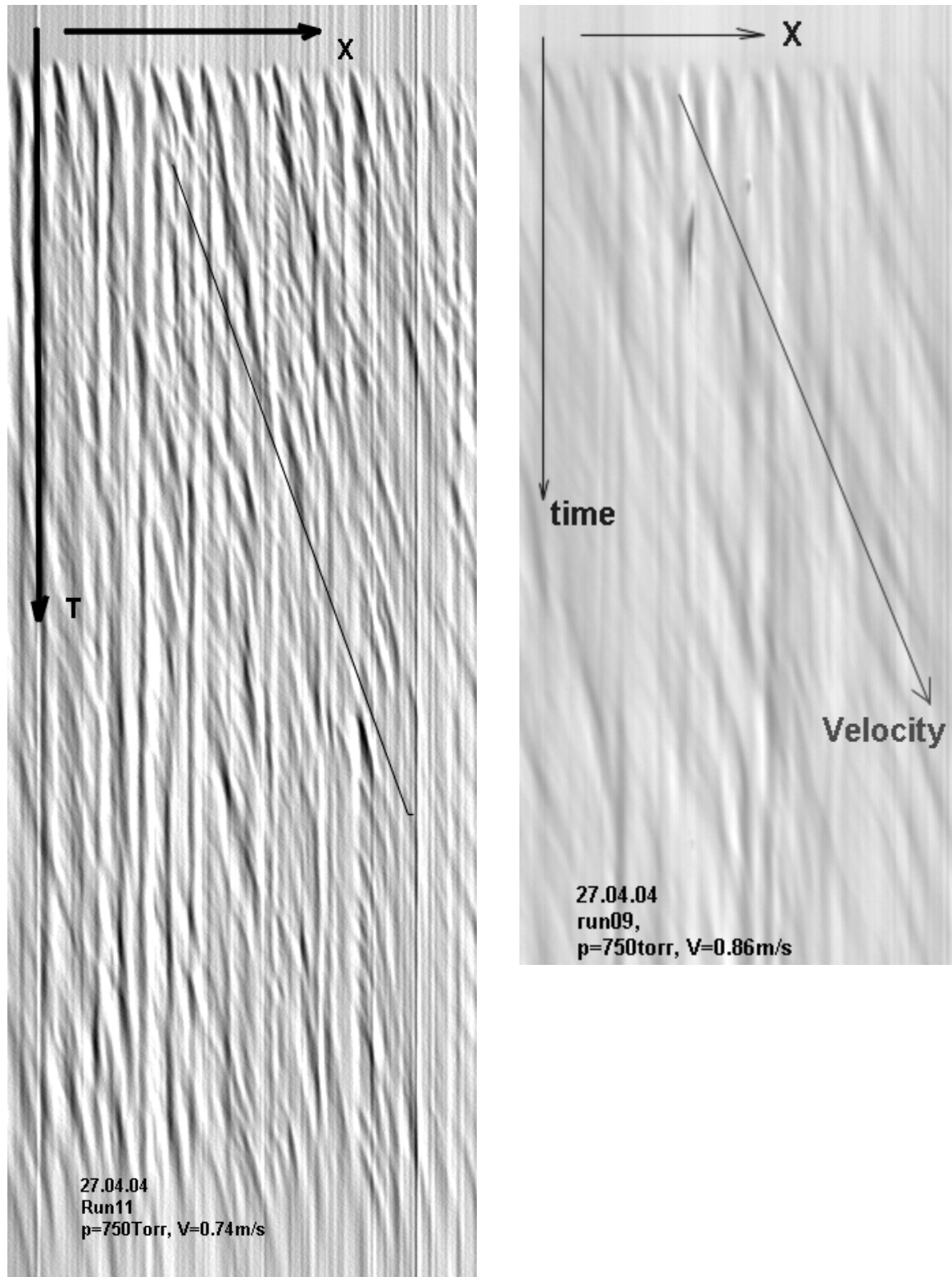


Fig.2.3.6.3. Schlieren streak images at $P=1\text{atm}$.

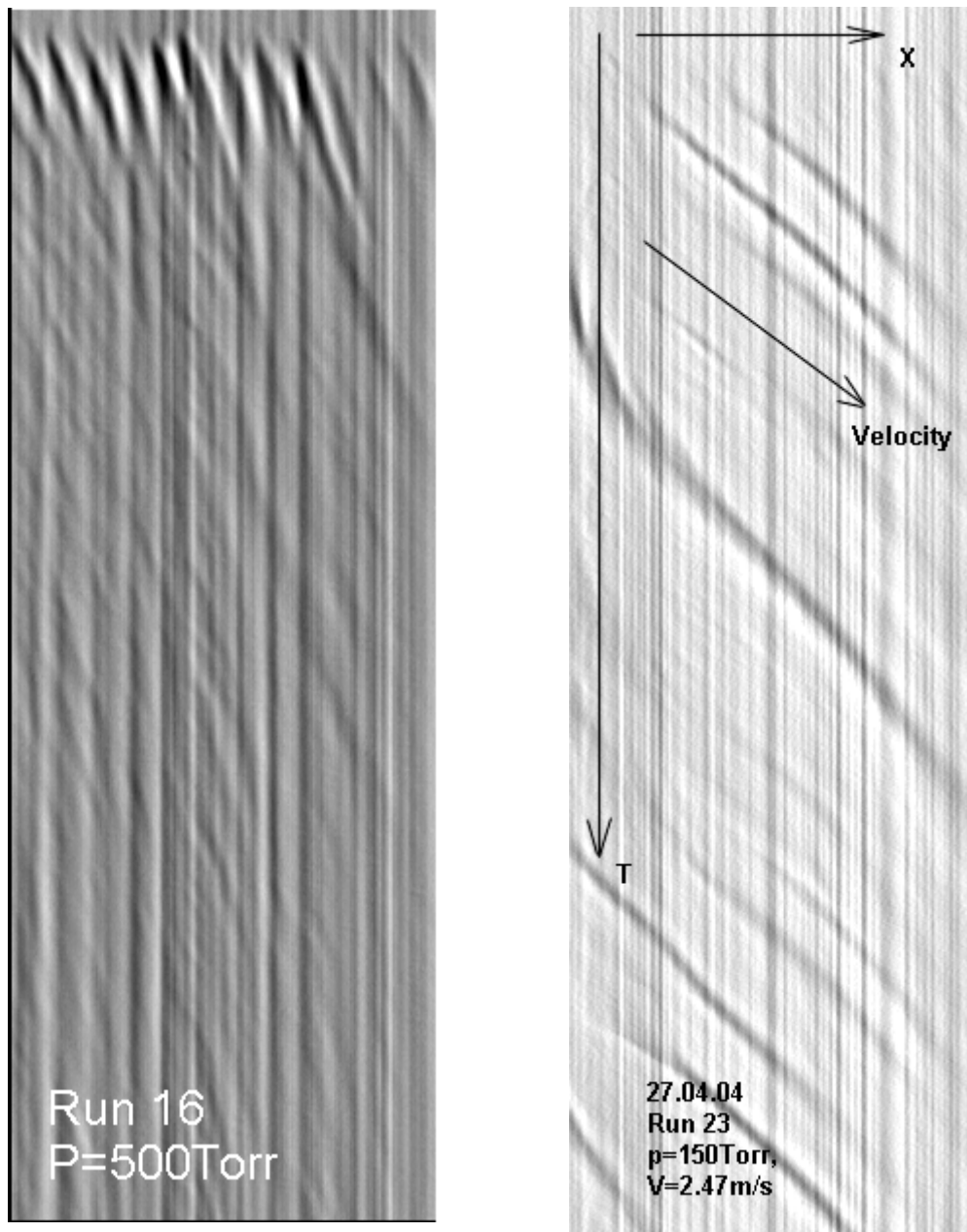


Fig.2.3.6.4. Schlieren streak images at different pressure.

Samples of Schlieren streak images are presented in Fig.2.3.6.4 at different pressure. All other parameters were conserved. The velocity measurements show that it is increased under reduced pressure. The result of such a measurement is presented in Fig.2.3.6.5. This curve reflects the fact that the electric field strength E is reduced with the pressure more slowly than the density of gas.

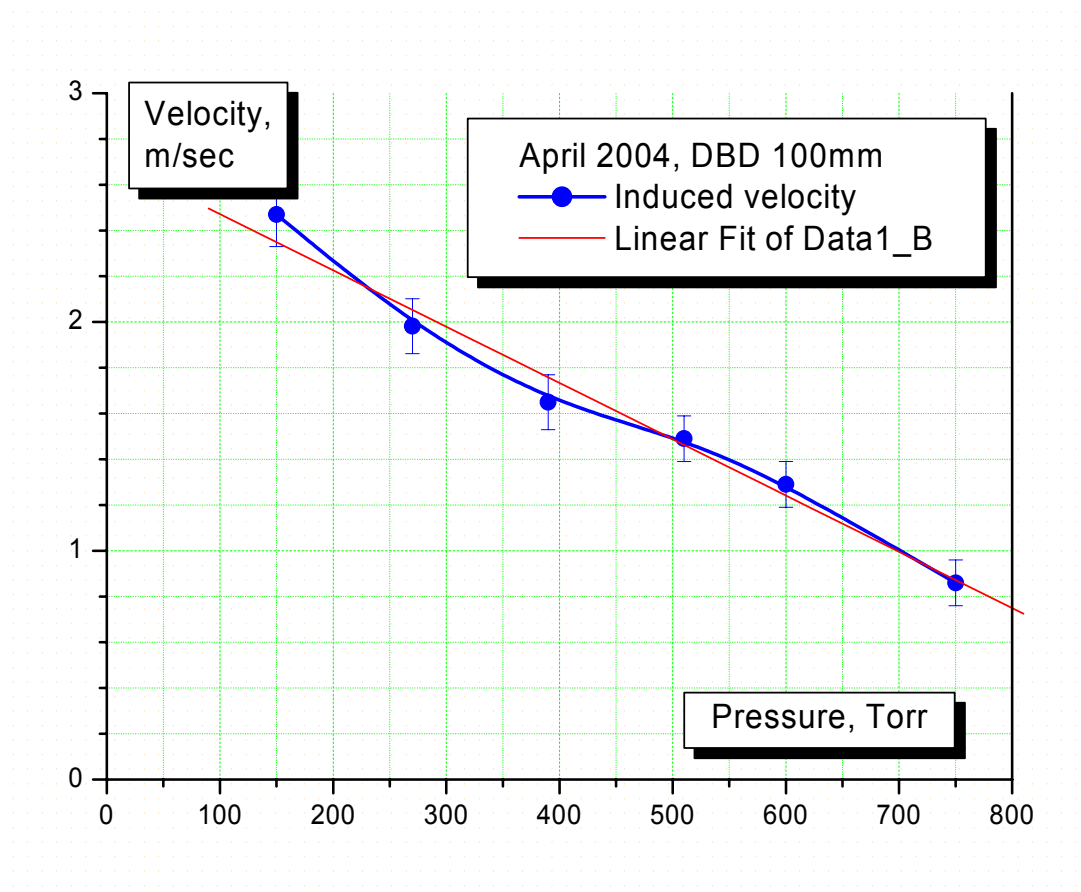


Fig.2.3.6.5. DBD-induced flow velocity in dependence on air pressure.

The DBD discharge properties in airflow are the same as in ambient air. It is quite understandable due to very short time of individual streamers generation $t < 0.1 \text{ mcs} \ll t_{\text{gd}}$ that is much less than characteristic gasdynamic time.

2.3.7. Subsonic Effects.

Well known that the corona and barrier types of electrical discharges effects of flow parameters under low flow velocity (see Reference below). It appears also in the effect of separation prevention at high angles of attack. Under the flow velocity $V=3-5\text{m/s}$ the authors have observed a plasma influence on external flow at non-symmetric mode of the discharge operation.

Separation Zone Visualization.

In order to visualize separation zone several methods have been tested. The shadow method of flow structure visualization is based on gas density gradients recognition. In our case of subsonic speed, when the flow velocity is relatively low, the artificial methods of gas density variation are needed. A different gases addition and the surface heating were tested.

Visualization of the flow structure by means of CO_2 and He jets was not successful and has not allowed us to see separation zone because of the fast turbulization of the jet in external airflow.

Another method was to heat DBD plate by the preliminary switched on discharge. Plate was heated under the discharge operation on about $\Delta T=20-40\text{K}$ and resolution of Schlieren shadow system is enough to visualize resulting air disturbances. The heating time was 10sec before the PWT-50 turning on. Sequence of Schlieren photos of DBD discharge under ambient conditions was shown in Fig.2.3.6.1. Well seen how the thermal disturbances move from right side to the left one.

As was mentioned above two types of light sources have been used: continuous source and pulsed flash lamp with pulse duration about 1mcs. The best visualization has been achieved under pulsed light source because resulting exposure time is equal to the duration of flash (i.e. 1mcs) while at continuous light source time exposure is limited by the camera shutter and in the most cases was about 4ms. As the result the structure of the disturbances becomes blurred at the larger exposure. The comparison of the Schlieren images in these two cases is shown in Fig.2.3.7.2 “a” and “b” correspondingly.

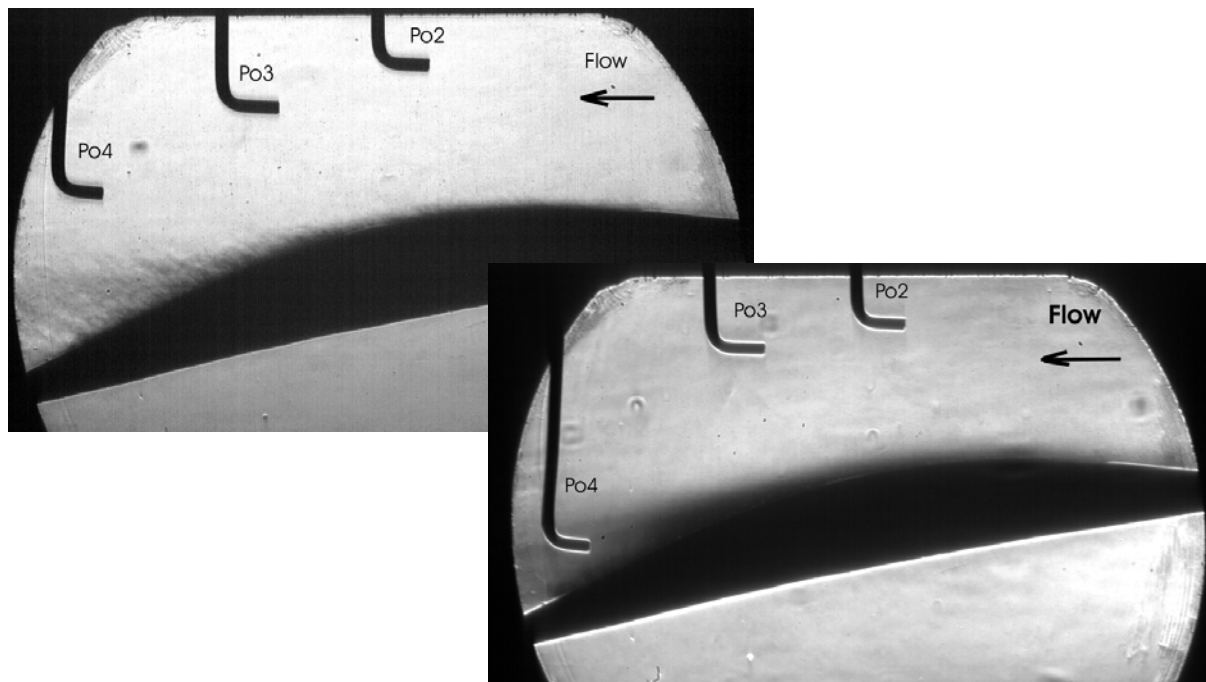


Fig.2.3.7.2. Typical Schlieren images at different exposure: “a”-1mcs, “b”-4ms.

A key component of the separation zone visualization was an image processing by means of program package Corel Photo-Paint ver.11.0. Two examples of such a processing of the Fig.2.3.7.2a are presented in Fig.2.3.7.3. As it could be seen the separation zone is visualized very clear.

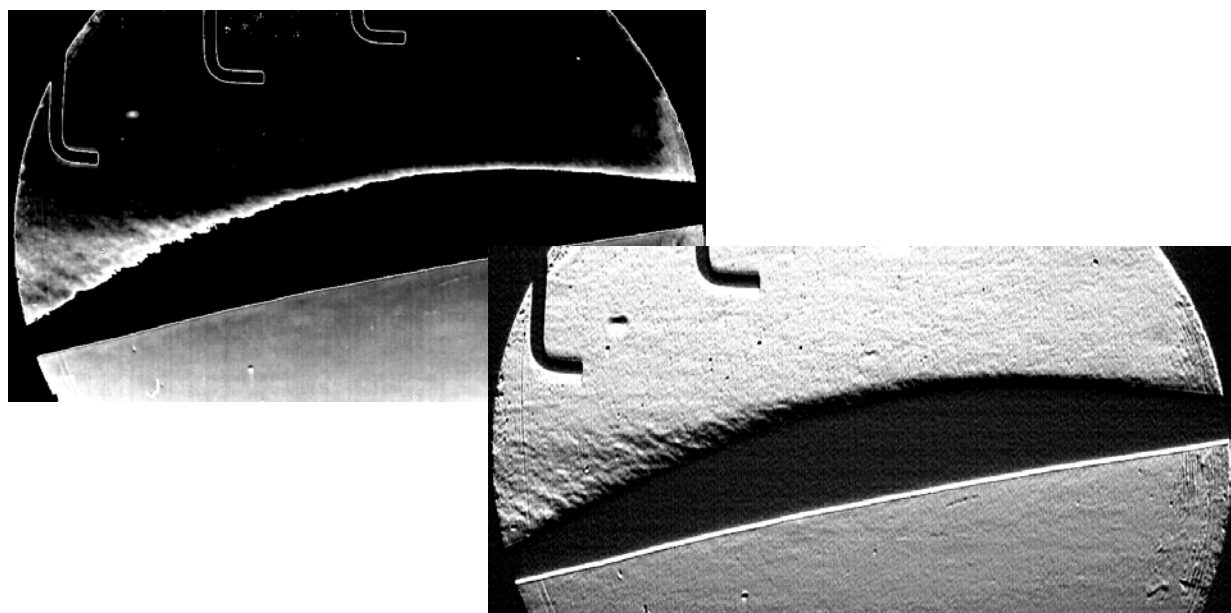


Fig.2.3.7.3. Samples of visualization technique. Image processing.

Discharge Effect on Separation Zone Position and Shape.

Typically the discharge was switched on in 100 ms after the valve actuation. Duration of discharge was 100 ms or 50 ms for some tests. Tests were performed under different velocity of the flow in a range 10-40m/s.

Experiments at angle of attack $\alpha=0^\circ$.

Sequence of separation zone visualization photos is shown in Fig.2.3.7.4.

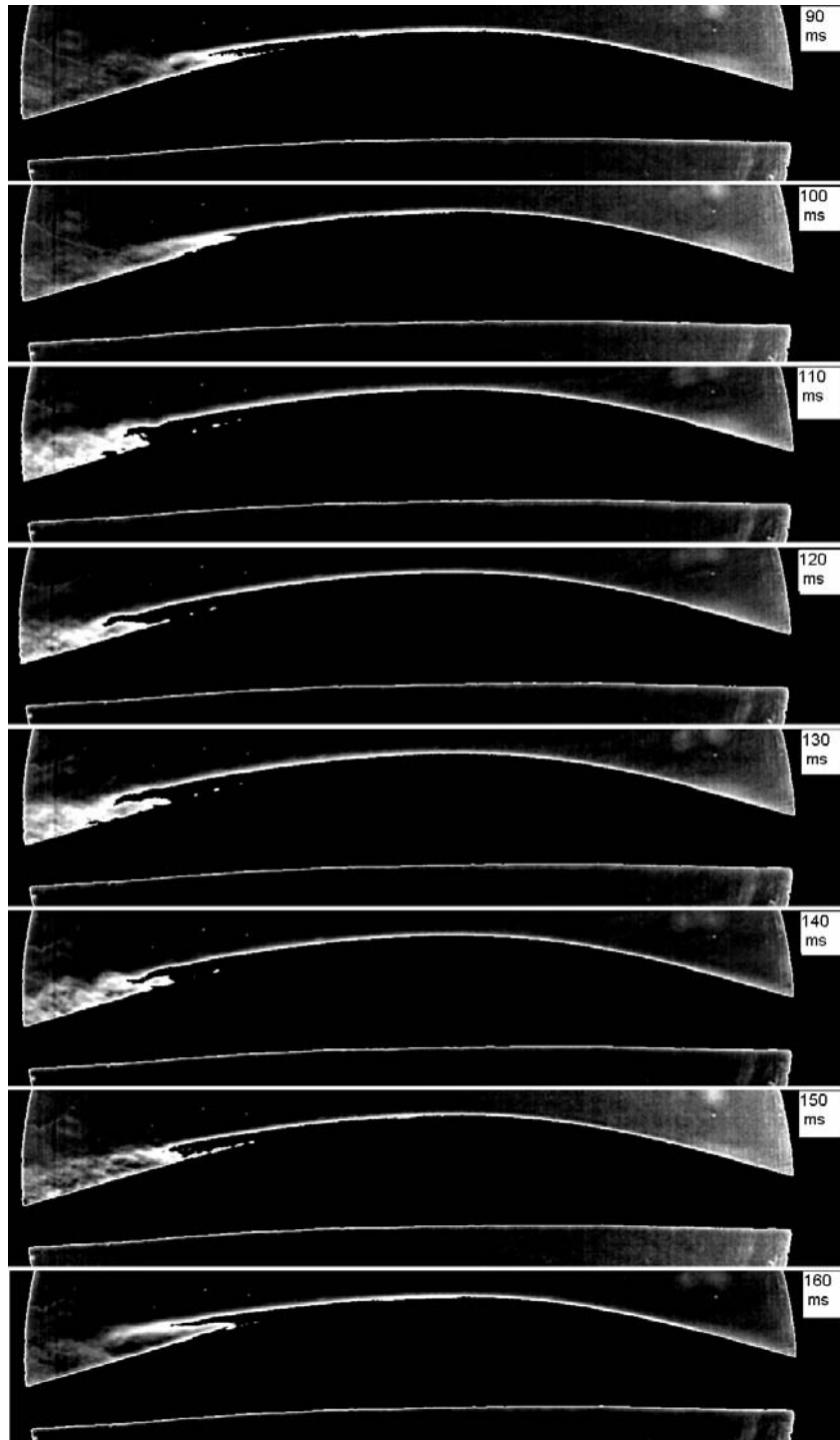


Fig.2.3.7.4.
Schlieren photos
under the DBD
operation. Flow
from right to left.

Discharge was turned on at 100ms after the start of the flow and it was turned off at 150ms. So, the first frame with the DBD is related to 110ms point. It is well seen that separation line changes its position after the discharge turning on.

In the case of attack angle $\alpha=0^\circ$ there was an obvious the effect dependence on flow velocity (the pressure in vacuum tank), namely, the lower the pressure the wider the separation zone. Processing photos of flow structure with and without discharge at different pressures are presented in Figs.2.3.7.5a,b and 2.3.7.6a,b.

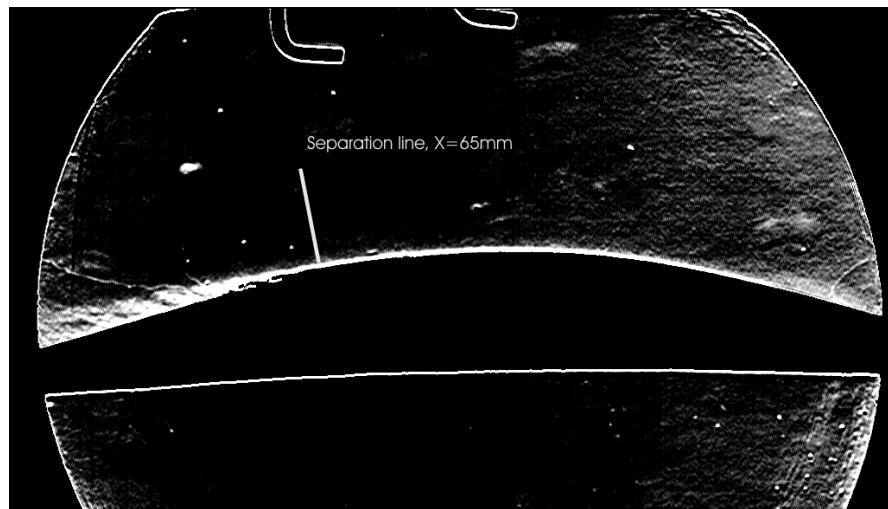


Fig.2.3.7.5a. Flow without discharge. $V=13\text{m/s}$.

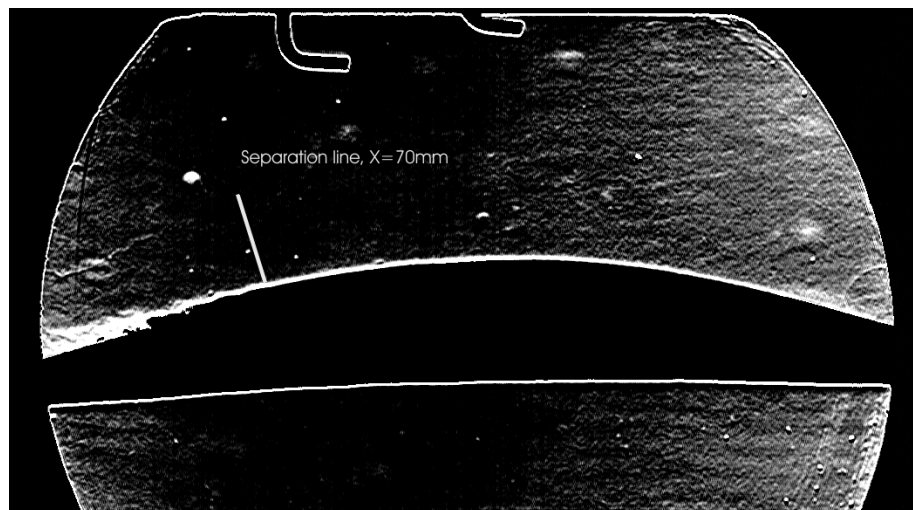


Fig.2.3.7.5b. Flow with discharge. $V=13\text{m/s}$.

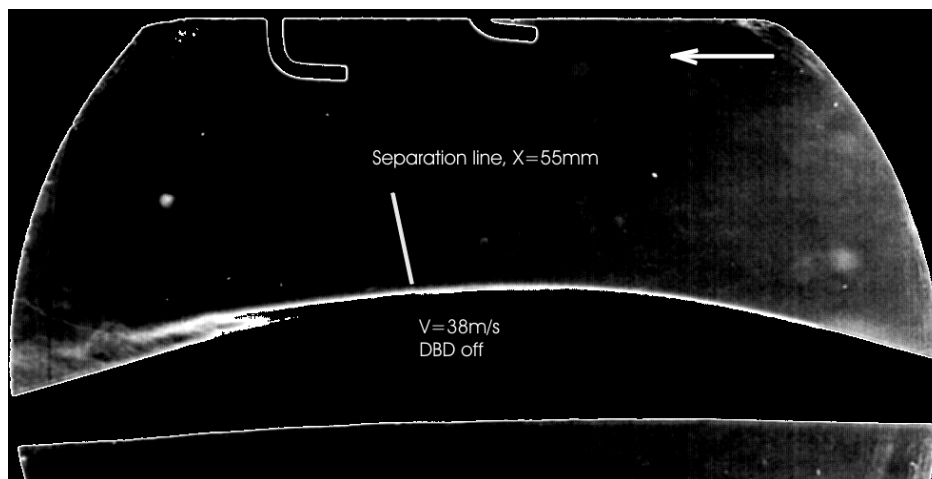


Fig.2.3.7.6a. Flow without discharge. V=38m/s.

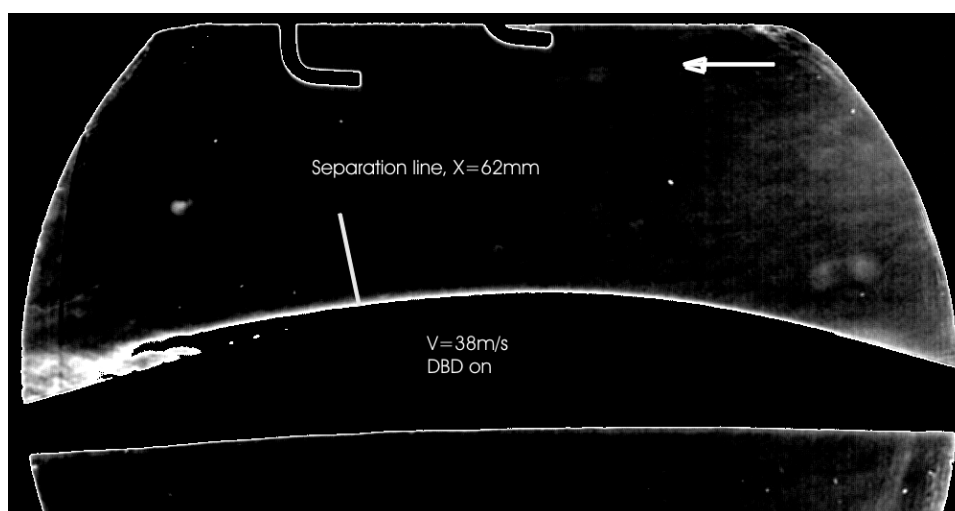


Fig.2.3.7.6b. Flow with discharge. V=38m/s.

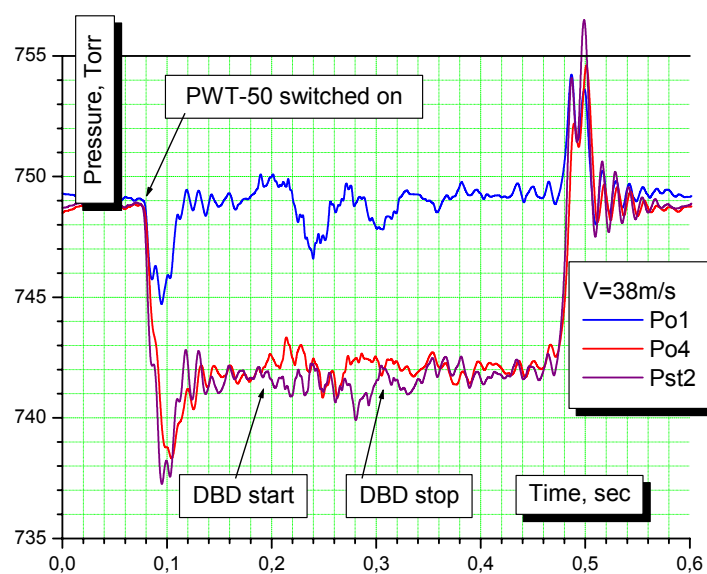


Fig.2.3.7.7. Sample of the pressure record at DBD operation.

The measurements of DBD effect on pressure in separation zone were done at different conditions. A sample of pressure record is shown in Fig.2.3.7.7. Here the data on three points are presented: total pressure upstream, Pitot pipe in separation zone and static pressure downstream. The EM noise was rejected by formalized procedure. It is easy to recognize that the DBD effect is not valuable but noticeable. It is appeared in some increase of the pressure in separation zone under the DBD operation.

The procedure of data averaging was applied for estimation of the value of pressure increase ΔP . It was found out that ΔP is almost independent on the initial flow velocity and the model orientation and was from $\Delta P = +0.12 \pm 0.8 \text{ Torr}$ up to $\Delta P = +0.6 \pm 0.5 \text{ Torr}$ for different realizations (runs). The accuracy of those measurements was limited by gasdynamic and electromagnetic noise.

Experiments at angle of attack $\alpha = 12^\circ$.

As well as in the case $\alpha = 0^\circ$ a slight dependence of separation zone width on the pressure in vacuum tank has been observed for DBD plate orientation $\alpha = 12^\circ$. In a contrary with that there were no valuable changes of separation zone width and position after the discharge switching on. At least we can't recognize it definitely. As a sample two processed Schlieren images of the flow structure without discharge and with it are presented in Fig.2.3.7.8 and 9. It should be noted that there were no experiments at flow velocity $V < 13 \text{ m/s}$.

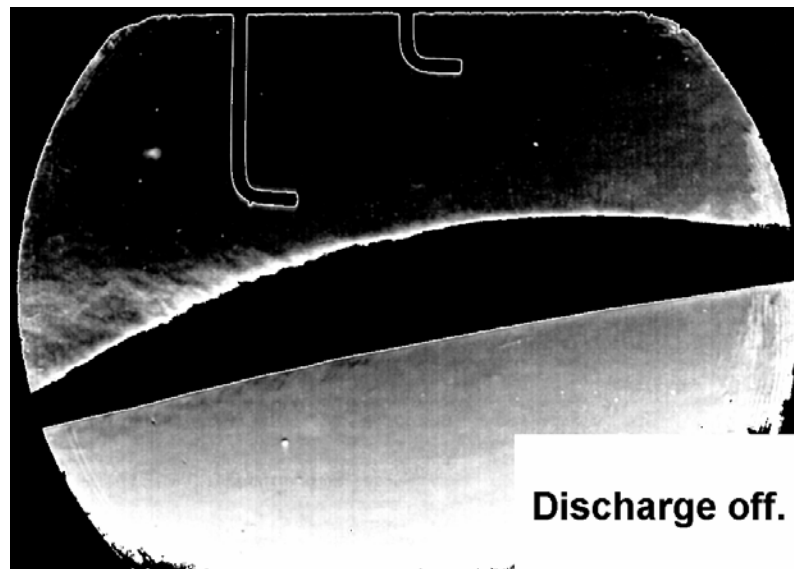


Fig.2.3.7.8. Flow structure without discharge.

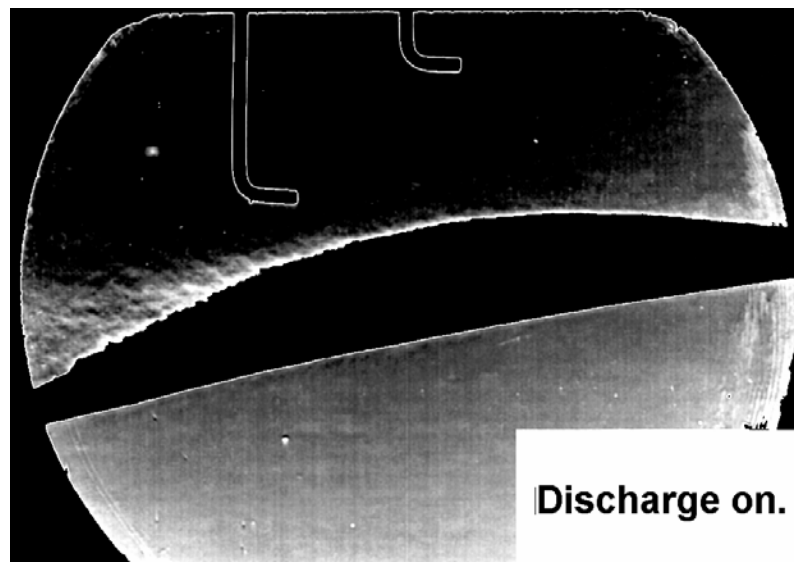


Fig.2.3.7.9. Flow structure under discharge operation.

Magnitude of Flow Disturbances at DBD Generation.

The scheme of flow disturbances measurements is shown in Fig.2.3.7.10. It contains a source of thin light beam (He-Ne or diode laser), diaphragm and photodiode sensor. The beam passes through the separation zone above the model parallel to the surface and perpendicular to the windows and flow direction. The disturbances refract the beam that leads to modulation of light intensity on the sensor.

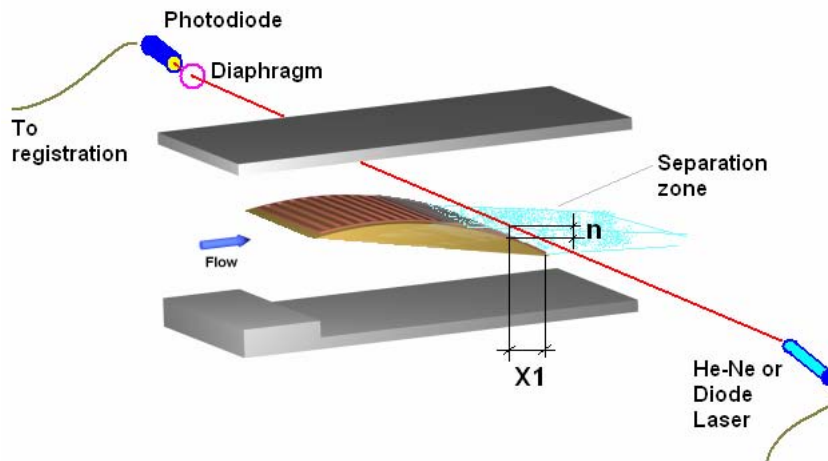


Fig.2.3.7.10. Scheme of the flow disturbances measurements.

The distance along the model surface from the end is $X1=x-100mm$ (pointed as “x” in the graphs), normally to the surface is n . The tests, which are presented in this section, were done at zero angle of attack of the model.

Such a sensor is sensitive to the flow disturbances as well as to the mean gradient of the gas density due to inhomogeneous heating. The reply of the system on the DBD generation without external airflow is shown in Fig.2.3.7.11 for the different n .

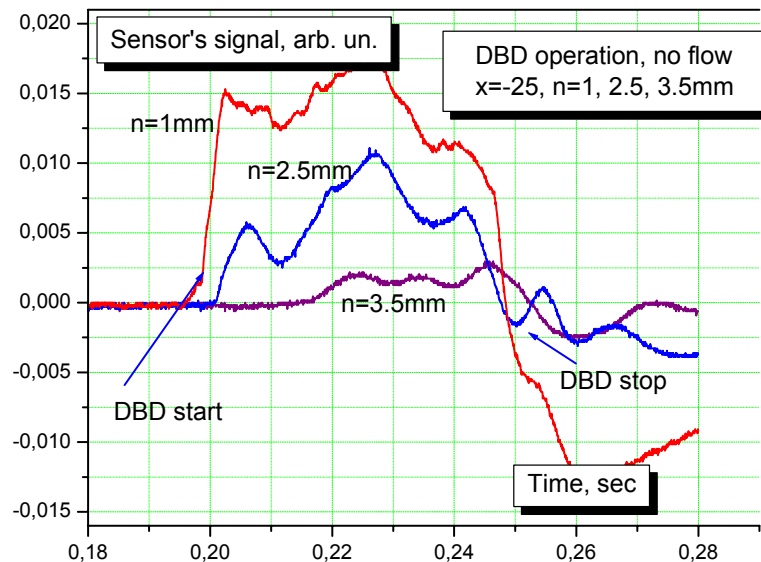


Fig.2.3.7.11. Schlieren sensor data at DBD operation. No flow.

The signal has a low frequency component only. Well seen that a thickness of heated layer is about 3-4mm and an expansion time is about 20ms. The results of measurement of flow disturbances at constant flow velocity and the different position of the sensor are shown in Fig.2.3.7.12. Sensor's beam was located in 10mm upstream a base edge of the model. A low frequency component (about 50Hz) occurs due to mechanical vibrations of facility. In this case one can see two types of response: shift of the signal level at the discharge operation when $n < 2$, and high frequency instability. If $n > 4mm$ the signal goes to an initial level, i.e. the beam is located outside the separation area.

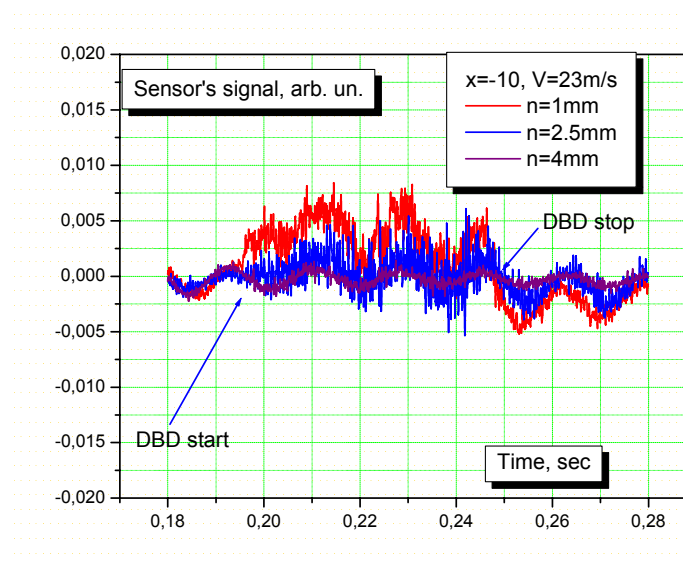


Fig.2.3.7.12. Schlieren sensor data at DBD operation and different beam position.

$X_1 = -10mm$.

The results of measurement at the same flow velocity, another beam location along the model (upstream, $X_1 = -25mm$) and the different position of the sensor on altitude n are shown in Fig.2.3.7.13. The thickness of separation zone at this position is about $n = 2.5mm$. In that beam position one can recognize an unmixed heated layer in 1-1.5mm above the surface. It was clear if the polarity of the signal was taking into account. In previous case ($X_1 = -10mm$) it was not so obvious. Well seen also the vortices generation (instability of separation line position) with the frequency about 200-300Hz.

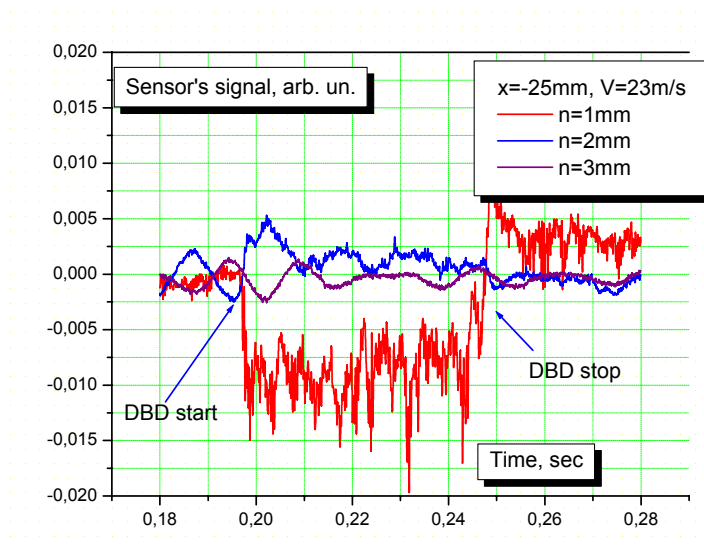


Fig.2.3.7.13. Schlieren sensor data at DBD operation and different beam location.

$X_1 = -25\text{mm}$.

The results of measurement of flow disturbances at different flow velocity and the fixed position of the sensor are shown in Figs.2.3.7.14a-c. Well seen that the results are differed each from other on the amplitude and the frequency of oscillation. At higher flow velocity the amplitude of gas density disturbances drops and the frequency grows simultaneously. The Furrier analysis of the disturbances effect on the Schlieren sensor was done at the different flow speed. The results are shown in Figs.2.3.7.15a-c. The figures position corresponds to the Fig.2.3.7.14.

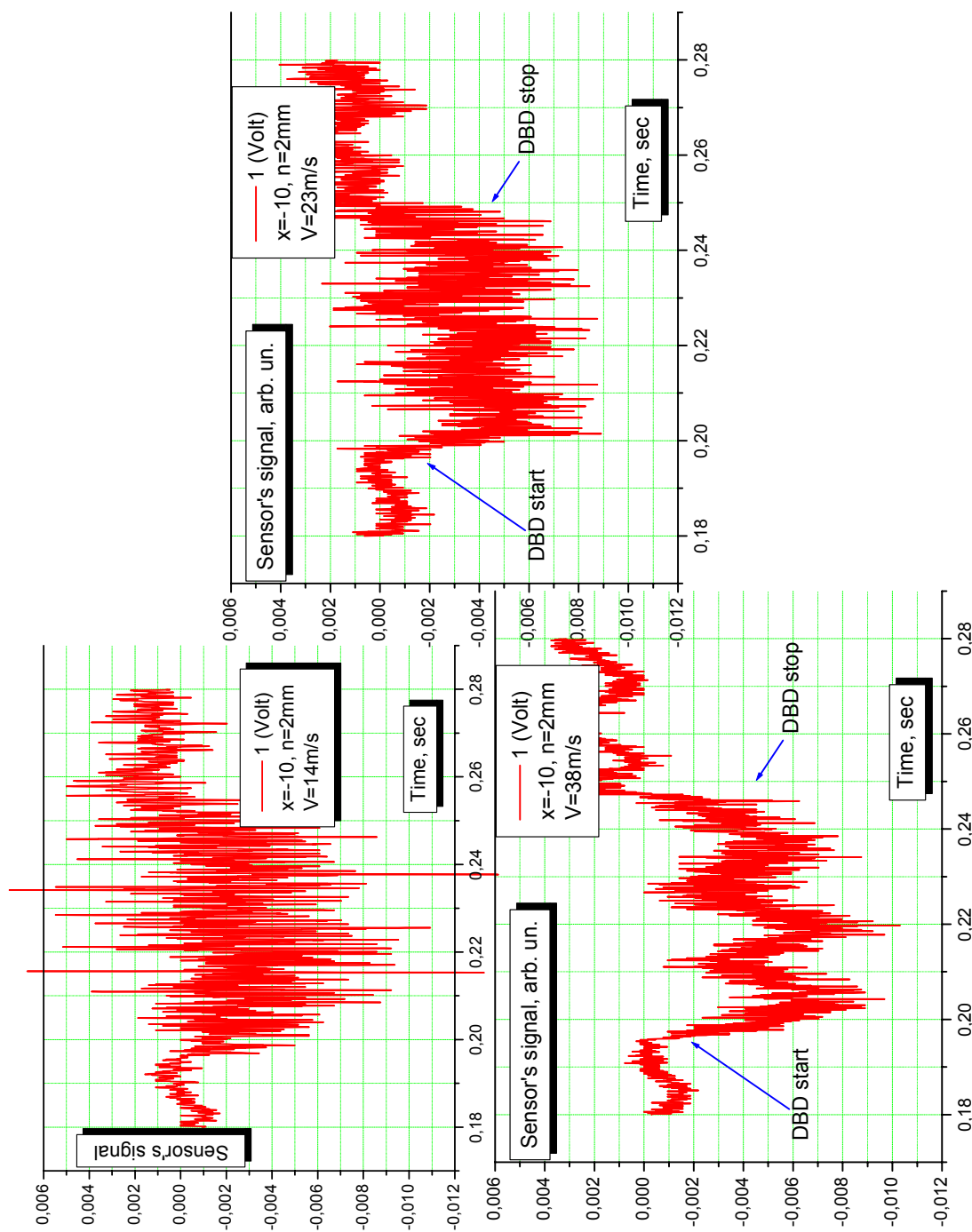


Fig.2.3.7.14. Schlieren sensor data at DBD operation and different flow speed.

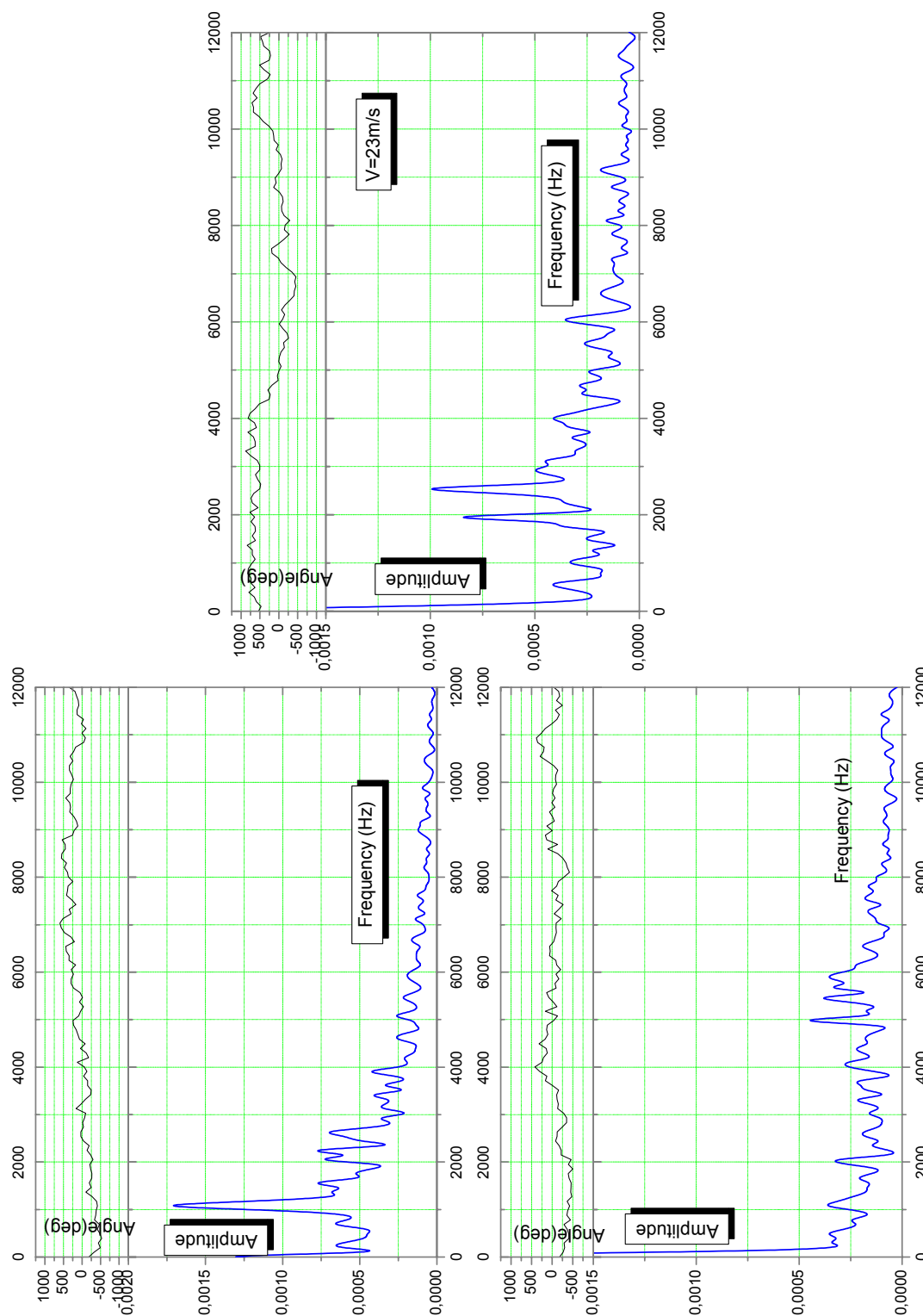


Fig.2.3.7.3.6. Result of Furrier analysis of flow disturbances in separation zone at different flow velocity.

The statement above is justified by the result of Furrier analysis: the main frequency of oscillation lies in a range $f=1-5kHz$ when the velocity of the flow is $V=13-38m/s$. A characteristic gasdynamic distance can be estimated from $l=13mm$ ($V=13m/s$) down to $l=8mm$ ($V=38m/s$). The most probable correlation of this distance is thickness of the separation zone width.

Reference to section 2.3.7.

1. J. R. Roth, H. Sin, R. Chandra, M. Madhan, S. P. Wilkinson "Flow re-attachment and acceleration by paraelectric and peristaltic EHD effects", 41th AIAA Aerospace Meeting and Exhibit, 6-10 January, Reno, NV, 2003.
2. Roth J. R., Sherman D. M. and Wilkinson S. P. "Electrohydrodynamic Flow Control with a Glow Discharge Surface Plasma" *AIAA Journal*, Vol. 38, No. 7, July 2000, pp 1166- 1172.
3. S. Khabiry, G. Colver, "Drag reduction by DC corona discharge along an electrically conductive flat plate for small Reynolds number flow", *Phys. Fluids*, 9 (3), March 1997, p. 587-599.
4. Yu.V. Shcherbakov, N.S. Ivanov, and others, Drag Reduction by AC Streamer Corona Discharges along a Wing-like profile Plate. AIAA Paper 2000-2670.
5. M. Post, T. Corke "Separation control on high angle of attack airfoil using plasma actuators", AIAA Paper 2003-1024, 41th AIAA Aerospace Meeting and Exhibit, 6-10 January, Reno, NV, 2003.

2.3.8. Transonic Effect.

Plasma effect on the airflow was observed when using contoured discharge plate with cylindrical profile. The transonic operation mode was realized in the test section, which has the arrangement shown in Fig.2.3.5.1.

The results of observation show that in some cases, when the aerodynamic situation is sensitive to weak influence, the surface plasma of barrier discharge can effect on transonic flow. Schlieren photos of such a mode are shown on the Fig.2.3.8.1. It is seen that transition zone between subsonic mode of the airflow and supersonic one is shifted down flow when the discharge is switched on (second photo).

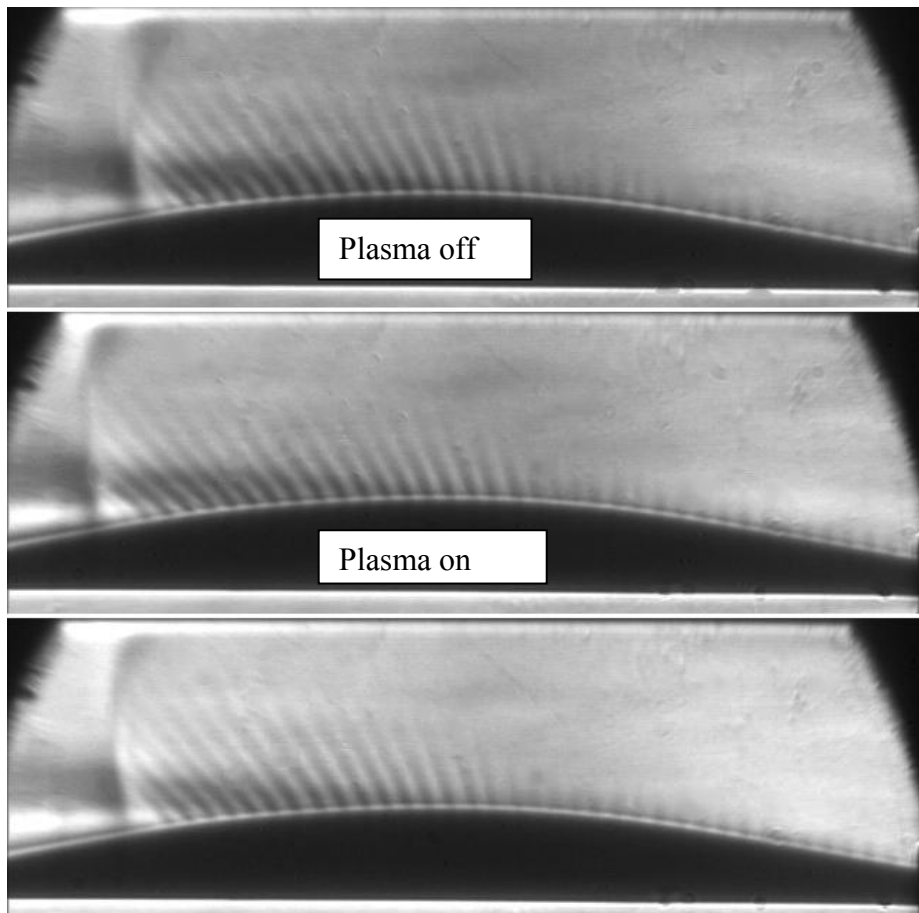


Fig.2.3.8.1. Schlieren photos of plasma flow interaction. Flow direction from right to left.

These effects are seen much better in processed Schlieren photo presented in Fig.2.3.8.2. Generally two main mechanisms may guide a shift of transonic shock over profiled airfoil:

thermal and electrostatic (non-thermal). In the first case the shock should be shifted upstream as it was observed in section 2.2.8. In the second case the effect may have both directions in dependence on the electrostatic force vector (direction of the plasma-induced flow). The fact that it is shifted downstream, when the additional force directed on the same manner, prove the conclusion on non-thermal mechanism of interaction.

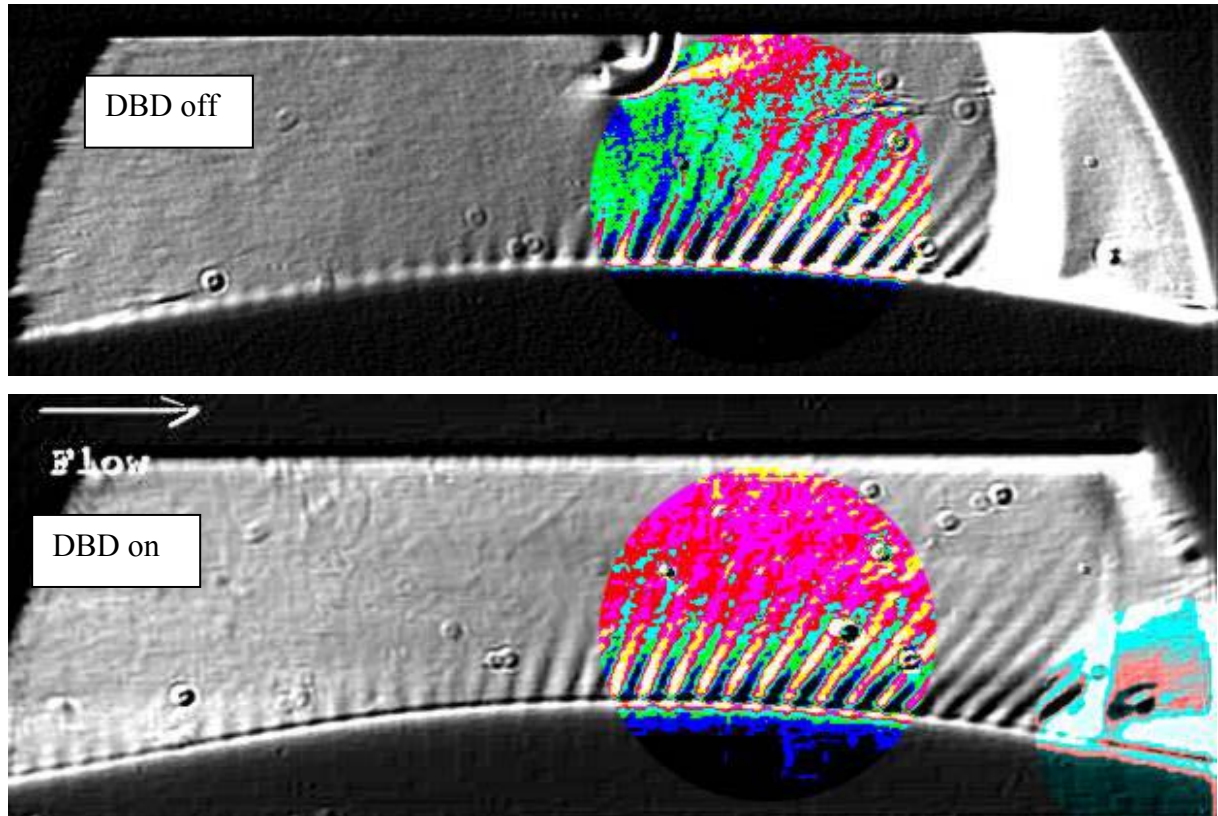


Fig.2.3.8.2. Processed Schlieren photos of the surface plasma effect on boundary layer under transonic flow. Flow direction from left to right.

2.3.9. Supersonic Effect.

As was mentioned above the electrostatic forces are too weak for high-speed dense flow modification. To find any valuable plasma effect a sensitive aerodynamic structure should be applied.

Short time wind tunnel's runs were executed for different configurations of the discharge. Schlieren photos on Fig.2.3.9.1 and Fig.2.3.9.2 show that there is no visible effect of the discharge influence on flow near plane plate and profiled plate. In that test the flow structure was observed, pressure distribution and flow fluctuations were measured. The flow direction was from right to left here. The top images correspond to time moment before the DBD switching on, the middle ones at the DBD operation and the bottom frames after this.

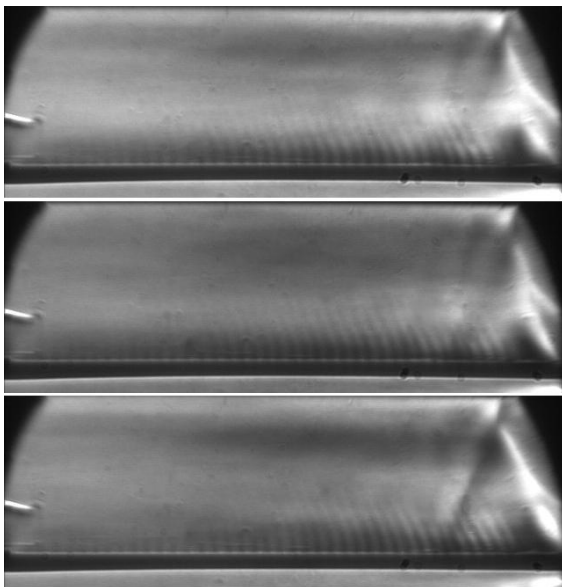


Fig.2.3.9.1. Plane model.

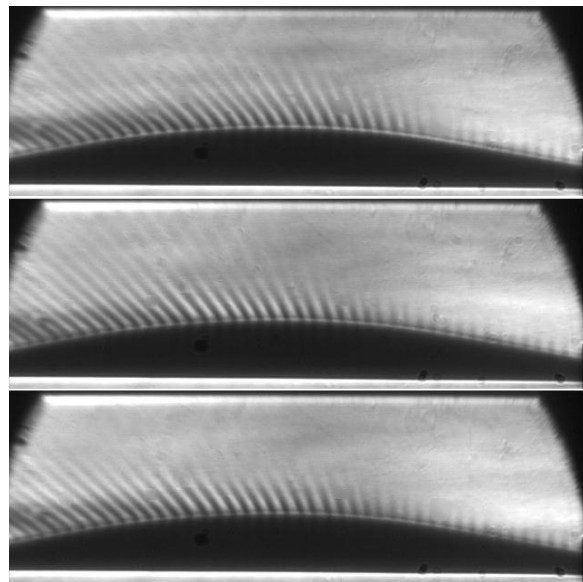


Fig.2.3.9.2. Contoured model.

The next test was fulfilled in modified aerodynamic configuration (see section 2.3.5) when an oblique shock wave reflection from DBD plate was examined. As the result an observable modification of reflection type was revealed. It appeared in some shift of reflection line upstream and growing of the stem in λ -type of shocks configuration. The result is shown in Fig.2.3.9.3. Such a modification could be explained by a thermal effect of the DBD plasma on the BL conditions.

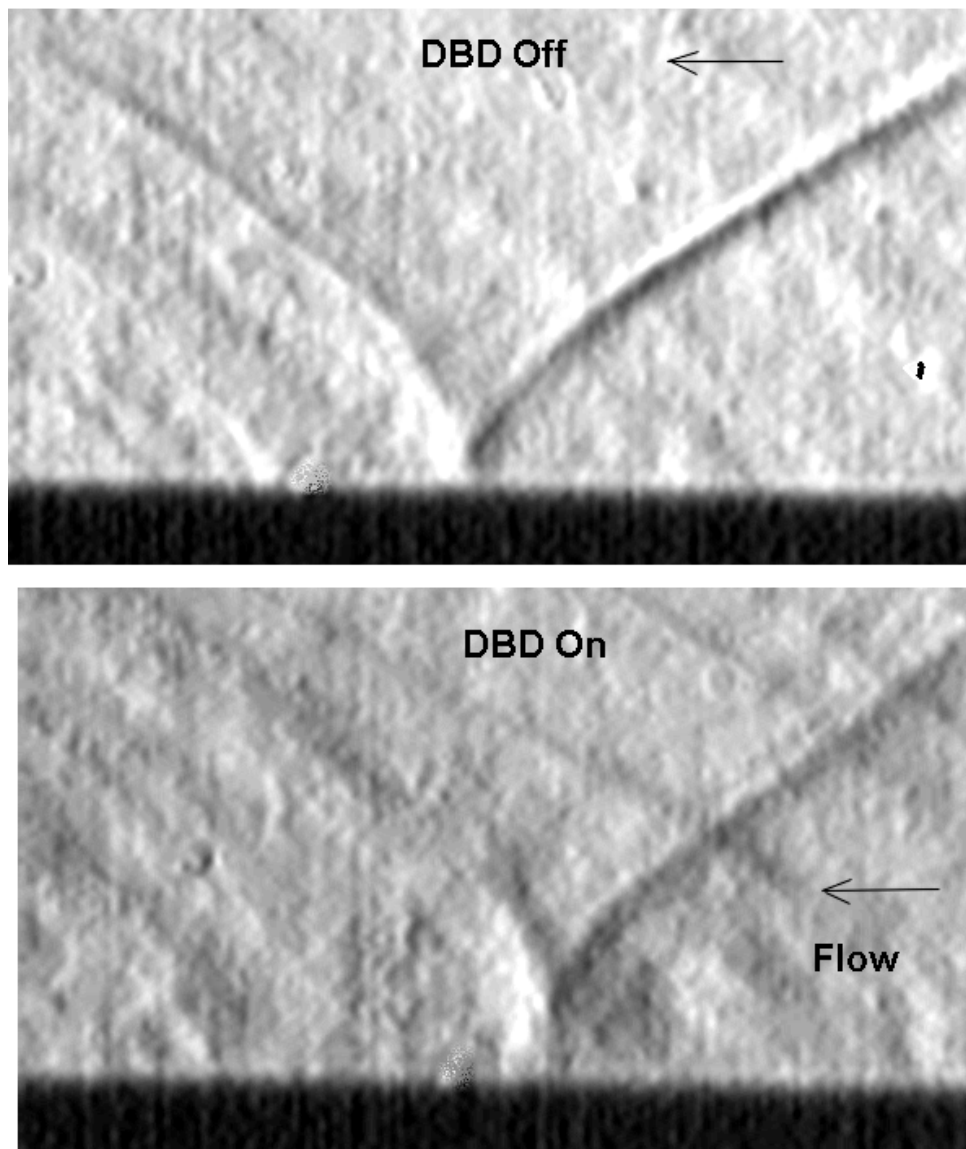


Fig.2.3.9.3. Shock reflection modification due to DBD plasma.

2.4. Numerical Simulation of Near-Surface Plasma Effect.

2.4.1. Near-Surface Thermal Power Deposition (Euler Approach).

Results of the numerical simulation of power deposition into the boundary layer on the plane plate at Mach number $M=2$ are presented in this section. A main attention was paid on the determination of the influence of power release into the boundary layer on the flow structure in the near-wall region and in the external supersonic flow in the vicinity of power-deposition region (Fig.2.4.1.1). Power deposition was realized in the rectangular region Ω with length L and height h . Region is situated on the distance L_{ps} from the front edge of the plate.

Numerical simulations has been carried out in the frames of inviscid perfect gas model by means of specially developed procedure. This procedure is based on the changing of subsonic part of the previously calculated boundary layer for inviscid subsonic layer at flow velocity that is constant over the section (Fig.2.4.1.2). According to this procedure calculation of the incompressible boundary layer by formula $\delta = A \cdot x / (Re)^n$ is carried out as the first step. Values of the constants A and n are chosen depending on the mode of the gas flow in the boundary layer (BL). After this recalculation of the BL thickness is carried out by means of the “determining” temperature method taking into consideration compressibility of the gas.

Thickness of the subsonic part of BL δ_s before the region Ω is determined during the second step by known velocity distribution law of the velocity over the BL on the plate. Changing of the BL for subsonic layer of this thickness with gasdynamic parameters that are constant over the section leads to the inviscid model problem with constant gap (Fig.2.4.1.2).

Temperature of this layer in the case of heat-insulated plate is assumed as one that is equal to the reduction temperature at number $Pr=0.7$. Density of the gas ρ^* in this fictitious layer is determined from the equation of state by the pressure of the unperturbed flow and by the reduction temperature. Velocity V^* is determined from the condition of the support of the same flow-rate as one in the subsonic region of the real boundary layer $\int_0^{\delta_s} \rho V dy = \rho^* V^* \delta_s$.

Eelier equations and energy equation describing gas flow in this model were solved by means of S.K.Godunov's method with using of difference scheme of Rodionov-Kolgan that

has a second order of accuracy. It must be noted that difference grid with dimension 120*80 was constructed with concentration in the boundary layer region along y axis and in the area of energy deposition along x axis. There were following varied parameters: longitudinal dimensions of the area of energy-deposition L (0.1, 0.5, 1 and 2m) and linear power of energy-deposition (50, 100, 150, 200 and 250 kW/m). Transversal dimension of heat-deposition region was 1mm in all cases. In the case of power-deposition 250 kW/m a mode of power that is linearly increased along the power-deposition region was considered (“wedge-shaped” power deposition).

Analyses of the results. The fields of calculated parameters are presented in Fig.2.4.1.5.

First of all, it is need to point out flow features that are common for all considered cases. In all cases a shock wave arose in the external flow. This shockwave approaches to the Mach compression wave at the low values of power. Shock wave intensity is increasing while power-deposition is increasing. It is indicated by growth of shock wave slope angle (see, for example, Fig.2.4.1.5 Pressure 50 and 250). However, there is a peculiarity that is related to the expansion of the backwise-circulation zone at power 250 kW/m. Lambda-shaped shock wave that arises in the upstream region of this zone causes to the intensity reduction of the main part of shock wave in the external flow.

The backwise circulation zone is absent at uniform power deposition to the expanded region (20mm) at low values of power. Generation of backwise circulation zone begins at nearly 100kW/m and further development begins at high values of power-deposition. The backwise circulation zone dimension increases (both downstream and upstream) when power increases.

Mach numbers are reduced in the trace beyond the power release region at increasing of the power deposition, while transversal dimensions of subsonic part of the trace is increasing (images Mach 50 - 250). Behavior of the gas density is the same (figures Density 50 - 250).

Concentrated power deposition (length of the power-deposition region is 0.1cm) causes to the boundary layer separation and backwise circulation zone generation for all considered levels of power.

There was no downstream opened separation zone in all considered cases.

The backwise circulation zone arises when power release is increasing linearly in the power-deposition region (“wedge-shaped” power deposition) at power deposition region

lengths of 0.1 and 0.5cm (this case is close to the concentrated power deposition) and power of 250kW/m. At the same time backwise circulation zone is absent when power deposition region length is from 1 to 2cm (mode of the length-distributed energy release), i.e. smoothly increased power deposition doesn't cause to the separation. It is well seen on Fig.2.4.1.3 and Fig.2.4.1.4. These figures demonstrate distribution of pressure coefficient and longitudinal component of the velocity along the plate.

It is need to note that static pressure beyond the power deposition region tends to the static pressure of unperturbed flow, while longitudinal component of velocity approximately one and a half times higher than velocity of the external flow, so power deposition causes to the increasing of the kinetic energy of the gas in the wall layer. The latter circumstance with consideration of gas heating allows us to assume that boundary layer will be more stable with respect to the separation downstream because it stays laminar one. Besides this, it is seen in the Fig.2.4.1.4 that backwise circulation zone can be localized behind the onset of the power deposition (green curve for $L=1\text{cm}$).

Reduction of the total pressure behind the power deposition region is determined by the gas expansion and by the static pressure fall at almost constant full velocity. Mode with backwise circulation zone presence is considered in the second file. Here, total pressure in the backwise circulation zone is almost equal to the static pressure because of the low velocities in this region. It is need to note that increasing of the static pressure and of the total pressure in the power deposition region is observed in the all examples that have been demonstrated.

Conclusion. Results of calculations that have been carried out by means of the method described above reflect properly the influence of the power deposition that is provided into the boundary layer on the flow structure. It is proved by the fact that all flow modes that were observed in the experiments and also in the solution of the similar task by means of the Navies-Stocks equations have been obtained. Further improvement of the method by means of the definition of the proper ratio of inviscid subsonic layer thickness δ_s (variable-length plate) to the power-deposition region height h , and also by means of the power generation law definition in the region Ω allows us to increase accuracy of the quantitative estimations.

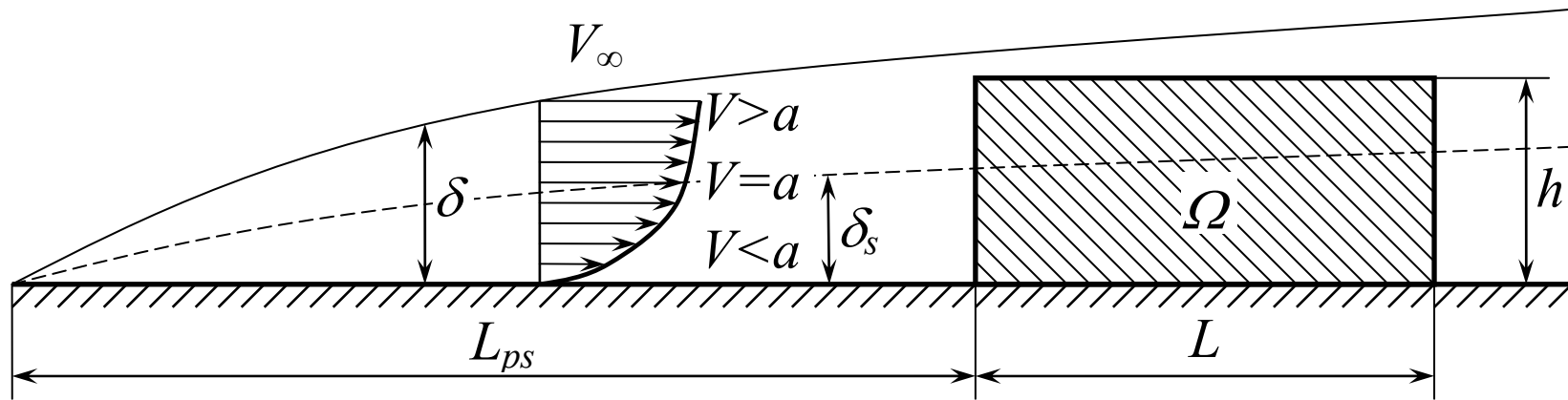


Fig.2.4.1.1. Scheme of the power feeding.

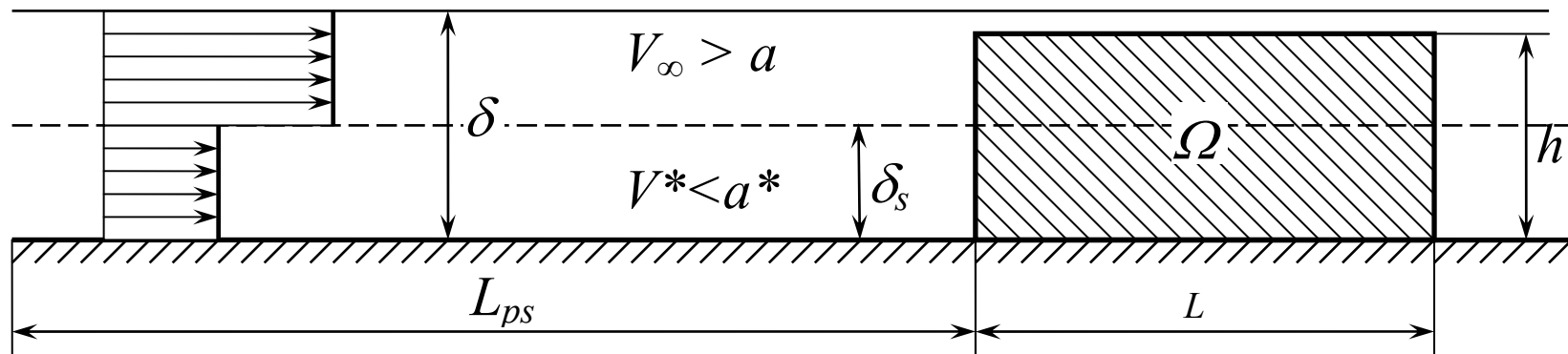


Fig.2.4.1.2. Physics model of the power deposition to the BL.

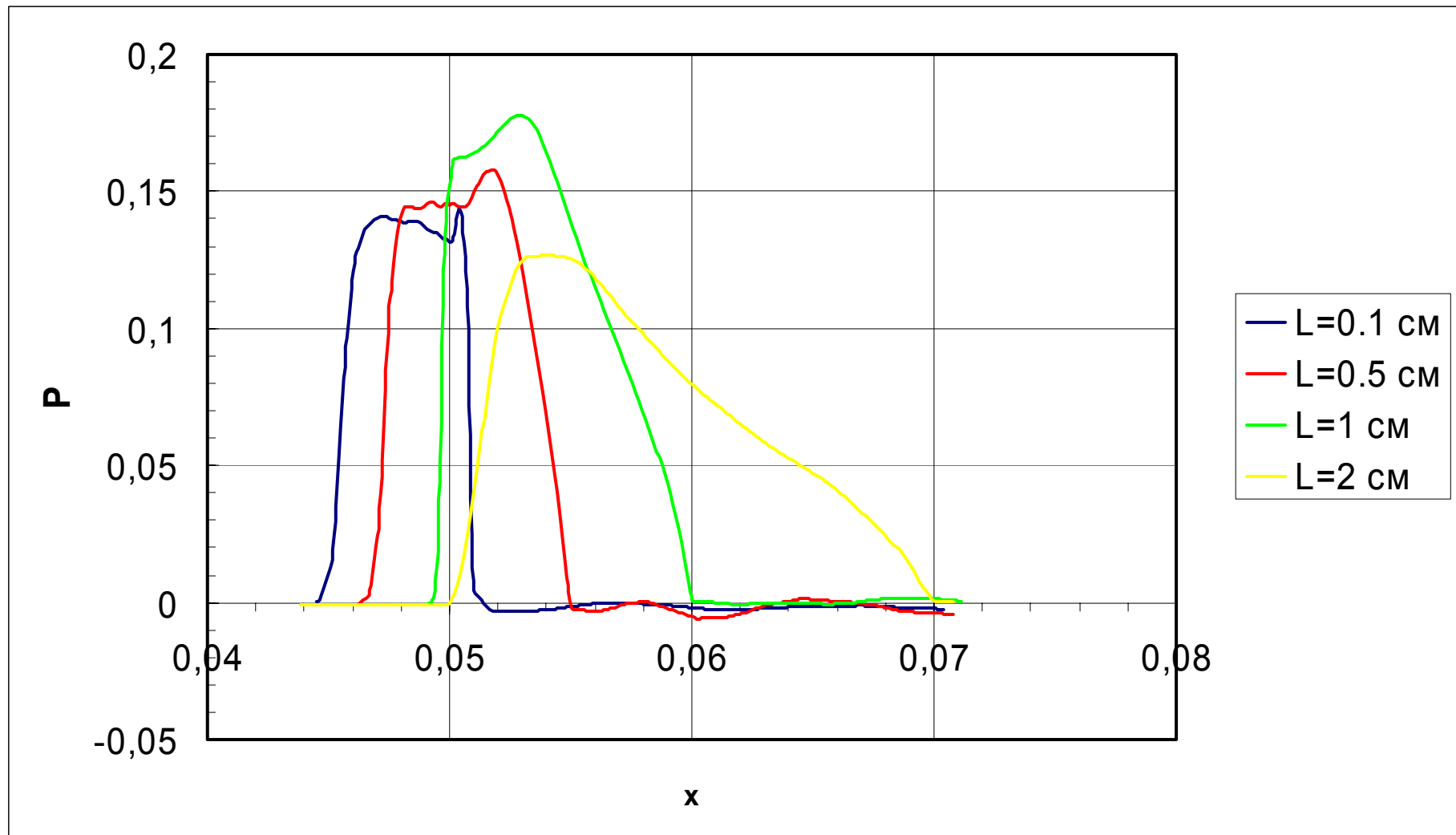


Fig.2.4.1.3. Pressure factor distribution on the surface
near the area of power deposition at different length of the zone.

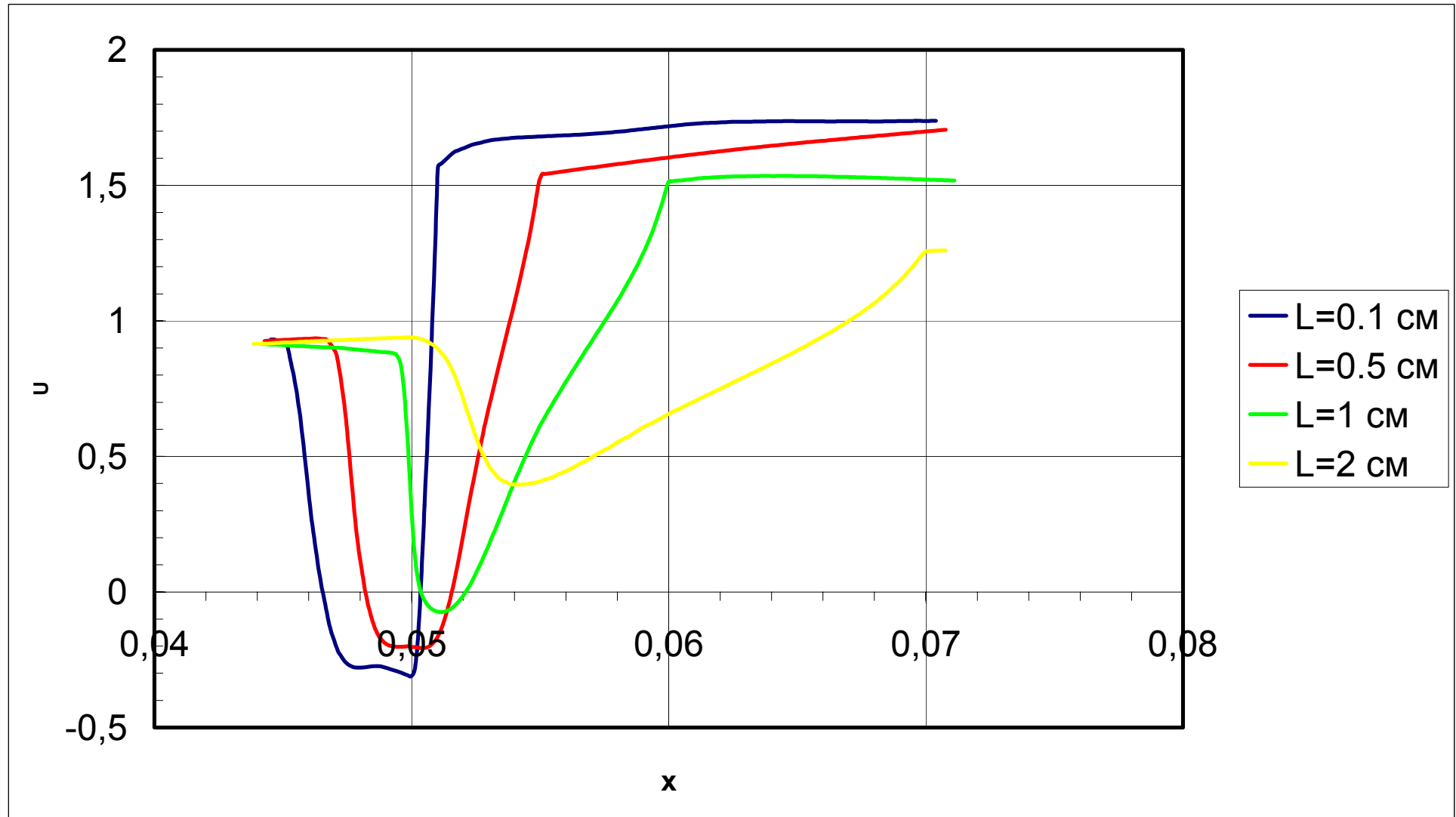
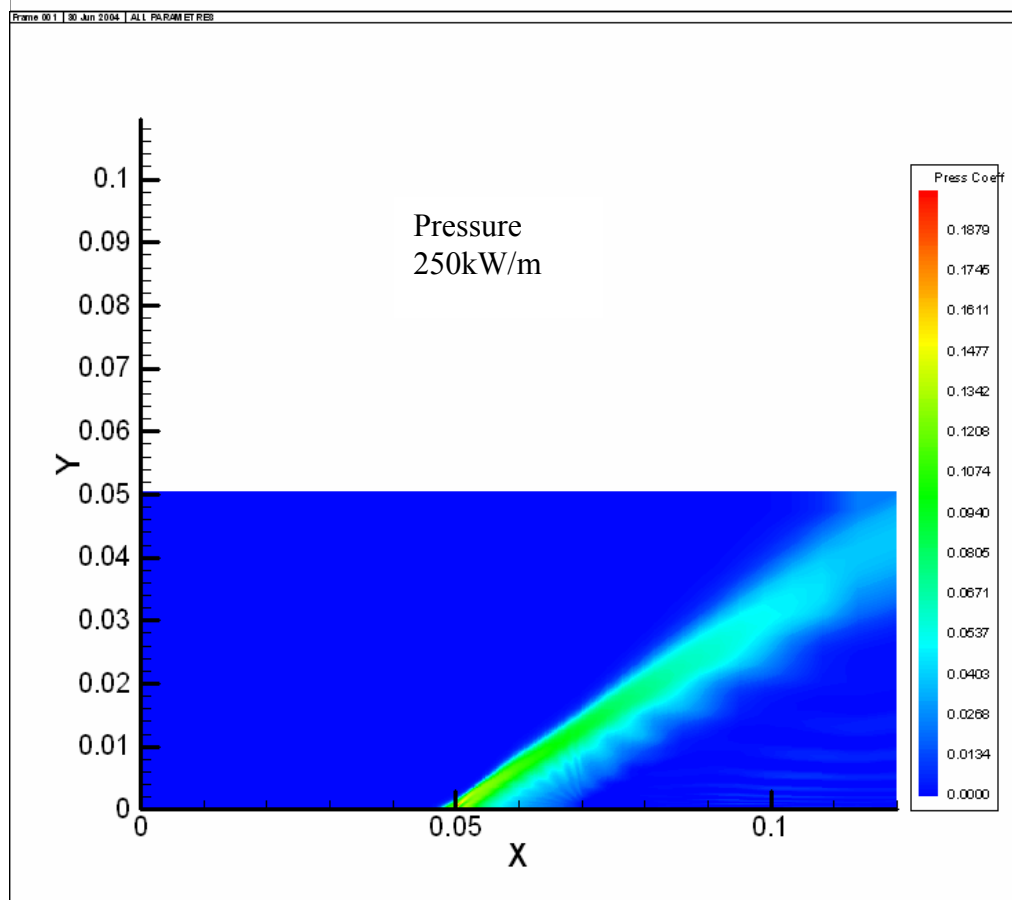
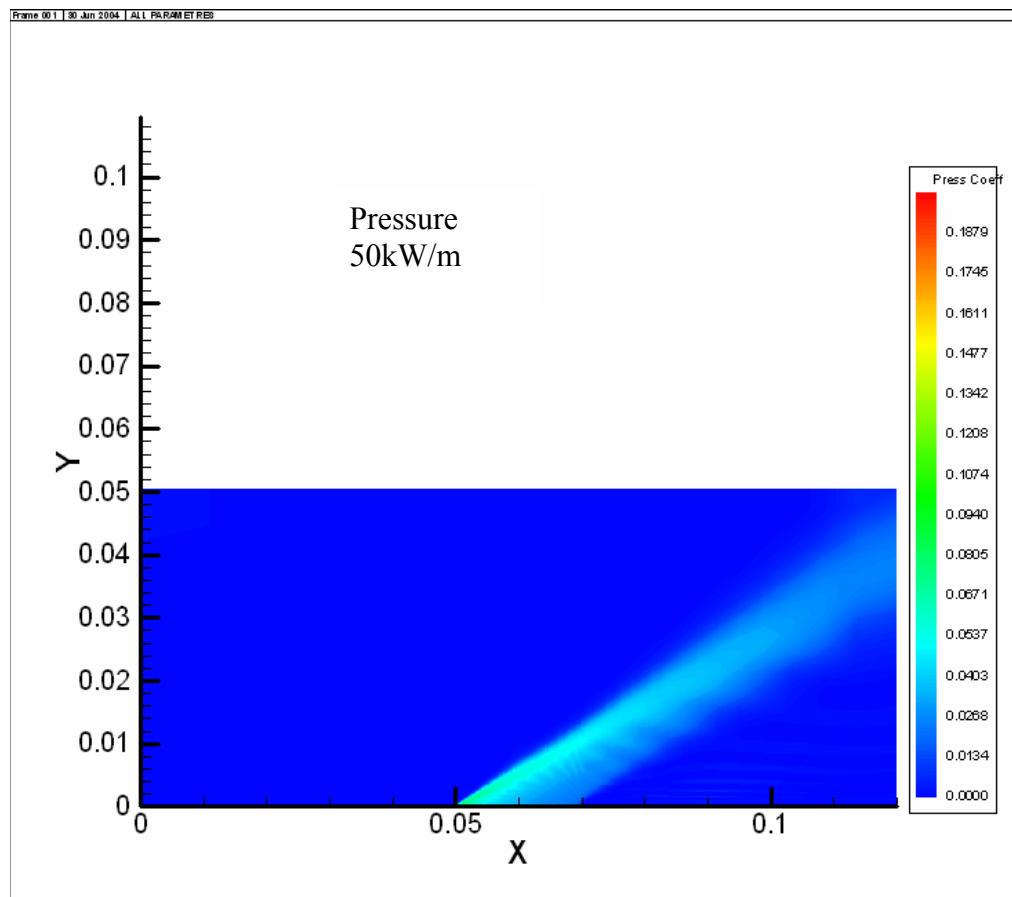
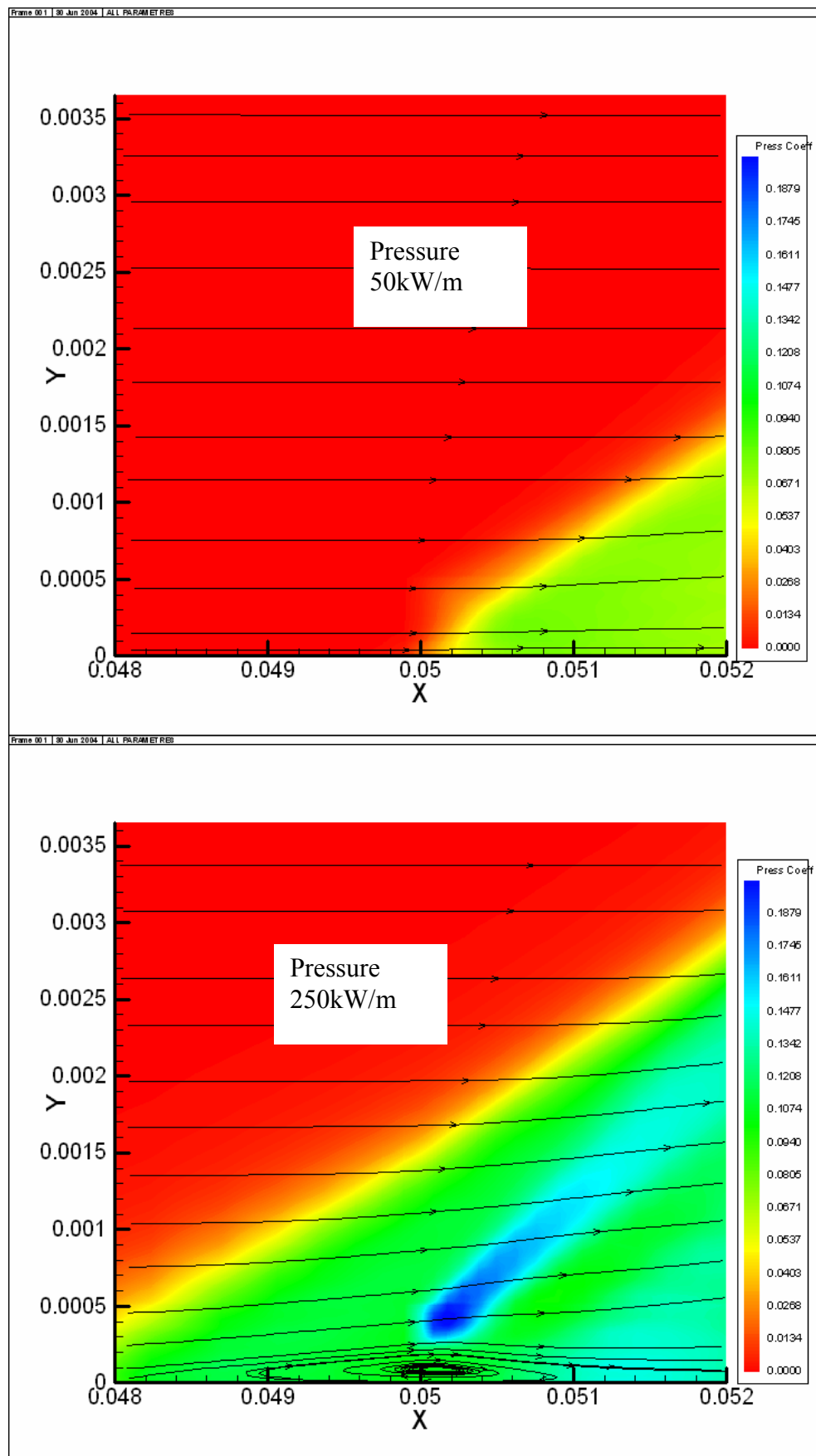
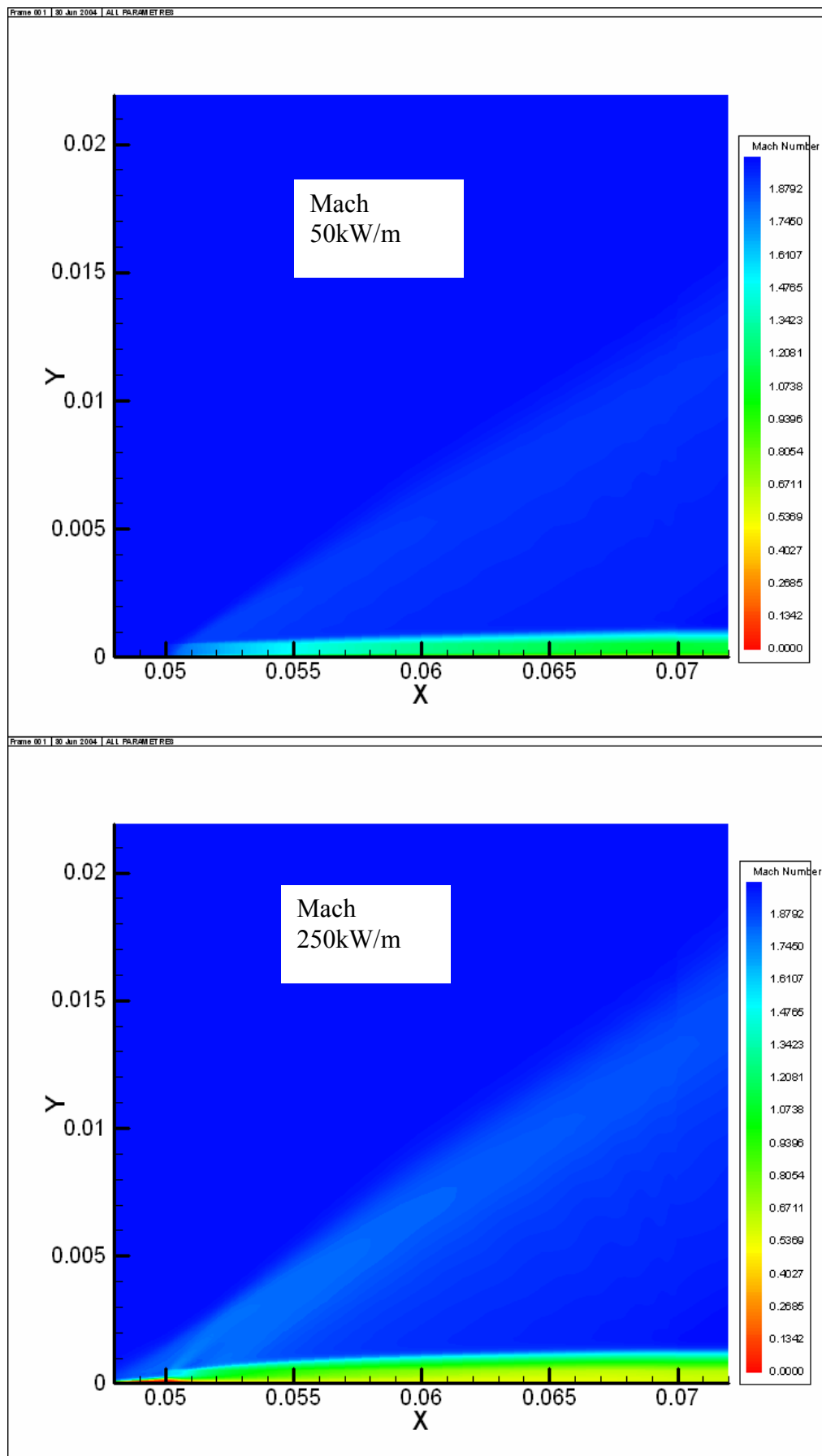
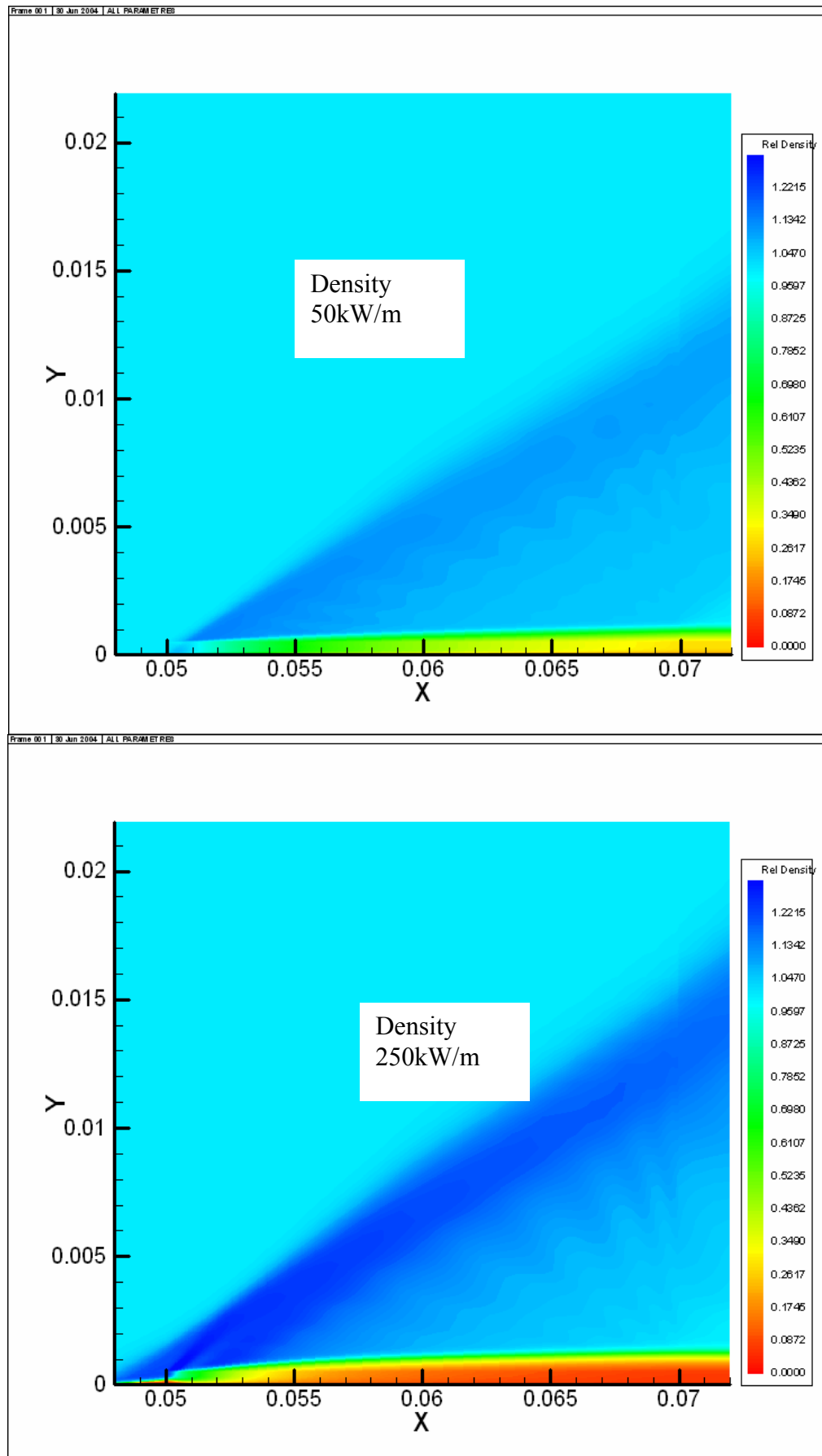


Fig.2.4.1.4. Axial velocity component distribution on the surface
at the different geometry of the power deposition.









2.4.2. Near-Surface Energy Deposition (Navier-Stokes Approach).

Stationary flow in plane duct was investigated numerically. The duct has a length of 50 mm and it is smoothly conjugated with plane supersonic nozzle. Turbulent gas flow in the duct is described by Favre-averaged equations of Navier-Stokes [1] for thermally equilibrium two-component model of air with constant chemical composition. Approach of Bussineks and two-parametric $k-\omega$ model of Wilkoks are used for turbulent transfer description [2]. Electric discharge influence on the flow is simulated by local heat application.

Numerical integration of equations is realized by means of second order of accuracy difference scheme of TVD type. This scheme is defined by final volume method on structured grid. The definite solution of Riman problem of the decay of undefined gap is used for calculation of inviscid flows through the cells' borders. Limit values of original variables are found out by means of one-dimensional "limited" extrapolation from cells' center to the corresponding borders. Viscous flows are calculated by central and one-sided difference-formulas of second order of accuracy. Calculations have been carried out on nonuniform grid with number of centers 280×200 . The centers are concentrated near surfaces in the region of boundary layer.

Some results of calculations are presented in the Fig.2.4.2.1-3. Conditions of numerical experiment were the following: heat-supply power of 2 kW/cm; heat-supply is uniformly distributed on the right-angle triangle with height of $h = 1$ or 3 mm and base of $d = 20$ mm that is situated on the bottom surface of the duct. Heat-supply is begun at the distance of 6 cm from the beginning of the duct that is in accordance with the electrodes arrangement in the experiment. It is assumed that duct surface is either cooled with constant temperature $T_w = 300\text{K}$ or heat-insulated. Uniform flow with Mach number $M=1$, stagnation temperature $T_0 = 300\text{K}$ and total pressure $P_0 = 1$ atm is assigned at the nozzle entrance (in the throat).

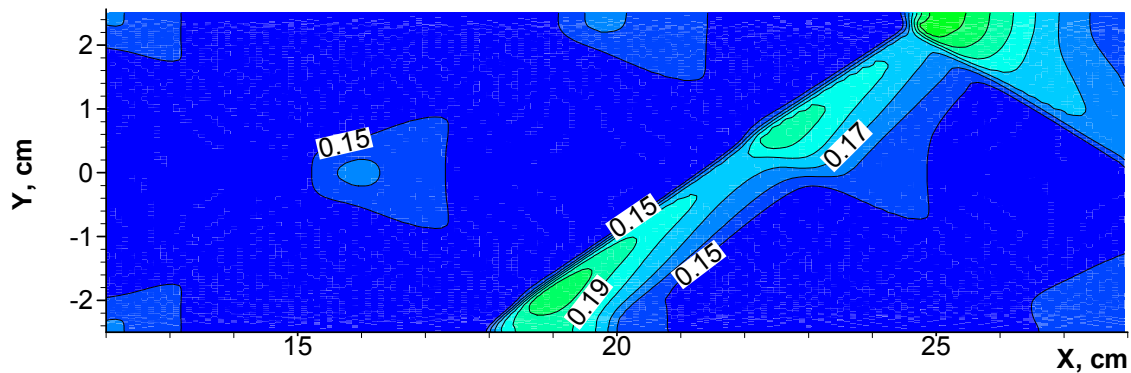
Distributions of static pressure P atm and density ρ that is divided by the air density in the nozzle throat ρ^* are presented in the Fig. 2.4.2.1a and 2a. These distributions have been obtained by calculations at $h = 1\text{mm}$ and $T_w = 300\text{ K}$. It is seen that wall heat-supply leads to the generation of the oblique shock wave that is caused by streamlines' deflection from surface as a result of the gas heating. A slope angle of shock wave is about 36° . Pattern of density distribution is close to the one that is obtained in experiment by means of shadow-photo method. Narrow separation zone arises in the vicinity of the beginning of heat-supply in the region of pressure increase on the duct surface.

Similar data at $h = 3$ mm is presented in the Fig.2.4.2.1b – 2b. Comparison shows that when increasing of h , slope angle of the shock wave is not changing almost while transversal dimension of the reduced density region is increasing proportionally to the changing of h .

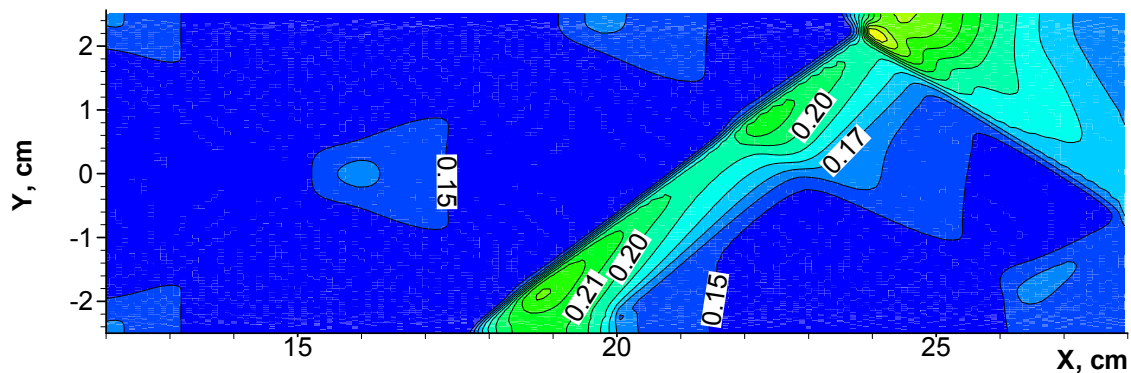
Distributions of total (solid line) and static (dash line) pressure over the two sections of wall layer – before heat-supply region (1) and behind its end (2) are presented in the Fig.2.4.2.3. Conditions were the following: $T_w=300$ K and $h = 3$ mm. It is seen that there is a considerable reduction of total pressure in the trace of the heat-supply region.

References to section 2.4.2.

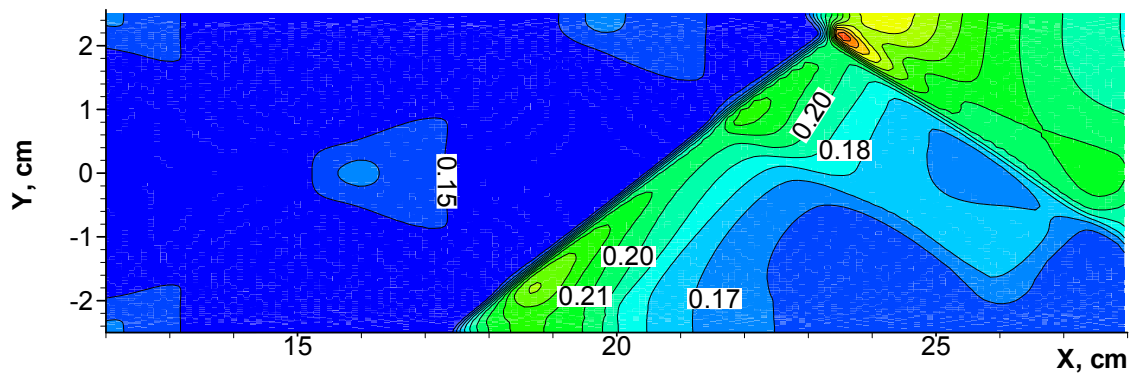
1. Favre, A. “Equations des gas turbulents compressibles”, Journal de Mecanique, 4, 1965.
2. Coakley, T.J. Development of Turbulence Models for Aerodynamic Applications,” AIAA Paper 97-2009, 1997, 11p



a.(P13) Pressure distribution $W=200\text{kW/m}$, $h=1\text{mm}$.

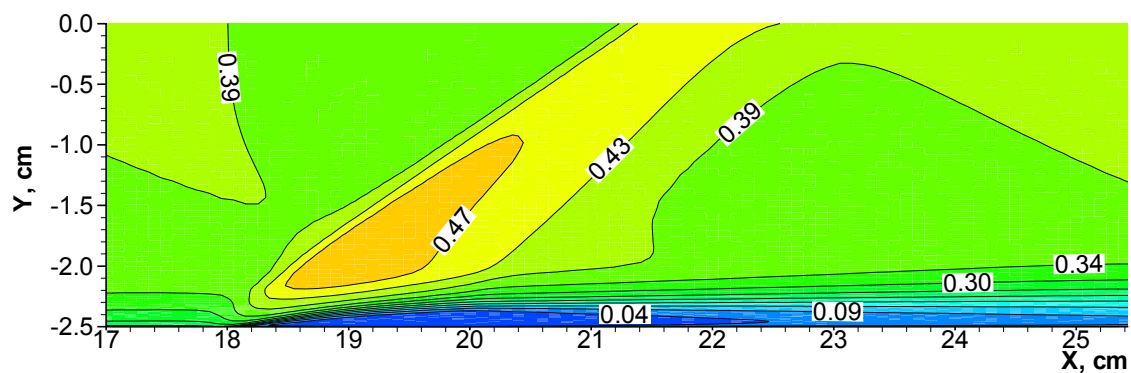


b.(P14) Pressure distribution $W=200\text{kW/m}$, $h=3\text{mm}$.

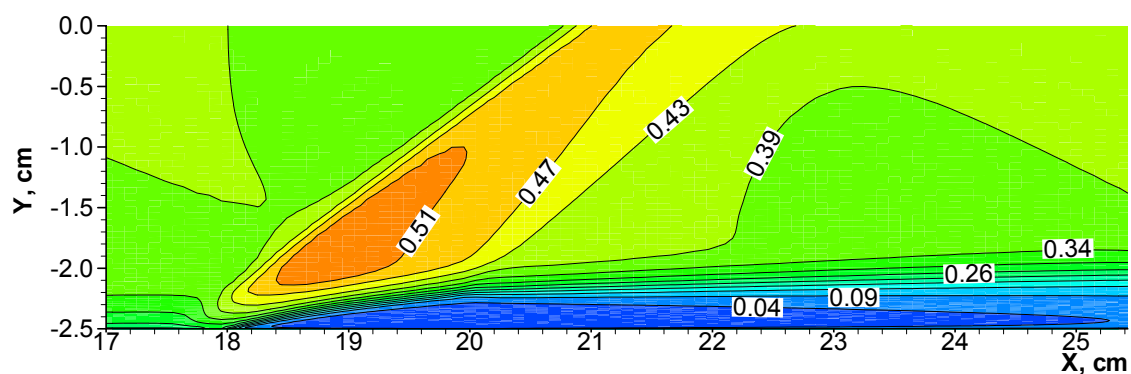


c.(P24) Pressure distribution $W=200\text{kW/m}$, $h=3\text{mm}$, thermo-insulated wall.

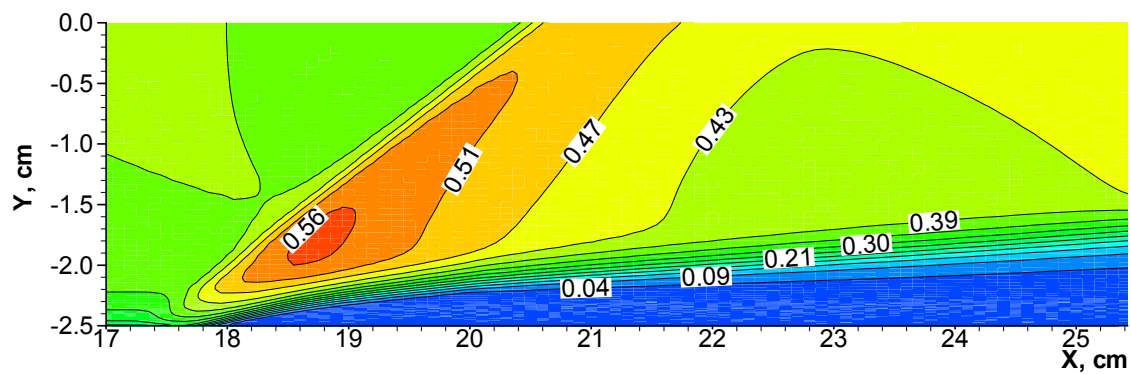
Fig.2.4.2.1. Pressure distribution calculated.



c. (Ro13). Density distribution $W=200\text{ kW/m}$, $h=1\text{ mm}$.



b. (Ro14). Density distribution $W=200\text{ kW/m}$, $h=3\text{ mm}$, thermo-conductive wall.



c. (Ro24). Density distribution $W=200\text{ kW/m}$, $h=3\text{ mm}$, thermo-insulated wall.

Fig.2.4.2.2. Density distribution calculated.

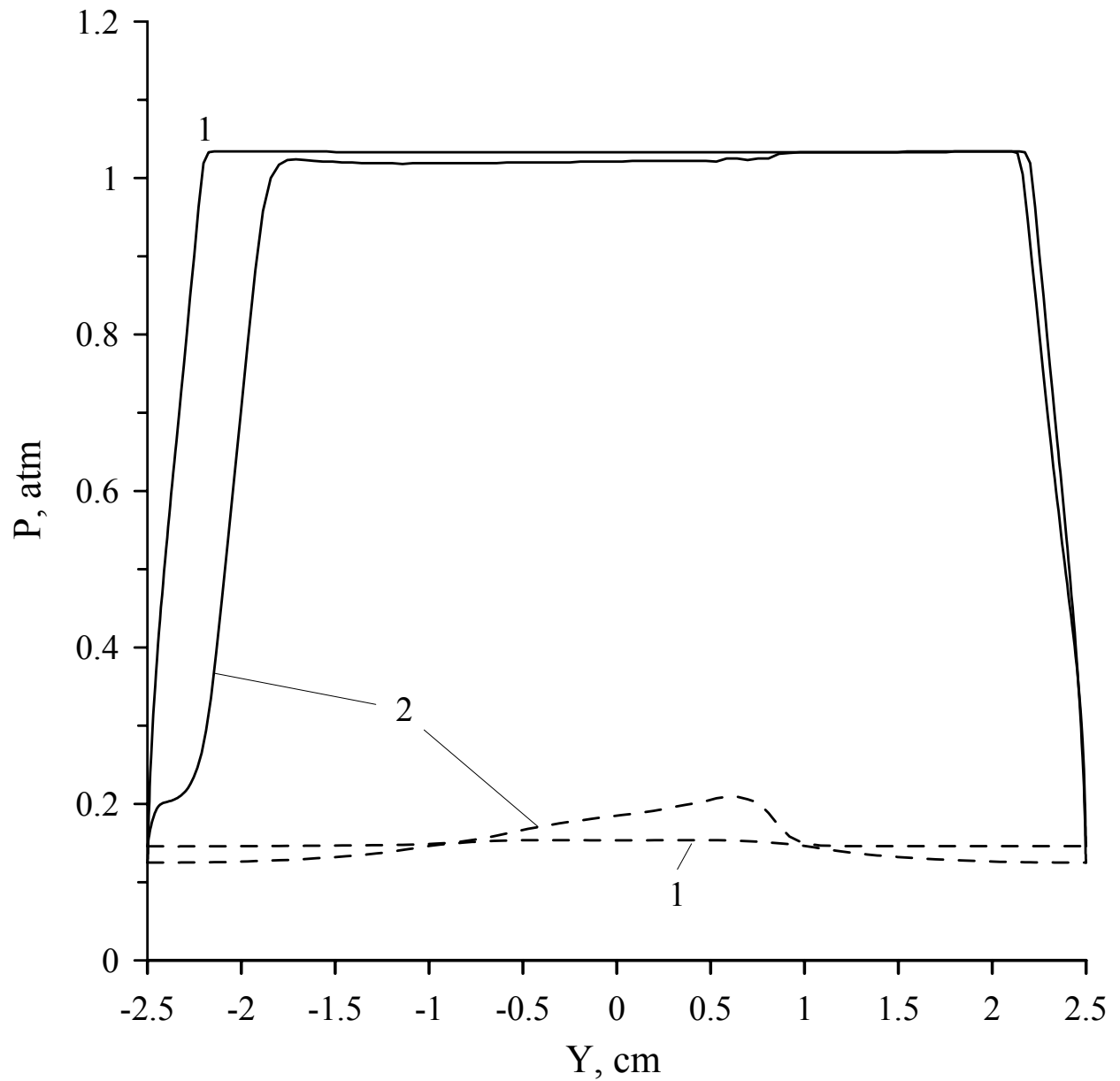


Fig.2.4.2.3. Pressure distribution modification due to surface heat transfer.

2.4.3. Electrodynamic Effects in Boundary Layer.

It is considered an air flow over a surface with a dielectric barrier discharge (DBD) that is generated on a set of thin and narrow electrodes placed on the streamlined surface perpendicular to the velocity vector of incident flow. It is supposed that the electrodes of opposite polarity are placed inside a streamlined body with a downstream shift with respect to external electrodes. In this case the DBD is generated from downstream edges of external electrodes.

Numerical simulation of the DBD influence on a boundary layer is carried out exclusively in the frame of equations of unsteady compressible laminar boundary layer with additional terms in momentum and energy equations which simulate a force and heat impact of the DBD. It means that an electrodynamic task describing physical phenomena in the discharge is not considered. However an influence of non-equilibrium degrees of freedom in total energy transfer is taken into account.

The non-equilibrium transfer of vibrational energy E_V^* (J/kg) to translational degrees of freedom is described in this approximation by source term S_{TR}^* in the total energy equation, which takes the form

$$S_{TR}^* = \rho^* \frac{E_V^* - E_{Ve}^*(T^*)}{\tau_{VT}^*} \quad (1)$$

Here ρ^* is the gas density, E_{Ve}^* is the equilibrium value of E_V^* , that is a function of gas temperature T^* , τ_{VT}^* is the effective vibrational relaxation time. The superscript $*$ denotes here and later dimensional quantities.

The conservation equation for vibrational energy is the usual equation of transfer for scalar function and in general case takes the following form:

$$\frac{\partial E_V^*}{\partial t^*} + \nabla^* \mathbf{j}^* = \frac{S_V^*}{\rho^*}, \quad S_V^* = r Q^* - S_{TR}^* \quad (2)$$

Here the source term Q^* (W/m³) simulates a total specific power revealed in the discharge, and the coefficient $r \leq 1$ defines a part of this power pumping in vibrational

degrees of freedom. The flux of scalar function E_V^* includes convective and diffusive components according to

$$\mathbf{j}^* = \mathbf{V}^* E_V^* - \rho^* D^* \nabla^* \left(\frac{E_V^*}{\rho^*} \right) \quad (3)$$

Here \mathbf{V}^* is the vector of gas velocity, D^* is the diffusion coefficient.

The system of equations and boundary conditions of the unsteady laminar boundary layer with the equation of vibrational energy transfer takes the form

$$\frac{\partial \rho^*}{\partial t^*} + \frac{\partial (\rho^* u^*)}{\partial x^*} + \frac{\partial (\rho^* v^*)}{\partial y^*} = 0 \quad (4)$$

$$\rho^* \frac{\partial u^*}{\partial t^*} + \rho^* u^* \frac{\partial u^*}{\partial x^*} + \rho^* v^* \frac{\partial u^*}{\partial y^*} = \frac{\partial}{\partial y^*} \left(\mu^* \frac{\partial u^*}{\partial y^*} \right) - \frac{\partial p^*}{\partial x^*} + F_x^* \quad (5)$$

$$\frac{\partial p^*}{\partial y^*} = F_y^* \quad (6)$$

$$\begin{aligned} \rho^* \frac{\partial h^*}{\partial t^*} + \rho^* u^* \frac{\partial h^*}{\partial x^*} + \rho^* v^* \frac{\partial h^*}{\partial y^*} &= \frac{\partial}{\partial y^*} \left(\frac{\mu^*}{\text{Pr}} \frac{\partial h^*}{\partial y^*} \right) + u^* \frac{\partial p^*}{\partial x^*} + v^* \frac{\partial p^*}{\partial y^*} + \\ &+ \mu^* \left(\frac{\partial u^*}{\partial y^*} \right)^2 + (1-r)Q^* + S_{TR}^*, \quad S_{TR}^* = \rho^{*2} \frac{H^* - H_e^*}{\tau_{VT}^*} \end{aligned} \quad (7)$$

$$p^* = \frac{\gamma-1}{\gamma} \rho^* h^* \quad (8)$$

$$\rho^* \frac{\partial H^*}{\partial t^*} + \rho^* u^* \frac{\partial H^*}{\partial x^*} + \rho^* v^* \frac{\partial H^*}{\partial y^*} = \frac{\partial}{\partial y^*} \left(\frac{\mu^*}{\text{Sc}} \frac{\partial H^*}{\partial y^*} \right) + \frac{1}{\rho^*} (rQ^* - S_{TR}^*) \quad (9)$$

$$t^* = 0: \quad (u^*, v^*) = (u_0^*, v_0^*), \quad p^* = p_0^*, \quad h^* = h_0^*, \quad H^* = H_e^* \quad (10)$$

$$y^* = 0: \quad u^* = v^* = \frac{\partial H^*}{\partial y^*} = 0, \quad C_w^* \frac{\partial h^*}{\partial t^*} = \lambda^* \frac{\partial h^*}{\partial y^*} \quad (11)$$

$$y^* = y_e^*: \quad u^* = u_e^*(x^*), \quad p^* = p_e^*(x^*), \quad h^* = h_e^*(x^*), \quad H^* = H_e^* \quad (12)$$

Here t^* is the time, (x^*, y^*) are the Cartesian coordinates, with the axis x^* directed along a streamlined surface, and the axis y^* directed perpendicular to it, (u^*, v^*) are the components of the velocity vector along the axes (x^*, y^*) , p^* is the pressure, $h^* = c_p^* T^*$ is the gas enthalpy, c_p^* is the specific heat capacity at a constant pressure, μ^* and λ^* are the coefficients of gas dynamic viscosity and heat conductivity respectively, $\gamma = 1.4$ is the adiabatic ratio, (F_x^*, F_y^*) are the components of volume force along the axes (x^*, y^*) , C_w^* is the heat capacity per unit surface of the streamlined body. The function $H^* = E_V^* / \rho^*$ is introduced in the equation of the vibrational energy transfer (9), obtained on the base of equations (1)–(4), for a simplification of the form of the equation (9).

The subscript 0 in the initial conditions (10) denotes the values of parameters corresponding to a steady boundary layer without force and heat impact. A finite value of heat capacity of the streamlined surface is taken into account in the last boundary condition (11). The subscript e in the boundary conditions (12) denotes the values outside the boundary layer.

Note, that the main feature of the boundary value problem (4)–(12) is the presence of the transversal pressure gradient defined by the equation (6).

The non-dimensional variables (without superscript $*$) are introduced for a convenience of numerical solution of the parabolic type equation system in the frame of the boundary layer approximation according to

$$t = \frac{t^*}{t_0^*}, \quad x = \frac{x^*}{l^*}, \quad y = \frac{y^*}{l^*} \sqrt{\frac{\text{Re}}{x}}, \quad u = \frac{u^*}{u_e u_\infty^*}, \quad v = \frac{1}{u_e u_\infty^*} \left(\sqrt{x \text{Re}} v^* - \frac{y}{2} u^* \right) \quad (13)$$

$$p = \frac{p^*}{p_\infty^*}, \quad h = \frac{h^*}{h_\infty^*}, \quad \rho = \frac{\rho^*}{\rho_\infty^*}, \quad \mu = \frac{\mu^*}{\mu_\infty^*}, \quad D = \frac{D^*}{D_\infty^*}$$

$$Q = \frac{l^*}{\rho_\infty^* u_\infty^{*3}} Q^*, \quad H = \frac{\rho_\infty^*}{u_\infty^{*2}} H^*, \quad F_x = \frac{l^*}{\rho_\infty^* u_\infty^{*2}} F_x^*, \quad F_y = \frac{1}{\sqrt{\text{Re}}} \frac{l^*}{\rho_\infty^* u_\infty^{*2}} F_y^*$$

$$\tau_{VT} = \frac{u_\infty^*}{l^*} \tau_{VT}^*, \quad \text{Re} = \frac{\rho_\infty^* u_\infty^* l^*}{\mu_\infty^*}, \quad \text{Sh} = \frac{l^*}{u_\infty^* t_0^*}, \quad \text{Pr} = \frac{\mu_\infty^* c_p^*}{\lambda_\infty^*}, \quad \text{Sc} = \frac{\mu_\infty^*}{\rho_\infty^* D_\infty^*}$$

Here t_0^* is the characteristic time, for example, the time interval between the beginnings of two successive charge pulses of the same sign, l^* is the characteristic line scale, $u_e(x)$ is the non-dimensional gas velocity outside the boundary layer, the subscript ∞ denotes the parameters of the incident flow, Re, Sh, Pr, Sc are the Reynolds, Strouhal, Prandtl and Schmidt numbers.

The system of equations and boundary conditions (4)–(12) takes the following form in the non-dimensional variables (13):

$$\frac{x}{u_e} \text{Sh} \frac{\partial \rho}{\partial t} + \left(\frac{x}{u_e} \frac{du_e}{dx} + \frac{1}{2} \right) \rho u + x \frac{\partial(\rho u)}{\partial x} + \frac{\partial(\rho v)}{\partial y} = 0 \quad (14)$$

$$\frac{\partial}{\partial y} \left(\mu \frac{\partial u}{\partial y} \right) = x \text{Sh} \rho \frac{\partial u}{\partial t} + u_e \left(x \rho u \frac{\partial u}{\partial x} + \rho v \frac{\partial u}{\partial y} \right) + \frac{x}{u_e} \left(\frac{1}{\gamma M_\infty^2} \frac{\partial p}{\partial x} - F_x \right) \quad (15)$$

$$\frac{\partial p}{\partial y} = \sqrt{x} \gamma M_\infty^2 F_y \quad (16)$$

$$\begin{aligned} \frac{\partial}{\partial y} \left(\frac{\mu}{\text{Pr}} \frac{\partial h}{\partial y} \right) = & x \text{Sh} \rho \frac{\partial h}{\partial t} + u_e \left(x \rho u \frac{\partial h}{\partial x} + \rho v \frac{\partial h}{\partial y} \right) - u_e \frac{\gamma - 1}{\gamma} \left(x u \frac{\partial p}{\partial x} + v \frac{\partial p}{\partial y} \right) - \\ & - (\gamma - 1) M_\infty^2 \left[u_e^2 \mu \left(\frac{\partial u}{\partial y} \right)^2 + x \left((1 - r) Q + x \rho^2 \frac{H - H_e}{\tau_{VT}} \right) \right] \end{aligned} \quad (17)$$

$$p = \rho h \quad (18)$$

$$\frac{\partial}{\partial y} \left(\frac{\mu}{\text{Sc}} \frac{\partial H}{\partial y} \right) = x \text{Sh} \rho \frac{\partial H}{\partial t} + u_e \left(x \rho u \frac{\partial H}{\partial x} + \rho v \frac{\partial H}{\partial y} \right) - \frac{x}{\rho} \left(r Q - \rho^2 \frac{H - H_e}{\tau_{VT}} \right) \quad (19)$$

$$\mu = h^{3/2} \frac{1 + A}{h + A}, \quad A = \frac{114}{T_\infty^*}$$

$$t = 0: \quad (u, v) = (u, v)_0, \quad p = p_0, \quad h = h_0, \quad H = H_e \quad (20)$$

$$y = 0: \quad u = v = \frac{\partial H}{\partial y} = 0, \quad \sqrt{x} \text{Re} \text{Sh} \text{Pr} C_w \frac{\partial h}{\partial t} = \mu \frac{\partial h}{\partial y}, \quad C_w = \frac{C_w^*}{c_p^* \rho_\infty^* l^*} \quad (21)$$

$$y = y_e : \quad u = u_e(x), \quad p = p_e(x), \quad h = h_e(x), \quad H = H_e \quad (22)$$

Explicit expressions for the pressure and its longitudinal gradient can be obtained from the equation (16) with taking into account the external boundary condition (22)

$$p(t, x, y) = p_e(x) - \sqrt{x} \gamma M_\infty^2 \int_y^{y_e} F_y(t, x, y) dy'$$

$$\frac{\partial p}{\partial x} = \frac{dp_e}{dx} - \frac{\gamma M_\infty^2}{\sqrt{x}} \int_y^{y_e} \left(\frac{F_y}{2} + x \frac{\partial F_y}{\partial x} \right) dy'$$

Unsteady source terms modeling the force and heat influence of the discharge are defined in the following form:

$$F_{x,y}(t, x, y) = F_{x0,y0} f_t(t) f_{xy}(x', y'), \quad Q(t, x, y) = \frac{12E}{\tau h_x h_y} f_t(t) f_{xy}(x', y')$$

$$f_t(t) = 2t' / \tau, \quad 0 \leq t' \equiv t - t_i \leq \tau / 2; \quad f_t(t) = 2(1 - t' / \tau), \quad \tau / 2 \leq t' \leq \tau$$

$$f_t(t) = 0, \quad \tau \leq t' \leq t_{i+1} - t$$

$$f_{xy}(x, y) = 1 - \frac{x'}{h_x} - \frac{y'}{h_y}, \quad 0 \leq x' \equiv x - x_i \leq h_x, \quad 0 \leq y' \equiv y - y_i \leq h_y \left(1 - \frac{x'}{h_x} \right)$$

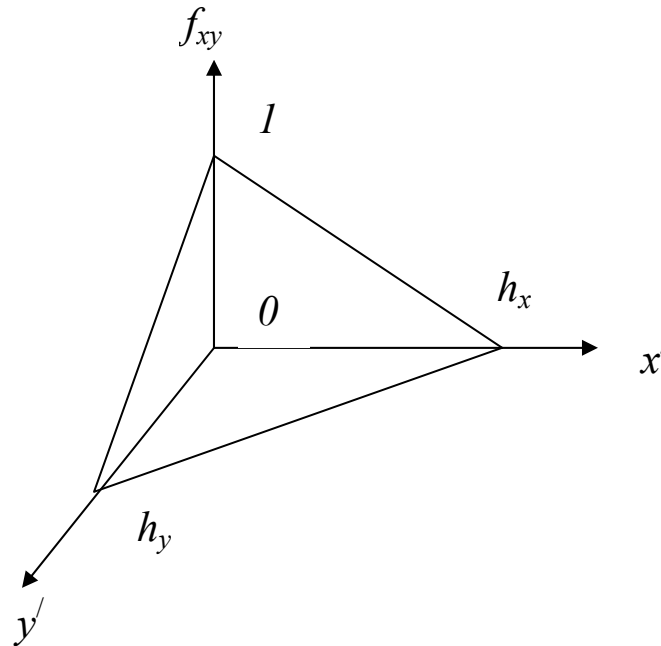


Fig. 2.4.3.1

Here $E = E^* / (\rho_\infty^* u_\infty^{*3} l^* t_0^*)$, E^* (J/m) is the energy of a single pulse on one electrode per length unit, $\tau = \tau^* / t_0^*$, τ^* is the duration of one pulse, h_x and h_y are the non-dimensional scales of every volume source in the x - and y - directions respectively, F_{x0} and F_{y0} are the maximum values of the corresponding components of the volume force, t_i is the time of the beginning of the i -th pulse ($t_1 = 0$), x_i is the coordinate of trailing edge of the i -th electrode. The form of the function f_{xy} is presented in Fig.2.4.3.1.

Calculation of flat plate boundary layer.

Statement of the boundary value problem. The air flow over a flat plate of the length l^* is considered. A set of flat electrodes is placed on the plate across an incident flow, as it is shown on Fig.2.4.3.2. An origin of the Cartesian co-ordinate system (x^*, y^*) is situated on a plate leading edge, x^* – axis is directed along a streamlined surface, and y^* – axis is perpendicular to it. The distance between downstream edges of two adjacent electrodes is constant and equal to $x_{i+1}^* - x_i^* = h_p^*$. The width both upper (active) and lower (placed into the plate) electrodes is similar too and equals h_x^* . Lower electrodes shift downstream relatively upper electrodes at a distance h_x^* . Downstream edge of the first active electrode is located at a distance x_0^* from the plate leading edge.

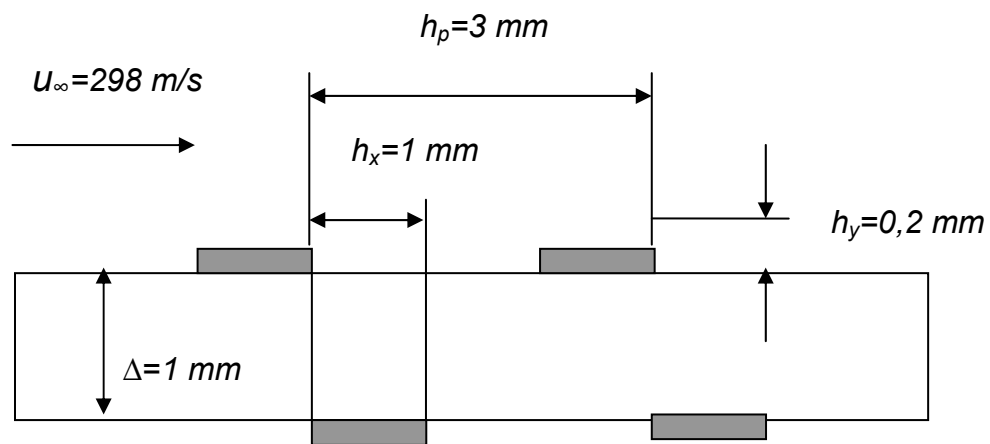


Fig.2.4.3.2. Sketch of the electrodes arrangement on a flat dielectric plate.

The statement of the boundary value problem simulating the considered flow is expounded in the previous report. Dimensionless variables and similarity criteria of the formulated problem have the following form:

$$\begin{aligned}
 t &= \frac{t^*}{t_0^*}, \quad x = \frac{x^*}{l^*}, \quad y = \frac{y^*}{l^*} \sqrt{\frac{\text{Re}}{x}}, \quad u = \frac{u^*}{u_\infty^*}, \quad v = \frac{1}{u_\infty^*} \left(\sqrt{x \text{Re}} v^* - \frac{y}{2} u^* \right) \quad (1) \\
 p &= \frac{p^*}{p_\infty^*}, \quad h = \frac{h^*}{h_\infty^*}, \quad \rho = \frac{\rho^*}{\rho_\infty^*}, \quad \mu = \frac{\mu^*}{\mu_\infty^*}, \quad D = \frac{D^*}{D_\infty^*}, \quad Q = \frac{l^*}{\rho_\infty^* u_\infty^{*3}} Q^*, \quad H = \frac{\rho_\infty^*}{u_\infty^{*2}} H^* \\
 F_x &= \frac{l^*}{\rho_\infty^* u_\infty^{*2}} F_x^*, \quad F_y = \frac{1}{\sqrt{\text{Re}}} \frac{l^*}{\rho_\infty^* u_\infty^{*2}} F_y^*, \quad E = \frac{E_{imp}^*}{\rho_\infty^* u_\infty^{*3} l^* t_0^*}, \quad \tau = \frac{\tau^*}{t_0^*} \\
 \tau_{VT} &= \frac{u_\infty^*}{l^*} \tau_{VT}^*, \quad \text{Re} = \frac{\rho_\infty^* u_\infty^* l^*}{\mu_\infty^*}, \quad \text{Sh} = \frac{l^*}{u_\infty^* t_0^*}, \quad \text{Pr} = \frac{\mu_\infty^* c_p^*}{\lambda_\infty^*}, \quad \text{Sc} = \frac{\mu_\infty^*}{\rho_\infty^* D_\infty^*}
 \end{aligned}$$

Here t^* is the time, (u^*, v^*) are the components of velocity vector along the axes (x^*, y^*) , p^* is the pressure, ρ^* is the gas density, D^* is the coefficient of diffusion, $h^* = c_p^* T^*$ is the gas enthalpy, c_p^* is the heat capacity at constant pressure, μ^* and λ^* are the coefficients of dynamic viscosity and heat conductivity of gas respectively, $\gamma = 1,4$ is the adiabatic ratio, (F_x^*, F_y^*) are the components of volume force along the axes (x^*, y^*) , Q^* is the total specific power revealed in the discharge, E_{imp}^* (J/m) is the energy of a single pulse on one electrode per length unit, H^* is the specific energy of vibrational degrees of freedom of gas molecules, t_0^* is the characteristic time, namely, time interval between the beginnings of two successive pulses of the discharge, τ_{VT}^* is the characteristic time of vibrational energy relaxation, τ^* is the duration of every pulse. The subscript ∞ denotes free stream parameters, Re, Sh, Pr, Sc are the Reynolds, Strouhal, Prandtl and Schmidt numbers.

The system of equations and boundary conditions describing boundary layer on a flat plate in non-dimensional variables (1) has the following form:

$$x \text{Sh} \frac{\partial \rho}{\partial t} + \frac{1}{2} \rho u + x \frac{\partial(\rho u)}{\partial x} + \frac{\partial(\rho v)}{\partial y} = 0 \quad (2)$$

$$\frac{\partial}{\partial y} \left(\mu \frac{\partial u}{\partial y} \right) = x \text{Sh} \rho \frac{\partial u}{\partial t} + x \rho u \frac{\partial u}{\partial x} + \rho v \frac{\partial u}{\partial y} + \frac{1}{\gamma M_\infty^2} \left(x \frac{\partial p}{\partial x} - \frac{y}{2} \frac{\partial p}{\partial y} \right) - x F_x \quad (3)$$

$$\frac{\partial p}{\partial y} = \sqrt{x} \gamma M_\infty^2 F_y, \text{ whence } p(t, x, y) = 1 - \sqrt{x} \gamma M_\infty^2 \int_y^{y_e} F_y(t, x, y') dy' \quad (4)$$

$$\begin{aligned} \frac{\partial}{\partial y} \left(\frac{\mu}{\text{Pr}} \frac{\partial h}{\partial y} \right) &= x \text{Sh} \rho \frac{\partial h}{\partial t} + x \rho u \frac{\partial h}{\partial x} + \rho v \frac{\partial h}{\partial y} - \frac{\gamma - 1}{\gamma} \left(x u \frac{\partial p}{\partial x} + v \frac{\partial p}{\partial y} \right) - \\ &- (\gamma - 1) M_\infty^2 \left[\mu \left(\frac{\partial u}{\partial y} \right)^2 + x(1 - r) Q + x \rho^2 \frac{H - H_e}{\tau_{VT}} \right] \end{aligned} \quad (5)$$

$$p = \rho h \quad (6)$$

$$\frac{\partial}{\partial y} \left(\frac{\mu}{\text{Sc}} \frac{\partial H}{\partial y} \right) = x \text{Sh} \rho \frac{\partial H}{\partial t} + x \rho u \frac{\partial H}{\partial x} + \rho v \frac{\partial H}{\partial y} - \frac{x}{\rho} \left(r Q - \rho^2 \frac{H - H_e}{\tau_{VT}} \right) \quad (7)$$

$$\mu = h^{3/2} \frac{1 + A}{h + A}, \quad A = \frac{114}{T_\infty^*}$$

$$t = 0: \quad (u, v) = (u, v)_0, \quad p = p_0, \quad h = h_0, \quad H = H_e \quad (8)$$

$$y = 0: \quad u = v = \frac{\partial H}{\partial y} = 0, \quad \sqrt{x} \text{Re Sh Pr } C_w \frac{\partial h}{\partial t} = \mu \frac{\partial h}{\partial y}, \quad C_w = \frac{C_w^*}{c_p^* \rho_\infty^* l^*} \quad (9)$$

$$y = y_e: \quad u = 1, \quad p = 1, \quad h = 1, \quad H = H_e \quad (10)$$

In equations (5) and (7) $0 \leq r \leq 1$ is the parameter which defines a part of discharge power pumping in vibrational degrees of freedom. In the last boundary condition (9) C_w^* is the heat capacity per unit surface of the plate, $H_e = 0$ in present calculations. In the initial conditions (8) the subscript 0 denotes the solution of steady-state boundary layer equation when $F_x = F_y = Q = 0$.

The time-dependent source terms modeling the force and thermal impact of the discharge are defined in the following form:

$$F_{x,y}(t, x, y) = F_{x0,y0} f_t(t) f_{xy}(x', y'), \quad Q(t, x, y) = \frac{12E}{\tau h_x h_y} f_t(t) f_{xy}(x', y')$$

$$f_t(t) = 2t' / \tau, \quad 0 \leq t' \equiv t - t_i \leq \tau / 2; \quad f_t(t) = 2(1 - t' / \tau), \quad \tau / 2 \leq t' \leq \tau$$

$$f_t(t) = 0, \quad \tau \leq t' \leq t_{i+1} - t$$

$$f_{xy}(x, y) = 1 - \frac{x'}{h_x} - \frac{y'}{h_y}, \quad 0 \leq x' \equiv x - x_i \leq h_x, \quad 0 \leq y' \equiv y - y_i \leq h_y \left(1 - \frac{x'}{h_x}\right)$$

Here h_x and h_y are the non-dimensional scales of every volume source in x - and y -directions respectively, t_i is the time of the beginning of the i -th pulse ($t_1 = 0$), the form of the function f_{xy} is presented in Fig.2.4.3.1.

Evaluation of the task parameters. One of aim of numerical simulation of the investigated complex phenomenon consists in the research of an influence of a large amount of its parameters on a prospective result, for example, the gas velocity induced by the discharge in the boundary layer. Another aim in the frame of the present work is a comparison of numerical results with experimental data described in [1]. Runing ahead, note that the second task is not solved for the time present, what will be explained below. Nevertheless, the main parameters of the formulated boundary value problem have been chosen in accordance with conditions of experiments [1].

The free stream parameters have been defined as follows: the total temperature is $T_0^* = 290$ K, the Mach number is $M_\infty = 0,95$, the static pressure is $p_\infty^* = 8 \cdot 10^4$ Pa, the plate length is $l^* = 0,1$ m, whence other parameters are defined, namely, the static pressure is $T_\infty^* = 245,7$ K, the viscosity coefficient is $\mu_\infty^* = 1,574 \cdot 10^{-5}$ kg/m s, the gas density is $\rho_\infty^* = 1,135$ kg/m³, the velocity is $u_\infty^* = 298,5$ m/s, the Reynolds number is $Re = 2,152 \cdot 10^6$. Non-dimensional distance up to first volume source is $x_0 = 0,11$, and the distance between two adjacent sources is $h_p = 0,03$. The longitudinal scale of every source corresponds approximately to the shift of lower electrode relatively upper one, the

vertical scale of the source has the order of the height of active electrode. For this reason the non-dimensional scales of the sources have been defined as $h_x = 0,01$ and $h_y = 0,002$.

The characteristic time of the vibrational energy relaxation is defined as $\tau_{VT}^* = 10^{-3}$ s, whence $\tau_{VT} = u_\infty^* \tau_{VT}^* / l^* \cong 3$. The value of the coefficient defining a part of discharge power pumping in the vibrational energy is defined as $r = 0,5$.

The energy of a single pulse has been defined as $E_{imp}^* = 2 \cdot 10^{-3}$ J/m. In this case for the frequency of pulses $n^* = 1/t_0^* = 2 \cdot 10^5$ s⁻¹ (when $t_0^* = 5 \cdot 10^{-6}$ s), the number of electrodes $N=28$ and the spanwise size of every electrode $h_z^* = 10^{-2}$ m, the total power of the discharge on the whole plate equals $W^* = E_{imp}^* n^* N h_z^* \cong 112$ W, what corresponds to experimental conditions [1]. The formula $\vec{F}^* = 1/2 \varepsilon_0^* \nabla \vec{E}^{*2}$ [2], where $\varepsilon_0^* = 8,854 \cdot 10^{-12}$ F/m is the dielectric permittivity of vacuum, \vec{E}^* is the vector of the electric field strength, has been used for an estimation of value of the volume force. For characteristic value of the electric field strength $E_0^* \cong 5 \cdot 10^6$ V/m the characteristic values of the components of the volume force vector have been estimated as $F_{x0}^* \cong \varepsilon_0^* E_0^{*2} / h_x^* \cong 2,2 \cdot 10^5$ N/m³ and $F_{y0}^* \cong -2 \varepsilon_0^* E_0^{*2} / h_y^* \cong -2,2 \cdot 10^6$ N/m³, whence $F_{x0} = 0,22$, $F_{y0} = -1,5 \cdot 10^{-3}$.

For the pulse frequency $n^* = 2 \cdot 10^5$ s⁻¹ ($t_0^* = 5 \cdot 10^{-6}$ s) taking place in experiments [1], the value of Strouhal number is equal to $Sh \cong 67$. But up to this moment it was failed to carry out calculations for so high value of Strouhal number. It is needed a further refinement of the used numerical method which was developed on the base of a method of solution of the stationary parabolic equation system [3]. In this connection the main attention in this stage was focused on a clarification of the qualitative influence of some problem parameters on the boundary layer flow.

The calculation results. The basic (first) variant of calculations was defined by the time interval between the pulses $t_0^* = 10^{-4}$ with pulse duration $\tau^* = 0,4 t_0^*$. The pulse energy was taken the same as in experiments [1], i.e. $E_{imp}^* = 2 \cdot 10^{-3}$ J/m. The set of the problem parameters in this variant was the next: $M_\infty = 0,95$, $Re = 2,152 \cdot 10^6$, $Sc = 0,9$,

$$\tau_{VT} = 3, \quad r = 0,5, \quad C_w = 1, \quad x_0 = 0,11, \quad h_p = 0,03, \quad h_x = 0,01, \quad h_y = 0,002, \\ F_{x0} = 0,22, F_{y0} = -1,5 \cdot 10^{-3}, E = 0,66 \cdot 10^{-5}, Sh = 3,35, \tau = 0,4.$$

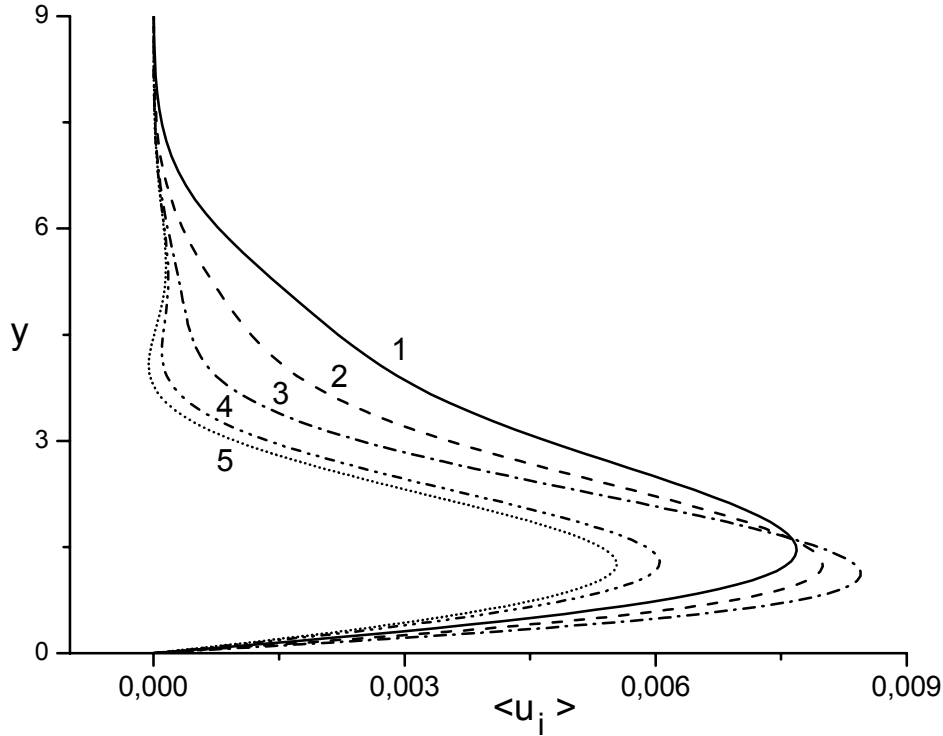


Fig.2.4.3.3. Profiles of averaged induced velocity in sections $x=0,24; 0,39; 0,54; 0,56$ (curves 1-4).

As calculations shown, the solution comes to almost time-periodic regime after 10 pulses. Along with the instantaneous parameters of the boundary layer, the values of the induced velocity as well as the gas temperature averaged during interval between 10th and 11th pulses have been calculated according to (the moment $t=9$ corresponds to the beginning of the 10th pulse):

$$\langle u_i \rangle = \int_9^{10} [u(x, y, t) - u_0(x, y)] dt, \quad \langle T \rangle = \int_9^{10} T(x, y, t) dt$$

Profiles of the averaged induced velocity obtained in 4 boundary layer sections are shown in Fig.2.4.3.3. The sections $x=0,24; 0,39; 0,54$ correspond to the ends of the volume sources besides 5th, 10th, and 15th electrodes respectively. One can see, that the maximum value of the induced velocity increases slightly with the increase of the number of sources,

and the region of the discharge influence converges. The latter is connected with the thickening of the boundary layer at a constant height of the sources. The last section $x=0,56$ separated up to 2 mm from the end of the 15th source. It is clear that the effect of the discharge influence decreases visibly even at so short distance.

The thermal influence of the discharge on the boundary layer is weak at the considered discharge power, as Fig.2.4.3.4 demonstrates, where the profiles of the averaged gas temperature are plotted in the same sections as in Fig.2.4.3.3. Insignificant temperature increase is observed near the plate surface and heat flux to its surface appears as a consequence of this temperature rise. This heat flux does not lead to remarkable change of the plate owing to its finite heat capacity.

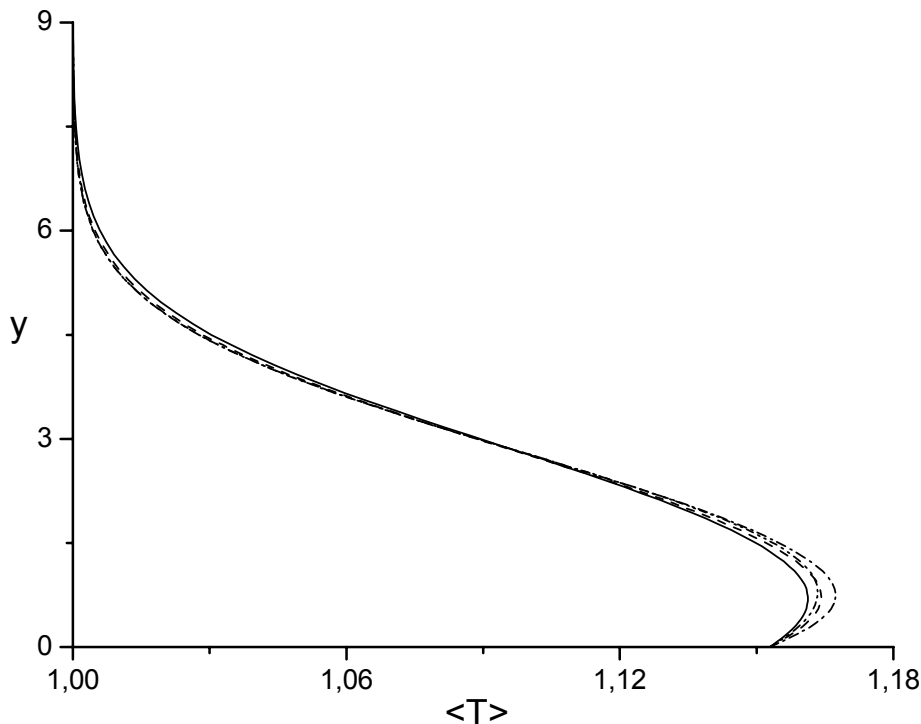


Fig.2.4.3.4. Profiles of the averaged gas temperature.

Figs.2.5.2.5-7 demonstrate the profiles of the instantaneous induced velocity in 3 boundary layer sections in various time moments. The curves 1 correspond to the moment $t_1 = 9 + 0,5\tau$, i.e. the middle of 10th pulse, when the source intensity is maximum; the curves 2 correspond to the moment $t_2 = 9 + \tau$, i.e. the end of 10th pulse; the curves 3 correspond to

the moment $t_3 = 9 + (1 + \tau)/2$, i.e. the middle of the “silence” interval between pulses; the curves 4 correspond to the moment $t_4 = 10$, i.e. immediately before the next pulse beginning.

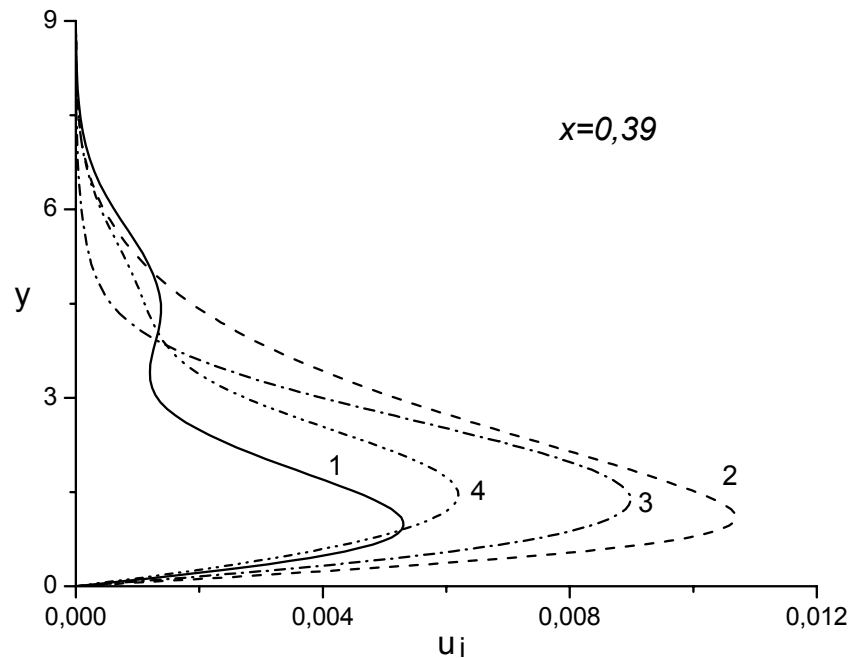


Fig.2.4.3.5. Profiles of the instantaneous induced velocity behind 10th source.

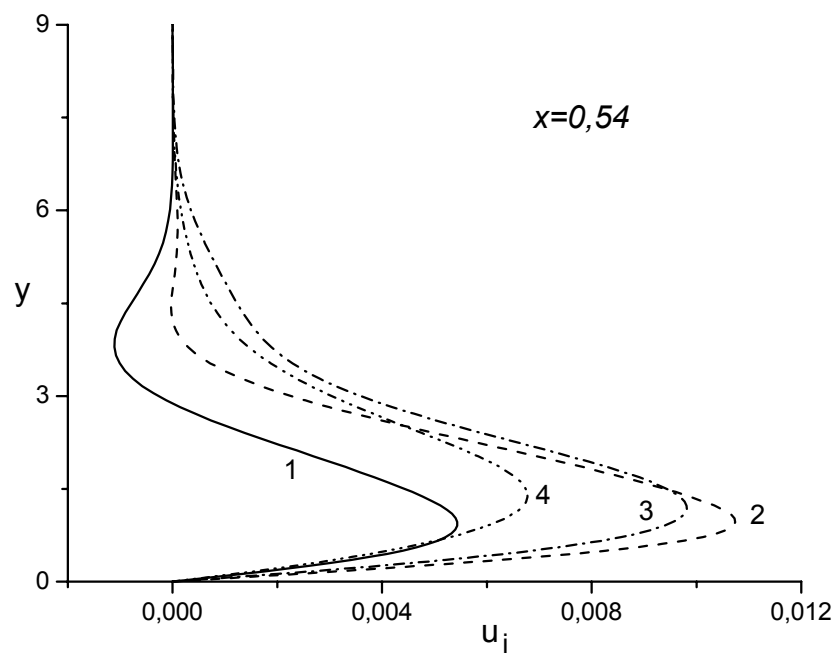


Fig.2.4.3.6. Profiles of the instantaneous induced velocity behind 15th source.

One can see, that behind both 10th and 15th sources the maximum induced velocity is achieved in the moment of the pulse end (curves 2), and the minimum velocity is achieved in the moment of maximum source intensity (curves 1). The induced velocity gradually fades after the pulse. The negative values of the induced velocity are observed behind 15th source in the moment of the maximum pulse intensity.

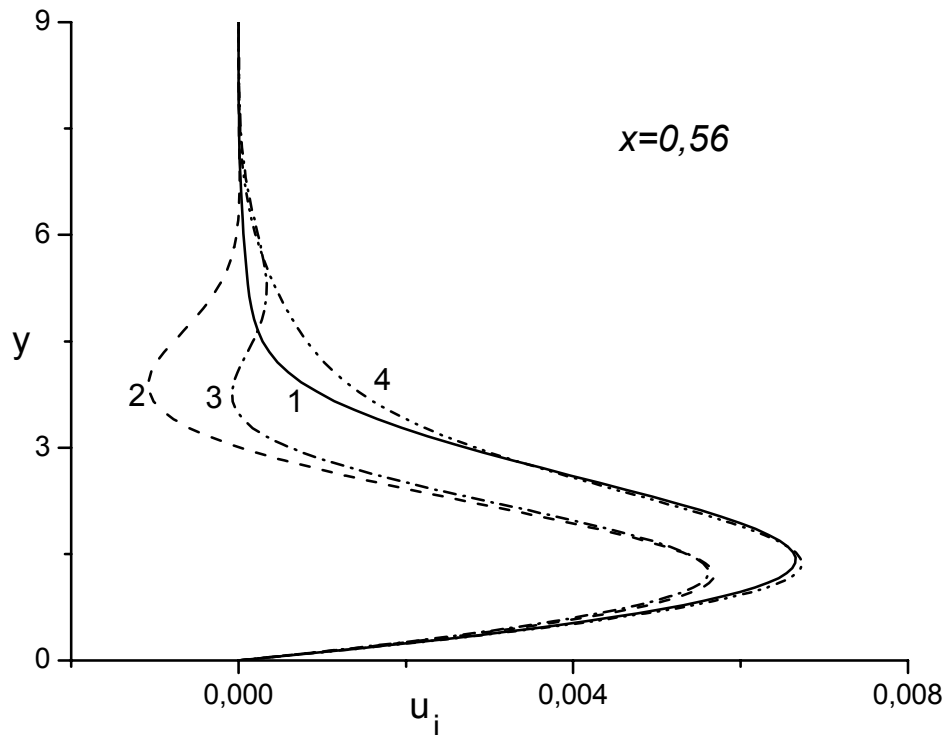


Fig.2.4.3.7. Profiles of the instantaneous induced velocity at a distance from 15th source.

In the last section $x=0,56$ the maximum value of the induced velocity vary insignificantly during considered interval and the negative induced velocity appears immediately after the pulse end.

The presented results show an extremely complex influence of the pulsatile volume force sources on the boundary layer both in space and in time.

In second variant of calculations the pulse frequency was increased two times, i.e. the interval between pulses was diminished down to $t_0^* = 5 \cdot 10^{-5}$ sec, with a decrease of pulse duration two times and a conservation of parameters F_{x0} и F_{y0} . In this case the integral momentum of volume forces remains the same as in first variant. The pulse energy was

decreased two times too. At that the discharge energy also remains constant. Thus the second variant differs from the first one only in the value of the Strouhal number $Sh = 6,7$. This increase of the Strouhal number has not been reflected on the profiles of the averaged induced velocity in sections $x=0,24; 0,39; 0,54$. Small diminishing of the velocity is visible only in the last section $x=0,56$, what is reflected by the curve 5 in the Fig.2.4.3.3. One can make preliminary conclusion that at a preservation of the integral momentum of volume forces the influence on the boundary layer depends on the pulse frequency weakly. But for final conclusion it is needed to consider the influence of the Strouhal number in more wide range of its variation.

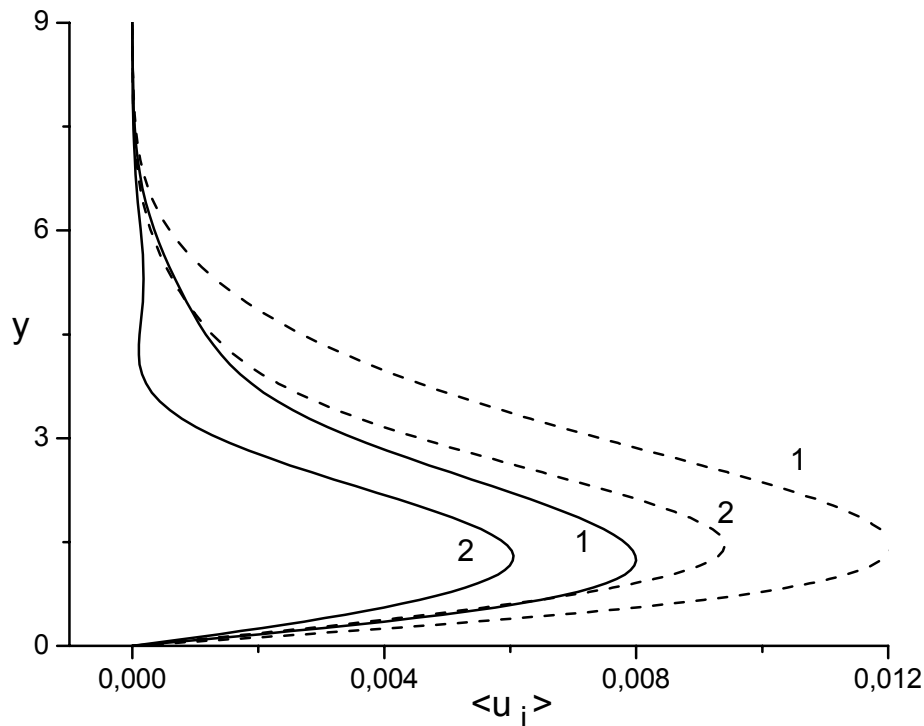


Fig.2.4.3.8. Influence of the longitudinal force F_x on averaged induced velocity.

The influence of the longitudinal force was estimated in the third variant. All parameters corresponded to the first variant except the parameter $F_{x0} = 0,44$ (the increase two times). Profiles of averaged velocity are shown in Fig.2.4.3.8 in sections $x=0,39$ (curves 1) and $x=0,56$ (curves 2) for $F_{x0} = 0,22$ (solid curves) and for $F_{x0} = 0,44$ (dashed curves). One can see that, the increase two times of the longitudinal accelerating force results

in the increase of the maximum induced velocity up to approximately 1,5 times in both sections. This effect seems to be sufficiently evident.

The fourth variant differs from the first one only by the parameter $F_{y0} = -0,003$, i.e. the increase two times an absolute value of the vertical pressing force. The result of the influence of this parameter is reflected in Fig.2.4.3.9 where the same symbols are used as in Fig.2.4.3.8. It is evident, that the impact of the pressing force is more significant than accelerating one: the increase of the parameter F_{y0} two times leads to the same increase of the maximum induced velocity.

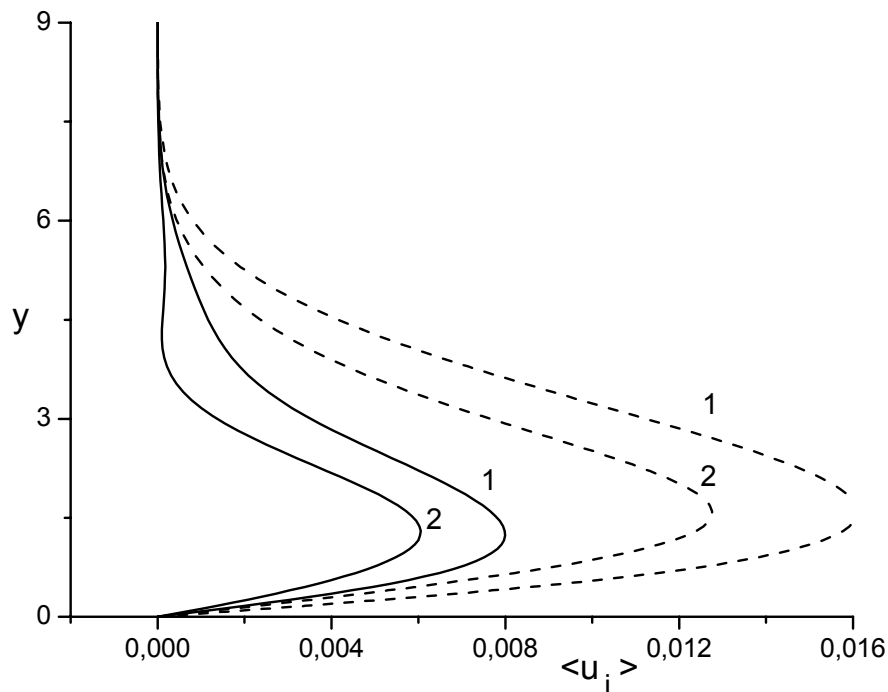


Fig.2.4.3.9. Influence of the vertical force F_y on induced velocity.

The influence of the relative pulse duration τ was found highly unexpected. Fig.2.4.3.10 demonstrates the profiles of the averaged induced velocity in four sections at $\tau = 0,2$ and other parameters corresponding to the first variant. In this case the force momentum and thermal influence are decreased two times in comparison with the first variant. As a result of this, the induced velocity becomes negative in the main part of the boundary layer except narrow near wall region. The profiles of the instantaneous induced velocity in section $x=0,39$ are shown in Fig.2.4.3.11. It is difficult to give physical explanation of this phenomenon for the present.

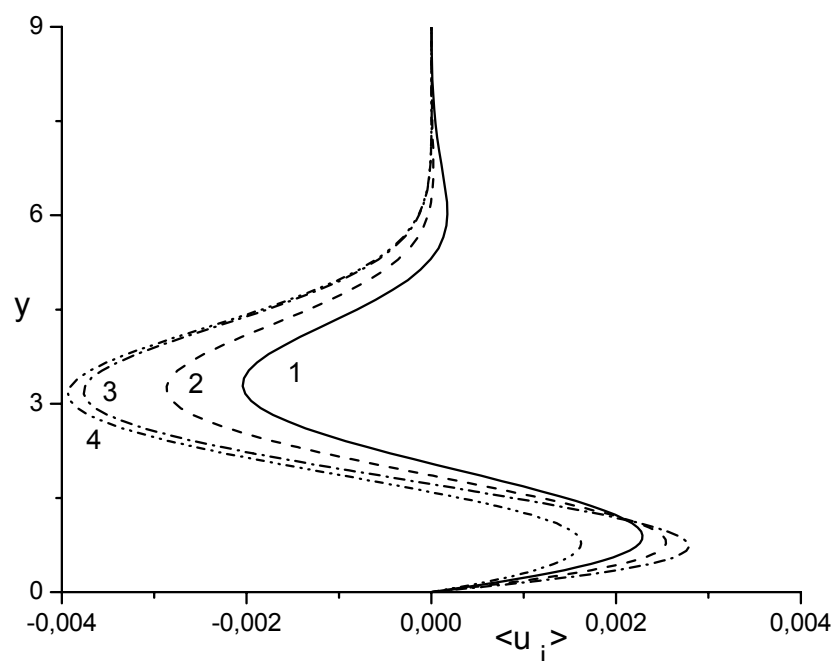


Fig.2.4.3.10. Influence of the relative pulse duration on averaged induced velocity in sections $x=0,24; 0,39; 0,54; 0,56$ (curves 1–4).

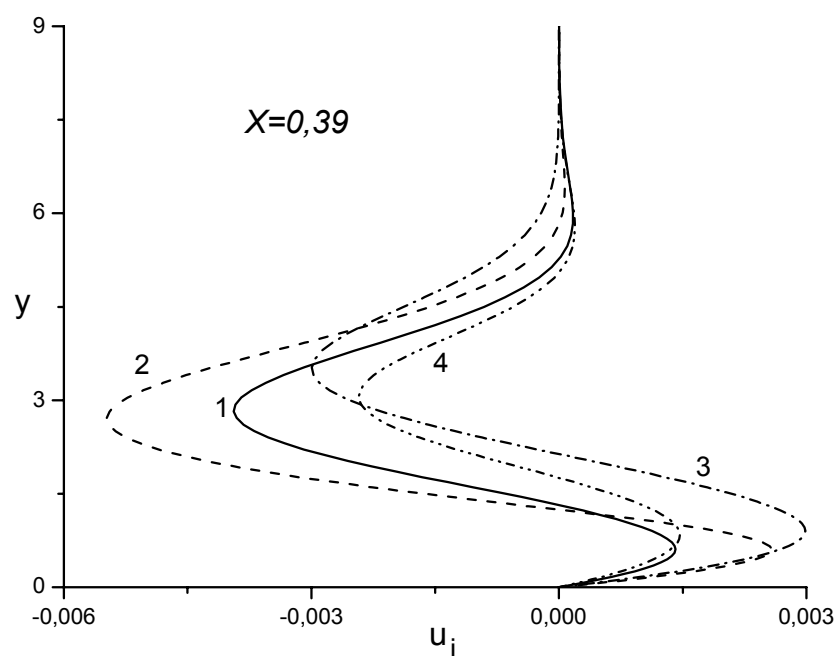


Fig.2.4.3.11. Profiles of instantaneous induced velocity at $\tau = 0,2$. Symbols correspond to Fig.2.4.3.5.

Some important remarks. Dielectric barrier discharge (DBD) seems to be prospective for an application with the aim, for example, of laminar-turbulent transition delay owing to gas acceleration in the boundary layer. Attraction of this discharge in comparison with, for example, DC corona discharge consists in a possibility of its relatively simple realization on sufficiently lengthy downstream part of a streamlined surface. As numerical estimation shows [4], it is sufficient to accelerate the laminar boundary layer up to some percents of the free stream velocity for transition delay. This acceleration seemingly may be achieved in the DBD. But the considered above results of the theoretical research, which, of course, are preliminary, indicate some difficulties on a way of DBD application for laminar-turbulent transition control.

First of all, as can see in Figs.2.5.2.3, 5, 6, the pulsations of the induced velocity are not small but of the order of its averaged value. Even for the discharge frequencies far enough from the characteristic frequencies of the Tollmien-Schlichting waves responsible for transition (what is needed evidently), so large disturbances of the induced velocity can result to more early transition without its linear stage. Secondly, the discharge regime corresponding to the last variant of calculations (Figs.2.5.2.10, 11) definitely will lead to a decrease of the boundary layer stability because the negative effect of gas braking in the main part of the boundary layer certainly will suppress the positive effect of gas acceleration in the narrow near wall region.

These remarks are not the demonstration of the pessimism in no circumstances. But they only emphasize the necessity of thorough both experimental and theoretical research of this complex and interesting phenomenon.

Estimation of an influence of the discharge frequency.

Task parameters definition. During this stage calculations of the flat plate laminar boundary layer have been executed under modeling of the DBD action on the boundary layer in the frame of the boundary value problem formulated in previous stage of research. Geometry of DBD electrodes is shown in Fig.2.4.3.12.

The free stream parameters have been defined the same as in previous calculations: follows the total temperature is $T_0^* = 290$ K, the Mach number is $M_\infty = 0,95$, the static pressure is $p_\infty^* = 8 \cdot 10^4$ Па, the plate length is $l^* = 0,1$ м (characteristic length scale), the static pressure is $T_\infty^* = 245,7$ K, the viscosity coefficient is $\mu_\infty^* = 1,574 \cdot 10^{-5}$ kg/m s, the

gas density is $\rho_{\infty}^* = 1,135 \text{ kg/m}^3$, the velocity is $u_{\infty}^* = 298,5 \text{ m/s}$, the Reynolds number is $Re = 2,152 \cdot 10^6$. Non-dimensional distance up to the first volume source is $x_0 = 0,11$, and the distance between two adjacent sources is $h_p = 0,03$. The non-dimensional longitudinal and vertical scales of the sources are $h_x = 0,01$ и $h_y = 0,002$ respectively. The non-dimensional time of the vibrational energy relaxation is defined as $\tau_{VT} = u_{\infty}^* \tau_{VT}^* / l^* \cong 3$. The single pulse energy $E_{imp}^* = 2 \cdot 10^{-3} \text{ J/m}$ and the maximum values of the volume force components $F_{x0}^* \cong \varepsilon_0^* E_0^{*2} / h_x^* \cong 2,2 \cdot 10^5 \text{ N/m}^3$ and $F_{y0}^* \cong -2\varepsilon_0^* E_0^{*2} / h_y^* \cong -2,2 \cdot 10^6 \text{ N/m}^3$ remained invariable too.

Calculations fulfillment at pulse frequency $n^* = 1/t_0^* = 2 \cdot 10^5 \text{ s}^{-1}$ (characteristic time of the task is $t_0^* = 5 \cdot 10^{-6} \text{ s}$) used in experiments [1] was the main purpose of this research stage. At $t_0^* = 5 \cdot 10^{-6} \text{ s}$ the value of non-dimensional parameter of source power equals $E = \frac{E_{imp}^*}{\rho_{\infty}^* u_{\infty}^{*3} l^* t_0^*} = 2,64 \cdot 10^{-4}$, and the Strouhal number is equal to $Sh=67$. Pulse duration equals $\tau^* = 0,4t_0^*$.

So, the values of task parameters are defined as follows: $M_{\infty} = 0,95$, $Re = 2,152 \cdot 10^6$, $Sc = 0,9$, $\tau_{VT} = 3$, $C_w = 1$, $x_0 = 0,11$, $h_p = 0,03$, $h_x = 0,01$, $h_y = 0,002$, $F_{x0} = 0,22$, $F_{y0} = -1,5 \cdot 10^{-3}$, $Sh = 67$, $\tau = 0,4$.

The Strouhal number influence. In this section the results of calculations carried out in the absence of energy input in the boundary layer, i. e. $E=0$ are described.

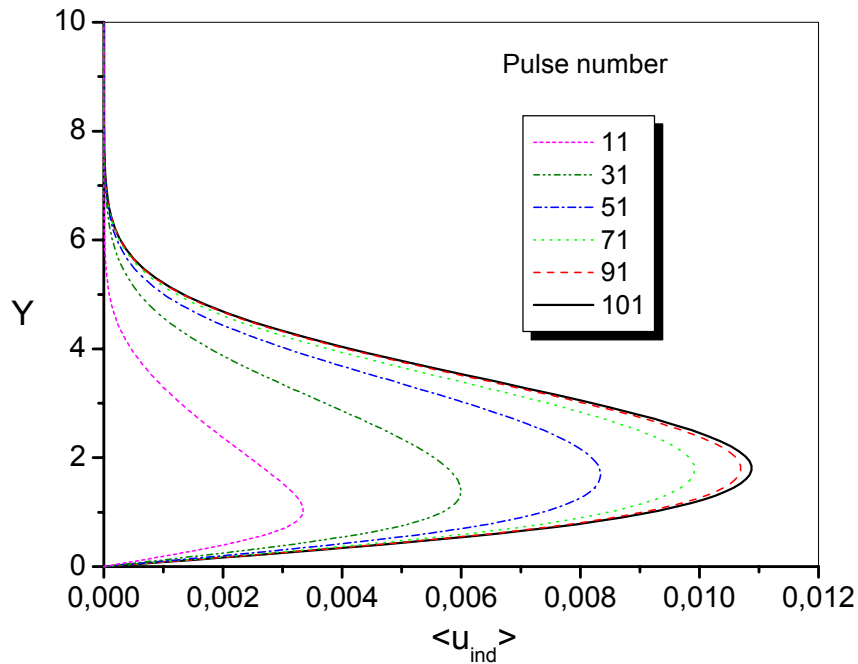


Fig.2.4.3.13. Establishment of the averaged induced velocity behind 12th source.

Note, that in previous calculations carried out at the Strouhal number $Sh = 6,7$, the solution achieved quasi-periodical regime (when flow parameters averaged during a time period between two pulses are independent on pulse number) after 10 pulses. When the Strouhal number increases up to order, the solution achieves quasi-steady regime after about 100 pulses, what Fig.2.4.3.13 demonstrates. Here the profiles of induced velocity averaged during the time period between two successive pulses behind 12th ($x=0,45$) are shown for various pulse numbers.

Fig.2.4.3.14 demonstrates the profiles of averaged induced velocity in different boundary layer sections, namely immediately behind 4th ($x=0,21$), 8th ($x=0,33$), 12th ($x=0,45$) sources and at distance of the 12th source end ($x=0,47$). As it was expected, the discharge force action monotone increases with an increase of source number. The forcing stopping leads to attenuation of the induced velocity (section $x=0,47$).

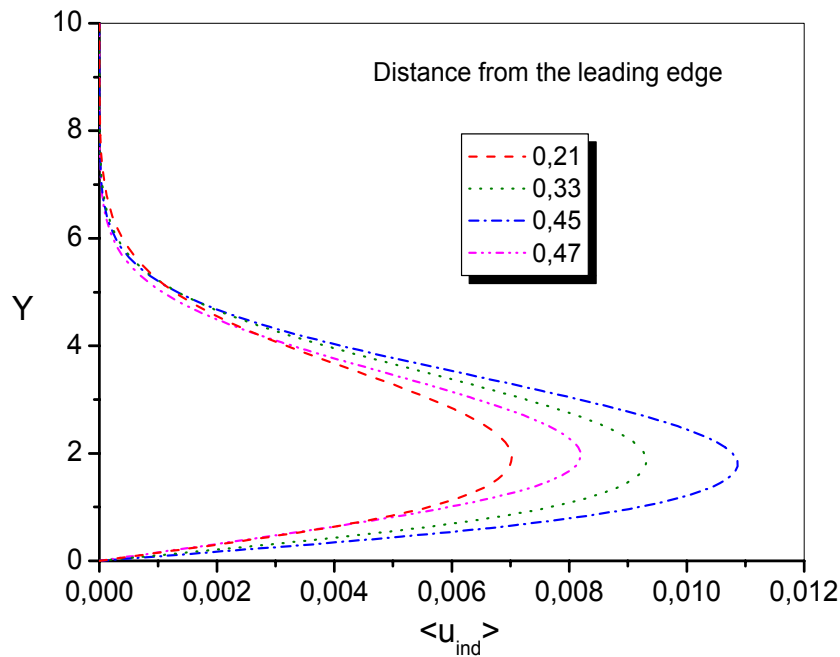


Fig.2.4.3.14. The induced velocity v.s. the distance from the plate leading edge.

As the present calculations shown, the main effect of the discharge frequency increase (the increase of the Strouhal number up to the order) consists in an achievement of quasi-steady regime of the boundary layer flow when flow parameters are almost independent on time, for example, fluctuations of the induced velocity don't exceed 0,1% in an interval between pulses. Remind, that at Strouhal number $Sh=6,7$ the variations of the maximum value of induced velocity between pulses achieved about 100%. The mentioned effect of the discharge frequency increase can has very important significance in the case of DBD application for boundary layer laminarization.

The second remarkable effect of the discharge frequency increase consists in an increase of the induced velocity in the boundary layer, what Fig.2.4.3.15 demonstrates. Here the profiles of averaged induced velocity immediately behind 8th and 12th sources at $Sh=67$ and behind 10th source at $Sh=6,7$ are shown.

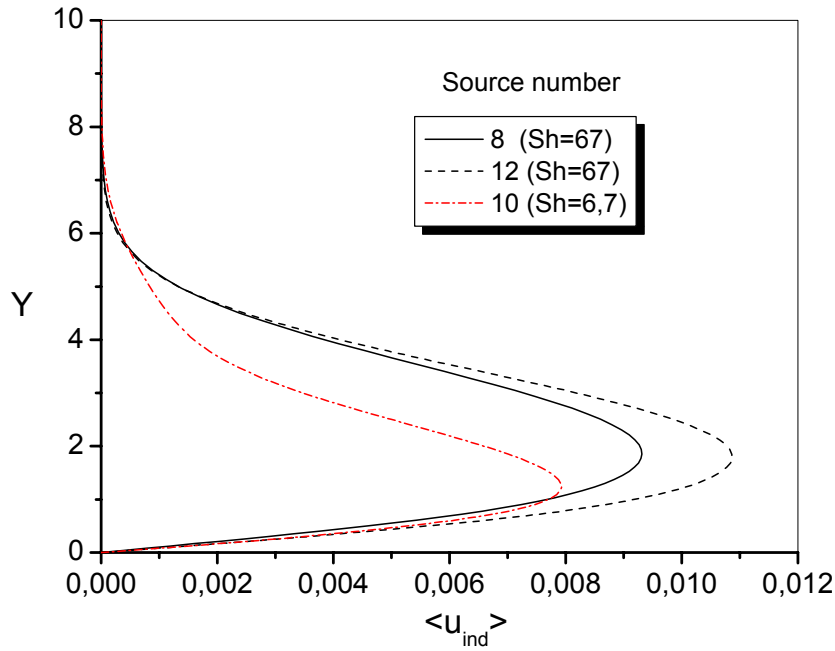


Fig.2.4.3.15. Influence of the Strouhal number on induced velocity.

As one can see from Fig.2.4.3.15, the maximum value of $\langle u_{ind} \rangle$ behind 10th source equals about 0,01 for $Sh=67$ and 0,008 for $Sh=6,7$. So, the discharge frequency increase up to the order results in induced velocity increase about up to 20%. Note, that the increase of the pulses frequency at a preservation of their relative duration $\tau = \tau^* / t_0^*$ and maximum values of the volume force components F_{x0} and F_{y0} doesn't change the value of the averaged force action on the boundary layer

$$\langle \vec{F}^* \rangle = \frac{1}{\Delta t^*} \int_{t^*}^{t^* + \Delta t^*} \vec{F}^* dt^*, \quad \Delta t^* \gg t_0^*$$

This circumstance explains not very significant influence of the Strouhal number on induced velocity.

Thermal influence of the discharge. It was pointed out in previous report that thermal influence of the DBD on boundary layer flow is insignificant. It is necessary to recognize this conclusion as wrong.

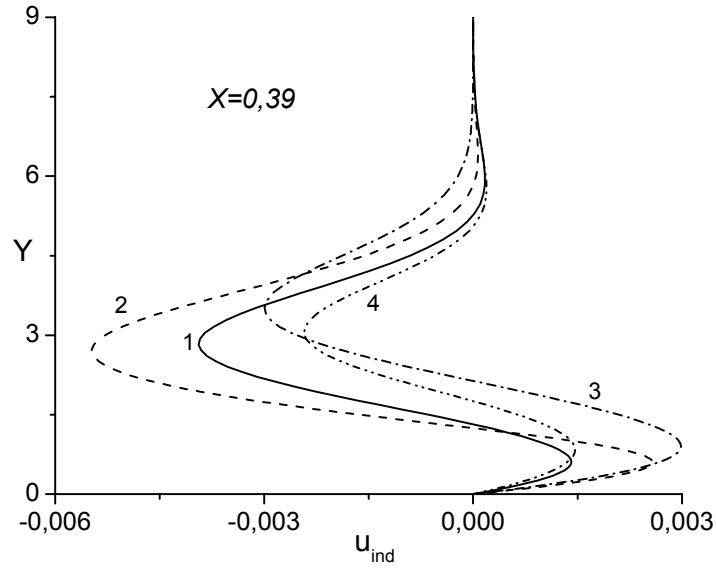


Fig.2.4.3.16. Profiles of the instantaneous induced velocity at $Sh=3,35$,
 $E = 0,66 \cdot 10^{-5}$ and $\tau = 0,2$.

Fig.2.4.3.16 demonstrates data from the previous report. The induced velocity was positive in all boundary layer sections in calculations conducted at $Sh=3,35$, $E = 0,66 \cdot 10^{-5}$ and $\tau = 0,4$ (variant 1). A decrease of the relative pulse duration down to $\tau = 0,2$ with the conservation all other task parameters results in an appearance of the negative values of the induced velocity according to Fig.2.4.3.16. In this case the force momentum decreases up two times as compared with variant 1 and the energy input remains the same.

The behavior of the induced velocity shown in Fig.2.4.3.16 is explained as follows. Convective terms in the longitudinal momentum equation can be neglected in the near-wall region $y \rightarrow 0$ and this equation takes the following form:

$$\mu^* \frac{\partial^2 u^*}{\partial y^{*2}} \approx -\frac{\partial \mu^*}{\partial T^*} \frac{\partial T^*}{\partial y^*} \frac{\partial u^*}{\partial y^*} + \frac{\partial p^*}{\partial x^*} - F_x^* \quad (1)$$

The absolute value of the curvature of the velocity profile will increase at a discharge action due to the presence of the positive temperature gradient, positive longitudinal volume force F_x , and negative longitudinal pressure gradient induced by the compressing volume

force F_y which decreases linear downstream. Therefore the induced velocity will be positive in this region.

The gas temperature increases with a moving from the wall and the gas density decreases. Some pressure increase given by volume force F_y doesn't compensate the density drop due to the heating. This decrease of the gas density leads to the boundary layer thickening. At that the stream-lines corresponding to some fixed values of the longitudinal velocity move from the wall. As a consequence of the boundary layer thickening a difference of the longitudinal velocities of disturbed and undisturbed flows will be negative at fixed distance from the wall. Thus thermal influence of the DBD at a deficient volume force momentum can prevail over its force action resulting in an appearance of negative induced velocity.

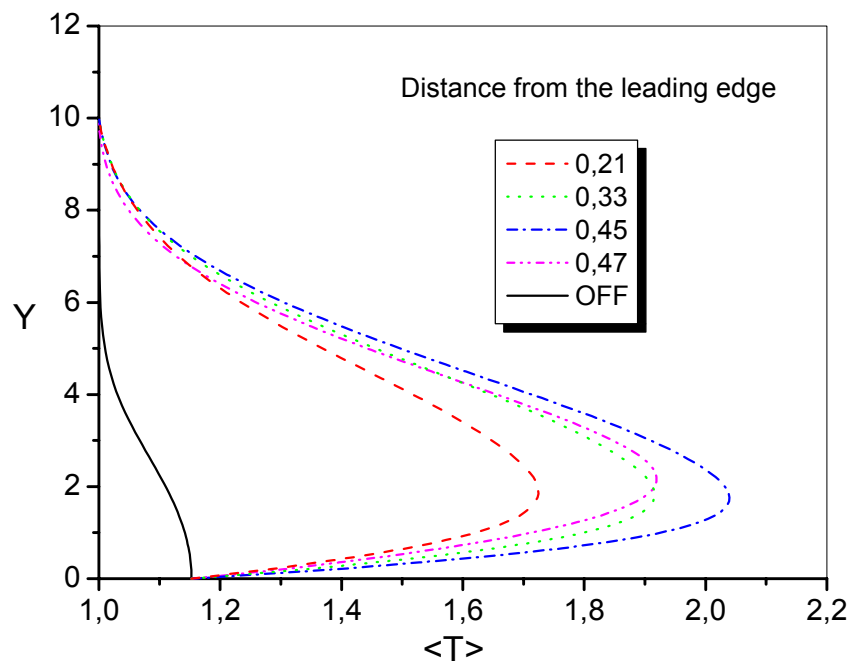


Fig.2.4.3.17. Profiles of the boundary layer temperature.

This conclusion is confirmed distinctly by calculations carried out at non-dimensional source power $E = 2,64 \cdot 10^{-4}$ and a coefficient defining the part of total energy incoming in translational degrees of freedom $r = 0,5$. Heat input in the boundary layer is greater up to the order in this case than in calculations executed in previous stage at $Sh=3,35$.

Fig.2.4.3.17. presents the gas temperature profiles in various boundary layer sections with and without DBD action. It is seen, that the temperature growth is very significant and sharp in this case. The velocity profiles in the same boundary layer sections are presented in Fig.2.4.3.18.

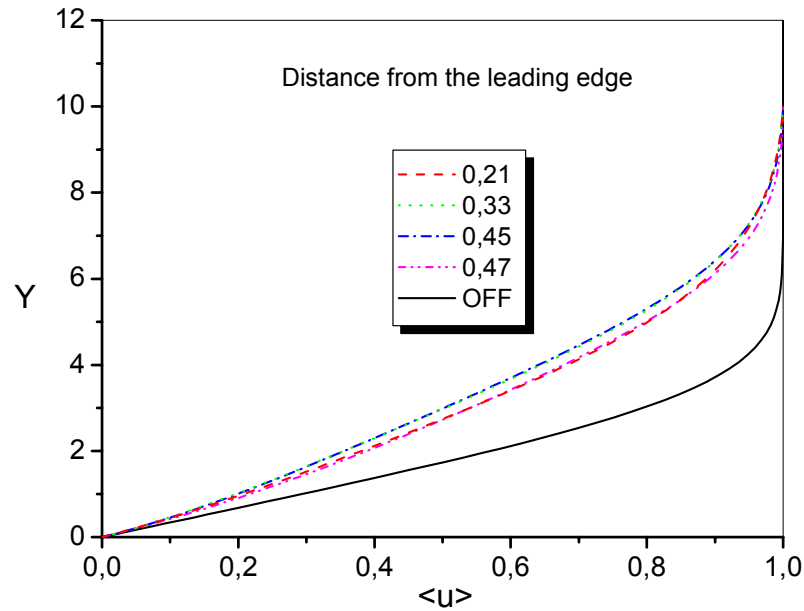


Fig.2.4.3.18. Velocity profiles.

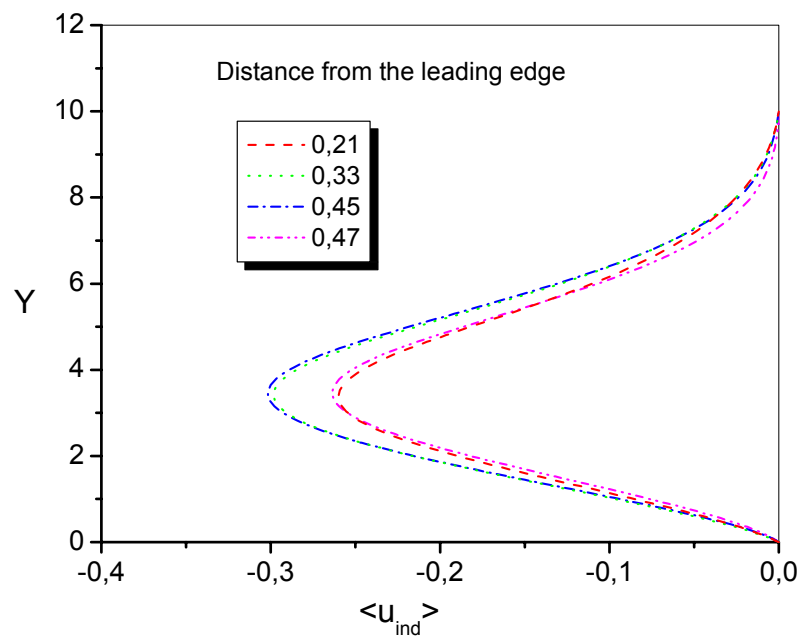


Fig.2.4.3.19. Induced velocity profiles.

The gas density decrease due to the heat input and corresponding boundary layer thickening are so significant in this case that induced velocity becomes negative across the whole boundary layer thickness what Fig.2.4.3.19 shows.

Conclusion. The main effect of the significant increase of the discharge frequency consists in an attainment of quasi-steady regime of the boundary layer flow. Fluctuations of flow parameters are very negligible in this case and it is an essential factor for DBD application for boundary layer laminar-turbulent transition control.

The discharge frequency increase up to the order with the preservation of the averaged force momentum results in an increase of maximum values of the induced velocity up to about 20%.

Thermal influence of the DBD on boundary layer at a deficient volume force momentum can prevail over its force action resulting in an appearance of negative induced velocity as a consequence of gas heating and boundary layer thickening.

References to section 2.4.3.

1. Leonov S., Yarantsev D., Kuryachii A., Yuriev A. Study of Friction and Separation Control by Surface Plasma // AIAA 2004-0512. 2004. 8p.
2. Roth J.R., Sherman D., Wilkinson D. Boundary-Layer Flow Control with One Atmosphere Uniform Glow Discharge Surface Plasma // AIAA-98-0328. 1998.
3. Denisenko O., Provotorov V., "Study of the viscous gas flow at intermediate Reynolds number" // TsAGI Proceedings 1985. vol.2269. P.111-127.
4. Kazakov A.V., Kuryachii A.P. Estimate of the Effectiveness of the Electrogasdynamic Method for Reducing Aerodynamic Drag // Fluid Dynamics. Vol. 36. No. 2. 2001. P. 236-243.

3. Conclusion.

3.1. Conclusion.

Two main aspects were aimed by this work and sequentially have been described in this Report: the features of the surface plasma generation in high-speed flow and such electrical discharges influence on the parameters of boundary layer including artificial separation.

It is clear that the local heat release near the surface in high-speed flow leads to boundary layer modification if the level of power is enough high. The execution of gas heating in predefined location, with needed magnitude and under high-speed dense flow is non-trivial technical problem. In the most cases it has to be done non-intrusively. The technique of electrical discharges is able to provide such characteristics. Moreover, the plasma generation is not equal to conventional heating. As a rule, the plasma structure is self-sustained with the flow structure. Besides of that the electromagnetic bulk forces can be excited inflow via the plasma of electric discharge. A scientific objective of this activity was in determination of mechanisms and features of near-surface plasma in airflow as well as in clarification of non-thermal (electrostatic, this time) mechanisms of interaction.

Several types of discharges were tested for this mean. Two arrangements were examined in details: transversal quasi-DC filamentary discharge of relaxation type, and surface dielectric barrier discharge (DBD plasma panel). These plasma generators were designed and constructed for aerodynamic applications on the base of experimental results, obtained during the previous study of pulse periodic discharges, and plasma generators of continuous and HF modulated types.

The transversal surface discharge between flush-mounted electrodes generates relatively equilibrium non-uniform unsteady plasma with significant share of heat deposition. The transversal discharge is an unstable system of relaxation type with hot plasma filaments, which moves with the flow. Such a discharge influences on the high-speed flow parameters and structure sufficiently.

From the other side the effective viscous friction reduction at reasonable power deposition requires an application of non-thermal mechanisms. There was considered that non-equilibrium surface plasma can be generated by multi-trace barrier discharge. Such a discharge can effect on the boundary layer parameters under relatively small power deposition. Now we don't see any technical limitation in manufacturing large plasma panels

on the base of multi-trace barrier MFD-HV discharge. The data on non-thermal non-equilibrium plasma behavior in high-speed flow were described.

The generation of near-surface filamentary discharge leads to significant modification of supersonic flow structure. The specific effects were demonstrated experimentally and described in publications, such as oblique shocks position and angle control, gasdynamic screening of obstacles, modification of shock's reflection, and control of flow parameters in a whole duct. The phenomenon of plasma-induced separation was described at the first time.

The control of parameters of fixed separation zone behind wall backstep was demonstrated as well. Two main regimes can be realized: expansion of circulation zone and flow mode transformation to separation-less one.

The influence of non-equilibrium plasma of DBD on flow parameters was demonstrated experimentally and simulated numerically. The separation control above a contoured airfoil was fulfilled at the flow velocity up to 30m/s. The resonant operation mode allowed us to demonstrate a weak non-thermal effect on the transonic shock position.

A large problem of plasma experiments generally and inflow specifically is the proper measurements of parameters at suitable time and spatial resolution. We paid a special attention to this. The detailed data on plasma parameters measured are shown in the Report. At the same time the specific conditions of plasma experiment forced us to apply the relatively rough methods of BL diagnostics.

The efforts were made in numerical simulation of near-surface plasma interaction with high-speed flow. Unfortunately, conventional gasdynamic approach didn't award a satisfactory agreement with experimental data. It seems that the applied model of plasma-gas interaction has to be adjusted deeply.

In the most condensed manner the results of the last three-year efforts can be formulated as following:

The plasma generators of filamentary type were designed and tested.

Structural evolution of plasma filaments at interaction with airflow has been studied.

Measuring system and application software have been made. Main parameters of plasma were measured.

The experimental apparatus was modified for test on viscous friction and separation control by filamentary and barrier-discharge plasma.

Numerous short-time wind tunnel's runs were fulfilled for examination of plasma effect on boundary layer conditions.

The specific effects of electrical discharges on near-surface layer in high-speed dense flow have been described in details. The plasma-induced artificial separation was demonstrated.

Non-thermal mechanisms of DBD interaction with gas flow have been investigated at subsonic speed. Weak influence of DBD plasma panel on BL characteristics at high-speed flow was considered in sensitive aerodynamic situations.

The numerical simulation was done of thermal and non-thermal effects on BL. A significant enhancement of CFD methodic is considered to be required.

Analysis of experimental data was done. The results were described in the Report.


3.2. Applications.

(A) "The Principal Investigator, Dr. Sergey Leonov, hereby declares that, to the best of its knowledge and belief, the technical data delivered herewith under ISTC Project No. 2084P is complete, accurate, and complies with all requirements of the contract."

(B) "Any opinions, findings and conclusions or recommendations expressed in this Report are those of the authors and do not necessarily reflect the views of any other persons and organizations."

DATE: _____November, 25, 2004_____

Dr. Sergey Leonov, Project Manager/Principal Investigator

A handwritten signature in black ink, appearing to be 'S. Leonov', written over a horizontal line.

Attachment 1.

Summary of publications.

S. Leonov, V. Bityurin, K. Savelkin, D. Yarantsev *“Effect of Electrical Discharge on Separation Processes and Shocks Position in Supersonic Airflow.”* 40th AIAA Aerospace Sciences Meeting & Exhibit, 13-17 January 2002 / Reno, NV, AIAA 2002-0355.

The paper analyses and discusses results of the last experimental works on influence of near-surface plasma formation on characteristics of separation zones and position of related shocks in high-speed airflow. Two different two-dimensional gasdynamic configurations have been tested: wall step and cline surface with angle 15-25 degrees. The study of the first configuration is important for base drag modification, and combustion processes at the separation, for instance. The study of the second configuration is important for a prediction of energy release result in a supersonic and hypersonic diffuser, for instance.

S. Leonov, V. Bityurin, K. Savelkin, D. VanWie D. Yarantsev , *“Hydrocarbon Fuel Ignition in Separation Zone of High Speed Duct by Discharge Plasma.”* Proceedings of 4th Workshop on Magneto Plasma Aerodynamics in Aerospace Applications, Moscow, IVTAN, April 2002.

The possibility of the fuel ignition at low temperature flow has been demonstrated. Experiments show that the volume and structure of separation zone are changed significantly due to plasma influence and the fuel combustion as well as gas parameters inside the zone depending on parameters of electrical discharge. The data on gas temperature inside of a separation area are given. Different variants of plasma ignition are discussed, including under the condition of artificial local separation zones.

S. Leonov, V. Bityurin, K. Savelkin, D. Yarantsev *“The Features of Electro-Discharge Plasma Control of High-Speed Gas Flows.”* AIAA-2002-2180, 33-th Plasmadynamic and Laser Conference, 20-24 May, 2002, Maui, HI.

The results of resent experimental works on influence of non-uniform plasma formations on characteristics of near-wall layers and separated areas in high-speed airflow are discussed in the paper. Experimental results are being presented, which are obtained at condition of small-scale model duct. Surface electrical discharge in different modes at variation of the power input is investigated. The discharge properties and structure are studied

as well as the change of the gasdynamic structure of the flow due to electric discharge excitation. Images of the flow interaction with the plasma layer observed by the Schlieren method are shown. The effect of artificial flow separation by the plasma energy deposition is demonstrated. The result, which is appeared in pressure redistribution in aerodynamic channel, is presented. Applications of the surface type of electric discharge for the flow modification in ducts and inlets are discussed. The work has been fulfilled in frames of Advance Flow/Flight Control (AFFC) concept.

S. Leonov, V. Bityurin, A. Klimov ***“Effectiveness of Plasma Method of Flow/Flight Control.”*** Proceedings of the Symposium on Thermal-Chemical Processes, St-Petersburg, “Leninets”, July, 2002.

The content of this paper is confined by the problem of aerodynamic drag reduction as the most popular in discussions last 10 years. From the other side such an approach allows one to consider important patterns in field of energetic method's application. The criterion of energy deposition effectiveness is defined more precisely. A short historical survey and the most important results of the last researches in this field are presented. An alternative to electrical discharge plasma method is proposed. Brief discussion on a scaling law is presented. The conclusions on the effectiveness of drag reduction by plasma are done. The results presented here are a part of extensive work on plasma formation influence on aerodynamic characteristics of models under the conditions of wind tunnels. Last years there were several attempts to organize a flight test. Unfortunately now there no any evidences on plasma behavior and effect in real flying system. So, all conclusions have a preliminary and prognostic nature.

S. Leonov, V. Bityurin ***“Hypersonic/Supersonic Flow Control by Electro-Discharge Plasma Application.”*** 11th AIAA/AAAF International Symposium Space Planes and Hypersonic Systems and Technologies, Orléans, 29 September – 4 October, 2002, AIAA-2002-5209.

Last time the possibilities of the electric discharge plasma application for flow control and enhancement of the characteristics of the external and internal flows are discussed widely. Results of the analysis show that the discharge plasma influents on the high-enthalpy flow on non-evident manner. This paper analyses the results of experimental work on effect of energy release from special organized surface electrical discharge on characteristics of duct-driven flows. Two gasdynamic configurations are under the examination: the separation area near

wall backstep and the channel with the constant cross-section. In the first case the experiments show that the volume and structure of the fixed separation zone are changed significantly due to plasma influence. The effect of the hydrocarbon fuel ignition at low temperature flow is demonstrated. In the second case the artificial separation effect as the result of the surface plasma generation is considered. The appropriate criteria are described. The scheme of plasma method for flame stabilization under the off-design operation is discussed.

S. Leonov, V. Bityurin, K. Savelkin, D. Yarantsev (IVTAN, Moscow). ***Progress in Investigation for Plasma Control of Duct-Driven Flows***. AIAA-2003-0699, 41th AIAA Aerospace Science Meeting and Exhibit, Reno, NV, January, 2003

This paper presents and discusses the results of experiments on the influence of specially organized electrical discharges on duct-driven flow characteristics. The ability of the plasma technology in the field of supersonic flow control has been demonstrated experimentally. It was done in two aspects: control of the structure and the parameters of the duct-driven flows and control of the shocks position in inlet-like configuration. A simplified model of the surface plasma effect on flow is proposed. It is shown that such a model gives a good result in comparison with the experimental data. A consequence of the surface plasma generation for whole duct is evaluated.

S. Leonov, V. Bityurin, D. Yarantsev (IVTAN, Moscow). ***The Effect of Plasma Induced Separation***. AIAA-2003-3853, 34th AIAA Plasmadynamics and Laser Conference, 23-26 June/ Orlando, FL

This work summarizes several experimental results on the plasma-induced separation effect in high-speed flow. It could be related to the fields of Weakly Ionized Plasma and Flow Control. Three different cases (levels of flow modification) were considered: subsonic plasma layer generation, local separation with reattachment and extensive separation zone creation. The required power level for each type of effect is defined experimentally. The effect of obstacle screening is considered as well. It is appears due to upstream flow separation. The control of parameters of fixed separation zone behind wall backstep is demonstrated. Two main regimes can be realized: expansion of circulation zone and transformation to separation-less mode. Those have been proved by numerical simulations.

Sergey B. Leonov, Institute of High Temperature RAS, Moscow. ***Plasma Assistance in Supersonic Combustion***. ONERA-CNRS Seminar, March 31 – April 01, 2003.

The paper is dedicated to the experimental demonstration of plasma technology abilities in the field of high-speed combustion. It is doing in three principal directions: control of the structure and the parameters of the duct-driven flows; the ignition of air-fuel composition at low mean gas temperature; and the mixing intensification inflow.

Global separation and unsteady local separation in duct-driven flow due to the surface plasma generation have been demonstrated experimentally. It can be used, probably, as the agent of the flame stabilization. The effect of plasma-induced ignition in non-premixed high-speed flow has been demonstrated under the conditions of fixed zone of separation. The energetic criteria have been found out. The plasma intensified mixing effects have been demonstrated by pulse discharge and due to MHD interaction.

S.B. Leonov, D.A. Yarantsev, K.V. Savelkin (IVT RAS). ***Temperature Measurements by Emission Spectroscopy Applied to the Plasma Assisted Combustion***. International Symposium Combustion and Atmospheric Pollution, 8-11 July 2003, St. Petersburg, Russia.

This paper describes and presents spectroscopic methods for plasma parameters measurement. Gas temperature measurements have been done by the method of fitting calculated spectrum and experimental one. It was pointed out that vibrational temperature of CN molecule is higher than rotational one. Rotational temperature that is measured by the N₂ Second positive band spectrum is lower than one, which is measured by CN spectrum. Strong heterogeneity of the plasma parameters under discharge assisted combustion was demonstrated.

S. Leonov, V. Bityurin, K. Savelkin, D. Yarantsev (IVTAN, Moscow, Russia). ***Plasma-Induced Ignition and Plasma-Assisted Combustion of Fuel in High Speed Flow***, 5th International Workshop “Magneto Plasma Aerodynamics in Aerospace Applications”, April, 2003, Moscow, IVTAN

This paper discusses a problem of plasma assistance in high-speed combustion, mainly. Several possible methods of plasma applications could be suggested in a field of propulsion. Different variants of plasma assistance are considered, including under the condition of artificial local separation zones. Also, the paper analyses and discusses results of experimental work on influence of energy release from special organized electrical discharge on

characteristics and dynamics of the fuel ignition under the non-premixed conditions. The advantages and possible penalties of plasma technique application in a field of supersonic propulsion are debated.

S. Leonov, A. Kuryachii, D. Yarantsev, A. Yuriev, ***“Study of Friction and Separation Control by Surface Plasma.”*** Paper AIAA-2004-0512, 42th AIAA Aerospace Sciences Meeting & Exhibit, 05-08 January 2004 / Reno, NV.

The paper describes some results of analytical and experimental study of plasma effects on a viscous friction and boundary layer separation. Two mechanisms of the electric discharge influence are considered here: thermal energy deposition and electrostatic force excitation. The modification of the fixed separation zone and generation of an artificial separation zone under supersonic and transonic flow are discussed. The data on the near-surface capacitive discharge effects in high-speed flow are presented. The experiments on separation control and transonic shock stabilization were conducted on a small-scale gasdynamic facility PWT-10. The plasma effects are demonstrated by the Schlieren observation. Results of pressure, temperature and volt-ampere measurements are shown. Characteristic energetic parameters are estimated.

S. Leonov ***“Near-Surface Plasma Effects in High-Speed Flows”***, Russian School-Workshop “MPA in Aerospace Applications”, 20-21 April 2004, IVTAN, Moscow.

The idea was announced as following. Energy release or plasma formation near surfaces in high-speed airflow influents on a near-wall layer itself, in particular, leads to a local/global separation, oblique shock and the plasma overlayer generation. These aerodynamic structures can be applied instead of mechanical arrangements, especially, under non-optimal operation mode of the combustor. The flame stabilization mode could occur at relatively low level of extra energy deposition. The plasma generator and fuel injector can be combined together in a single device. The paper presents the experimental and analytical results in frames of that method development.

S. Leonov, K. Savelkin, D. Yarantsev ***“Electrical Discharge Effect on Structure and Parameters of Supersonic Airflow”***. Proceedings of the Symposium on Thermal-Chemical Processes and Plasma Applications in Aerodynamics, St-Petersburg, “Leninets”, 12-14 July, 2004.

The paper is devoted mainly to problem of flow management by the discharge plasma excited inflow. It could be related to the newly-developed field of Magneto Plasma Aerodynamics. Conventional methods to advance aerodynamic characteristics of aerovehicles and its parts or to adjust the trajectory are based on application of mechanical elements, which use energy of approach airflow for re-distribution of pressure on surfaces, and application of jets' power in local areas near the surfaces. There are no doubts now that other (energetic) methods for flow/flight control have a practical potential. Among known methods for flow characteristics control the plasma generation is, probably, the most prospective. Recently the potential of enhancing the characteristics of supersonic flow in ducts using electric discharge plasma has been widely discussed. Two main ideas stimulate efforts in this field: the control of the inlet/diffuser performance and the improvement of the supersonic combustion efficiency. In both cases the electrical discharge changes the structure of flow, and the thermo-chemical and electro-magnetic properties of the medium.

S. Leonov, K. Savelkin, D. Yarantsev, A.Yuriev ***“Supersonic Gas Flow Control by Electrical Discharges”*** International Scientific Conference “High-Speed Flow: Fundamental Problems”, Zhukovsky, 21-24 September 2004.

The paper describes the problem of flow guiding by the discharge plasma excited cross-flow and near the surface of high-speed channel. A main attention is paid for the results of the surface discharge effect on structure of separation zone in supersonic airflow in a duct with backwise wallstep.